SOLID PHASE SYNTHESIS OF FLUORESCENT DYE LIBRARIES AND THEIR APPLICATIONS IN BIO-IMAGING

RAJ KUMAR DAS

(M. Sc., Indian Institute of Technology Bombay, Mumbai, India)

A THESIS SUBMITTED

FOR THE DEGREE OF DOCTOR OF PHILOSOPHY

DEPARTMENT OF CHEMISTRY

NATIONAL UNIVERSITY OF SINGAPORE

2013

Thesis Declaration

The work in this thesis is the original work of Raj Kumar Das, performed independently under the supervision of Professor Young Tae Chang, (in the Chemical Bioimaging Lab, S9-03-03), Chemistry Department, National University of Singapore, between 07/01/2009 and 07/01/2013. Content of the thesis has been partially published in:

1) Development of photostable near-IR cyanine dyes, Samanta, A.; Vendrell, M.; **Das, R**.; Chang, Y. T.* *Chem. Commun*., 2010, *46*, 7406-7408.

2) Solid Phase Synthesis of Ultra-Photostable Cyanine NIR dye library, **Das, R. K**.; Samanta, A.; Ha, H. H.; Chang, Y. T.* *RSC Advances*, 2011, *1*, 573.

3) *ChemInform Abstract*: Development of Photostable Near-Infrared Cyanine Dye, Samanta, A.; Vendrell, M.; **Das, R.**; Chang, Y. T.* *ChemInform*, 2011, 42, 204.

4) Development of Rhodol Based Fluorescent Cell Cycle Probe, Chang, Y.T.; **Das, R. K.**; Yun, S. W.; Jeong, Y. M.; Kang, N. Y.; Park, S. J. US Provisional Appl. 61/780,116, 2013.

Raj Kumar Das	*Rajkuman Das*	15.08.2013
Name	Signature	Date

MyungWon, Yoges, Emmiline, Jow Zhi Yen, Chee Geng, Physilia, Jimmy, Pamela, Fronia, Tang Mui Kee, Yogesh, CheeGeng, Justin, Xuwang, Dongdong, Elton, Amanda, Jun Cheng and Xiaojun Liao.

Table of Contents

Chapter 3 Monocyte/Macrophage specific Fluorescent Probe

Development to Assess inflammation *in vivo*

Chapter 5 Possibility of live B-Lymphocytes imaging by novel BODIPY probe: CDg6

Chapter 8   Conclusions and Future prospective

Summary

It is quite obvious from the available wide range of literature reports that the progress of diversity oriented fluorescent library approach along with the high throughput screening lead to novel bio-imaging probes/sensors discovery in a relatively faster manner. However, for the case presented here, efficient solid phase chemistry needs to be devised to provide a robust synthetic route for generating a large number of fluorescent libraries in a short span of time. In this view, I developed an elegant solid phase route to systemically apply in the synthesis of fluorescent libraries that cover wide emission color spectra from VIS to NIR. We designed the novel diversity oriented fluorescent libraries where each library contains single emission wavelength to develop both cell imaging and *in vivo* imaging probe. Single wavelength with different structural diversity provided a useful toolbox as it allowed easier structural activity relationships studies (B cell probe development).

In the chapter 2, based on the previous work by our group, I have synthesized ultra-photostable , NIR cyanine dye libraries (CyR and its CA, AC and lipoic acid derivatives) utilizing CyNA-414 , the most photostable dye from CyNA library. In Chapter 3, from macrophage screening of CyR derivatives, we developed a novel *in vivo* imaging macrophage probe (CyRCA-341). From the SERS screening of the CyRLA compounds (Chapter 4), we discovered the highly SERS-active compound CyRLA-572 which has been utilized as the multiplexing partner with the Cy7LA and Cy7.5LA compounds to detect three germ layers of mESc *in vitro*.

Modifying the stable tetramethyl BODIPY scaffold, in the chapter 5, I have synthesized BDR library and its CA and AC derivatives to generate green emission compounds. From the cell based screening, we discovered a B-cell selective probe CDg6 (BDRCA-656). For the SARs study, I synthesized BODIPY derivatives containing long alkyl chains (upto 24 carbons).

In the chapter 6, Rhodol scaffold, a mixed hybrid from rhodamine and fluorescein was employed to produce longer wavelength, dye library (RDR and its CA, AC derivatives) in the range of orange emission color. Rhodol library inherited excellent photophysical properties such as good quantum yield, high extinction coefficient. Using cell based screening, we obtained primary results for discovering mitotic phase specific probe, RDR-567 which specifically stains to the mitosis compared to the inter phase cells.

I synthesized COR library (chapter 7) and its respective chloroacetyl (CA) and acetyl derivatives (AC) to cover the large stokes shift (150 nm), green emission dyes. Here, based on the previous work and the studies, I opted a coumarin scaffold which contains dimethyl amino group at 7- position for better photophysical property and acid group at 4-position for diversification. Over all, I constructed a coumarin library (COR, CORCA and CORAC) with diversity at the 4-position using our efficient solid phase synthesis to explore these compounds in the evaluation of biological function via cell based and *in vitro* screening.

List of Tables

List of Figures

Chapter 1

Chapter 2

CORCA and CORAC compound. 197

List of Charts

List of Schemes

Abbreviation and symbols

AcOH	Acetic acid
Ac$_2$O	Acetic anhydride
ACN	Acetonitrile
GFP	Green fluorescent protein
BuOH	Butanol
CDCl$_3$	Deuterated chloroform
CHCl$_3$	Chloroform
CO$_2$	Carbondioxide
Methanol-d4	Deuterated methanol
DAD	Diode array detector
DCC	N,N'-Dicyclohexylcarbodiimide
DCM	Dichloromethane
DIC	N,N'-Diisopropylcarbodiimide
DIEA	Diisopropyl ethylamine
DMAP	Dimethylaminopyridine
DMF	N, N-Dimethylformamide
DMSO	Dimethyl sulfoxide
DMSO-d6	Deuterated dimethyl sulfoxide
DOS	Diversity oriented synthesis
DOFLA	Diversity oriented fluorescence library approach
EA	Ethyl acetate
ESI	Electrospray ionization
Ex	Excitation
Em	Emission
FRET	Fluorescence resonance energy transfer

HATU	2-(1H-7-Azabenzotriazol-1-yl) 1,1,3,3-tetramethyluronium hexafluorophosphate methanaminium
HCl	Hydrochloric acid
HEPES	4-(2-Hydroxyethyl)-1-piperazineethanesulfonic acid
HPLC	High-performance liquid chromatography
HPLC-MS	High-performance liquid chromatography mass spectrometry
HTS	High throughput screening
mESC	Mouse Embryonic Stem Cell
MeOH	Methanol
MeOD	Deuterated methanol
ACN	Acetonitrile
MS	Mass spectrometry
NMR	Nuclear magnetic resonance
ϕ	Quantum yield
Mϕ	Macrophage
RT	Room temperature
TFA	Trifluoroacetic acid
THF	Tetrahydrofuran
TLC	Thin layer chromatography
TOS	Target oriented synthesis
TRITC	Tetramethylrhodamine-5-isothiocyanate
UV	Ultraviolet

List of Publications

1) Target Identification: A Challenging Step in Forward Chemical Genetics, **Das, R. K**.; Samanta, A.; Ghosh, K.; Zhai, D.; Xu, W.; Su, D.; Leong, C.; Chang, Y. T.* *Interdiscip. Bio Central* 2011, *3*, 1.

2) Development of photostable near-IR cyanine dyes, Samanta, A.; Vendrell, M.; **Das, R**.; Chang, Y. T.* *Chem. Commun*., 2010, *46*, 7406.

3) *ChemInform Abstract*: Development of Photostable Near-Infrared Cyanine Dye, Samanta, A.; Vendrell, M.; **Das, R.**; Chang, Y. T.* *ChemInform*, 2011, *42*, 204.

4) Solid Phase Synthesis of Ultra-Photostable Cyanine NIR dye library, **Das, R. K**.; Samanta, A.; Ha, H. H.; Chang, Y. T.* *RSC Advances*, 2011, *1*, 573.

5) Development of Photostable Near-IR Cyanine Dyes for *In Vivo* Imaging, Chang. Y. T.; Samanta. A.; Vendrell. M.; Kang, N. Y.; Maiti, K. K.; Soh, K. S.; Dinis. U. S.; Olivo. M.; Park, S.J.; **Das, R.K**.; U.S.Application No: 13/625,832.; Ref: 09227N-USCIP.; Docket No. 4459.1016-001.

6)) Development of Rhodol Based Fluorescent Cell Cycle Probe, Chang, Y.T.; **Das, R. K.**; Yun, S. W.; Jeong, Y. M.; Kang, N. Y.; Park, S. J. US Provisional Appl. 61/780,116, 2013.

7) Monocyte/Macrophage Specific Fluorescent Probe Development to Assess Inflammation *In Vivo*. ***Manuscript under preparation.***

8) Multiplex detection of different germ layers in teratoma by SERS nanotags with cyanine Raman reporters**.** ***Manuscript under preparation.***

9) Possibility of live B-Lymphocytes imaging by novel BODIPY probe: CDg6 ***Manuscript under preparation.***

Chapter 1

Introduction

Of late, the use of fluorescent molecules in biological research is the benchmark in many applications, and their utilization is constantly mounting owing to their adaptability, sensitivity and quantitative potentiality. Moreover, the use of fluorescence small molecules remarkably diminishes the most challenging task in the process of the identification of small molecule probes with a high selectivity towards the specific targets. In this case, the ligands of specific targets from the organelles in complex biological systems are usually labeled with fluorescent molecules and subsequently visualized by taking images using fluorescence microscopy. As a result, in recent times, the fluorescent probes or sensors are widely being utilized to detect protein location, to recognize protein complex formation as well as activation, to detect conformational changes and to examine biological processes both *in vitro* and *in vivo*.

The conventional strategy for the design of fluorescent probes or sensors is based on the target oriented synthesis (TOS) where the combination of fluorescent dye molecules and designed receptors for specific analytes is used for the recognition of the receptor-analyte complex which in turn can induce the photophysical property changes of the dye moiety. Though, this approach has played a critical role throughout the decades, it has its own limitation in the process of novel sensor discovery. Recently, the application of combinatorial chemistry techniques along with the diversity-oriented strategy has impelled the emergence of diversity-oriented fluorescence library approach (DOFLA) to the discovery of novel fluorescence sensors. By

applying this approach, the fluorescent dye libraries are generated to avoid the concept of recognition of specific analytes. Here, during the process of synthesis, the fluorophore scaffolds are typically designed with certain functionality to introduce the diversity and the efficient synthetic routes are customized to produce a diverse set of dyes. So far several DOFLA scaffolds have already been reported which include coumarin, dapoxyl, styryl, hemicyanine, rosamine, and BODIPY and their applications have been demonstrated.

The following sections of this thesis will review the research of the expansion of combinatorial approach on fluorescent small molecules in sensor or probes development using different fluorescent scaffolds and their recent applications.

1.1 Overview of Small Molecule Fluorophores

Fluorescence is a form of optical spectroscopy where a molecule usually absorbs ultraviolet, visible, or near infrared radiation to be promoted to an electronically excited state. The excited molecule then discharges the energy in the form of light emission to return to the ground state, or to a lower-lying excited electronic state. The emitted light can be detected either visually or through the detectors. Due to its high flexibility, sensitivity and quantitative capabilities, fluorescence technique[1] has been applied in biological research for over 100 years. The developments in fluorescence chemistry along with technical discoveries have stimulated the advancement of many different kinds of fluorophores. Three general groups of fluorophores are developed due to enormous research. These are biological fluorophores, quantum dots and organic dyes. Bioluminescence, generated from biological

fluorophore is quite well known for a long time as the first use of a biological fluorophore for research applications took place in the 1990s, when green fluorescent protein (GFP)[2] was utilized as a gene expression reporter. Since then, derivatives of the original GFP and many other proteins have been designed for application in biological expression systems. However, the biological fluorophores or fluorescent proteins are quite bulky in size. Hence in the biological research, the fluorescent proteins become slow labeling, and difficult handling agents[3].Quantum dots also used as fluorophores, were developed in the 1980s by Alexei Ekimov and since the 1990s have gradually been used more in fluorescence applications in biological research. While the use of quantum dots in biological applications is increasing, there are reports of cell toxicity[4] in response to the breakdown of the particles and their use can be cost-prohibitive. Additionally, in case of QDs, the fact that these behave not as molecules but as nanocolloids complicates their application in biological environments[5]. In biological research, organic synthetic dyes are the most useful dyes. However, there are a very limited number of scaffolds found to be fluorophores. Interestingly, these few fluorescent scaffolds cover almost all colors in the spectra, from UV-visible to near–infrared (NIR).

Figure 1.1 Spectral range of different well known fluorophores

Well known fluorophores[6] with different wavelengths used as DOFLA scaffolds are: DAPI, FITC, TRITC, Texas Red , BODIPY, Rhodol, rosamine, styryl, xanthone, oxazine and cyanine. These DOFLA scaffolds have been utilized for a range of applications in the bioorganic field. Among the different fluorophores, NIR dyes (i.e., molecules absorbing light in the range

of 700 to 1000 nm) are more suitable for the optical imaging *in vivo*[7], while the shorter wavelength dyes ranging from blue to red are mainly used for *in vitro*[8] cell imaging studies. Therefore, NIR light absorbing dyes have attracted much attention for the development of the *in vivo* optical imaging probes[9].
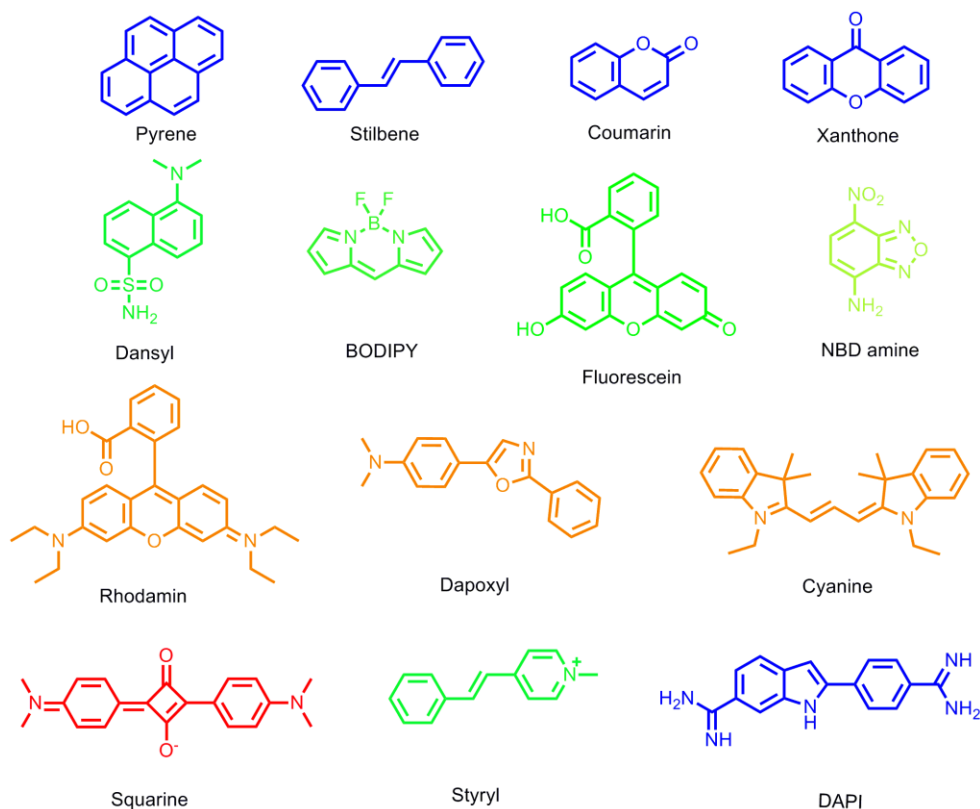
Figure 1.2 Representative fluorophores with emission ranging from blue to NIR.

1.2 Synthetic strategies for novel fluorescent probes

1.2.1 Target oriented approach

There are two commonly used synthetic strategies for probes development in chemical biology. These are the target-oriented approach (TOS)[10] and diversity oriented approach[11]. In the target oriented approach, the target recognition moiety of the molecule is designed on the basis of empirical knowledge, and the fluorophore is simply used as a signal amplifier. However, in this approach, the complex designed receptor structures usually need bulky

synthetic work for each individual sensor. Also, the sensor's scope of application is intrinsically limited to the preselected analytes that the sensor was designed for.
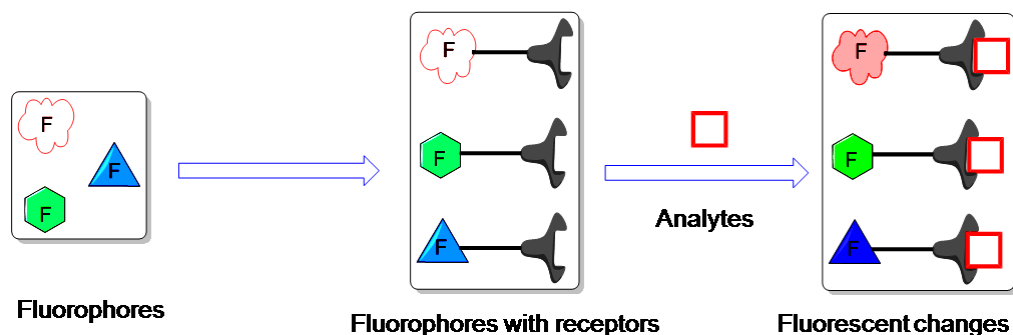
Figure 1.3 Schematic diagram for Target-oriented fluorescent sensor design

1.2.2 Diversity oriented approach

In the diversity oriented approach, the library of diversified synthesized fluorescent compounds is screened against a broad range of analytes without a limitation[12]. The application of combinatorial chemistry techniques and the diversity-oriented strategy have spurred the appearance of diversity-oriented fluorescence library approach (DOFLA)[13] to the discovery of novel fluorescence sensors. Here, the design and preparation of the dye library is unbiased to any specific target analyte so the library can be evaluated with quite distinct analytes to maximize the chance of applications in different fields. The effectiveness of this approach has been demonstrated with the impressive discoveries of novel sensors for organelle[14], polymers such as DNA and heparin[15] or for small molecules such as GTP[16] and glutathione.[17]
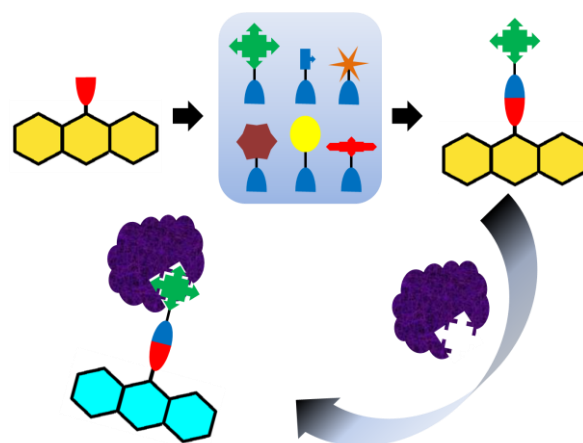
Figure 1.4 Schematic diagram for diversity-oriented fluorescent sensor design

1.3 Solid Phase Synthesis

This DOFL approach needs quite efficient synthetic work with relatively easier chemistry to acquire a diverse set of dyes. A number of parallel synthesis methods for the synthesis of dye molecules in solution phase have already been reported[18] in literatures. However, the methods comprise tedious purification steps along with typical low recovery yields. Although the synthesis of individual compounds could overcome this limitation, it would critically trouble the combinatorial derivatization of the fluorescent scaffold because of its labour intensive purification processes. The challenges have been overcome by incorporating the solid phase methodologies in the synthesis process pioneered by Bruce Merrifield who first introduced this method for synthesizing peptide molecules[19]. In the process of solid phase synthesis, one of the reactant molecules is attached to an insoluble material i.e the solid support which can be easily modified in to the products by means of appropriate chemical reactions. Although this technique initially was used for peptide synthesis, later it was adopted for oligonucleotide[20] synthesis. Recently, solid phase synthesis is broadly employed in combinatorial

6

chemistry for the development of the huge number of molecules in a very short time. One of the major advantages of the solid phase synthesis is that it can help to circumvent the technical difficulties related with the solubility and purification. In this method, purification is basically carried out by washing the resin with a variety of solvents. The use of suitable washing solvents or solvent mixtures can remove all the unbound impurities, by-products and the excess solution phase reagents entirely. An additional advantage of this solid phase synthesis is that the use of excess reagent can lead to the completion of the reaction with relatively higher yields. So far, a number of solid-phase methodologies have been successfully applied for diversifying the various fluorescent scaffolds encompassing challenging purification steps. Syntheses of libraries of cyanine [21,22] and other dyes (e.g. diazonium salts,[23] coumarins,[24] thiazoles,[25] benzimidazolium,[26] rosamines[27]) have been carried out on solid supports and hence demonstrated the effectiveness of this technique. One of the general Schemes for the solid phase synthesis is given in the **Figure 1.5**.
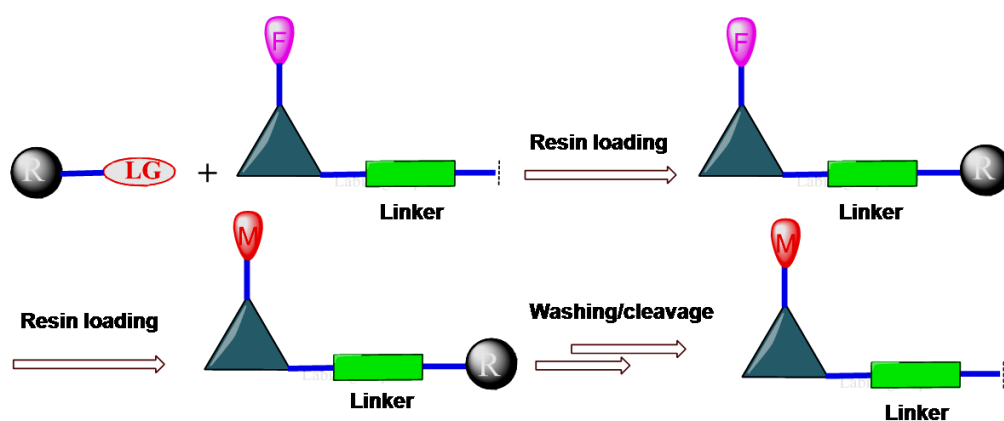
Figure 1.5 Schematic diagrams for solid phase synthesis

1.4 Bioimaging

Optical bio-imaging research labs mainly focus on the development of fluorescent probes, which allow visualization of metal ions such as Ca^{2+},[28] Zn^{2+},[29] Na^{+},[30] K^{+} [31] etc., small biomolecules such as nitric oxide (NO)[32] or enzyme activities [33] in living cells by means of fluorescence microscopy. At present, fluorescent probes based on small organic molecules have turn out to be crucial tools in modern biology as they offer dynamic information regarding the localization and quantification of the molecules of interest, exclusive of the requirement for genetic engineering of the sample. Practically, it is also quite desirable in the field of life science research that the techniques used should not comprise any invasive method, in other way it should not involve any experiment related with cutting into the body or isolating cellular components. Therefore, methods to visualize physiological or pathophysiological changes in the body or in other word *in vivo* imaging have become gradually more crucial in biomedical sciences. The bio-imaging probe consists of two apparent classes of probes. One is cell-based imaging probe to study the cellular events thoroughly and another is *in vivo* imaging probe for non-invasive detection and monitoring the different events.

1.4.1 Cell imaging Probes or sensor: target oriented design

Application of modern synthetic organic chemistry allows proficient modification on the chemical structure to obtain probes for particular biological experiments inside the cell. Here, often, the chemistry are used to activate fluorogenic compounds (fluorophores) by means of substrate specific enzymes and photoactivatable compounds that can facilitate the improvement of imaging experiments with low background fluorescence. Many cases, rationally designed ligands attached in the fluorescent molecules which are

essentially cell permeable are used to discover the probes or sensors to understand the cell biology. There are many reports on the development of cell imaging probes using the targeted design strategies with the various fluorescent scaffolds in the literatures. For instance, Jung *et. al.* in 2009 developed a fluorescence quenching based copper sensor[34] (**Figure 1.6**) where coumarin scaffold was intentionally attached with 2-picolyl group to obtain the selective coordination with the Cu^{2+} over other heavy metal ions. They also demonstrated the utility of this sensor in the cell imaging study.
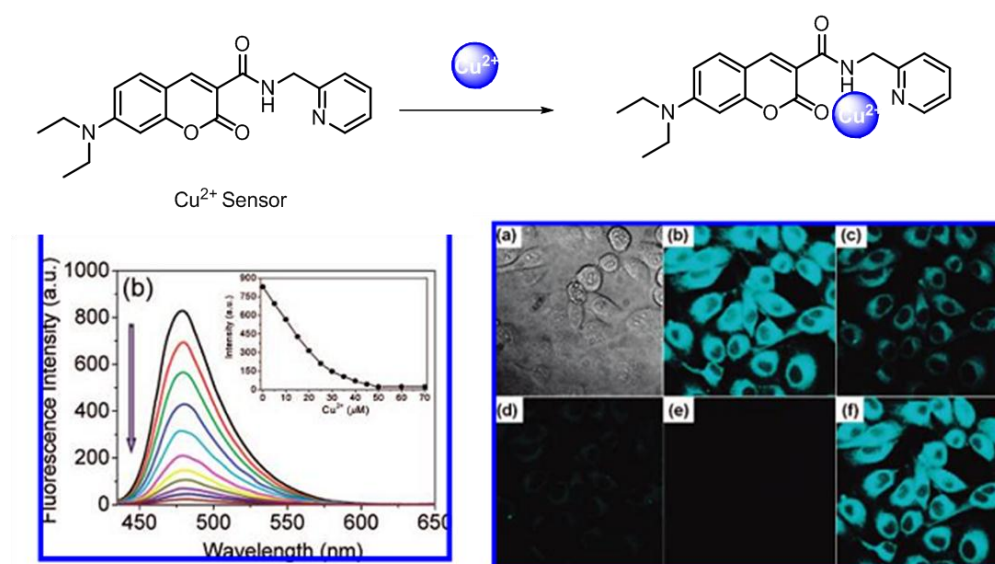
Figure 1.6 Confocal fluorescence images of Cu^{2+} in LLC-MK2 cells. (a) Represents the brightfield transmission image of LLC-MK2 cells. (b) Represents the fluorescence image of LLC-MK2 cells after incubation with Cu^{2+} sensor. (c) to (e) stands for the fluorescence image of further incubation with addition of various concentrations of $CuCl_2$ [(c) 5, (d) 10, and (e) 20 equiv, respectively] and finally (f) fluorescence image corresponds to return of intracellular Cu^{2+} to the resting level was achieved by addition of EDTA (500 µM). This picture has been copied from reference 34 under copyright permission.

1.4.2 Cell imaging Probes or sensor: diversity oriented design

In connection to the development of imaging sensors or probes, the deficit of enough information at a molecular level for many biological events (e.g. protein–protein interactions, cellular differentiation stages[35]) and major dissimilarities between *in vitro* and living cell situations have barred the design of imaging probes by rational-based methodologies[36]. A useful substitute would be the diversity-oriented strategies, which methodically diversify the chemical structure and consequently facilitate the research in the development of imaging probes or sensors. Combinatorial approach for fluorescent libraries syntheses and their extensive cell based screening (**Figure 1.7**) enable us to develop multiple probes or sensors efficiently and that would partially overcome our restricted capability of envisaging particular interaction between the biological actions and the designed fluorescent molecules.
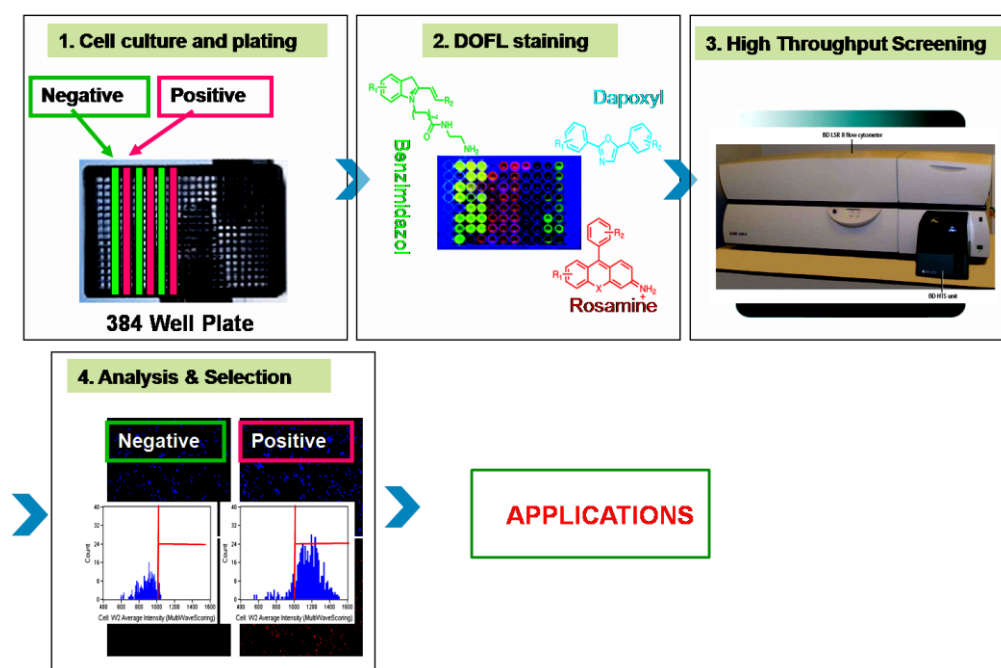
Figure 1.7 Schematic diagram for a development method of cell imaging probe or sensors using diversity oriented approach.

Recently our group (Chang and co-workers) reported a neural stem cell specific boron-dipyrromethane (BODIPY) derivative, compound of designation red 3 (CDr3)[37] which has been developed through a high throughput/content screening of in-house generated diversity oriented fluorescence library in stem cells at different developmental stages. This novel compound specifically detects living neural stem cells of both human and mouse origin.
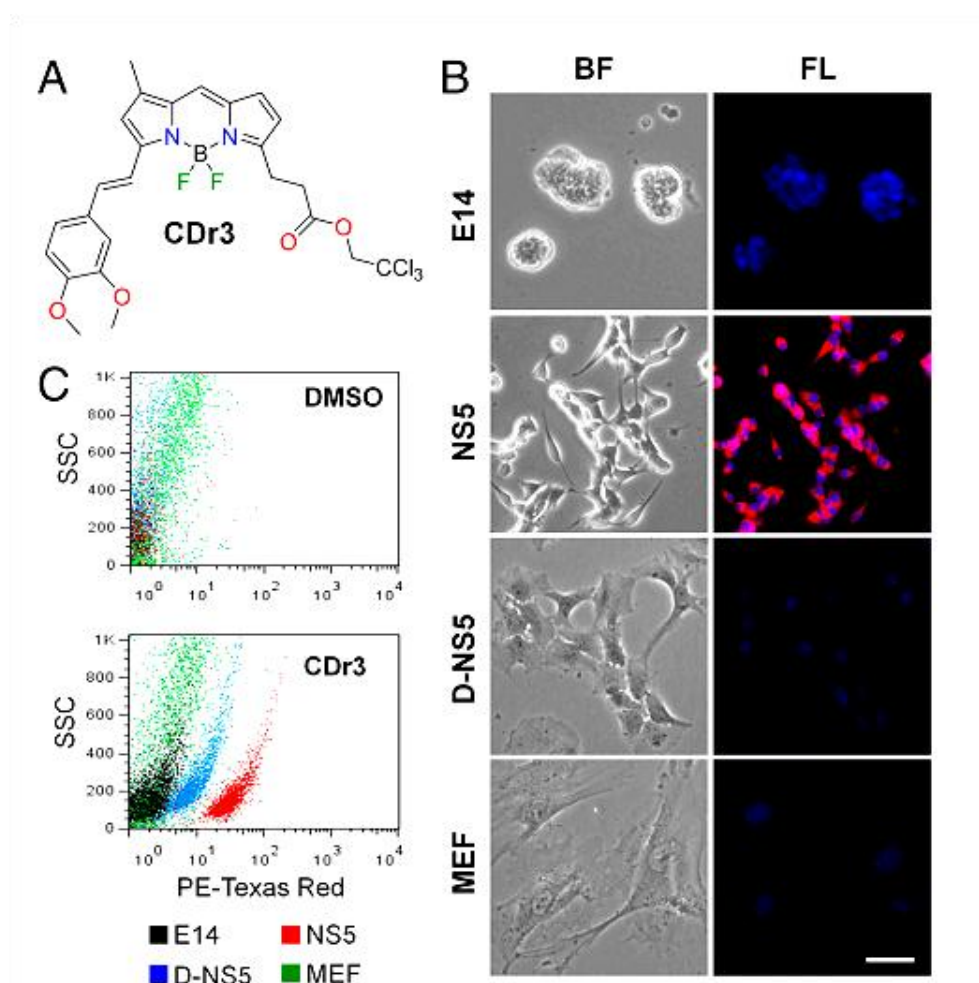
Figure 1.8 Development of neural stem cell specific probe; **Figure 1.8B** image represent the selective Staining of NS5 by CDr3 where nuclei of E14, NS5, D-NS5, and MEF were visualized by Hoechst 33342; but only NS5 was selectively stained by CDr3. **Figure 1.8C** is the flow cytometry dot plot images of E14, NS5, D-NS5, and MEF incubated with CDr3. In this case, they

have added DMSO for unstained control cells. This picture has been copied from reference 37 under copyright permission.

Chang *et al*. have also synthesized several diversity oriented libraries including rosamine, cyanine, chalcone, dapoxyl, bemzimidazol, libraries and evaluated their photophysical properties and successfully applied them in live cell imaging study that includes β-amyloid[38], human serum albumin[39], embyronic stem cell probe[40], etc.

1.5 *In vivo* imaging

In vivo imaging is an approach where biology is studied at an organismal instead of the cellular, level. During the *in vivo* imaging, light is shone on animal subjects which are commonly mice or rats and then an answer in the form of a map of emitted light intensity as a function of anatomic position is derived (**Figure 1.9**)
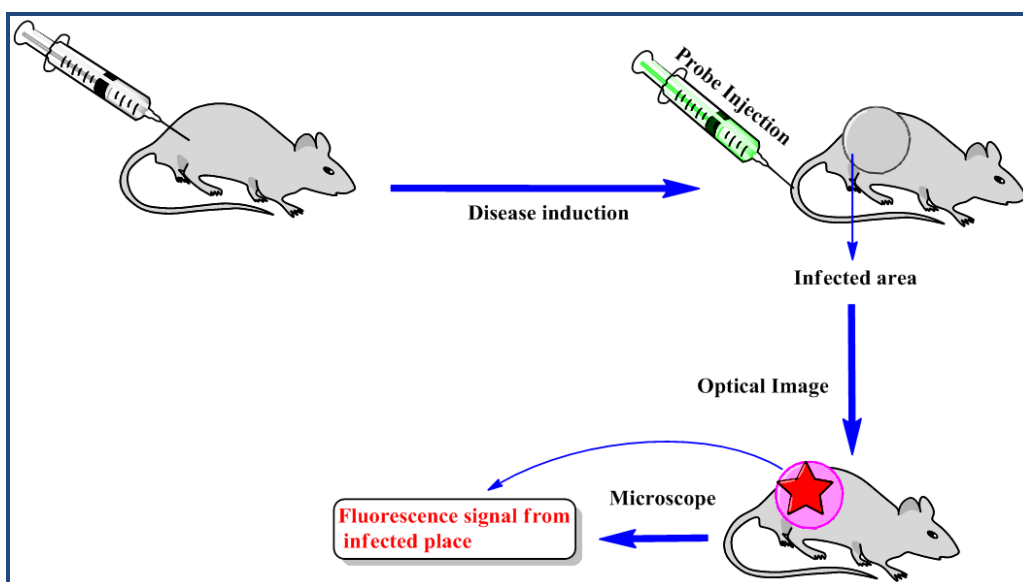
Figure 1.9 Schematic diagram for a development method of *in vivo* imaging probe

Among the different techniques of *in vivo* imaging, *in vivo* fluorescence imaging using NIR light has a great potential for molecular diagnostics and therapeutic studies. In addition, there is another practical benefit too. As the *in vivo* imaging is non-invasive, animals may be tracked over time, for example to investigate as a tumor grows.

1.6 NIR fluorophores

As it is well known that the shorter wavelength dyes in the range of UV-Vis emissions are mainly used for *in vitro* or cell imaging studies, therefore, NIR light absorbing dyes have attracted much interest for the development of the *in vivo* optical imaging probes. NIR light has been used enormously in biomedical applications due to its deep tissue penetration. UV-visible light often has high autofluorescence and background limitations. In contrast, NIR light reduces the background problems and therefore paves the way for the NIR light absorbing dyes in the bio-imaging research. The benefits of imaging in NIR region are numerous: (a) the low absorbance from tissue allows a deeper tissue penetration; (b) low auto-fluorescence decreases the fluorescence background and (c) low Raman scattering makes very high signal to noise ratio. In recent time, the research spotlights on tissue imaging or *in vivo* imaging lead to the development of different NIR fluorophores. Till now, a very few number of scaffolds are available to develop NIR fluorophores (e.g. squaraine,[41] quinone,[42] triphenylmethane,[43] cyanine[44]). Recently few limited structures from the BODIPY and rhodamine scaffolds have been reported as the Near-infrared dyes (**Figure 1.10**).
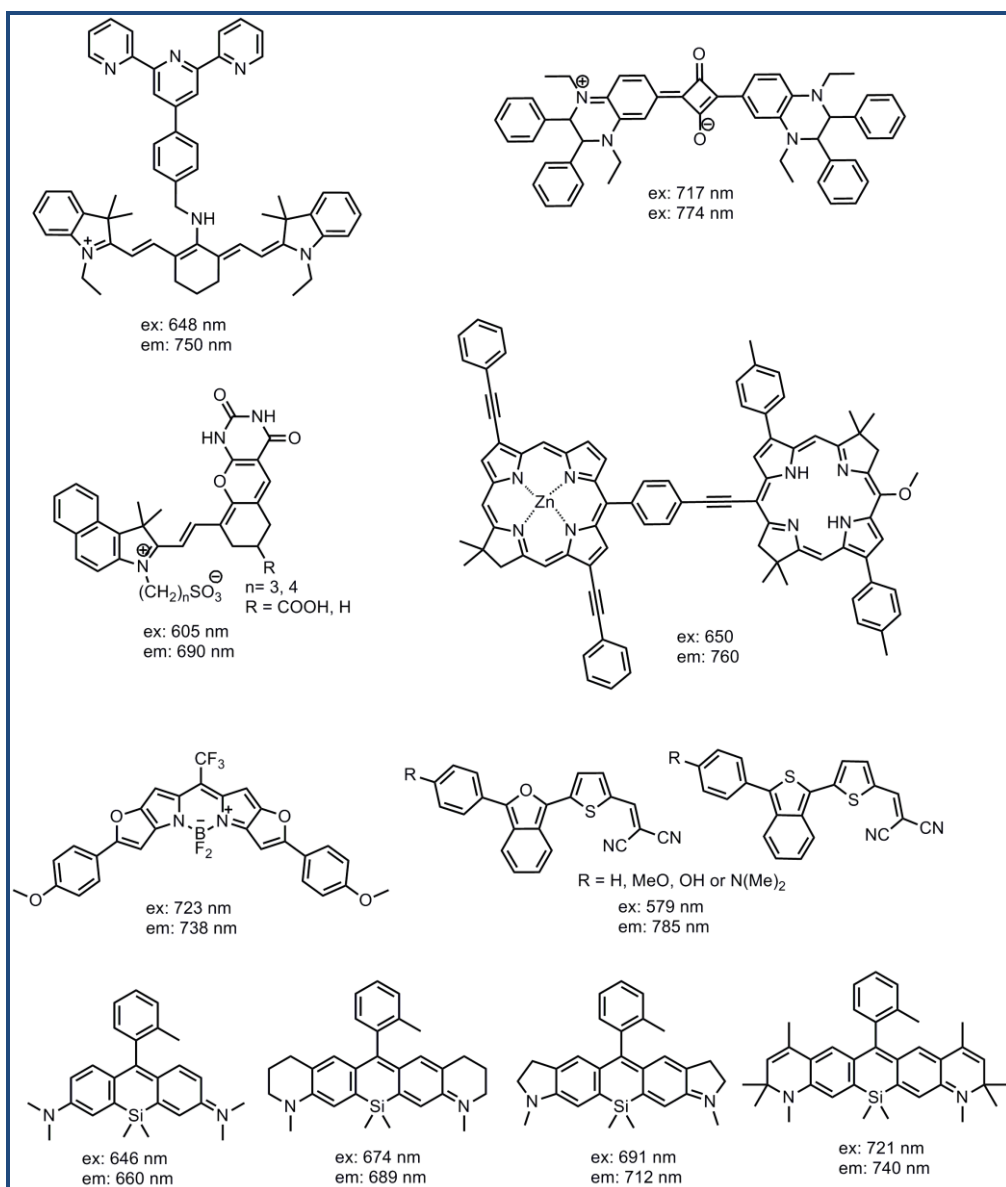
Figure 1.10 Representative examples of NIR fluorescent structures[45]

1.6.1 Tricarbocyanine dyes: *in vivo* imaging

Among the available fluorophores, cyanine structures[44] have been accepted as one of the best scaffolds compared to the other NIR dye scaffolds, especially for the development of imaging probes due to their synthetic accessibility, large molar extinction coefficient and broad wavelength tunability. Moreover, photo-switchable cyanine dyes are useful for high resolution microscopy (e.g. STORM and PALM[46]). However, major limitation

of cyanine dyes is the photobleaching or photodestruction characteristics. Cyanine dyes upon irradiation of light in presence of aqueous media undergoes the chemical reactions with the various reactive oxygen species such as singlet oxygen $(^1O_2)$[47], peroxide, superoxide and redox active metabolites and that leads to their degradation. Particularly, tricarbocyanine dyes are identified to be comparatively low photostable owing to their long conjugation. Very few reports about the photostability of cyanine dyes are available in the literature. To take up this challenge, our group developed a combinatorial approach to develop photostable tricarbocyanine library and screened them to identify best stable candidate, CyNA-414[48] which has the stronger emission intensity and higher photostability than the NIR standard IndoCyanine Green (ICG). The possible reason hypothesized by our group that the modification of the bridgehead nitrogen atom by removing lone pair electron would restrict the likelihood of forming iminium intermediate which is the presumed culprit for facilitating the incorporation of the reactive oxygen species in to the dye scaffolds. Therefore, various structurally diverse amine tricarbocyanine (CyN) compounds were modified with an electron-withdrawing acetyl group to afford the corresponding acetylated compounds (CyNA) which showed remarkably improved photostability over the CyN (**Figure 1.11**). Later, Chang and co-worker modified the CyNA-414 derivatives with the succcinimidyl ester (CyNE790)[49] for the bioconjugation. The CyN790 dye was labled with the EGFR monocholnal antibody preserving the excellent photostability and NIR fluorescence intensity of the amine acetylated tricarbocyanine scaffold and applied this dye for *in vivo* NIR imaging. Theses superior property attracts me to opt out the CyNE-790

derivative to generate another set of NIR compounds which may have wide possibility to develop *in vivo* imaging probe (**Figure 1.12**).
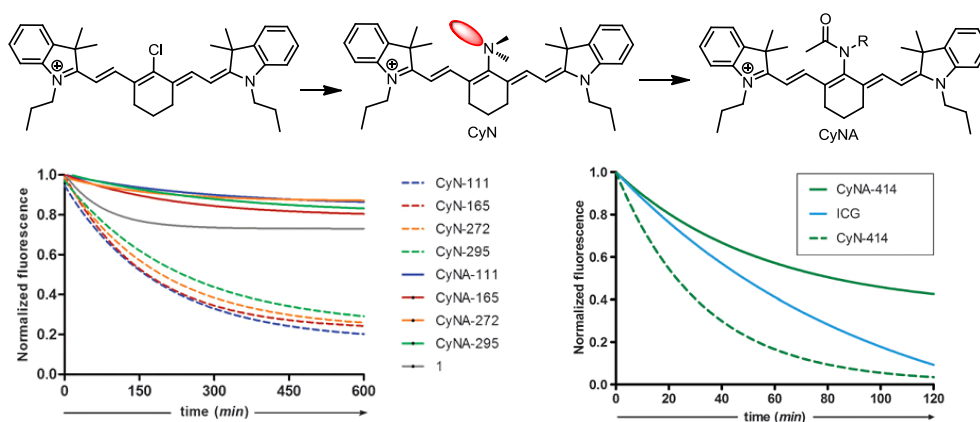
Figure 1.11 Design and synthesis for the photostbale cyanine compounds. This picture has been copied from reference 48 under copyright permission.
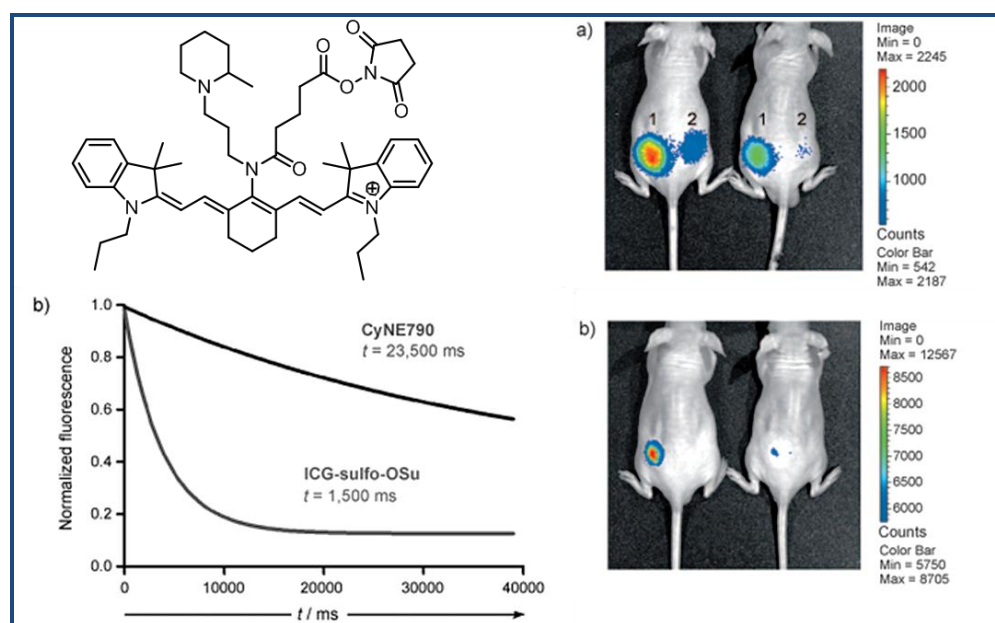
Figure 1.12 Application of photostbale cyanine compounds in *in vivo* imaging. This picture has been copied from reference 49 under copyright permission.

1.6.2 Tricarbocyanine dyes: SERS imaging

In recent times, the application of SERS in the sensitive detection of biomolecules inside living cells,[50] glucose sensing,[51] protein analysis,[52] or the investigation of sensitive biological samples are continuously increasing[53]. In this view, reporter molecules (i.e. Raman-active dyes) having thiol functionality are used to attach with the surface of silver or gold NPs with variable sizes (10–80 nm) to acquire SERS nanotags. The reproducibility and spectral intensity of these nanotags can be monitored by encapsulation and shielding from the environment. Now-a-days, the stable and biocompatible nanoparticles (NPs) have widely been used for SERS cellular imaging.
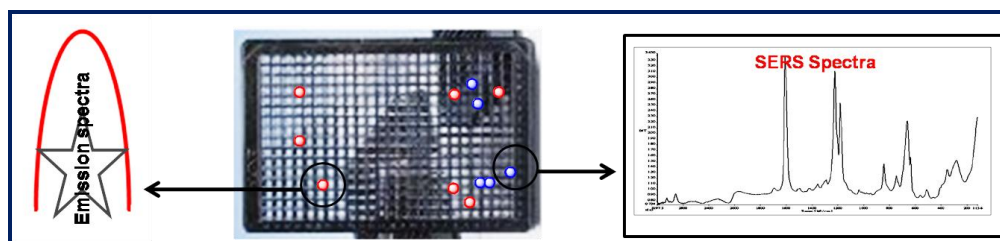
Figure 1.13 Schematic diagram for high-throughput SERS screening strategy

Antibody-conjugated gold nanoparticles (AuNPs) and nanorods have also been utilized to detect cancer using the target specific imaging technique where the cell surface of the cancer cell is highly expressed by the cancer markers. Therefore, the antibody-conjugated AuNPs which are attached with Raman reporter can selectively target the cancers cells and thereby provide the higher intensity SERS signal from the targeted cancer cells and allow their imaging and detection capability. For instance, epidermal growth factor receptor (EGFR)[54] recognizing anitbodies have been conjugated to SERS nanotags and applied them to detect *in vivo* where the EGFR are over-expressed in the human tumors[54]. NIR dyes (e.g.diethylthiatricarbocyanine

17

(DTTC)) have also been in used as the specific Raman reporters for *in vivo* surface-enhanced resonance Raman scattering (SERRS).[55] Recently, Samanta *et.al.* synthesized lipoic acid-containing NIR-active tricarbocyanine library (CyNAMLA), and screened their SERS properties after chemisorption in AuNPs. Among them, they identified CyNAMLA-381 NIR SERS reporter[56] molecule which has a 12-fold higher sensitivity than the current standard DTTC. Next, they applied CyNAMLA-381 as the SERS probe for *in vivo* cancer imaging by conjugating CyNAMLA-381–AuNPs to scFv anti-HER2 antibodies and that exhibits a very good SERS intensity and selectivity towards HER2-positive cancer cells under both Raman and dark-field microscopes. Later, Maiti *et. al.* developed a novel multiplex SERS partners using the combination of triphenylmethine and cyanine Raman reporters (B2LA and Cy3LA)[57]. Then, they derivatized nanotags (B2LA and Cy3LA) with anti- EGFR and anti-HER2 antibodies and demonstrated the specific recognition of their nanotags towards the respective cancer cells (e.g. OSCC and SKBR-3) with non-overlapping SERS peaks. Maiti *et al.* also developed another multiplexing partner (Cy7LA, Cy7.5LA and CyNAMLA-381)[58] and demonstrated their *in vivo* use capability using HER2 and EGFR recognizing antibody.
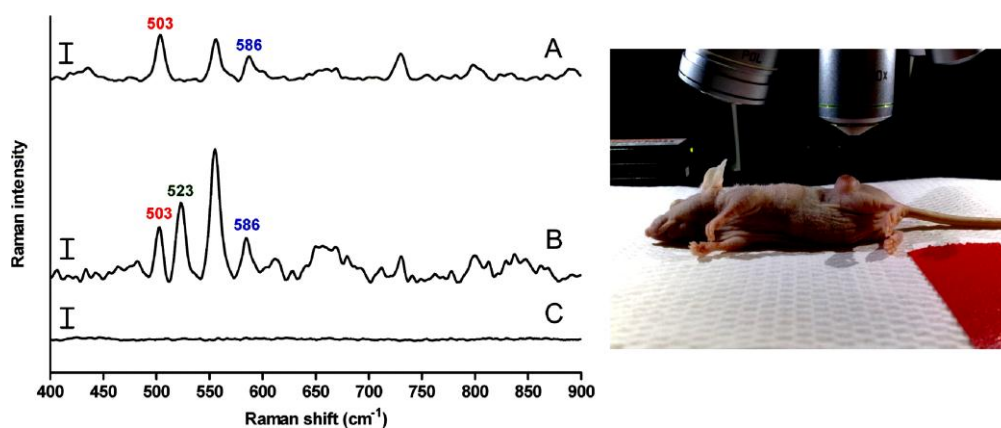
Figure 1.14 *In vivo* multiplex detection in xenograft tumor: SERS spectra from tumor site from EGFR positive nanotags. This picture has been taken from reference 58 under copyright permission.

1.7 Scope and Outline

It is quite obvious from the wide literature reports discussed in the earlier section that the progress of diversity oriented fluorescent library approach along with the high throughput screening lead to the novel bio-imaging probes/sensors discovery in a relatively faster manner. However, the case presented here, efficient solid phase chemistry needs to be devised to provide a robust synthetic route for generating a large number of fluorescent libraries in a short span of time. In this view, I aim to develop an elegant solid phase route to systemically apply in the synthesis of fluorescent libraries that cover wide emission color spectra from Vis to NIR. We aim to design the novel diversity oriented fluorescent libraries where each library contains single emission wavelength to develop both cell imaging and *in vivo* imaging probe. Single wavelength with different structural diversity may be useful as it allows easier structural activity relationships studies.

The aims of this thesis are:

1) Photostability is one of the key issues in NIR dyes and we previously reported a photostable CyNA library. To develop an ultra-photostable cyanine-based NIR fluorescence library, I designed and synthesized CyR library, utilizing the stability component of CyNA. Efficient solid phase chemistry was also devised to provide a robust synthetic route to the new NIR dye library.

2) To develop *in vivo* bioimaging probes, first, I derivatized CyR library with acetyl and chloroacetyl moiety to make CyRAC and CyRAC compounds respectively. Then, we screened these compounds against macrophage cells and found out an *in vivo* macrophage probe CyRCA-341 in mouse inflammation model.

3) To design multiplex partners using three different surface-enhanced Raman scattering (SERS) cyanine dyes (CyRLA-572, Cy7LA, and Cy7.5LA) for the multiplex detection of 3 different germ layers of differentiated mouse embryonic stem cells *in vitro*. To find out CyRLA as the novel cyanine based Raman active dye, I incorporated a thiol linker motif (lipoic acid) to chemisorb an 55-member CyRLA library on gold nanoparticles (AuNPs) and then screened the full library and selected the most responsive compounds.

4) To develop novel fluorescent small molecule probe for B-lymphocytes cell, cell-based screening was performed with the BDR library and its chlororacetyl (BDRAC) and actyl derivatives (BDRAC). Then, we found that the BDRCA-656 (CDg6) showed excellent B-cell staining selectivity over T-cell. Here, I synthesized BDR and its derivatives (BDRCA and BDRAC) using BODIPY as the core fluorescent scaffold and solid phase route as the synthetic technique.

5) To develop M phase probe, Rhodol scaffold based library, RDR and its chloroacetyl (RDRCA) and acetyl derivatives (RDRAC) were screened and found a mitotic phase staining compound RDR-567, as the primary hit. The solid phase synthetic methodology was adopted to diversify the Rhodol scaffold to generate RDR and its derivatives.

6) To develop a coumarin based library and to apply in bio-imaging, I synthesized COR library, using diversity oriented solid phase synthetic methodology. Then, I derivatized COR library with chloroacetyl and acetyl moiety to generate CORCA and CORAC library. In order to explore the photo physical properties of COR, CORCA and CORAC compounds, full spectral characterisation was also carried out.

1.8 References

1) W. Liu, *Ca-Cancer J. Clin.*, 1961, **11**, 55.

2) M. Chalfie, Y. Tu, G. Euskirchen, W. W. Ward and D. C. Prasher, *Science*, 1994, **263**, 802.

3) A. Miyawaki, A. Sawano and T. Kogure, *Nat. Cell. Biol.*, 2003, S1.

4) J. Lovric, S. J. Cho, F. M. Winnik and D. Maysinger, *Chem. Biol.*, 2005, **12**, 1227.

5) U. Resch-Genger, M. Grabolle, S. Cavaliere-Jaricot, R. Nitschke and T. Nann, *Nat .Methods*, 2008, **5**, 763.

6) L. D. Lavis and R. T. Raines, *Acs. Chem. Biol.*, 2008, **3**, 142.

7) R. Araki and I. Nashimoto, *Adv. Exp. Med. Biol.*, 1992, **316**, 155.

8) H. Ke, H. Wang, W. K. Wong, N. K. Mak, D. W. Kwong, K. L. Wong and H. L. Tam, *Chem. Commun.*, 2010, **46**, 6678.

9) J. Rao, A. Dragulescu-Andrasi and H. Yao, *Curr. Opin. Biotechnol.*, 2007, **18**, 17.

10) J. S. Lee, Y. K. Kim, M. Vendrell and Y. T. Chang, *Mol. Biosyst.*, 2009, **5**, 411.

11) W. R. J. D. Galloway, A. Isidro-Llobet and D. R. Spring, *Nat. Commun.*, 2010, **1**.

12) J. S. Lee, M. Vendrell and Y. T. Chang, *Curr. Opin. Chem. Biol.*, 2011, **15**, 760.

13) S. L. Wang, Y. K. Kim and Y. T. Chang, *J. Comb. Chem.*, 2008, **10**, 460.

14) G. R. Rosania, J. W. Lee, L. Ding, H. S. Yoon and Y. T. Chang, *J. Am. Chem. Soc.*, 2003, **125**, 1130.

15) S. L. Wang and Y. T. Chang, *Chem. Commun.*, 2008, 1173.

16) S. L. Wang and Y. T. Chang, *J. Am. Chem. Soc.*, 2006, **128**, 10380.

17) Y. H. Ahn, J. S. Lee and Y. T. Chang, *J. Am. Chem. Soc.*, 2007, **129**, 4510.

18) (a) J. S. Lee, N. Y. Kang, Y. K. Kim, A. Samanta, S. Feng, H. K. Kim, M. Vendrell, J. H. Park and Y. T. Chang, *J. Am. Chem. Soc.*, 2009, **131**, 10077.; (b) A. Samanta, M. Vendrell, M., R. Das and Y.T. Chang, *Chem. Commun.*, 2010, **46**, 7406.

19) R. B. Merrifield, *J. Am. Chem. Soc.*, 1963, **85**, 2149.

20) M. H. Caruthers, *Science*, 1985, **230**, 281.

21) J. Isacsson and G. Westman, *Tetrahedron Lett.*, 2001, **42**, 3207.

22) S. J. Mason, J. L. Hake, J. Nairne, W. J. Cummins and S. Balasubramanian, *J. Org. Chem.*, 2005, **70**, 2939.

23) J.Merrington, M. James and M. Bradley, *Chem. Commun.*, 2002, 140.

24) A. Song, J. Zhang and K. S. Lam, *J. Comb. Chem.*, 2004, **6**, 112.

25) X. Fei, S. Yang, B. Zhang, Z. Liu and Y. Gu, *J. Comb. Chem.*, 2007, **9**, 943.

26) S. Wang and Y. T. Chang, *J. Am. Chem. Soc.*, 2006, **128**, 10380.

27) Y. H. Ahn, J. S. Lee and Y. T. Chang, *J. Am. Chem. Soc.*, 2007, **129**, 4510.

28) A. Matsui, K. Umezawa, Y. Shindo, T. Fujii, D. Citterio, K. Oka and K. Suzuki, *Chem. Commun.*, 2011, **47**, 10407.

29) S. Atilgan, T. Ozdemir and E. U. Akkaya, *Org. Lett.*, 2008, **10**, 4065.

30) I. Leray, F. O'Reilly, J. L. H. Jiwan, J. P. Soumillion and B. Valeur, *Chem. Commun.*, 1999, 795.

31) M. Baruah, W. Qin, R. A. Vallee, D. Beljonne, T. Rohand, W. Dehaen and N. Boens, *Org. Lett.*, 2005, **7**, 4377.

32) Y. Gabe, Y. Urano, K. Kikuchi, H. Kojima and T. Nagano, *J. Am. Chem. Soc.*, 2004, **126**, 3357.

33) C. A. Combs and R. S. Balaban, *Biophys J*, 2001, **80**, 2018.

34) H. S. Jung, P. S. Kwon, J. W. Lee, J. I. Kim, C. S. Hong, J. W. Kim, S. H. Yan, J. Y. Lee, J. H. Lee, T. Joo and J. S. Kim, *J. Am. Chem. Soc.* **2009**, 131, 2008.

35) B. K. Wagner, H. A. Carrinski, Y. H. Ahn, Y. K. Kim, T. J. Gilbert, D. A. Fomina, S. L. Schreiber, Y. T. Chang and P. A. Clemons, *J. Am. Chem. Soc.*, 2008, **130**, 4208.

36) N. S. Finney, *Curr. Opin. Chem. Biol.*, 2006, **10**, 238.

37) S. W. Yun, C. Leong, D. Zhai, Y. L. Tan, L. Lim, X. Bi, J. J. Lee, H. J. Kim, N. Y. Kang, S. H. Ng, L. W. Stanton and Y. T. Chang, *Proc. Natl. Acad. Sci. U S A*, 2012, **109**, 10214.

38) Q. Li, J. K. Min, Y. H. Ahn, J. H. Namm, E. M. Kim, R. Lui, H. Y. Kim, Y. Ji, H. Z. Wu, T. Wisniewski and Y. T. Chang, *Chembiochem*, 2007, **8**, 1679.

39) Y. H. Ahn, J. S. Lee and Y. T. Chang, *J. Comb. Chem.*, 2008, **10**, 376.

40) S. C. Lee, N. Y. Kang, S. J. Park, S. W. Yun, Y. Chandran and Y. T. Chang, *Chem. Commun.*, 2012, **48**, 6681.

41) K. Jyothish, K. T. Arun and D. Ramaiah, *Org. Lett.* 2004, **6**, 3965.

42) K. Takagi, M. Kawabe, M. Matauoka and T. Kitao, *Dyes Pigm.* 1985, **6**, 177.

43) W. B. Tuemmler and B. S. Wildi, *J. Am. Chem. Soc.* 1958, **80**, 3772.

44) (a) J. Chen, I. R. Corbin, H. Li, W. Cao, J. D. Glickson and G. Zheng, *J. Am. Chem. Soc.* 2007, **129**, 5798.; (b) S. A. Hilderbrand and R. Weissleder, Curr. Opin. Chem. Biol.2010,**14**,71.

45) (a) J. O. Escobedo, O. Rusin, S. Lim and R. M. Strongin, *Curr. Opin. Chem. Biol.*, 2010, **14**, 64 (b) Y. Koide, Y. Urano, K. Hanaoka, W. Piao, M. Kusakabe, N. Saito, T. Terai, T. Okabe and T. Nagano, *J. Am. Chem. Soc.*, 2012, **134**, 5029.

46) (a) M. Bates, B. Huang, G. T. Dempsey and X. Zhuang, *Science* 2007, **317**, 1749.; b) M. Bates, B. Huang and X. Zhuang, *Curr. Opin. Chem. Biol.* 2008, **12**, 505.

47) C. S. Foote, *Science* 1968, **162**, 963.

48) A. Samanta, M. Vendrell, R. Das and Y. T. Chang, *Chem. Commun.*, 2010, **46**, 7406.

49) A. Samanta, M. Vendrell, S. W. Yun, Z. P. Guan, Q. H. Xu and Y. T. Chang, *Chem-Asian J.*, 2011, **6**, 1353.

50) S. Boca, D. Rugina, A. Pintea, L. Barbu-Tudoran and S. Astilean, *Nanotechnology*, 2011, **22**.

51) U. S. Dinish, F. C. Yaw, A. Agarwal and M. Olivo, *Biosens. Bioelectron.*, 2011, **26**, 1987.

52) G. Das, F. Mecarini, F. Gentile, F. De Angelis, H. G. M. Kumar, P. Candeloro, C. Liberale, G. Cuda and E. Di Fabrizio, *Biosens. Bioelectron.*, 2009, **24**, 1693.

53) R. Gessner, P. Rosch, R. Petry, M. Schmitt, M. A. Strehle, W. Kiefer and J. Popp, *Analyst*, 2004, **129**, 1193.

54) L. Sun, K. B. Sung, C. Dentinger, B. Lutz, L. Nguyen, J. W. Zhang, H. Y. Qin, M. Yamakawa, M. Q. Cao, Y. Lu, A. J. Chmura, J. Zhu, X. Su, A. A. Berlin, S. Chan and B. Knudsen, *Nano Lett.*, 2007, **7**, 351.

55) X. M. Qian, X. H. Peng, D. O. Ansari, Q. Yin-Goen, G. Z. Chen, D. M. Shin, L. Yang, A. N. Young, M. D. Wang and S. M. Nie, *Nat. Biotechnol.*, 2008, **26**, 83.

56) A. Samanta, K. K. Maiti, K. S. Soh, X. J. Liao, M. Vendrell, U. S. Dinish, S. W. Yun, R. Bhuvaneswari, H. Kim, S. Rautela, J. H. Chung, M. Olivo and Y. T. Chang, *Angew. Chem. Int. Edit.*, 2011, **50**, 6089.

57) K. K. Maiti, A. Samanta, M. Vendrell, K. S. Soh, M. Olivo and Y. T. Chang, *Chem. Commun.*, 2011, **47**, 3514.

58) K. K. Maiti, U. S. Dinish, A. Samanta, M. Vendrell, K. S. Soh, S. J. Park, M. Olivo and Y. T. Chang, *Nano Today*, 2012, **7**, 85.

Chapter 2

Solid Phase Synthesis of Ultra-Photostable Cyanine NIR dye library
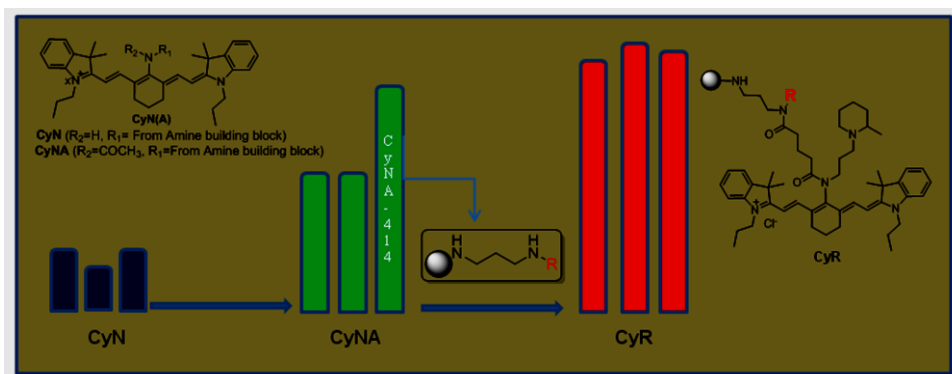
2.1 Introduction

Near-infrared (NIR) fluorescence (λ_{max}: 700-1000 nm) has recently received substantial attention in various chemical and biological studies[1,2]. The advantages of NIR fluorescence are the deep penetrating ability through tissue and the significant reduction of auto fluorescence which often come across in visible light emission. Therefore, NIR probes are extensively used in a broad range of biological research as in vivo imaging probe[3], proteins labelling agent[4] and fluorescence tag in DNA sequencing[5]. To date, a very limited scaffold such as squarine,[6] quinone[7], triphenylmethane[8] and cyanine[9] have been employed for organic NIR fluorophores. Among them, cyanine dyes[10] have attracted the most attention, due to their synthetic accessibility, broad wavelength tunability, and large molar extinction coefficient with moderate fluorescence quantum yields. However, the photostabilty of the dyes diminishes significantly along with the increase of the Π-conjugation system. Especially, the photodegradation is a serious problem for the NIR cyanine dyes having absorbance λ_{max} longer than 700 nm[11]. To overcome this limitation, our group has recently developed a photostable NIR cyanine dye library CyNA in which amine group of CyN was acetylated and thus the photoactivating lone pair electron was removed[12]. As a result, CyNA was much more stable than CyN in general, and CyNA-414 was selected as the most photostable dye among CyNA library (discussed in previous chapter).

2.2 Objectives

While a derivative of CyNA-414 was proved to be superior to currently available commercial NIR dye in *in vivo* mouse imaging[13], to further improve the photostability, I aimed to design a new library utilizing CyNA-

414 structure as the key component. Here, I aimed to synthesize the ultra-photostable cyanine library using highly efficient and clean solid phase chemistry. The previous CyNA library was synthesized by solution phase chemistry and the laborious purification step was unavoidable. Inspired by an efficient solid phase chemistry reported for cyanine dyes[14], I designed a new solid phase route to secure pure NIR cyanine dyes library (CyR) in high speed manners by minimizing crucial purification step.

2.3 Results and discussion

2.3.1 Library design, characterization and photostability studies

In order to synthesize CyR library (**Scheme 2.1**), firstly, 3-bromopropylamine was loaded to the 2-chlorotrityl resin quite efficiently, and then, a broad range of structural diversity was introduced by a series of primary amines (**Chart 2.1**). Here, the nucleophilic displacement of bromide occurred in N-methyl-2-pyrrolidone (NMP) solvent under moderate heating condition, was carried out with primary amines to lead structurally diversified solid supported secondary amines. The key intermediate **1** (CyNA-414 derivative)[13] was coupled to this solid phase amine building blocks (**scheme 2.1**) by using standard acid-amine coupling protocol[15]. The final step of acidic cleavage from the solid supported compounds **2** yielded highly pure 80-members of CyR library (average purity is 94% without further purification at 365 nm, **Table 2.2**). It is noteworthy that the current synthetic protocol provides a linker motif with amino group incorporated in cyanine scaffold in addition to the structural diversity. The amino linker will be useful for further derivatization of the library compounds with various reporter or affinity tags for bio-conjugation depending on the biological study requirements.

Scheme 2.1 Synthesis of CyR library
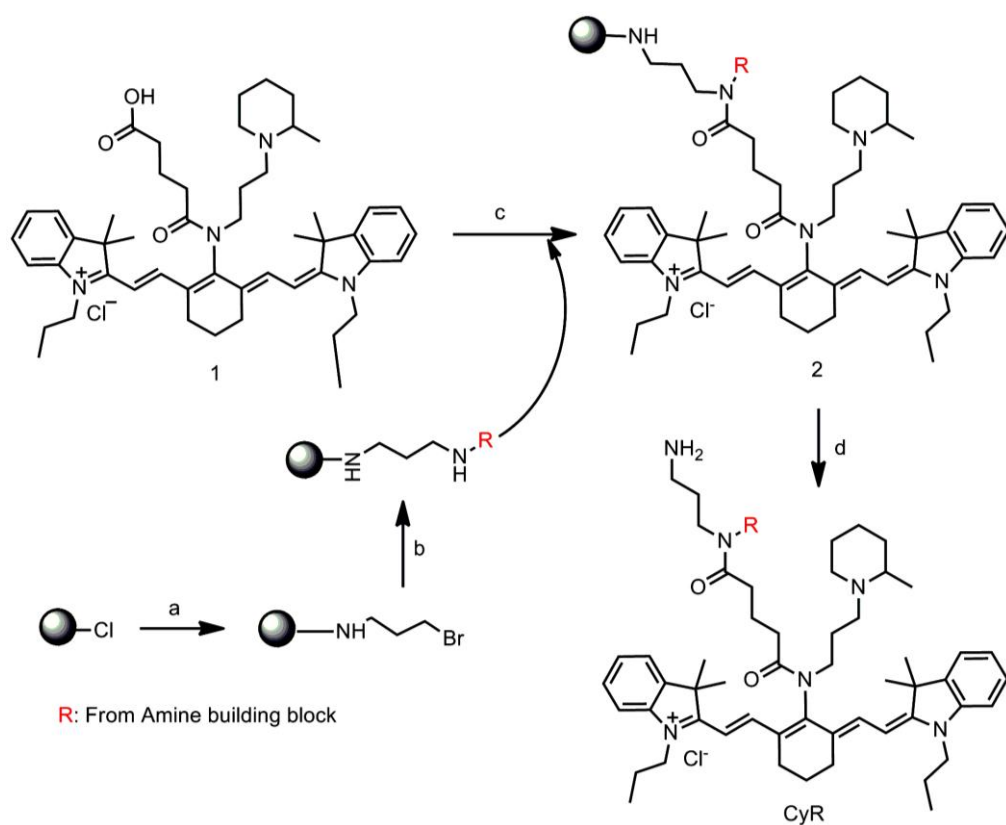
R: From Amine building block

Reagents and conditions: (a) DIEA, THF, 3-bromopropylamine, r.t., 12 h.; (b) DIEA, RNH$_2$, NMP, 70 ^{o}C, 12 h.; (c) HATU, DIEA, r.t. 24 h.; (d) 2% TFA in DCM , r.t., 10 min.

Chart 2.1 Amine building blocks for **CyR** library
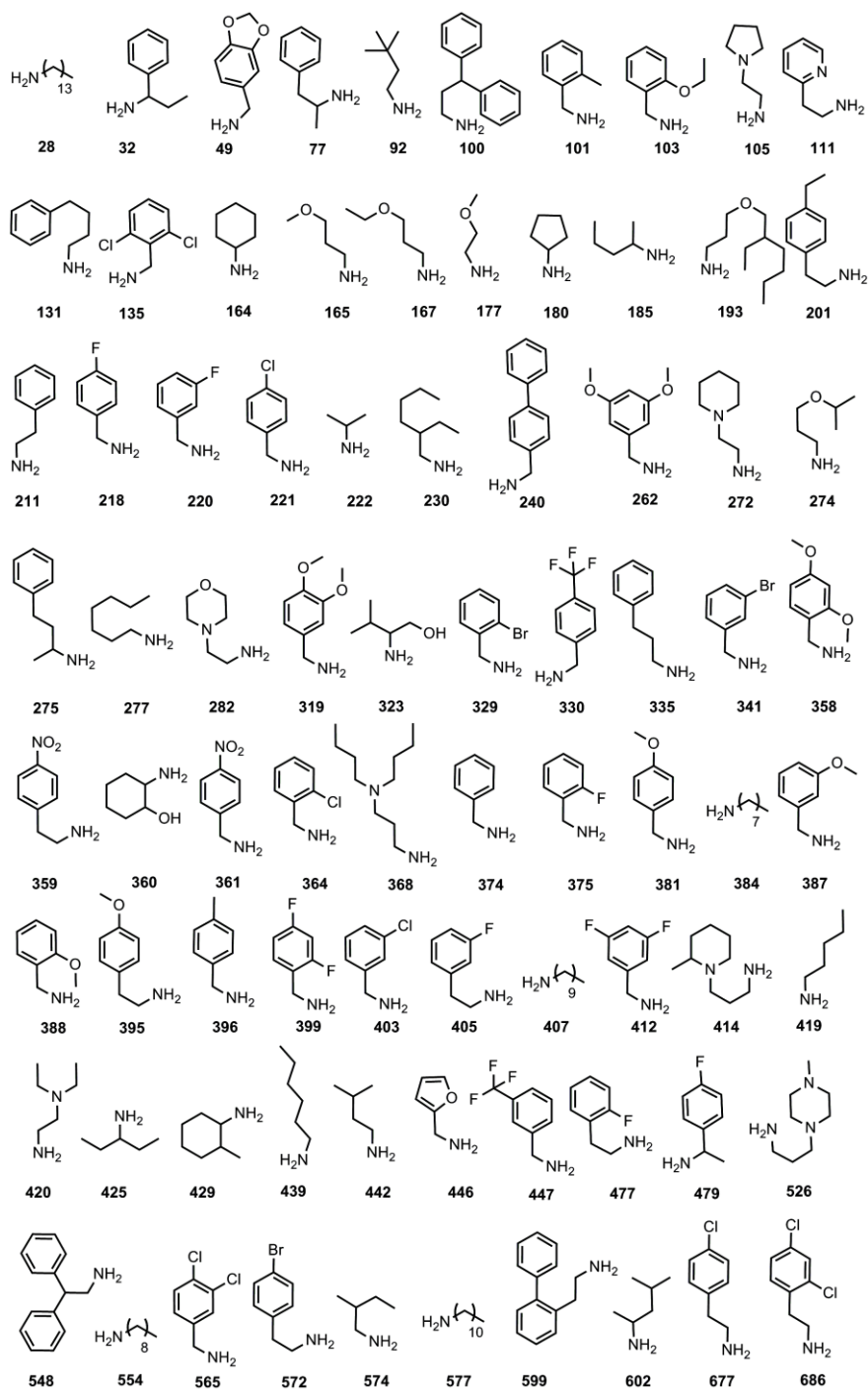
Table 2.1 Characterization and purity determination by HPLC-MS, photophysical properties and preliminary photostability assessment of CyR library compounds and CyNA-414 by using the SpectraMax M2 spectrophotometer under the xenon lamp

Compound	M^+(calc.)	M^+(found)	λ_{abs}(nm)	λ_{em}(nm)	ϕ*[1]	Purity*[2]	F/F_o*[3]
CyR 28	1025.8	1025.9	807	824	0.12	93	98
CyR 32	947.6	947.6	806	822	0.11	92	89
CyR 49	963.6	963.6	807	823	0.13	93	91
CyR 77	947.6	947.7	806	824	0.10	96	90
CyR 92	913.7	913.6	807	823	0.08	93	86
CyR 100	1023.7	1023.6	807	823	0.12	92	92
CyR 101	933.6	933.7	807	825	0.10	97	90
CyR 103	963.6	963.7	807	822	0.10	95	93
CyR 105	926.7	926.6	807	822	0.12	95	94
CyR 111	934.6	935.6	807	823	0.10	92	92
CyR 131	961.7	961.8	807	822	0.16	95	91
CyR 135	987.5	987.5	806	822	0.08	91	89
CyR 164	911.6	911.8	806	824	0.10	91	92
CyR 165	901.6	901.6	807	822	0.10	93	94
CyR 167	915.6	915.6	807	824	0.11	92	100
CyR 177	887.6	887.6	806	823	0.10	92	93
CyR 180	897.6	897.6	807	822	0.12	92	98
CyR 185	899.6	899.6	807	824	0.10	91	96
CyR 193	999.7	999.7	806	823	0.12	93	100
CyR 201	961.7	961.7	807	822	0.09	90	93
CyR 211	933.6	933.6	807	823	0.14	91	89
CyR 218	937.6	937.6	807	822	0.13	92	82
CyR 220	937.6	937.7	806	823	0.09	92	97
CyR 221	953.6	953.6	807	822	0.12	93	91
CyR 222	871.6	871.7	807	824	0.10	95	97
CyR 230	941.7	941.7	807	823	0.10	91	96
CyR 240	995.5	995.6	806	822	0.11	88	93

CyR 262	979.6	979.6	806	823	0.10	91	93
CyR 272	940.7	940.6	806	822	0.11	91	95
CyR 274	929.7	929.6	806	821	0.10	96	91
CyR 275	961.7	961.6	807	822	0.08	91	88
CyR 277	927.7	927.7	806	823	0.10	92	95
CyR 282	942.7	942.7	807	822	0.10	90	91
CyR 319	979.6	979.7	806	822	0.08	91	95
CyR 323	915.6	915.6	806	821	0.14	90	94
CyR 329	997.57	997.6	806	822	0.11	91	100
CyR 330	988.3	988.6	806	823	0.10	96	91
CyR 335	947.6	947.7	806	821	0.08	94	92
CyR 341	997.5	997.7	806	821	0.11	94	100
CyR 358	979.6	979.7	806	822	0.10	94	95
CyR 359	978.6	978.5	807	823	0.10	94	94
CyR 360	941.7	941.7	806	822	0.11	94	94
CyR 361	964.6	964.5	807	822	0.13	95	90
CyR 364	953.6	953.5	807	822	0.11	93	93
CyR 368	998.7	998.7	807	822	0.13	95	91
CyR 374	919.6	919.6	807	822	0.11	96	97
CyR 375	937.6	937.6	807	823	0.09	94	94
CyR 381	949.6	949.7	807	825	0.10	89	95
CyR 384	941.7	941.7	807	822	0.13	96	100
CyR 387	949.6	949.7	807	823	0.10	91	98
CyR 388	949.6	949.7	806	823	0.12	92	89
CyR 395	963.6	963.7	806	823	0.10	90	100
CyR 396	933.6	997.8	807	822	0.10	98	100
CyR 399	955.6	955.7	806	822	0.11	91	80
CyR 403	953.6	953.6	807	823	0.11	93	100
CyR 405	951.6	951.6	807	822	0.12	91	100
CyR 407	969.7	969.7	806	821	0.10	92	100
CyR 412	955.6	955.6	806	824	0.11	96	86
CyR 414	968.7	968.6	807	823	0.12	94	94
CyR 419	899.6	899.6	807	823	0.10	93	100
CyR 420	928.7	928.6	806	823	0.13	95	100

CyR 425	899.6	899.7	806	824	0.09	94	94
CyR 429	925.7	925.6	807	824	0.10	93	96
CyR 439	913.7	913.6	807	823	0.12	94	94
CyR 442	899.6	899.6	806	823	0.11	94	91
CyR 446	909.6	909.7	806	821	0.12	93	92
CyR 447	987.6	987.6	806	822	0.10	93	100
CyR 477	951.6	951.5	806	823	0.10	91	91
CyR 479	951.6	951.7	807	820	0.10	93	95
CyR 526	969.7	969.7	807	824	0.12	92	100
CyR 548	1009.7	1009.8	807	823	0.12	91	100
CyR 554	955.7	955.6	807	822	0.12	92	92
CyR 565	989.2	989.6	807	823	0.12	92	93
CyR 572	933.6	1013.5	807	822	0.11	96	100
CyR 574	899.6	899.7	806	822	0.10	92	100
CyR 577	997.8	933.7	807	822	0.13	93	92
CyR 599	1009.7	1009.7	807	823	0.12	89	90
CyR 602	913.7	913.6	806	822	0.11	93	93
CyR 677	967.6	967.6	806	824	0.10	91	100
CyR 686	1001.6	1001.6	807	822	0.11	92	94
CyNA-4144	701.5	701.2	804	819	0.10	96	100

[*1] Quantum yields were measured in DMSO, using Cardiogreen as a standard (φ:0.13, in DMSO).[16] [*3] Quotients of fluorescent intensities after 8 h vs. fluorescent intensities (after 0 h), in a time-course fluorescence measurement using 10 μM (1% DMSO) solutions in HEPES buffer (10 mM, pH 7.4). [*2] Purities were determined according to UV absorption at 365 nm. [*4] CyNA-414 was used as the standard for the photostability evaluation.

2.3.2 Spectral properties of CyR library

These compounds show the maximum absorption wavelengths around 800 nm and emission around 820 nm with an average quantum yield 0.1 (**Table 2.1**).
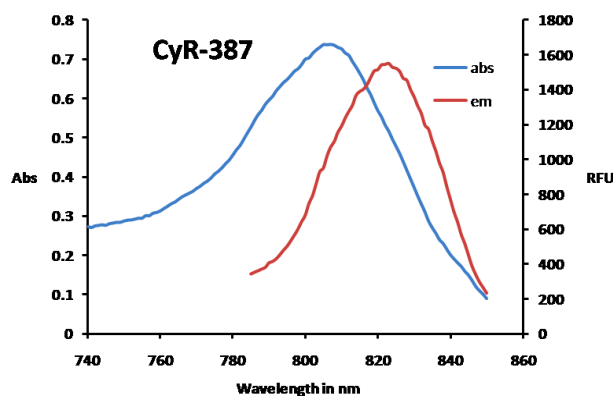
Figure 2.1 Absorption and Emission spectra of a representative CyR library compounds

2.3.3 Photostability evaluation

To evaluate the photostability of CyR in comparison with CyNA and CyN, I examined the decrease of fluorescence intensity of the compounds under xenon lamp ($6W/cm^2$) for 8 h. The average fluorescence intensity decreases of CyNA and CyN compounds[12] were around 17% and 70% respectively, whereas newly synthesized CyR library shows only 5% decrease by average (**Table 2.1**) reflecting the superior photostability in general. To differentiate the relative photostability among CyR compounds, we introduced a stronger light condition (UV Blak-Ray® B-100AP high intensity mercury lamp, 100W, 365 nm) to the whole CyR compounds and monitored the relative fluorescence intensity (F/F_0) at 1 h and 2 h respectively (**Table 2.2**). Three most stable CyR compounds (CyR 167, CyR 387, CyR 526) were selected and further compared with representative CyN and CyNA compounds including CyNA-414 (structures available in **Table 2.3**, **2.4**, **2.5**) and the results are summarized in **figure 2.1** It clearly shows that the three selected CyR compounds exhibit much better photostability compared to CyN and CyNA, even the previous best compound CyNA-414.

34

Table 2.2 Photostability evaluation of **CyR** library compounds and **CyNA-414** by using the UVP Blak-Ray® B-100AP high intensity mercury lamp

Compound	F/F_o*5	F/F_o*6
CyR 28	44	34
CyR 32	55	43
CyR 49	48	37
CyR 77	44	39
CyR 92	50	40
CyR 100	56	48
CyR 101	46	44
CyR 103	52	39
CyR 105	62	53
CyR 111	51	41
CyR 131	43	36
CyR 135	54	42
CyR 164	58	45
CyR 165	60	47
CyR 167	67	63($)
CyR 177	59	50
CyR 180	48	40
CyR 185	55	43
CyR 193	43	36
CyR 201	57	48
CyR 211	62	55
CyR 218	51	39
CyR 220	49	46
CyR 221	41	37
CyR 222	43	34
CyR 230	63	52
CyR 240	48	33
CyR 262	43	32
CyR 272	47	37
CyR 274	48	42

CyR 275	43	35
CyR 277	45	38
CyR 282	48	43
CyR 319	42	36
CyR 323	61	58
CyR 329	51	40
CyR 330	44	39
CyR 335	51	37
CyR 341	59	50
CyR 358	45	40
CyR 359	45	38
CyR 360	57	39
CyR 361	45	37
CyR 364	56	47
CyR 368	51	40
CyR 374	62	57
CyR 375	58	49
CyR 381	45	39
CyR 384	52	46
CyR 387	70	68($)
CyR 388	43	39
CyR 395	62	50
CyR 396	37	35
CyR 399	49	41
CyR 403	48	39
CyR 405	45	36
CyR 407	47	37
CyR 412	47	36
CyR 414	49	39
CyR 419	42	36
CyR 420	48	34
CyR 425	61	57
CyR 429	47	38

CyR 439	48	39
CyR 442	45	38
CyR 446	55	49
CyR 447	41	32
CyR 477	48	38
CyR 479	49	41
CyR 526	69	60 ($)
CyR 548	62	60
CyR 554	48	38
CyR 565	57	44
CyR 572	61	54
CyR 574	48	46
CyR 577	44	35
CyR 599	49	38
CyR 602	53	40
CyR 677	48	43
CyR 686	51	36
CyNA-414	51	47

($) Best selected three compounds

*[5] Quotients of fluorescent intensities after 1 h vs. fluorescent intensities (after 0 h), in a time-course fluorescence measurement under the strong Hg-lamp (high intensity UV radiation) using 10 μM (1% DMSO) solutions in HEPES buffer (10 mM, pH 7.4). *[6] Quotients of fluorescent intensities after 2 h vs. fluorescent intensities (after 0 h), in a time-course fluorescence measurement under the strong Hg-lamp (high intensity UV radiation) using 10 μM (1% DMSO) solutions in HEPES buffer (10 mM, pH 7.4).

2.3.4 Photostability comparison of best selected compounds
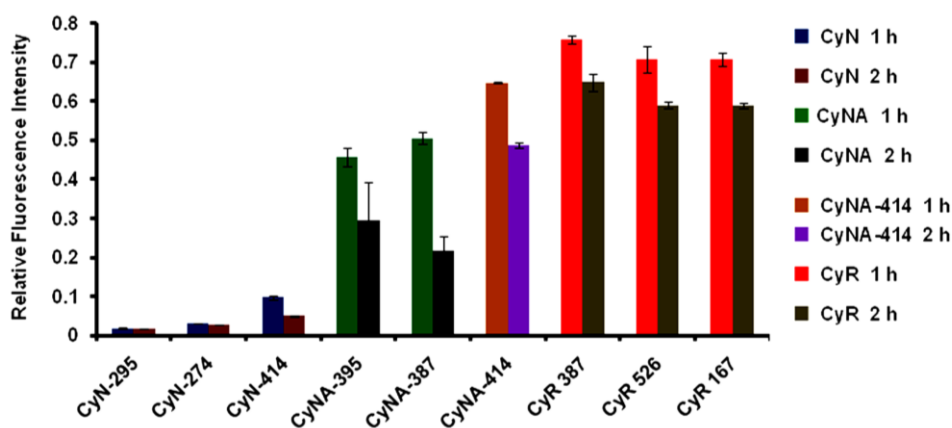
Figure 2.2 Photostability assessments under strong UV irradiation in each 10 min interval for 2 h of CyN, CyNA (including CyNA-414) and 3 selected CyR compounds. 1% DMSO in 10 mM HEPES buffer (pH 7.4) was used to dissolve the compounds at final concentration 10 μM. The bar graphs exhibit mean fluorescence intensity after 1 h and 2 h. Values are means ± s.d acquired from three experiments.

Table 2.3 Structures of best selected photostable CyR compounds compared with **CyNA-414** under high intensity UV radiation
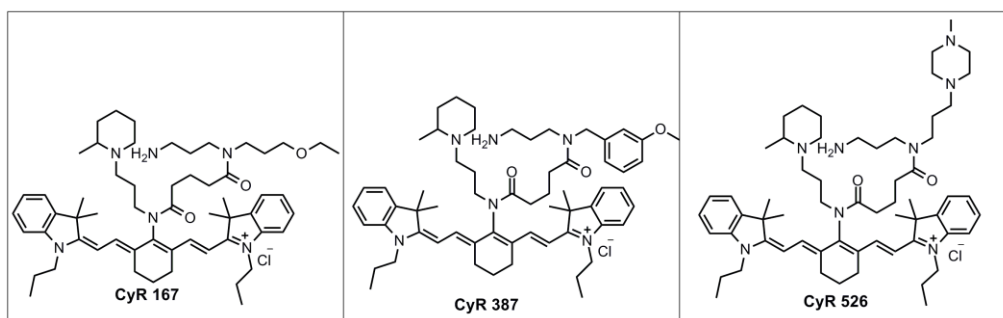
Table 2.4 structures of the CyNA compounds used in high intensity UV condition

CyNA-387   CyNA-395   CyNA-414
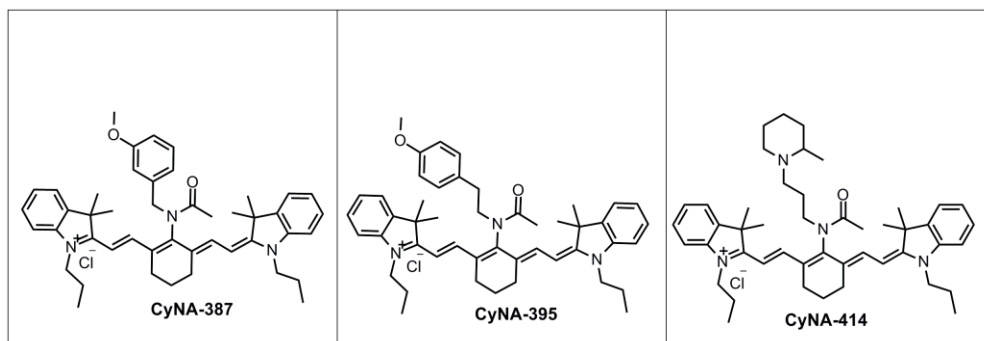
Table 2.5 Structure of CyN used in high intensity UV condition

CyN-274   CyN-295   CyN-414
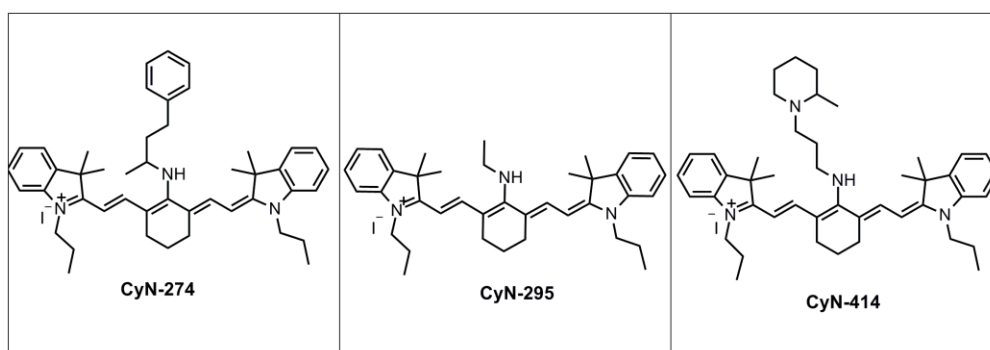
2.3.5 Kinetic analysis

A further detailed kinetic analysis was performed for the three CyR dyes in comparison with CyNA-414 and the kinetic constant was measured (**Table 2.6, Figure 2.3**) showing the superior photostability of new CyR compounds to CyNA-414.

Table 2.6 Decomposition rate constants of three selected compounds

Compound	$k(s^{-1})$
CyNA-414	11.16×10^{-5}
CyR 167	8.16×10^{-5}
CyR 387	7.00×10^{-5}
CyR 526	8.33×10^{-5}

2.3.6 Detailed photodecomposition Study

Here for the photodecomposition study, 10 µM CyR 526, CyR 387, CyR 167 and CyNA-414 solutions in 10 mM HEPES buffer (pH 7.4) containing 1% DMSO were placed in a 96-well black plate under the strong UV light, and fluorescence intensity measurements were performed every 10 min for a total period of 2 h (excitation-emission: 790-820 nm).Values are fitted to a non-linear regression one-phase exponential decay (**Figure 2.3**). Rate constants of dye photodecomposition were acquired from the plots of -ln(F/F$_0$) vs. time, considering $-\ln(F/F_0) = k*t$ as a pseudo-first order rate equation[17].
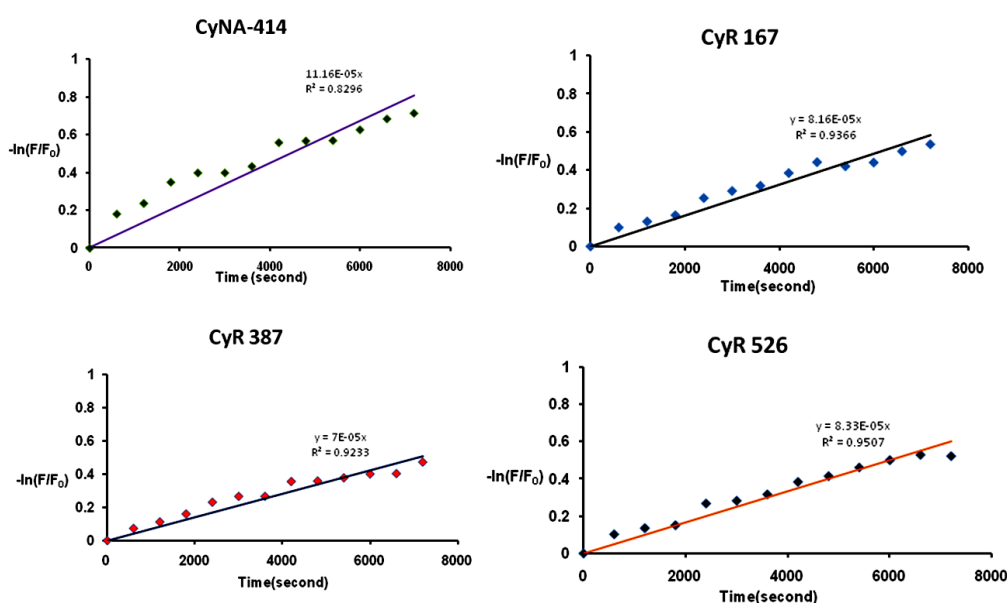
Figure 2.3 Photodecomposition of CyR 167, CyR 387, CyR 526 and CyNA-414

2.4 Conclusions

Photostability is one of the key issues in NIR dyes and we have previously reported photostable CyNA library. Here, we successfully designed

and developed an ultra-photostable cyanine-based NIR fluorescence library, CyR, utilizing the stability component of CyNA. Photostability evaluation reveals that the CyR library, in general, consists of the better photostable compounds compared to previous reported CyNA compounds. Moreover, three selected CyR compounds exhibit much better photostability compared to the previous best compound CyNA-414. The reported synthetic procedure is quite straightforward and practical to be applied to much bigger library construction with almost no purification step required. Therefore, the CyR library and derivatives might be an extremely useful tool box to develop novel *in vivo* bioimaging probes.

2.5 Experimental methods

Materials and Methods

Amine building block and all other chemicals and solvents for the synthesis were purchased from the Alfa Aesar, Fluka, Acros, MERCK, and Sigma Aldrich and were used without any purification. Merck Silica Gel 60 (particle size: 0.04-0.063 mm, 230-400 mesh) was used for the normal phase column chromatographic purification. From BeadTech Inc., Korea, 2-chlorotrityl alcohol resin (1.37 mmol/g) was purchased. All the, CyN, CyNA derivatives which were previously synthesized by our group were used for the comparative photostability study with CyR derivatives. For analytical characterization of CyR compounds HPLC-MS (Agilent-1200 series) with a DAD detector and a single quadrupole mass spectrometer (6130 series) with an ESI probe was routinely used. Analytical process, except specified: eluents: A: H_2O (0.1% HCOOH), B: ACN (0.1% HCOOH), gradient from 0 to 100% B in 4 min; C_{18} (2) Luna column (4.6 x 50mm^2, 5 μm particle size) was used.

^{1}H-NMR and ^{13}C-NMR spectra were recorded on both Bruker Avance 300 MHz and 500 MHz NMR spectrometer, and chemical shifts are expressed in parts per million (ppm) and approximate coupling constants were calculated in Hz. Quantum yields and all other photophysical properties, photostability evaluation study of CyN, CyR and CyNA derivatives were performed in SpectraMax M2 spectrophotometer (Molecular Devices) instrument and the obtained data were analyzed using the Microsoft Office Excel 2007. In order to employ the strong UV irradiation to the compounds of interest, UVP Blak-Ray® B-100AP high intensity mercury lamp (100W, 365 nm) at 2 cm distance was used.

2.5.1 Synthesis and characeterization of cyanine derivatives

For the synthesis of compound **IR-780 iodide**, we followed the reported procedure[3].
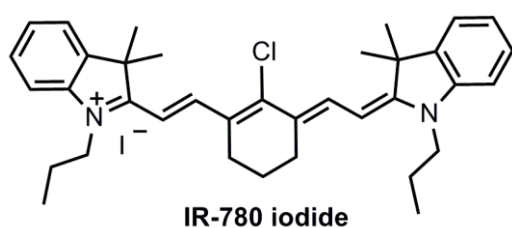
IR-780 iodide

Synthesis of CyN-414

CyN-414
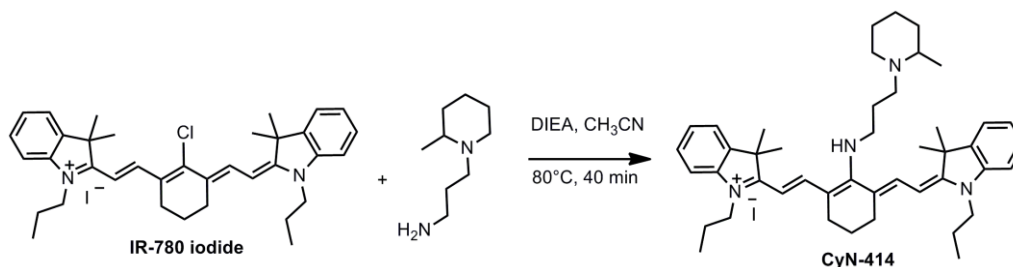
IR-780 iodide (600 mg, 0.9 mmol, 1 eq.) and 1-(3-aminopropyl)-2-pipecoline (340 mg, 1.8 mmol, 2 eq.) were dissolved in ACN (2 mL), and N,N-diisopropylethylamine (DIEA) (174 μL, 1.34 mmol, 1.5 eq.) was added.

The reaction mixture was heated to 80 °C for 40 min, and the resulting blue color crude CyN-414 was neutralized with 0.1 N HCl (aq.) and concentrated under vacuum. The crude product obtained was directly used for the next step synthesis of **1**.

Synthesis of 1
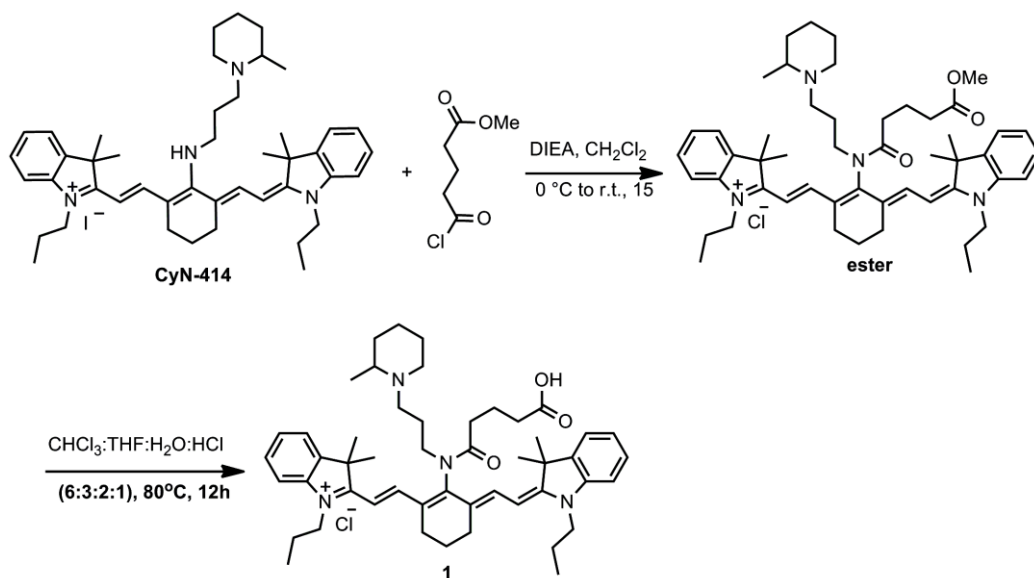
The crude compound CyN-414 was dissolved in DCM under N_2 atmosphere, and treated with excess DIEA (1.4 mL, 10.8 mmol, 12 eq.) and methyl 4-(chloroformyl)butyrate (220 μL, 1.34 mmol, 1.5 eq.) at 0 °C for 15 min. The resulting green product (ester) was washed with 0.1 (N) HCl and brine, concentrated under vacuum. The obtained crude product (ester) was directly employed for next step synthesis.

The crude product (ester) was dissolved in solvent mixture of $CHCl_3$:THF:H_2O:HCl(conc) (6:3:2:1)(v/v/v/v) (90 mL). The resulting mixture was stirred at 0° C. After 5 min., the reaction mixture was refluxed at 80 °C for 12 h, and monitored by LC-MS. After complete hydrolysis of the methyl ester, $CHCl_3$ was added to the reaction mixture, and the organic layer was collected (3 x 40 mL), washed with water and purified by a normal-phase

silica column using DCM-MeOH (ranging from 100:0 to 88:12) as the eluting solvent.

Characterization data for 1 (140 mg, 20% from IR-780 iodide)

Characterization of Compound 1

^{1}H-NMR (300 MHz, CDCl$_3$): δ 1.06 (t, 6H, J=7.5Hz), 1.24 (d, 3H, J=6.6 Hz), 1.39 (m, 2H), 1.61 (s, 6H), 1.62 (s, 6H), 1.79-1.95 (m, 6H), 2.22 (t, 2H, J=7.8 Hz), 2.33 (t, 2H, J=6.6 Hz), 2.52-2.56 (m, 4H), 2.82 (t, 2H, J=5.4 Hz), 2.87 (t, 2H, J=5.4 Hz), 2.96-2.98 (m, 2H), 3.09-3.12 (m, 1H), 3.36 (t, 4H), 3.53 (t, 2H, J=6.6 Hz), 3.67 (t, 2H, J=6.6 Hz), 4.06 (t, 2H, J=4.2 Hz), 4.15 (t, 2H, J=4.8 Hz), 6.15 (d, 1H, J=14.1Hz), 6.20 (d, 1H, J=14.1Hz), 7.07-7.38 (m,8H), 7.51 (d, 1H, J=14.1Hz), 7.60 (d, 1H, J=14.1Hz). ^{13}C-NMR (75 MHz, CDCl$_3$): δ 106.2, 110.6, 110.8, 114.9, 118.8, 122.3, 125.5, 125.6, 127.7, 128.1, 128.6, 140.6, 140.9, 141.4, 142.1, 142.2, 144.6, 153.9, 160.9, 161.4, 171.7, 172.5, 173.6, 174.3, 101.5, 101.9, 102.4, 11.6, 12.2, 19.5, 20.4, 20.6, 20.7, 22.2, 22.9, 24.8, 28.1, 28.2, 28.3, 31.3, 32.3, 41.9, 43.9, 48.3, 49.1, 49.3, 50.2, 51.8, 53.7, 60.4,

ESI (HRMS) m/z (C$_{50}$H$_{69}$N$_4$O$_3{}^+$), calc: 773.5364; found: 773.5351.

Synthesis of CyNA-414

The **CyNA-414** was synthesized according to the reported procedure.[12]

Preparation of 2-chlorotrityl chloride from 2-chlorotrityl alcohol resin

Thionyl chloride (1.2 mL, 16.48 mmol, 3 eq) was added to 2-Chlorotrityl alcohol resin (4g, 1.37mmol/g, 5.48 mmol, 1 eq) suspended in 40 mL of anhydrous DCM. Then the solution mixture was shaken for overnight at room temperature. Then the resin was filtered and washed thoroughly with

DMF (3X 40 mL) followed by DCM (3X40 mL) and then the resin was dried in vacuum.

General procedure for loading of solid supported 3-bromopropylamine

(3.5 g, 15.75 mmol, 5 eq) 3-bromopropylamine was dissolved in THF (5 mL/g) and then (6 mL, 32.5 mmol, 10 eq) DIEA was added to the solution. The resulting solution was then added to 2-chlorotrityl chloride resin (2.5 g, 3.25 mmol, 1 eq, 1.3 mmol/g) suspended in dichloromethane (10 mL/g). After stirring for 12 h, the resin was filtered through 10 mL cartridge and washed with DMF (5X 40 mL), methanol (5X 40 mL), and dichloromethane (10X 40 mL). The resin was then shaken with 20% MeOH in DMF for 2 h for the capping of excess 2-chlorotrityl chloride resin. The resin obtained was again washed with DMF (5X 40 mL), methanol (5X 40 mL), and dichloromethane (5X 40 mL) and then was dried using high vacuum.

General procedure for synthesis of solid supported secondary amines

For each reaction, resin (solid supported 3-bromopropylamine) (100 mg, 0.1 mmol, 1 eq, 1 mmol/g) was suspended in 2 mL of N-Methylpyrrolidone (NMP) in a 20 mL of glass vial. 7 eq of each amine (0.7 mmol) and 14 eq of DIEA (1.4 mmol) were then added in 2 ml of the same solvent The reaction mixture was shaken for overnight at 70 °C temperature in the heat block and the resin was filtered through 10 mL cartridge and washed with DMF (5X 5 mL), methanol (5X 5mL), and dichloromethane (5X 5mL). The solid supported secondary amine resins obtained, were dried and used for next step reactions.

General procedure for synthesis of CyR library

To synthesize **CyR** library, each of (solid supported secondary amine) resin (50 mg, 0.035 mmol, 1eq, 0.7 mmol/g) was suspended in 3 mL of DMF in a 10 mL syringe then (28 mg, 0.07 mmol, 1 eq) **1** (30 mg, 0.77 mmol, 2.2 eq),2-(7-Aza-1H-benzotriazole-1-yl)-1,1,3,3-tetramethyluronium hexafluorophosphate (HATU) and (30 μL, 0.168 mmol, 4.8 eq) DIEA were added. At a time 40 individual reaction mixtures were placed on orbital shaker for 24 h at room temperature and after complete the reaction the resin was filtered through 10 mL cartridge washed with DMF (5X 5mL), methanol (5X 5mL), and dichloromethane (5X 5mL). The resin was dried under high vacuum to afford solid supported compounds resin **2** and then the subsequently the dried resin of 50 mg was treated with 2% TFA in dichloromethane (5 mL) for 10 min. The solution was drained to the 20 mL vial and then organic layer was washed with the saturated NaHCO$_3$ solution, and then the organic layer was separated and dried using Speed Vacuum to afford the CyR library products. Each of CyR compound was solid and primarily characterized by LC-MS. The representative products are characterized by LC-MS, HR-MS, ^{1}H-NMR, ^{13}CNMR.

Representative CyR compounds characterization

CyR 167 (14 mg, 60%)
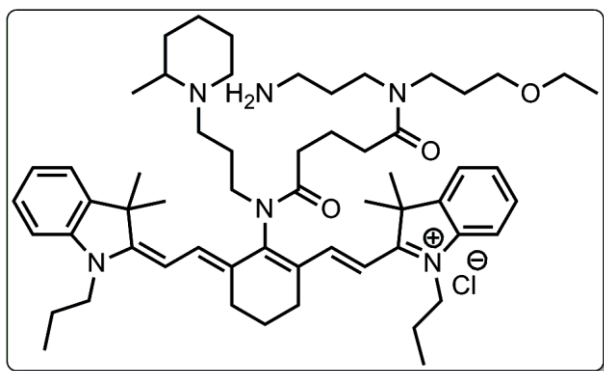
¹H-NMR (500 MHz, CDCl$_3$): δ 1.03-1.64 (m, 18H), 1.61 (s, 6H), 1.64 (s, 6H), 1.70-1.89 (m, 6H), 2.05 (m, 2H), 2.19-2.34 (m, 5H), 2.62-2.87 (m, 11H), 3.38-3.60 (m, 4H), 3.67 (m, 2H), 3.69 (s, 3H), 3.8 (s, 2H), 3.99-4.06 (m, 6H), 6.15 (d, 1H, *J*=13.85 Hz), 6.17 (d, 1H, *J*=13.85 Hz), 6.6-6.89 (m, 4H), 7.07-7.37 (m, 8H), 7.54 (d, 1H, *J*=13.85 Hz), 7.57 (d, 1H, *J*=13.85). ¹³C-NMR (75 MHz, CDCl$_3$): δ 11.60, 14.09, 15.02, 15.11, 20.41, 20.76, 22.66, 23.53, 24.74, 25.08, 27.70, 27.75, 27.77, 28.02, 28.70, 29.67, 31.93, 32.21, 36.87, 41.34, 44.80, 45.93, 48.61, 49.22, 49.26, 49.30, 66.11, 66.14, 66.84, 67.87, 101.76, 101.96, 110.48, 110.54, 115.64, 117.97, 122.67, 125.49, 125.58, 127.89, 128.52, 128.59, 140.87, 141.11, 141.23, 141.31, 141.94, 142.05, 142.09, 153.36, 153.39, 161.76, 162.03, 172.38, 172.63, 173.90, 175.16

ESI (HRMS) m/z (C$_{58}$H$_{87}$N$_6$O$_3^+$) calc: 915.6834; found: 915.6864.

CyR 387 (12 mg, 52%)
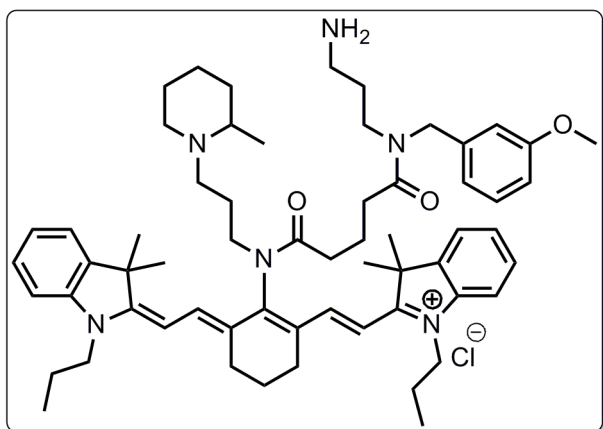
^{1}H-NMR (500 MHz, CDCl$_3$): δ 1.04-1.59 (m, 12H), 1.65 (s, 6H), 1.66 (s, 6H), 1.71-2.06 (m, 20H), 2.25-2.39 (m, 6H), 2.57-2.77 (m, 6H), 2.90-3.0 (m, 2H), 3.30-3.46 (m, 11H), 3.67 (m, 2H), 4.01 (m, 4H), 6.14 (d, 1H, *J*=13.9 Hz), 6.13 (d, 1H, *J*=13.85 Hz), 7.07-7.44 (m, 8H), 7.52 (d, 1H, *J*=13.85 Hz), 7.54 (d, 1H, *J*=13.25 Hz). ^{13}C-NMR (75 MHz, CDCl$_3$): δ 11.51, 11.56, 20.58, 20.78, 21.02, 24.76, 28.03, 28.11, 28.13, 32.32, 32.64, 37.57, 42.33, 44.63, 44.98, 45.93, 47.97, 49.09, 49.13, 49.20, 49.26, 50.44, 50.77, 51.46, 55.09, 55.17, 56.59, 59.79, 101.66, 101.91, 110.64, 110.74, 110.82, 11.94, 112.60, 112.79, 113.39, 114.47. 118.08, 118.26, 120.07, 121.38, 122.26, 122.45, 125.27, 125.36, 125.42, 125.51, 128.31, 128.66, 129.89, 138.07, 141.00, 141.25, 141.53, 142.22, 142.25, 150.30, 160.04, 161.69, 171.96, 172.16, 173.21, 174.38

ESI (HRMS) m/z (C$_{61}$H$_{85}$N$_6$O$_3^+$) calc: 949.6678; found: 915.6671.

CyR 526 (17 mg, 55%)
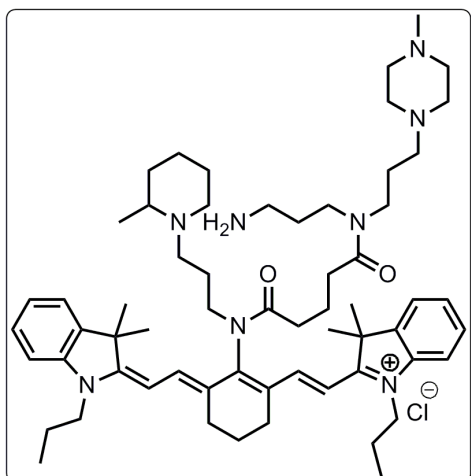
[^1]H-NMR (500 MHz, CDCl$_3$):δ 0.88-1.77 (m, 16H), 1.24 (s, 6H), 1.20 (s, 6H), 2.2 (m, 7H), 2.61 (s, 3H), 2.98 (m, 10H), 3.17 (m, 5H), 3.32 (m, 8H), 3.45-3.65 (m, 11H), 3.98 (m, 2H), 4.21 (m, 1H), 5.35 (m, 2H), 6.42-7.13 (m, 12H).

[^13]C-NMR (125 MHz, CDCl3): δ 14.17, 14.23, 22.58, 22.60, 22.68, 26.40, 29.15, 29.20, 29.38, 29.41, 29.62, 29.69, 30.68, 31.73, 31.75, 31.92, 39.50, 39.68, 39.84, 40.01, 40.17, 40.34, 40.5, 59.00, 59.05, 59.13, 63.78, 64.06, 67.80, 67.93, 114.62, 114.83, 115.15, 123.61, 124.28, 126.35, 131.80, 132.21, 132.35, 133.68, 140.30, 140.46,   141.74, 141.83, 154.80, 155.01, 161.43, 161.72, 162.22, 162.35, 162.70, 168.13, 168.59

ESI (HRMS) m/z (C$_{61}$H$_{93}$N$_8$O$_2{}^+$) calc: 969.7416; found: 969.7410.

CyR 275 (9 mg, 61%)
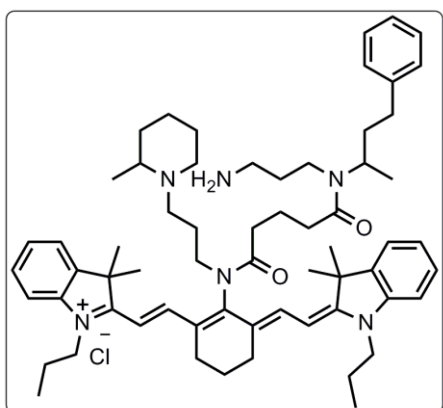
^{1}H-NMR (500 MHz, CDCl$_3$): δ 1.10 (t, 6H, J=4Hz), 1.18 (d, 3H, J=5Hz), 1.2(d, 3H, J=8.5Hz), 1.33(m, 2H), 1.43-1.45(m, 2H), 1.66(s, 12H), 1.88-1.92(m, 6H), 2.02-2.04(m, 1H), 2.22(t, 2H, J=8Hz), 2.33 (t, 2H, J=5Hz), 2.51-2.55(m, 4H), 2.75 (t, 4H, J=5Hz), 3.12 (m, 2H), 3.22-3.24 (m, 1H), 3.29 (t, 4H, J=5Hz), 3.68 (t, 2H, J=5Hz), 4.03 (t, 2H, J=4.7Hz), 4.33 (t, 2H, J=5Hz), 6.15 (d, 1H, J=14.5Hz), 6.34 (d, 1H, J=15Hz), 7.08-7.13 (m, 5H), 7.21-7.28 (m, 5H), 7.49 (d, 1H, J=14Hz). 7.55 (d, 1H, J=15 Hz).

ESI (HRMS) m/z (C$_{63}$H$_{89}$N$_6$O$_2^+$), calc: 961.7042; found 961.7057

CyR 477 (13 mg, 56%)
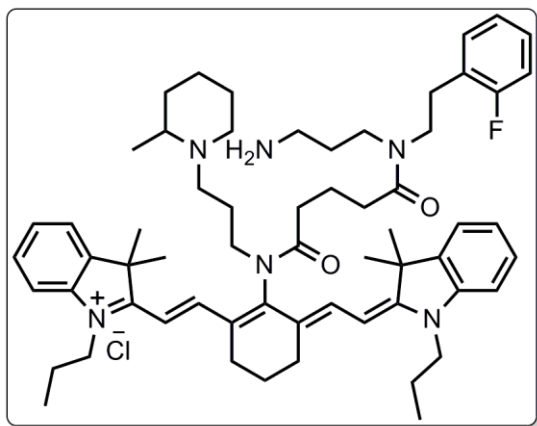
^{1}H-NMR (500 MHz, CDCl$_3$): δ 0.89 (t, 6H, J=7Hz), 1.10 (d, 3H, J=5Hz), 1.28-1.34 (m, 2H), 1.64 (s, 12H), 1.828 (m, 2H), 1.91-1.94 (m, 2H), 2.04 (t, 2H, J= 6Hz), 2.22 (t, 2H, J=8Hz), 2.228 (t, 2H, J=7Hz), 2.33 (t, 2H, J=5), 2.37 (t, 2H), 2.49-2.58 (m, 4H), 2.77 (t, 2H, J=6Hz), 2.86 (t, 2H, J=7Hz), 2.89 (t, 2H, J=7.5Hz), 2.94-2.96 (m, 2H), 3.03-3.05 (m, 1H), 3.45 (t, 4H), 3.58 (t, 2H, J=7Hz), 3.64 (t, 2H, J=8Hz), 4.01 (t, 2H, J=8Hz), 4.13 (t, 2H, J=6.5Hz), 6.07 (d, 1H. J=14 Hz), 6.11 (d, 1H, J=14Hz), 6.97-7.05 (m, 4H), 7.07-7.2 (m, 8H), 7.48 (d, 1H, J=14Hz), 7.54 (d, 1H, J=14Hz)

ESI (HRMS) m/z (C$_{61}$H$_{84}$FN$_6$O$_2^+$), calc: 951.6634; found 951.6651

CyR 164 (15 mg, 52%)
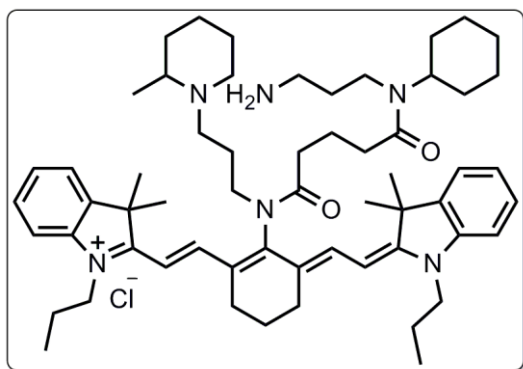
^{1}H-NMR (300 MHz,CDCl$_3$): δ 0.825 (t, 6H, J=7.2Hz), 1.03 (d, 3H, J=7.2Hz), 1.25-1.4 (m, 12 H), 1.61 (s, 12H), 1.79-1.91 (m, 6H), 1.84-1.89 (m, 2H), 2.0 (t, 2H), 2.12 (t, 2H, J=3.3 Hz), 2.21 (t, 2H, J=7.8Hz), 2.31 (t, 2H, J=2.1Hz), 2.41-2.52 (m, 4H), 2.71-2.76 (m, 4H), 2.95-3.0 (m, 4H), 3.25-3.26 (m, 1H), 3.34 (t, 4H), 3.5-3.62 (m, 4H), 3.93 (t, 4H, J=3.9Hz), 6.0 (d, 1H. J=14.1 Hz), 6.17 (d, 1H, J=14.1Hz), 7.0-7.39 (m, 8H), 7.54 (d, 1H, J=14.1 Hz), 7.47 (d, 1H, J=14.1 Hz)

ESI (HRMS) m/z (C$_{61}$H$_{84}$FN$_6$O$_2^+$), calc: 911.6885; found 911.6882

2.5.2 Photostability experiment

Procedure: 1% DMSO in10 mM HEPES buffer (pH 7.4) was used for dissolving all the **CyR** derivatives and CyNA-414 compound. The final concentrations of all the compounds were 10 μM. The compound solution were taken in 96-well black plate and then fluorescence intensity measurements were carried out in each 10 min interval for a total period of 8 h (excitation-emission 790-820 nm for CyR and CyNA compounds). For the strong UV condition, same stock solution was used for the photostability study.

2.6 References

1) (a) V. Ntziachristos, C. H. Tung, C. Bremer and R. Weissleder, *Nat. Med.* (N. Y.), 2002, **8**, 757–760; (b) J. Fabian, H. Kakazumi and M. Matsuoka, *Chem. Rev.*, 1992, **92**, 1197–1226; (c) M. Matsuoka, Infrared *Absorbing Dyes*, Plenum Press, New York, 1990; (d) J. V. Frangioni, *Curr. Opin. Chem. Biol.*, 2003, **7**, 626–634; (e) W. M. Leevy, S. T. Gammon, J. R. Johnson, A. J. Lampkins, H. Jiang, M. Marquez, D. Piwnica-Worms, M. A. Suckow and B. D. Smith, *Bioconjugate Chem.*, 2008, **19**, 686.; (f) E. M. Sevick-Muraca, J. P. Houston and M. Gurfinkel, *Curr. Opin. Chem. Biol.*, 2002, **6**, 642.

2) R. B. Mujumdar, L. A. Ernst, S. R. Mujumdar, C. J. Lewis and A. S. Waggoner, *Bioconjugate Chem.*, 1993, **4**, 105.

3) W. K. Moon, Y. H. Lin, T. O'Loughlin, Y. Tang, D. E. Kim, R. Weissleder and C. H. Tung, *Bioconjugate Chem.*, 2003, **14**, 539.

4) W. Pham, W. F. Lai, R. Weissleder and C. H. Tung, *Bioconjugate Chem.*, 2003, **14**, 1048.

5) D. B. Shealy, M. Lipowska, J. Lipowski, N. Narayanan, S. Sutter, L. Strekowski and G. Patonay, *Anal. Chem.*, 1995, **67**, 247.

6) K. Jyothish, K. T. Arun and D. Ramaiah, *Org. Lett.*, 2004, **6**, 3965.

7) K. Takagi, M. Kawabe, M. Matauoka and T. Kitao, *Dyes Pigm.*, 1985, **6,** 177.

8) W. B. Tuemmler and B. S. Wildi, *J. Am. Chem. Soc.*, 1958, **80**, 3772.

9) (a) J. Chen, I. R. Corbin, H. Li, W. Cao, J. D. Glickson and G. Zheng, *J. Am. Chem. Soc.*, 2007, 129, 5798; (b) S. A. Hilderbrand and R. Weissleder, *Curr. Opin. Chem. Biol.*, 2010, **14**, 71.

10) (a) J. Panda, P. R. Virkler and M. R. Detty, *J. Org. Chem.*, 2003, **68**, 1804.; (b) G. A. Reynolds and K. H. Drexhage, *J. Org. Chem.*, 1977, **42**, 885.; (c) N. Narayanan and G. Patonay, *J. Org. Chem.*, 1995, **60**, 2391.; (d) P. J. Sims, A. S. Waggoner, C. H. Wang and J. F. Hoffman, *Biochemistry*, 1974, **13**, 3315.; (e) S. J. Mason and S. Balasubrumanian, *Org. Lett.*, 2002, **4**, 4261.; (f) S. J. Mason, J. L. Hake, J. Nairne, W. J. Cummins and S. Balasubrumanian, *J. Org. Chem.*, 2005, **70**, 2939.; (g) M. Lopalco, E. N. Koini, J. K. Cho and M. Bradley, *Org. Biomol. Chem.*, 2009, **7**, 856.

11) M. Lipowska, G. Patonay and L. Strekowski, *Synthetic Commun.*, 1993, **23**, 3087.

12) A. Samanta, M. Vendrell, R. Das and Y. T. Chang, *Chem. Commun.*, 2010, **46**, 7406.

13) A. Samanta, M. Vendrell, S. W. Yun, Z. Guan, Q. H. Xu, and Y. T. Chang, *Chem.-Asian J.,* 2011, DOI: 10.1002/asia.201100041.

14) M. Lopalco, E. N. Koini, J. K. Choa and M. Bradley, *Org. Biomol. Chem.*, 2009, 7, 856.

15) C. Ornelas, R. Lodescar, A. Durandin, J. W. Canary, R. Pennell, L. F. Liebes, and M. Weck, *Chem. Eur. J.,* 2011, **17**, 3619.

16) K. Licha, B. Riefke, V. Ntziachristos, A. Becker, B. Chance, W. Semmler. *Photochem. Photobiol.* 2000, **72**, 392-398.

17) A. Toutchkine, D.V. Nguyen, K.M. Hahn. *Org. Lett.* 2007, **9**, 2775-2777.

Chapter 3

Monocyte/Macrophage Specific Fluorescent Probe Development to Assess Inflammation *in vivo*

a)

b)

c)

3.1 Introduction

The advances in molecular imaging enable development of tools to display and quantify molecular and cellular targets[1] for *in vivo* disease imaging. This is especially due to the richness of new fluorescent/nuclear medicinal reporter technologies for tagging of many cellular and subcellular processes *in vivo*. Non-invasive molecular imaging methods allow detection of early pathophysiological changes before conventional radiological imaging techniques including ultrasound, MRI (Magnetic Resonance Imaging) and CT (Computed tomography) detect anatomical changes[2]. Furthermore, this targeted imaging may detect molecular and cellular changes associated with inflammation prior to the onset of diseases. Therefore the application of molecular imaging to target inflammation has significant importance in clinical diagnosis of several major diseases. This is because chronic inflammation[3] is related to the onset of many diseases that do not have permanent cure. Alzheimer disease (AD) is a neurodegenerative disease characterized by progressive memory loss and dementia[4]. The effective treatment to AD is defied unless the important factors leading to the cause of the disease is known. The initial stages of the disease involve oxidative induced inflammatory damaged to blood vessels and dysregulated amyloid metabolism and this has implications for early detection and therapy[5].

The use of radiopharmaceuticals, ^{111}In-oxine and ^{99m}Tc-hexa-methylpro-pylenamine oxime (HMPAO) are still considered as 'gold standard'[9] nuclear medicine technique for imaging inflammation. ^{111}In-oxine and [99m]Tc- hexa-methylpro-pylenamine oxime (HMPAO) are lipophilic[6] compounds that can label leucocytes *ex vivo*. The effectiveness of ^{111}In-oxine and ^{99m}Tc-hexa-

methylpro-pylenamine oxime (HMPAO) in imaging lies in its specificity as compared to other non-specific inflammation tracers such as ^{67}Ga citrate[7], radiolabelled avidin and biotin. However, ^{111}In-oxine and ^{99m}Tc-hexa-methylpro-pylenamine oxime (HMPAO) requires the *ex-vivo* labeling of the leucocytes and re-injecting the leucocytes back into the patient. This can lead to potential blood contamination, and possible transmission of blood borne pathogens. Furthermore, ^{18}F-FDG[8] has emerged as inflammation targeting agent for PET imaging since immune cells including monocyte/macrophage show relatively high metabolic ability. ^{18}F-FDG is a well-established diagnostic tool in oncology and suitable for clinical PET imaging due to relatively long physical half-life of [18]F (110 min). However, ^{18}F-FDG is a very non-specific tracer because it shows uptake in any type of cell with high glycolytic activity and may therefore provide a false-positive result.

The characteristics of an ideal probe includes efficient accumulation and good retention in inflammatory foci, rapid clearance from background, no accumulation in non-target organs, no toxicity, early diagnostic imaging, ready availability and low cost, easy low-hazard preparation, differentiation between infection and low radiation burden[9]. Since no current tracer including ^{111}In-oxine, ^{99m}Tc-HMPAO and ^{18}F-FDG meet all the criteria for an ideal probe, this project aims to develop a specific fluorescence probe that can bind to monocytes/macrophage cell lineage specifically offering accurate assessment ability of inflammation *in vivo*.

NIR region is highly suitable for *in vivo* imaging (e.g., deep tissue penetration, low auto-fluorescence background) and the utility of the NIR dyes extensively described[11-13]. Diversity oriented solid phase synthesis enables us

to provide a number of NIR compounds and subsequently apply them in live cell based high-throughput image screening technology, intending to find novel chemical probes to stain monocyte/macrophage specifically which have the potential for clinical application to assess inflammation *in vivo*.

3.2 Objectives

I synthesized CyRCA and CyRAC compounds by modifying the CyR library. By using cell based high throughput screening with these compounds, we found a macrophage probe, CyRCA-341 which specifically stained to the monocyte/macrophage cells. Then, the compound was utilized to detect inflammation *in vivo* of mouse to demonstrate the applicability of this NIR fluorescent.

3.3 Results and discussion

3.3.1 Design and synthesis

In the Chapter 2, I have mentioned that the availability of reactive primary amine group in the CyR library allows us to modify the structure in further. Utilizing that possibility, I synthesized CyRCA and CyRAC compounds by applying the solid phase activated ester chemistry. To do that, firstly, active ester resins were prepared by treating the nitrophenol resin with chloroacetyl chloride (for CA) and acetyl chloride (for AC). The reaction between the resulting resin with the highly reactive primary amine of CyR library in the presence of catalytic amount of mild base $NaHCO_3$ afforded the corresponding CyRCA and CyRAC compounds (**Scheme 3.1, Chart 3.1**). The reaction was completed within 2 hours and the products were obtained after a simple filtration with an average purity of above 90% without further

purification (at 365 nm, **Table 3.2 & 3.3**). These compounds show fluorescence in the NIR range (average absorption 805 nm and emission at 820 nm). The quantum yield of each molecule varied from 0.01 to 0.08 (**Table 3.1 & 3.2, Figure 3.1**).

Scheme 3.1: Synthesis of CyRCA and CyRAC compounds
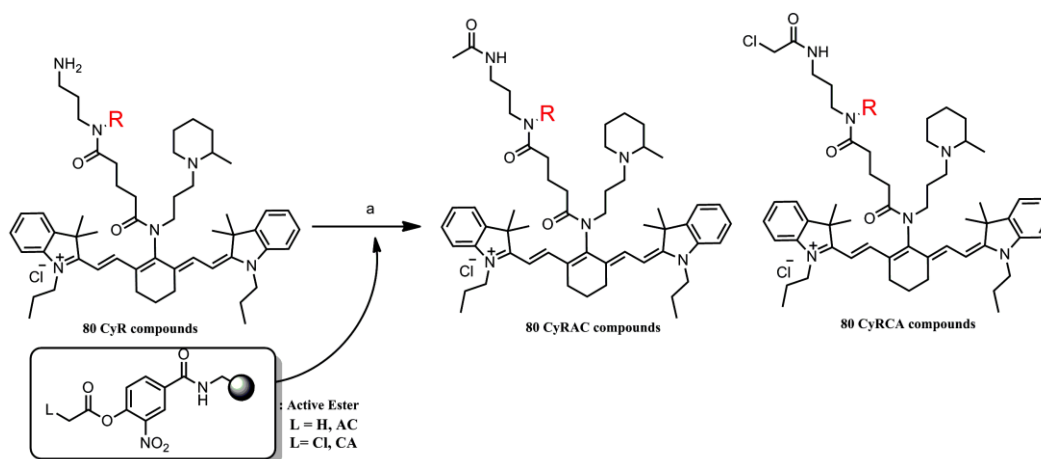
Reagents and conditions: (a) DCM/ACN (7:1), NaHCO$_3$, r.t., 2 h.
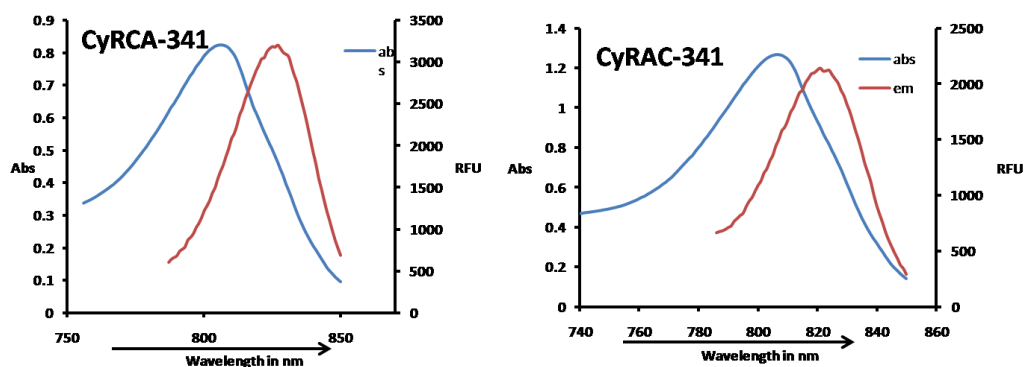
Figure 3.1 Absorption and Emission spectra of representative CyRCA and CyRAC compound

Table 3.1 Characterization by HPLC-MS and photophysical property of CyRCA library (*1 and *2 stands same meaning as chapter 2)

Compound	M$^+$(calc.)	M$^+$(exp.)	λ_{abs}(nm)	λ_{em}(nm)	ϕ*^{1}	purity*^{2}
CyRCA 28	1101.8	1101.4	806	825	0.05	91
CyRCA 32	1023.6	1024.3	806	825	0.05	90

CyRCA 49	1039.6	1039.2	806	825	0.02	89
CyRCA 77	1023.6	1023.3	806	825	0.06	92
CyRCA 92	989.7	989.3	806	825	0.05	92
CyRCA 100	1099.7	1100.8	806	825	0.04	91
CyRCA 101	1009.6	1009.3	806	825	0.05	90
CyRCA 103	1039.6	1039.3	806	825	0.05	88
CyRCA 105	1002.7	1002.3	806	825	0.04	92
CyRCA 111	1010.6	1010.3	806	825	0.04	91
CyRCA 131	1037.7	1038.3	806	825	0.03	91
CyRCA 135	1063.5	1064.2	806	825	0.02	90
CyRCA 164	987.6	987.3	806	825	0.05	89
CyRCA 165	977.6	978.3	806	825	0.04	92
CyRCA 167	991.6	992.3	806	825	0.05	92
CyRCA 177	963.6	963.6	806	825	0.04	91
CyRCA 180	973.6	973.3	806	825	0.04	90
CyRCA 185	975.6	976.3	806	825	0.02	88
CyRCA 193	1075.7	1076.3	806	825	0.01	92
CyRCA 201	1037.6	1037.3	806	825	0.01	91
CyRCA 211	1009.6	1009.3	806	825	0.05	92
CyRCA 218	1013.6	1013.3	806	825	0.03	93
CyRCA 220	1013.6	1013.2	806	825	0.05	94
CyRCA 221	1029.6	1030.2	806	825	0.05	94
CyRCA 222	947.6	948.3	806	825	0.03	92
CyRCA 230	1017.7	1018.3	806	825	0.02	95
CyRCA 240	1071.6	1071.2	806	825	0.01	89
CyRCA 262	1055.6	1055.2	806	825	0.05	91
CyRCA 272	1016.6	1017.3	806	825	0.02	91
CyRCA 274	1005.6	1005.3	806	825	0.05	90
CyRCA 275	1037.6	1037.3	806	825	0.02	89
CyRCA 277	1003.7	1003.3	806	825	0.04	92
CyRCA 282	1018.6	1018.3	806	825	0.04	92
CyRCA 319	1055.6	1055.3	806	825	0.04	91
CyRCA 323	991.6	991.3	806	825	0.04	90
CyRCA 329	1073.5	1074.6	806	825	0.04	88

CyRCA 330	1063.6	1063.3	806	825	0.05	92
CyRCA 335	1023.6	1024.8	806	825	0.05	91
CyRCA 341	1073.5	1075.1	806	825	0.05	91
CyRCA 358	1055.6	1055.3	806	825	0.05	90
CyRCA 359	1054.6	1055.2	806	825	0.04	89
CyRCA 360	1017.7	1017.3	806	825	0.05	92
CyRCA 361	1040.6	1040.3	806	825	0.03	92
CyRCA 364	1029.6	1030.2	806	825	0.04	91
CyRCA 368	1074.7	1074.4	806	825	0.05	90
CyRCA 374	995.6	996.2	806	825	0.02	88
CyRCA 375	1013.6	1013.2	806	825	0.05	92
CyRCA 381	1025.6	1025.3	806	825	0.01	91
CyRCA 384	1017.7	1017.3	806	825	0.03	90
CyRCA 387	1025.6	1025.2	806	825	0.05	89
CyRCA 388	1025.6	1026.2	806	825	0.05	92
CyRCA 395	1039.6	1040.3	806	825	0.03	92
CyRCA 396	1009.6	1009.3	806	825	0.05	91
CyRCA 399	1031.6	1031.2	806	825	0.05	90
CyRCA 403	1029.6	1030.2	806	825	0.05	88
CyRCA 405	1027.6	1029.3	806	825	0.03	92
CyRCA 407	1045.7	1046.7	806	825	0.01	91
CyRCA 412	1031.6	1031.2	806	825	0.04	92
CyRCA 414	1044.7	1045.3	806	825	0.03	93
CyRCA 419	975.6	975.3	806	825	0.06	94
CyRCA 420	1004.6	1005.3	806	825	0.02	94
CyRCA 425	975.6	975.3	806	825	0.05	92
CyRCA 429	1001.6	1002.3	806	825	0.03	95
CyRCA 439	989.6	990.3	806	825	0.05	89
CyRCA 442	975.6	976.3	806	825	0.04	91
CyRCA 446	985.6	985.2	806	825	0.05	91
CyRCA 447	1063.6	1063.2	806	825	0.05	90
CyRCA 477	1027.6	1029.2	806	825	0.05	89
CyRCA 479	1027.6	1027.2	806	825	0.05	93

Compound	M⁺(calc.)	M⁺(exp.)	λ_abs(nm)	λ_em(nm)	φ*¹	purity*²
CyRCA 526	1045.7	1045.2	806	825	0.02	95
CyRCA 548	1085.6	1086.3	806	825	0.05	94
CyRCA 554	1031.7	1031.3	806	825	0.04	93
CyRCA 565	1063.5	1063.2	806	825	0.05	94
CyRCA 572	1087.5	1087.3	806	825	0.04	94
CyRCA 574	975.6	975.3	806	825	0.05	93
CyRCA 577	1073.7	1073.4	806	825	0.02	90
CyRCA 599	1085.6	1085.3	806	825	0.05	89
CyRCA 602	989.6	989.3	806	825	0.03	92
CyRCA 677	1043.6	1044.2	806	825	0.05	92
CyRCA 686	1077.5	1078.2	806	825	0.03	91

Table 3.2 Characterization by HPLC-MS and photophysical property of CyRAC library (*1 and *2 stands same meaning as chapter 2)

Compound	M⁺(calc.)	M⁺(exp.)	λ_abs(nm)	λ_em(nm)	φ*¹	purity*²
CyRAC 28	1067.8	1067.7	805	825	0.06	90
CyRAC 32	989.7	989.6	805	825	0.05	90
CyRAC 49	1005.6	1005.6	805	825	0.03	95
CyRAC 77	989.7	989.6	805	825	0.02	94
CyRAC 92	955.7	955.6	805	825	0.04	91
CyRAC 100	1065.7	1065.6	805	825	0.05	90
CyRAC 101	975.7	976.6	805	825	0.05	95
CyRAC 103	1005.7	1006.6	805	825	0.05	93
CyRAC 105	968.7	968.6	805	825	0.05	93
CyRAC 111	976.6	976.6	805	825	0.05	90
CyRAC 131	1003.7	1004.6	805	825	0.04	93
CyRAC 135	1029.6	1029.5	805	825	0.05	93
CyRAC 164	953.7	953.6	805	825	0.02	94
CyRAC 165	943.6	943.6	805	825	0.05	91
CyRAC 167	957.7	957.6	805	825	0.05	90
CyRAC 177	929.6	929.6	805	825	0.05	90
CyRAC 180	939.6	939.6	805	825	0.02	90

CyRAC 185	941.7	941.6	805	825	0.04	89
CyRAC 193	1041.7	1041.7	805	825	0.02	91
CyRAC 201	1003.7	1041.6	805	825	0.05	92
CyRAC 211	975.6	975.6	805	825	0.03	93
CyRAC 218	979.6	980.6	805	825	0.05	94
CyRAC 220	979.6	980.6	805	825	0.04	94
CyRAC 221	995.6	995.5	805	825	0.03	95
CyRAC 222	913.6	914.6	805	825	0.05	93
CyRAC 230	983.7	983.6	805	825	0.04	93
CyRAC 240	1037.7	1037.6	805	825	0.04	90
CyRAC 262	1021.6	1022.6	805	825	0.05	93
CyRAC 272	982.7	982.6	805	825	0.02	93
CyRAC 274	971.7	971.6	805	825	0.03	94
CyRAC 275	1003.7	1004.6	805	825	0.05	91
CyRAC 277	969.7	970.7	805	825	0.05	92
CyRAC 282	984.7	984.6	805	825	0.03	92
CyRAC 319	1021.6	1021.6	805	825	0.02	90
CyRAC 323	957.7	957.6	805	825	0.01	90
CyRAC 329	1025.6	1025.6	805	825	0.01	93
CyRAC 330	1029.6	1030.6	805	825	0.03	91
CyRAC 335	989.7	990.6	805	825	0.05	91
CyRAC 341	1025.6	1025.6	805	825	0.03	91
CyRAC 358	1021.7	1021.6	805	825	0.05	93
CyRAC 359	1020.7	1021.6	805	825	0.05	94
CyRAC 360	983.7	983.6	805	825	0.03	95
CyRAC 361	1006.7	1006.7	805	825	0.04	94
CyRAC 364	995.6	995.5	805	825	0.04	92
CyRAC 368	1040.8	1041.7	805	825	0.02	93
CyRAC 374	961.7	961.6	805	825	0.04	93
CyRAC 375	979.7	979.5	805	825	0.05	96
CyRAC 381	991.7	992.6	805	825	0.02	90
CyRAC 384	983.7	983.6	805	825	0.02	91
CyRAC 387	991.6	992.6	805	825	0.05	88

CyRAC 388	991.6	992.6	805	825	0.05	90
CyRAC 395	1005.7	1006.6	805	825	0.05	91
CyRAC 396	975.6	976.6	805	825	0.05	91
CyRAC 399	997.6	997.6	805	825	0.05	90
CyRAC 403	995.6	995.5	805	825	0.04	92
CyRAC 405	993.6	993.6	805	825	0.02	91
CyRAC 407	1011.7	1011.7	805	825	0.02	91
CyRAC 412	997.6	997.6	805	825	0.04	93
CyRAC 414	1010.7	1010.7	805	825	0.05	92
CyRAC 419	941.7	941.6	805	825	0.05	91
CyRAC 420	970.7	970.6	805	825	0.04	93
CyRAC 425	941.7	942.6	805	825	0.05	93
CyRAC 429	967.7	968.6	805	825	0.05	90
CyRAC 439	955.7	956.6	805	825	0.02	90
CyRAC 442	941.6	941.6	805	825	0.04	91
CyRAC 446	951.6	952.6	805	825	0.05	92
CyRAC 447	1029.6	1029.6	805	825	0.04	93
CyRAC 477	993.6	993.5	805	825	0.01	93
CyRAC 479	993.6	994.6	805	825	0.03	91
CyRAC 526	1011.7	1011.6	805	825	0.02	90
CyRAC 548	1051.7	1051.6	805	825	0.02	90
CyRAC 554	997.7	997.7	805	825	0.02	91
CyRAC 565	1029.6	1030.5	805	825	0.03	93
CyRAC 572	1054.0	1055.5	805	825	0.01	92
CyRAC 574	941.7	942.6	805	825	0.02	90
CyRAC 577	1039.8	1040.7	805	825	0.01	91
CyRAC 599	1051.7	1052.6	805	825	0.05	90
CyRAC 602	955.7	955.6	805	825	0.03	91
CyRAC 677	1009.6	1009.6	805	825	0.02	92
CyRAC 686	1043.6	1043.5	805	825	0.02	92

3.3.2 Human Blood Cell Line Screening

In order to discover macrophage probe, CyRCA and CyRAC compounds were screened against a set of human macrophage/ macrophage related cells (cancer cells: HL60, U937, Mφ) in presence of negative control Molt4 cell (T cells). After the fluorescence image intensity based analysis as well as visual confirmation, we found that one CyRCA compound (CyRCA-341/CyRCA-E4) stained macrophage/ macrophage related cells more brightly than the negative control Molt4 cell (**Figure 3.2**). It is noted that the compound name CyRCA-341 and CyRCA-E4 are same where 341 represents the amine building block number according to our chemical inventory and E4 represents the plate position of the compounds we screened. For the screening, dye has been used in 1 μM concentration with 1 h incubation at 37 °C.
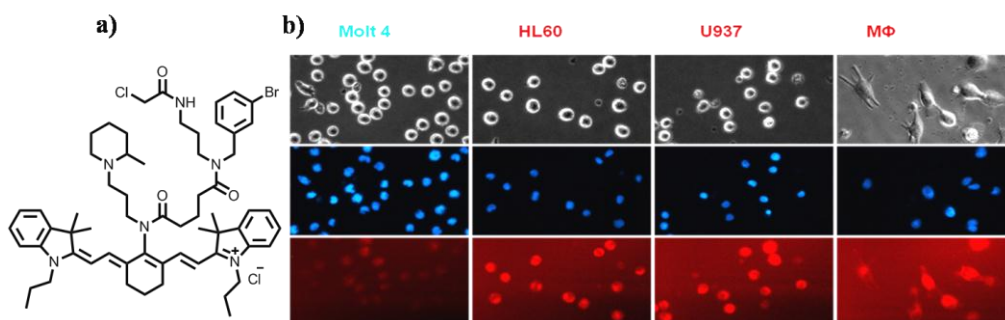
Figure 3.2 Discovery of Macrophage probe a) Chemical structure of macrophage probe, CyRCA-341 b) Nuclei of Molt4 (negative control cells) and HL-60, U937, Mφ (macrophage related cells) were visualized by Hoechst 33342 (middle panel); macrophage related cells were selectively stained by CyRCA-341(lower panel). (Upper panel represents phase contrast bright-field (BF) images; fluorescent (FL) images obtained with DAPI and Cy7 filter set. Scale bar, 50 μm.

3.3.3 Human Peripheral Blood Leucocytes Screening

Molt 4, HL60 and U937 (T cell, myeloid cell and monocytes respectively) are all cancer cell lines which are derived from patients

diagnosed with leukemia. The difference in genetic expressions between cancer cell and normal cell can result in different phenotypic expressions. As such, compound staining specificity in cancer cell lines (Molt 4, HL60, and U937) might differ from normal cells (T cell, myeloid cell and monocytes). Therefore, the compounds were further tested on peripheral human blood and the result demonstrates that the compound shows specificity towards monocytes/macrophage (**Figure 3.3**). CyRCA-E4/341 was incubated at 5 μM concentration at 37 °C for 1 h.
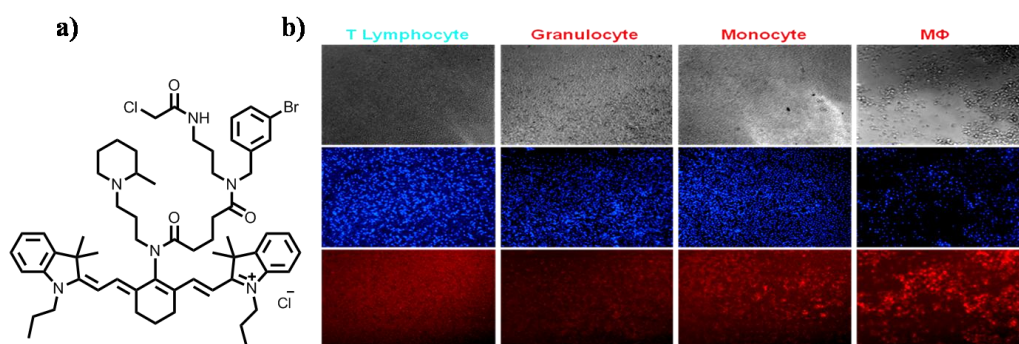
Figure 3.3 Discovery of Monocyte/macrophage probe **a**) Chemical structure of macrophage probe, CyRCA-341 **b**) Nuclei of T Lymphocytes , Granulocytes , Monocytes and Mφ were visualized by Hoechst 33342 (middle panel); monocytes and macrophage cells were selectively stained by CyRCA-341(lower panel). (Upper panel represents phase contrast bright-field (BF) images; fluorescent (FL) images obtained with DAPI and Cy7 filter set. Scale bar, 200 μm.

3.3.4 Mouse macrophage probe

After discovering the human monocytes/macrophage probes, it is time to check quickly whether the same compound can be applied in mouse macrophage case or not, as our eventual goal is to apply our probe into the mouse inflammation model. To quickly verify this, RAW (mouse macrophage cell line) cells were treated with CyRCA-E4/341 and the staining was

investigated. Our probe nicely stained to the mouse macrophage too (**Figure 3.4**).
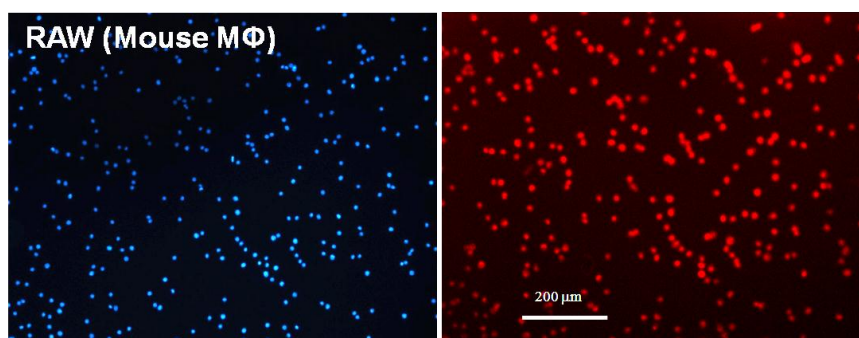
Figure 3.4 Mouse macrophage staining; nuclei of RAW cells were visualized by Hoechst 33342 (left); RAW cells were stained by CyRCA-341(right) fluorescent (FL) images obtained with DAPI and Cy7 filter set. Scale bar, 50 µm. Total x100 magnification.

3.3.5 *In Vivo* imaging with LPS Induce inflammation Model

To check the applicability of our probe, first, inflammation was generated to the right paw of a mouse by using LPS injection (3 days, 1mg/kg LPS). Then, the NIR fluorescence image (IVIS: Perkin Elmer) was taken after intravenous (tail vein injection) treatment of CyRCA-E4/341 compound. The imaging result indicates that our probe can comparatively enter more into the inflammation area over the healthy regions (**Figure 3.5**). CyRCA-341 was treated with 100 µM concentration and the image was taken after 1 h.
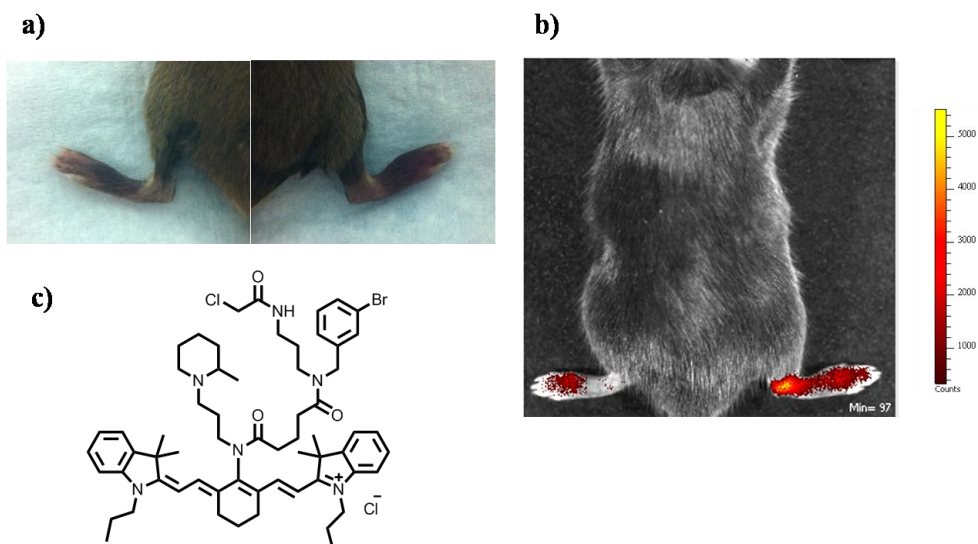
Figure 3.5 Inflammation detection *in vivo* **a**) LPS induced inflammation (three day after injection of 1 mg/Kg LPS) into the right paw of the mouse **b**) NIR fluorescence image (excitation 745 nm and emission 820 nm); Image was taken using IVIS (Perkin Elmer) machine, 1 h after the tail vein injection of 200 μL (100 μM) probe **c**) (CyRCA-341).

3.3.6 *In Vivo* Imaging with Hind Limb Ischemia Model[10]

Applicability of this probe was further tested by comparing our probe with ICG which is known to be regularly used in macrophage detection. To do that Hind limb Ischemia model was utilized to produce inflammation (Ischemia) in the hind limb area of a mouse using artery ligation method. 5 days after artery ligation, 100 μM of ICG and CyRCA-E4/341 were treated separately through the tail vein injection of two individual mice and then 2 h after fluorescence images were taken with IVIS machine. Imaging results show that our probe can more specifically enter to the inflammation area compared to the commercial standard ICG (**Figure 3.6**).

ICG

CyRCA-341
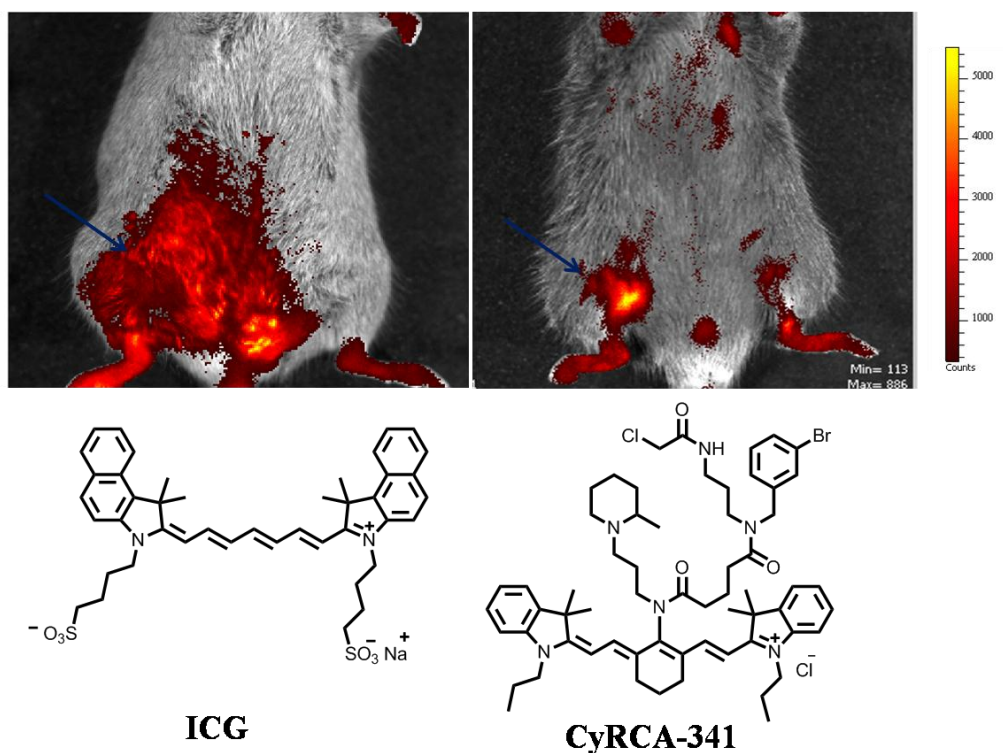
Figure 3.6 Inflammation detection *in vivo* **;** (Right panel) NIR fluorescence image was taken using IVIS (Perkin Elmer) machine, 1 h after the tail vein injection of 200 µL of 100 µM ICG. (Left) NIR fluorescence image (excitation 745 nm and emission 820 nm) was taken using IVIS (Perkin Elmer) machine, 1 h after the tail vein injection of 200 µL (100 µM) CyRCA-341.

To have a better view of the image from Ischemia model, fluorescence combined with X-ray image was taken using *In Vivo* MS FX PRO (Carestream) machine. The inflammation area in the hind limb area can now be well visualized from the **figure 3.7** image.

1.58 inch
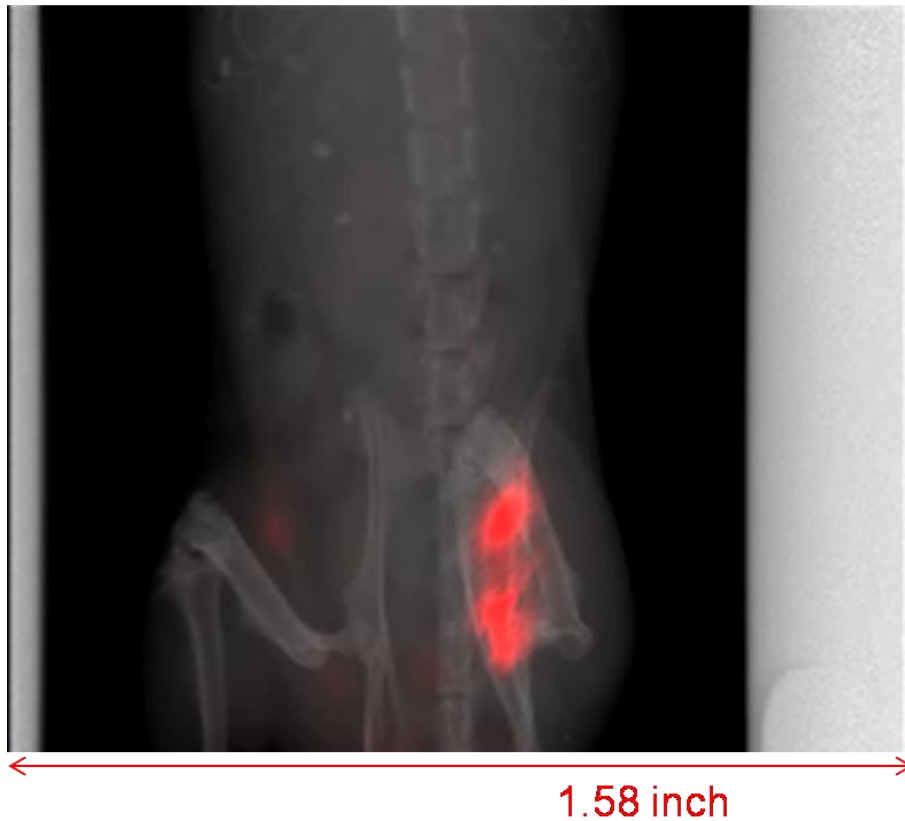
Figure 3.7 Inflammation detection *in vivo* using Hind Limb Ischemia Model**;** inflammation was induced 5 day after femoral artery ligation of mouse. Fluorescence plus X-ray image was taken using MS FX PRO (Carestream) machine, 2 h after tail vein injection of CyRCA-341. Scale bar 1.58 inch. Cy7 filter set.

3.3.7 Histological Identification of macrophage staining area

To confirm the specificity of macrophage probe and also to validate that the inflammation causes due to macrophage, the macrophage staining area from the hind limb inflammation region was identified. **Figure 3.8** demonstrates the histological identification experiment where macrophage specific antibody (CD11b+) was employed to identify the existence of macrophage in the inflammation area. 'Hot spot' area identified by *in vivo* animal imaging (orange frame in **a)**) is characterized by CD11b+ monocyte/macrophageinflux. Immunohistochemistry for CD11b was

69

performed on 10-mm cryosection corresponding to the area that revealed enhanced CyRCA-341 signal by *in vivo* fluorescence imaging. The CD11b expression in the entire region of interest, indicated by the frame in a), is shown in b), where both the 'hot spot' area (orange frame) and the 'cold spot' area (blue frame) were identified.
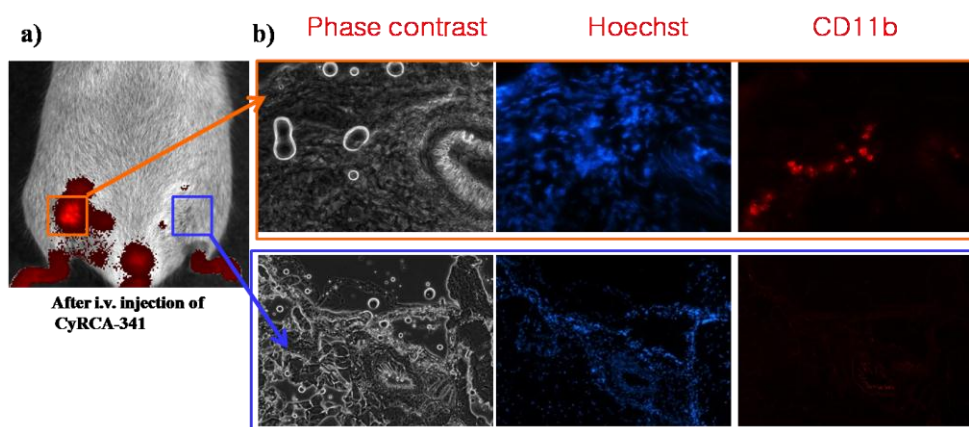
Figure 3.8 Histological Identification of macrophage staining area; The 'hot spot' area was characterized by massive macrophage infiltration (upper panel) compared with the 'cold spot' area (lower panel). (Upper panel) (left) bright field phase contrast image, (middle) Hoechst staining image, (right) fluorescence image of Cy7 conjugated CD11b+ antibody ; (lower panel) Images for non inflammation area; (left) bright field phase contrast image, (middle) Hoechst staining image, (right) fluorescence image of Cy7 conjugated CD11b+ antibody. Filter sets used, DAPI and Cy7.Scale bar 50 μm.

3.4 Conclusions

In summary, I have synthesized the acetyl and chloroacetyl version of NIR-cyanine dye library. Then, we have developed a novel *in vivo* imaging probe, CyRCA-341 for inflammation detection which exhibits comparable staining selectivity as well as monocyte/macrophage specificity.

3.5 Experiment and Methodology

3.5.1 Characterization data of representative CyRCA and CyRACcompounds

CyRCA-341(10 mg, 30%)
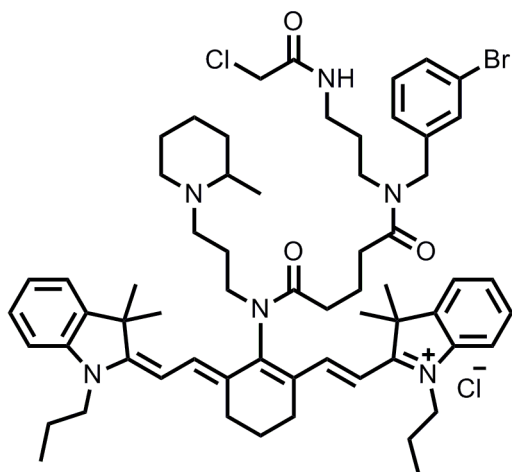
^{1}H-NMR (500 MHz, CDCl$_3$); δ 1.05-1.58(m, 12H), 1.63 (s, 6H), 1.64 (s, 6H), 1.67-2.0 (m, 9H), 2.19-2.23 (m, 6H), 2.45-2.72(m, 6H), 2.91 (m, 2H), 3.16-3.36 (m, 11H), 3.68 (m, 2H), 3.98 (m, 4H), 4.14 (s, 2H), 6.10 (d, 1H, *J*=14 Hz), 6.11 (d, 1H, *J*=14 Hz), 7.06-7.39 (m, 11H), 7.53 (d, 1H, *J*=11.5 Hz), 7.54 (d, 1H, *J*= 14 Hz), 7.71 (m, 1H). ESI-MS *m/z* (M $^+$), calc'd: 1073.5, found 1075.1 (due to bromine isotope)

LC-MS spectra of CyRCA-341

DAD1 D, Sig=640,4 Ref=off (RAJU\RAJ 2010-11-11 22-39-41\1ED-4301.D)

DAD1 E, Sig=780,4 Ref=off (RAJU\RAJ 2010-11-11 22-39-41\1ED-4301.D)

*MSD1 SPC, time=3.637 of D:\DATA\RAJU\RAJ 2010-11-11 22-39-41\1ED-43

Max: 3.62701e+006

538.3

537.3

1075.1

1077.1

DAD1, 3.483 (854 mAU,Up2) of 1ED-4301.D
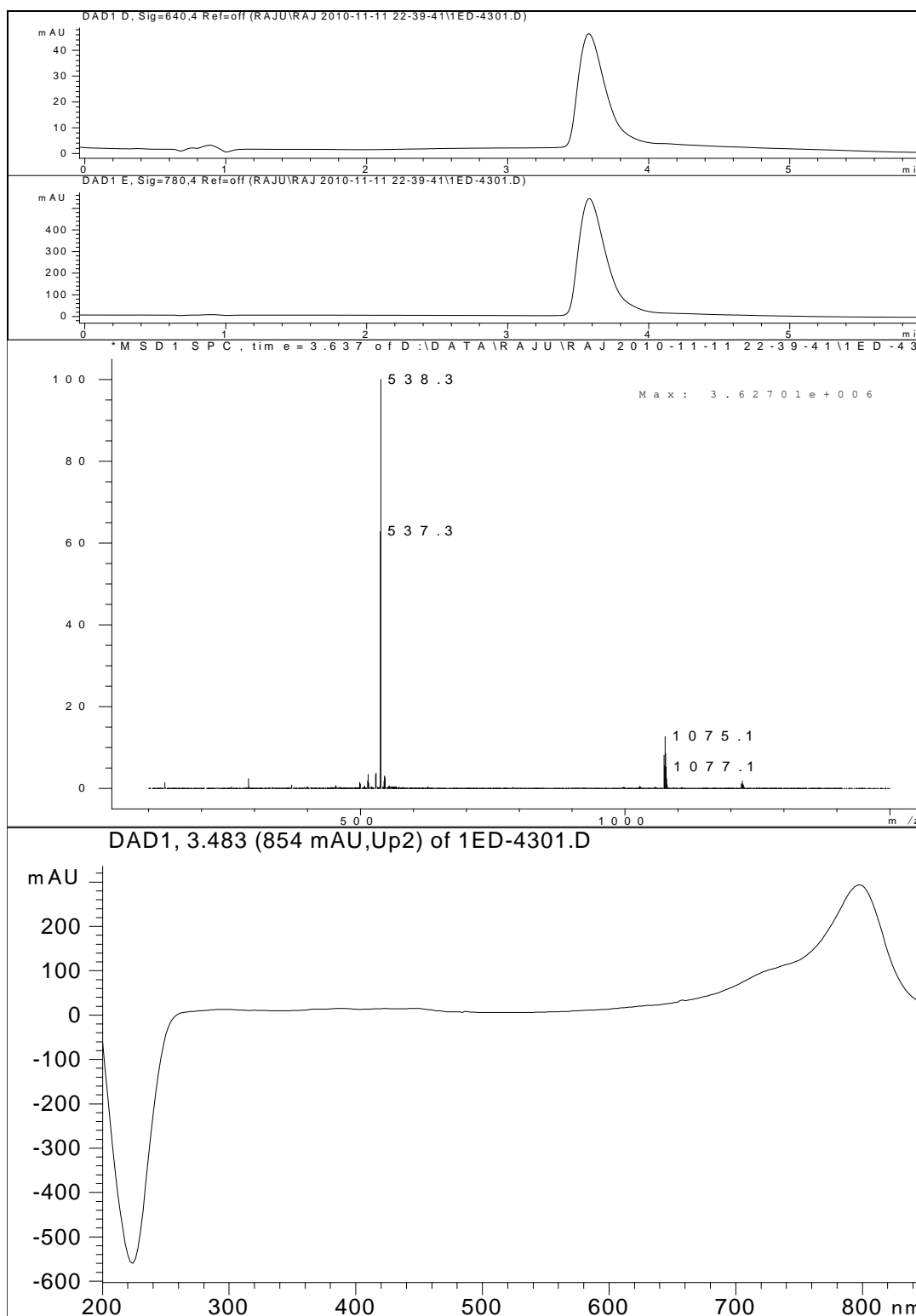
CyRCA-477 (12 mg, 32%)
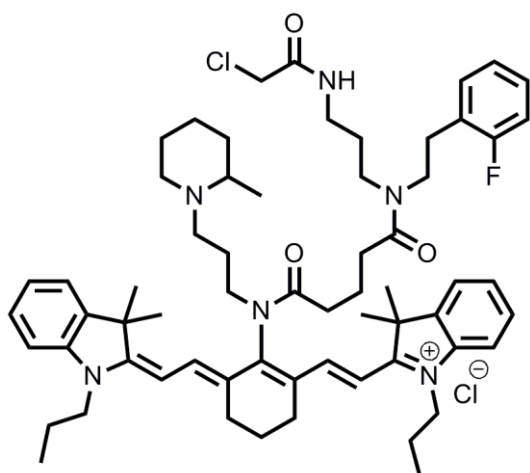
^{1}H-NMR (500 MHz, CDCl$_3$): δ 1.19-1.52(m, 12H), 1.57 (s, 6H), 1.58 (s, 6H), 1.72-1.90 (m, 9H), 2.14-2.20 (m, 6H), 2.66-2.83(m, 6H), 2.92 -3.11 (m, 15H), 3.27-3.30 (m, 2H), 3.94 (s, 2H), 3.95 (m, 4H), 6.04 (d, 1H, J=13.5 Hz), 6.07 (d, 1H, J=13 Hz), 6.95-7.20 (m, 12H), 7.43 (d, 1H, J=13 Hz), 7.49 (d, 1H, J=13 Hz). ESI-MS m/z (M$^+$), calc'd: 1027.6, found 1027.4

CyRCA-167 (9 mg, 27%)
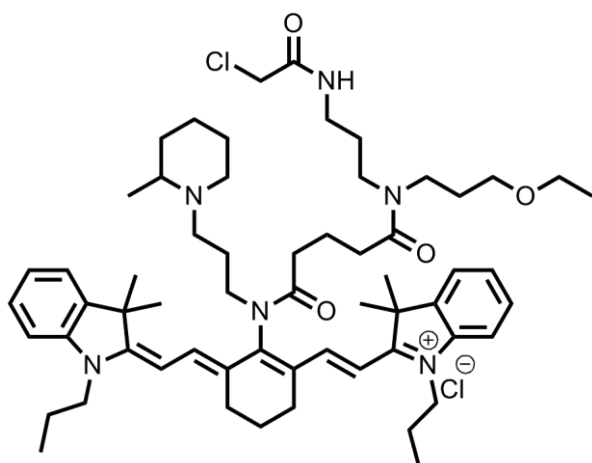
^{1}H-NMR (500 MHz, CDCl$_3$): δ 1.05-1.64 (m, 20H), 1.63 (s, 6H), 1.65 (s, 6H), 1.69-1.97 (m, 8H), 2.01-2.37 (m, 5H), 2.51 -3.12 (m, 11H), 3.21-3.36 (m, 11H), 3.68 (m, 2H), 3.97-399 (m, 6H), 6.10 (d, 1H, J=14 Hz), 6.12 (d, 1H, J=14 Hz), 7.05-7.37 (m, 8H), 7.52 (d, 1H, J=14 Hz), 7.53 (d, 1H, J=14.5 Hz). ESI-MS m/z (M$^+$), calc'd: 991.7, found 991.6

CyRCA-358 (12 mg, 35%)
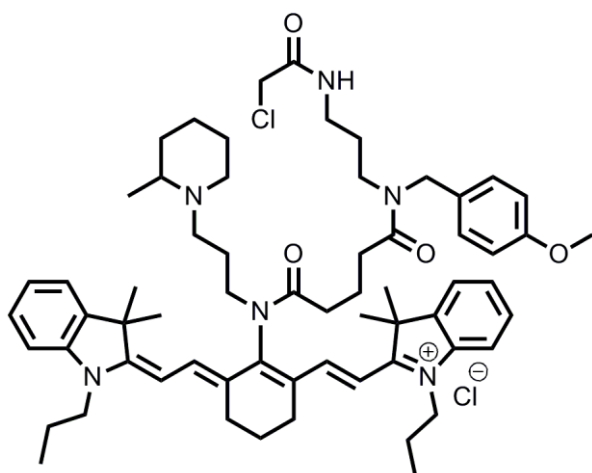
^{1}H-NMR (500 MHz, CDCl$_3$): δ 1.06-1.59 (m, 12H), 1.66 (s, 6H), 1.67 (s, 6H), 1.70-2.0 (m, 14H), 2.21-2.77 (m, 12H), 3.29 (m, 2H), 3.64-3.86 (m, 13H), 3.99-4.03 (m, 4H), 6.10 (d, 1H, *J*=13 Hz), 6.13 (d, 1H, *J*=13 Hz), 7.06-7.36 (m, 12H), 7.53 (d, 1H, *J*=13.5 Hz), 7.54 (d, 1H, *J*=13.5 Hz). ESI-MS *m/z* (M $^+$), calc'd: 1025.6, found 1025.1

CyRAC-341 (8 mg, 28%)
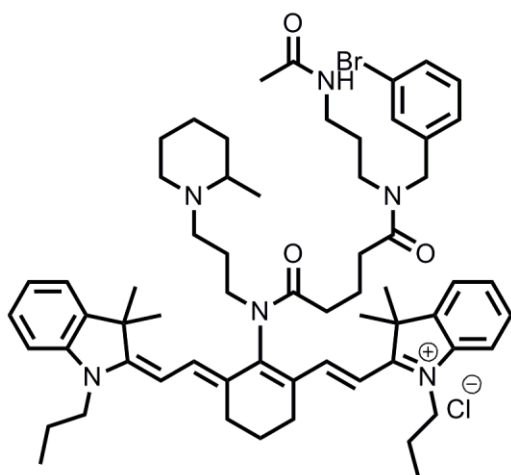
^{1}H-NMR (500 MHz, CDCl$_3$): δ 1.05-1.58(m, 12H), 1.63 (s, 6H), 1.64 (s, 6H), 1.67-2.0 (m, 9H), 2.19-2.23 (m, 6H), 2.45-2.72(m, 6H), 2.91 (m, 2H), 3.16-3.36 (m, 11H), 3.68 (m, 2H), 3.98 (m, 4H), 4.14 (s, 2H), 6.14 (d, 1H, *J*=14 Hz), 6.17 (d, 1H, *J*=14 Hz), 7.04-7.39 (m, 11H), 7.53 (d, 1H, *J*= 4 Hz), 7.56

(d, 1H, *J*=15 Hz), 7.70 (m, 1H). ESI-MS *m/z* (M $^+$), calc'd: 1039.6, found 1041.1(due to bromine isotope).

Materials and Methods

Amine and few bromide building block and all other chemicals and solvents for the synthesis were purchased from the Alfa Aesar, Fluka, Acros, MERCK, and Sigma Aldrich and were used without any purification. Merck Silica Gel 60 (particle size: 0.04-0.063 mm, 230-400 mesh) was used for the normal phase column chromatographic purification. From BeadTech Inc., Korea, 2-chlorotrityl alcohol resin (1.37 mmol/g) was purchased. For analytical characterization of CyRCA and CyRAC compounds HPLC-MS (Agilent-1200 series) with a DAD detector and a single quadrupole mass spectrometer (6130 series) with an ESI probe were used. Analytical process, except specified: eluents: A: H_2O (0.1% HCOOH), B: ACN (0.1% HCOOH), C_{18} (2) Luna column (4.6 x 50mm^2, 5μm particle size) was used. ^{1}H-NMR spectra were recorded on 500 MHz NMR spectrometer, and chemical shifts are expressed in parts per million (ppm) and approximate coupling constants were calculated in Hz. Quantum yields and all other photophysical properties of CyRCA and CyRAC derivatives were performed in Spectramax M2 instrument and the obtained data were analyzed using the Microsoft Office Excel 2007.

3.5.2 Cell preparation and screening

Preparation of U937 Medium: U937 medium was prepared by adding 500mL of RPMI medium, 5% (vol/vol) FBS (Fetal Bovine Serum), 1%(vol/vol) Glutamax, 1% (vol/vol) Pen Strep (Penicillin Streptomycin) and

1%(vol/vol) NEM NEA (NEM non-essential amino acids). The medium was mixed and filtered using 0.22um filter system and stored at 4 ^{0}C.

Preparation of Freezing Medium: Freezing medium was prepared by adding 50mL of FBS (Fetal Bovine Serum) and 5% (vol/vol) DMSO (Dimethyl Sulfoxide). DMSO was filtered using 0.20um filter before it was added into FBS. The medium was stored at -20 ^{0}C.

Cell Growth and Cell Storage

The cell lines (Molt 4, HL60 and U937) were purchased and grown in 200 mL, growth area 75cm^2 cell flask, containing 10 mL of U937 medium at 37 ^{0}C. Cells growth was maintained by replacement of fresh U937 medium every 1 to 2 days. To change cell medium, the cell solution contained in the cell flask was transferred to a 50mL tube and was centrifuged at 1500 rpm, 10 minutes and 21 ^{0}C. After centrifugation, the supernatant was aspirated and 20 mL of U937 medium was added to the cell pellet and re-suspended. Next, 10 mL of cell solution was transferred to a new cell flask and the remaining 10 mL of cell solution was transferred to a 15 mL tube, centrifuged using the same setting and the supernatant was aspirated and cell pellet was re-suspended in freezing medium. The cells suspended in freezing medium were counted using manual cell counting (appendix) and was stored at -80 ^{0}C.

Macrophages were derived from U937 cell line by adding 15 μL of 100 μM of PMA (Phorbol 12-myristate 13-acetate dissolved in DMSO)[8] in a 10 cm cell dish containing $2x10^6$ U937 cells in 10 mL medium. The cells were incubated for 1 day at 37 ^{0}C. The attached macrophages were removed from cell dish by firstly aspirating the cell medium. Next, the cells were washed with 10 mL of DPBS (Dulbecco's Phosphate-Buffered Saline w/o

Ca^{2+} & Mg^{2+} at pH 7.3) and DPBS was aspirated. 1 mL of 0.25% Trypsin-EDTA 1x was added to cell dish and incubated for 4 minutes at 37 ^{0}C. After 4 minutes, macrophages were detached as (observed from microscope) from cell dish and 10mL of U937 medium was added. The cell solution was transferred into a 15mL tube and centrifuged at 1500 rpm, 10 minutes and 21 ^{0}C. The supernatant was removed and the cell pellet was re-suspended in U937 medium and the number of macrophages was counted.

Human Blood Screening Experiment

40 mL of human blood was extracted by Pilip William Kuchel, M.D from a volunteer (Ethnic group: Indian, Age: 30+, Sex: Male). Mononuclear cells and granulocytes were isolated from human blood using Ficoll- Paque separation media (GE Healthcare, Isolation of mononuclear cells, methodology and applications). Monocytes and T cells were further separated from mononuclear cells by negative magnetic separation. Monocytes were obtained by using BD IMag Streptavidin particles and BD IMag human monocyte Enrichment set (BD IMag, Human Monocyte Enrichment Set DM) while T cells were obtained by using BD IMag Streptavidin particles and BD IMag Human T lymphocyte Enrichment Set(BD IMag, Human T Lymphocyte Enrichment Set). Macrophages were differentiated from monocytes by incubation of 1×10^7 monocytes with 10 mL of RPMI medium containing 40 µL of 50 µL/mL M-CSF (Macrophage Colony-stimulating factor). After the cells were separated, (T cell, granulocytes, Monocytes and Macrophages), the cells were screened with Nikon Ti microscope.

3.5.3 General synthesis procedure

General procedure for the synthesis of p-nitrophenol resin

In a 50 mL polystyrene cartridge, to an amino polystyrene resin (1 g, 1.2 mmol) in DMF (15 mL) were added 4-hydroxy-3-nitrobenzoic acid (1 g, 5.5 mmol), HOBt (1 g, 7.4 mmol), and DIC (1 mL, 6.4 mmol). After overnight shaking, the reaction mixture was washed with DMF (20 mL, 5 times), DCM, and methanol (20 mL, 5 times alternatively). To remove any undesirable side product, DMF (5 mL) and piperidine (0.5 mL) were added to the cartridge and allowed to shake for 1.5 h. The resin was filtered and washed with DMF (20 mL, 5 times). The resulting piperidine salt was removed via the addition of a 10% HCl solution (in DMF, 20 mL) and was allowed to shake for 1.5 h. The resin (1 g) was then filtered; washed with DMF, methanol, and DCM (20 mL, 5 times each); and dried by nitrogen gas flow. This nitrophenol resin (1 g, 1 mmol, 1eq.) was then suspended in DCM and then 7 eq. of DIEA (7 mmol, 1.22 mL) followed by 5eq of chloroacetyl chloride at 0 $^{\circ}$C was added under nitrogen and then the stirred slowly at room temperature for 4 hours. Resin was filtered through the syringe fitted with cartridge and then washed with DMF (5X 10 mL) , DCM (5X 10mL) and then dried over vacuum to get active ester resin.

General procedure for synthesis of CyRCA and CyRAC library

To synthesized CyRCA library, each of 1 μmol CyR library compound (80 compounds) was taken according to their plate code in the 2 mL of 96-deep well plate. About 30 mg (~ 20 μmol, 20 eq.) of active-ester resin was added to the each well of the CyR library containing plate. Then, DCM:ACN (7:1) solvent mixture of around 500 μL and catalytic amount of saturated solution of NaHCO$_3$ were poured in to each well. The plate was kept in the

shaker with moderate shaking for 2 hours. Then, the solution was filtered from the resin and dried to obtain pure products.

3.6 References

1) F. A. Jaffer and R. Weissleder, *Circulation Research*, 2004, **94**, 433. A. Signore and A. W. J. M. Glaudemans, *Ann. Nucl. Med.*, 2011, **25**, 681.

2) M. Provinciali, M. Cardelli and F. Marchegiani, *Curr. Opin. Pulm. Med.*, 2011, **17 Suppl 1**, S3.

3) (a) C. K. Combs, *J. Neuroimmune. Pharm.*, 2009, **4**, 380. (b) D. Gautrin, S. Froda, H. Tetreault and D. Gauvreau, *Can. J. Psychiatry.*, 1990, **35**, 162.; (c) E. Masliah, *Histol. Histopathol.*, 1995, **10**, 509-519.

4) V. T. Marchesi, *Faseb. J.*, 2011, **25**, 5.

5) R. Laitinen, J. Tahtinen, T. Lantto and M. Vorne, *Clin. Nucl. Med.*, 1990, **15**, 597. (c) F. J. van Hemert, R. Thurlings, S. E. Dohmen, C. Voermans, P. P. Tak, B. L. van Eck-Smit and R. J. Bennink, *Nucl. Med. Biol.*, 2007, **34**, 933.; (d) M. Djekidel, R. K. Brown and M. Piert, *Clin. Nucl. Med.*, 2011, **36**, e50. (a) S. Vallabhajosula, S. J. Goldsmith, H. Lipszyc, A. P. Chahinian and T. Ohnuma, *Eur. J. Nucl. Med.*, 1983, **8**, 354. (b) L. J. Anghileri, M. Ottaviani and C. Raynaud, *Nuklearmedizin*, 1982, **21**, 8.

6) L. W. Locke, M. B. Williams, K. D. Fairchild, M. Zhong, B. K. Kundu and S. S. Berr, *Int. J. Mol. Imaging.*, 2011, **2011**, 356730.; (b) C. D. Beer, K. Potter, N. Lenzo, D. Blacker, L. F. Arnolda, G. J. Hankey and I. B. Puddey, *Clin. Neurol. Neurosurg.*, 2012, **114**, 613.;

(c) A. Almuhaideb, R. Syed, L. Iordanidou, Z. Saad and J. Bomanji, *Brit. J. Radiol.*, 2011, **84**, E202.

7) H. J. Rennen, O. C. Boerman, W. J. Oyen and F. H. Corstens, *Eur. J. Nucl. Med.*, 2001, **28**, 241. A. Limbourg, T. Korff, L. C. Napp, W. Schaper, H. Drexler and F. P. Limbourg, *Nat. Protoc.*, 2009, **4**, 1737.

8) D. S. Miller, S. Letcher, D. M. Barnes, *Am. J. Physiol.* 1996, 271, F508.

9) G. Di Chiro, E. Oldfield, D. Bairamian, N. J. Patronas, R. A. Brooks, L. Mansi, B. H. Smith, P. L. Kornblith, R. Margolin, *J. Comput. Assist. Tomogr.* 1983, **7**, 937.

10) J. N. Talbot, D. Grahek, K. Kerrou, N. Younsi, V. de Beco, C. Colombet-Lamau, Y. Petegnief, N. Cailleux, F. Montravers, *Gynecol. Obstet. Fertil.* 2001, **29**,775.

Chapter 4

Multiplexing SERS nanotags for in vitro Detection of Differentiated Mouse Embryonic stem cells (mESc)
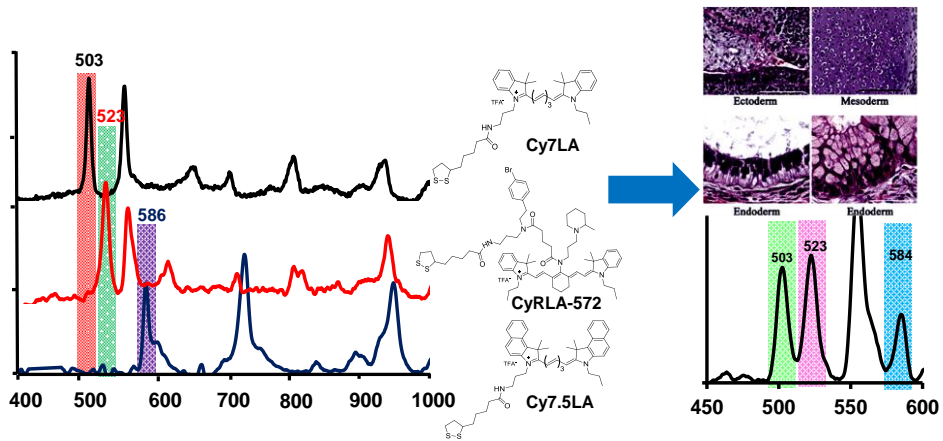
4.1 Introduction

High spectral sensitivity of SERS nanotags is extensively useful in multiplexing detection in the bio-analytical applications. The multiplexing capability derives because of its narrow bandwidths of the Raman spectra of the associated reporter molecules. Therefore, it offers a precious chance for the simultaneous identification of closely connected targets.[1-3] Maiti *et al* recently accomplished the multiplex detection of cancer cells using cyanine and triphenylmethine based SERS nanotags.[4] Here, they used the different antibody-conjugated SERS nanotags simultaneously (e.g. anti-EGFR and anti-HER2) to recognize different types of cancer cells (i.e. OSCC and SKBR-3 respectively) utilizing a single excitation wavelength. *In vitro* multiplexing of cell lines detection using SERS nanotags of commercial RMs has also been recently studied.[5] Additionally, Maiti *et al* demonstrated the applicability of polymethine cyanine dyes as multiplex partners that can clearly identify the various tumors *in vivo*[6]. Recently, the application of pluripotent stem cell therapies in clinical study faces a major threat due to the potential teratoma[7] formation. A teratoma is a monstrous mass/tumor[7] that consists of tissue from all three germ layer (ectoderm, mesoderm, and endoderm) formation. Hentze *et al.* demonstrates the semiquantitative histopathological analysis of the teratomas[8] that includes several cell lines, injection sites and cell numbers. Motivated by all these researches, we aimed to simultaneously detect different germ layer of a mESc *in vitro* as it exists in teratoma. As a tool, SERS technique is adopted due to its well known characteristics of multiplexing aptitude.

4.2 Objectives

Here, SERS nanotags were prepared to obtain the simultaneous detection of three different germ layer of teratoma. To do that, we first synthesized the lipoic acid-containing cyanine derivatives, CyRLA a 55 memberd library and screened them to identify CyRLA-572 as an NIR SERS reporter with excellent sensitivity. Later, we evaluated the multiplexing capacity of this CyRLA-572 with our previously reported highly sensitive SERS active cyanine dyes, Cy7LA and Cy7.5LA under a single excitation wavelength (e.g. 785 nm laser). These cyanine based SERS nanotags have been then applied for the detection of different layers of mESc in *in vitro* using different antibodies. Specifically, multiplex antibody-conjugated SERS nanotags (anti-CD34, anti-CD184, anti-Notch1) that recognize different types of germ layer of teratoma (mesoderm, endoderm and ectoderm respectively) were applied to detect different layer of differentiated mESc using a single excitation wavelength. Multiplex peaks were also identified from three different nanotags.

4.3 Results and discussion

4.3.1 Design and synthesis

Chang *et al*. recently, developed the combinatorial approach to identify cyanine based Raman reporter. Encouraged by this strategy, I have synthesized the lipoid acid containing 55 memeber, cyanine dye library, CyRLA (**Chart 2.1, Scheme 4.1, Table 4.1**), by adopting solid phase active ester method.

Scheme 4.1: Synthesis of CyRLA library
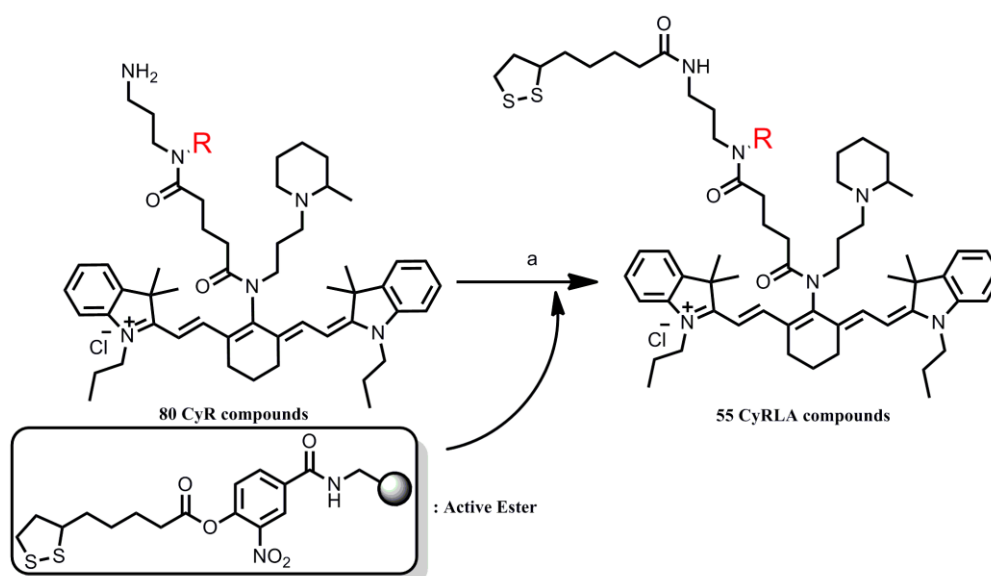
Reagents and conditions: (a) DCM/ACN (7:1), NaHCO$_3$, r.t., 6 h.

Table 4.1 Characterization by HPLC-MS and photophysical property of CyRLA library

Compound Code	M$^+$(calc.)	M$^+$(exp.)*[a]	Purity(%)*[b]	λ_{abs}/nm	λ_{em}/nm
CyRLA-677	1155.7	1155.6	90	803	820
CyRLA-599	1197.7	1197.6	94	803	820
CyRLA-396	1121.7	1121.6	82	803	821
CyRLA-221	1141.7	1141.6	84	805	820
CyRLA-358	1137.7	1137.6	93	804	822
CyRLA-574	1087.7	1087.6	90	802	820
CyRLA-262	1167.7	1167.6	86	803	820
CyRLA-565	1175.6	1175.5	93	801	819
CyRLA-330	1175.7	1175.5	92	804	820
CyRLA-329	1185.6	1185.7	89	802	823
CyRLA-335	1135.7	1135.6	93	801	820
CyRLA-388	1137.7	1137.6	92	802	819
CyRLA-399	1143.7	1143.6	92	803	820
CyRLA-479	1139.7	1139.6	93	804	823
CyRLA-548	1197.7	1197.6	82	803	820
CyRLA-222	1059.7	1059.6	90	802	821

CyRLA-447	1175.7	1175.6	81	803	822
CyRLA-360	1129.7	1129.6	91	804	823
CyRLA-319	1167.7	1167.6	89	801	820
CyRLA-240	1183.7	1183.6	92	802	820
CyRLA-193	1187.8	1187.7	93	803	819
CyRLA-384	1129.8	1129.7	83	802	820
CyRLA-275	1149.7	1149.6	84	804	820
CyRLA-92	1101.7	1101.7	89	801	820
CyRLA-111	1122.7	1122.6	72	803	821
CyRLA-165	1089.7	1089.6	89	802	820
CyRLA-167	1103.7	1103.6	92	803	822
CyRLA-405	1139.7	1139.6	93	801	820
CyRLA-341	1185.6	1185.5	92	803	820
CyRLA-414	1156.8	1156.7	93	801	819
CyRLA-477	1139.7	1139.6	92	803	820
CyRLA-554	1143.8	1143.7	93	802	823
CyRLA-572	1199.6	1199.5	92	805	820
CyRLA-100	1211.8	1211.7	91	803	819
CyRLA-180	1085.7	1085.6	92	804	820
CyRLA-211	1121.7	1121.6	93	803	823
CyRLA-274	1117.7	1117.6	92	802	820
CyRLA-359	1166.7	1166.6	90	803	821
CyRLA-403	1141.7	1041.6	91	802	822
CyRLA-442	1087.7	11087.7	92	803	823
CyRLA-602	1101.7	1101. 6	85	804	820
CyRLA-32	1121.7	1121.6	89	802	820
CyRLA-177	1075.7	1075.6	81	803	821
CyRLA-361	1152.7	1152.6	82	802	820
CyRLA-375	1125.7	1125.6	75	804	822
CyRLA-412	1143.7	1143.6	85	803	820
CyRLA-429	1113.7	1113.6	90	803	820
CyRLA-135	1175.6	1175.5	92	801	819
CyRLA-201	1149.7	1149.6	92	804	820
CyRLA-374	1107.7	1107.6	91	805	823

CyRLA-364	1141.7	1141.6	92	802	820
CyRLA-185	1087.7	1087.6	92	801	819
CyRLA-164	1099.7	1099.6	89	802	820
CyRLA-395	1151.7	1151.6	85	803	823

(a) ESI-MS m/z corresponding to [M+] values.

*(b) Purities were determined by integration of the UV absorbance signal at 780 nm.

55-member CyRLA compounds were characterized by HPLC-MS analysis. The purities of the whole library were determined by integration of the UV absorbance signal at 780 nm. The spectra of 10 μM in DMSO solution was recorded in SpectraMax M2 plate reader.

4.3.2 SERS Measurement

For CyRLA library, 60 nm diameter AuNPs were employed for the SERS measurement. CyRLA are NIR compounds having absorbance maximum wavelengths around 800 nm in DMSO (**Figure 4.1**).
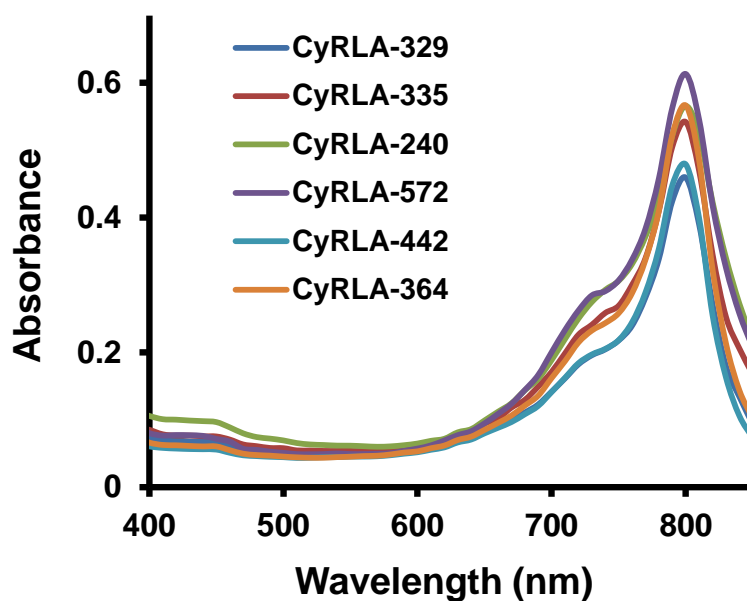
Figure 4.1 Absorbance spectra of the 6 selected CyRLA compounds (10 μM concentration, pH=7.4, 20 mM PBS).

As, 800 nm is the excitation maxima for the CyRLA compounds, 785 nm laser sources were used for the excitation of Au-nanotags. In practice, there are two available laser sources for SERS microscopes; these are 633 nm and 785 nm. Among them, 785 nm sources produce a higher SERS signal intensity because of its resonance between the excitation frequency and electronic transition of NIR reporter molecules. The SERS property of every CyRLA compound was evaluated under a compact Raman scanner after incubating them with citrate-stabilized gold nanoparticles. It is noted from the primary screening that the SERS intensities of CyRLA compounds varied significantly throughout the library (**Figure 4.2**) indicating that the SERS properties depend on the amine structures.
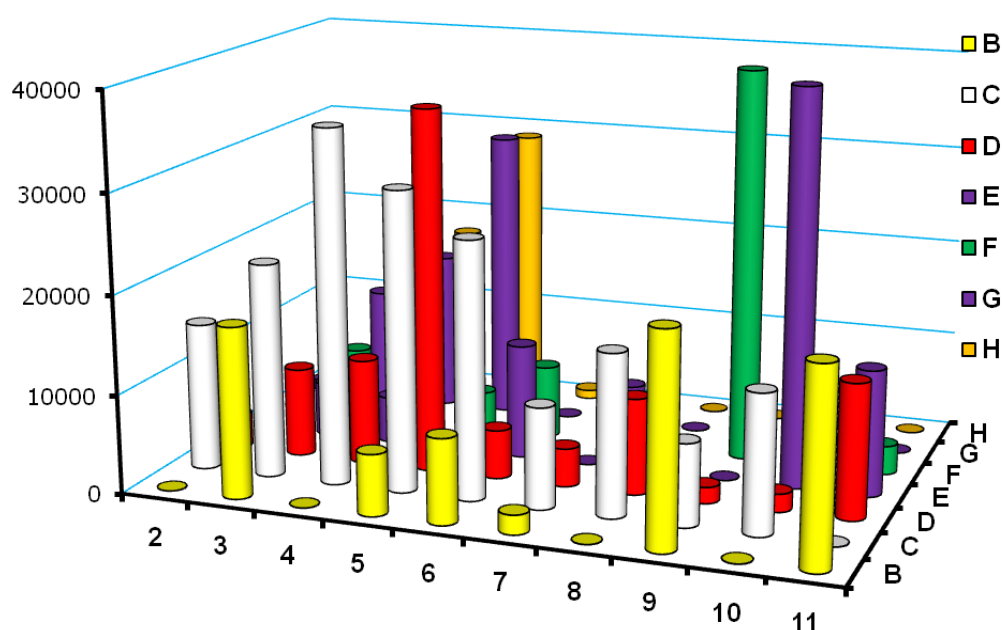
Figure 4.2. Comparative SERS intensities of the whole CyRLA library. SERS spectra were measured in a compact Raman scanner with excitation at 785 nm and 60 mW laser power.

Notably, six derivatives (CyRLA-335, 329, 240, 364, 572 and 442, represented in **figure 4.2** as C5, C4, D5, H5, E10 and F9 respectively)

exhibited very high SERS intensities. The selected SERS active reporter molecules were further carried out in a Renishaw InVia Raman microscope (Renishaw, UK, model: HPNIR785) using an excitation wavelength of 785 nm.
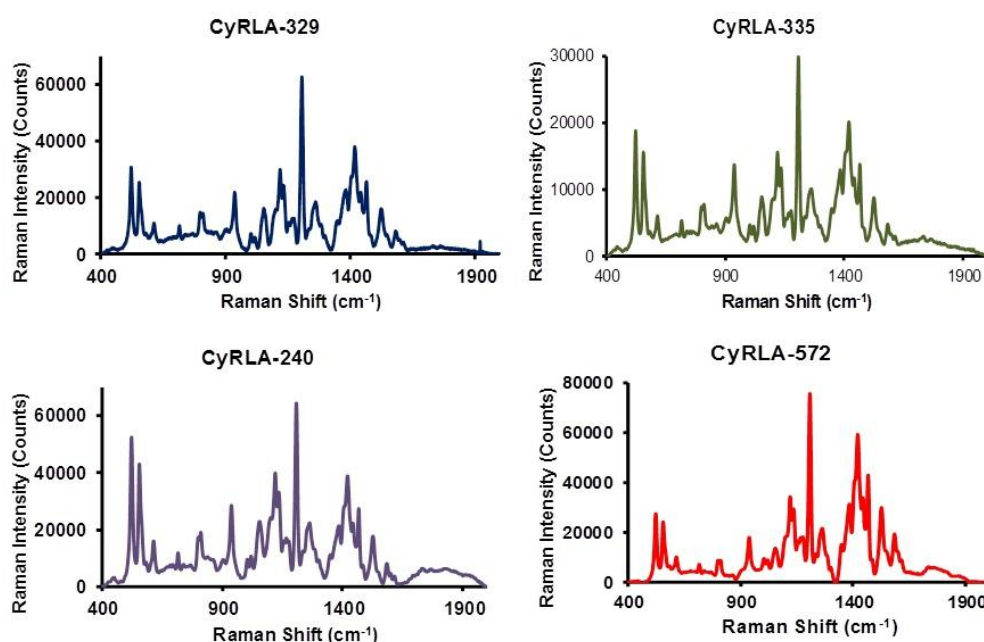
Figure 4.3 SERS spectra of BSA-encapsulated nanotags; that were derivatized with CyRLA-329, CyRLA-335, CyRLA-240, CyRLA-572; Raman spectral range: 400 to 2000 cm^{-1}, resolution: 1 cm^{-1}, acquisition time: 10s.

4.3.3 Design and synthesis of Cy7 and Cy7.5 based NIR Raman reporters

Here, I applied the same (like CyRLA synthesis) lipoic acid (LA) linker strategy to NIR dyes Cy7 and Cy7.5 to form two new RMs (Cy7LA and Cy7.5LA) that could be chemisorbed on the Au-NPs for SERS studies.[31-32] First, I prepared the Cy7 and Cy7.5 with an aminopropyl linker according to the previously synthesized protocol.[6] The amine intermediates then reacted with activated ester resin of lipoic acid (**Scheme 4.2**) to obtain the target compounds Cy7LA and Cy7.5LA with an average purity of 90%.

Scheme 4.2 Synthesis of Cy7LA and Cy7.5LA
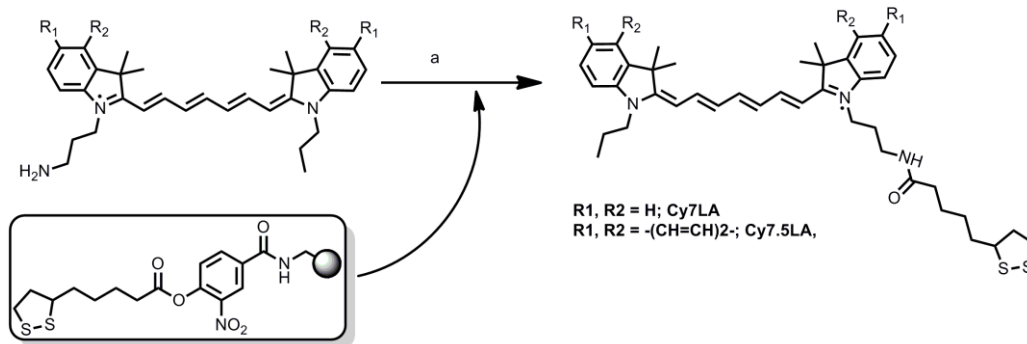
Reagents and conditions: (a) DCM/ACN (7:1), NaHCO$_3$, r.t., 6 h

4.3.4 Encapsulation of AuNPs and TEM characterization

Encapsulation strategy for SERS-active nanoparticles is very important due to its aggregation prevention characteristics.[9-12] Moreover, encapsulated nanoparticles can be used for bioconjugation by introducing the functional groups on their surface. Long-term stability of the six selected CyRLA-NPs was evaluated after bovine serum albumin (BSA) and glutaraldehyde modification. Here, coated cross-linked organic layer of BSA contains carboxylic acid group on the surface that can be modified further with amine-containing molecules (i.e. antibodies, proteins or other macromolecules) (Scheme 5.2).[13] Previously Qian et al. reported that, under harsh conditions the gold nanoparticles rapidly undergo precipitation or aggregation .[14] Samanta et al. adopted BSA encapsulation strategy to increase the stability of SERS signal intensity and minimize the aggregation among the nanoparticles.[6] The same strategy has been adopted for the coating of the CyRLA compounds. The increased size (65-70 nm) of the BSA-encapsulated CyRLA-AuNPs was confirmed by transmission electron microscopy (TEM). Additionally, a minor band around 600 nm of the plasmon spectra in **Figure 4.4** indicates that there is no significant aggregation among the Au-colloids.
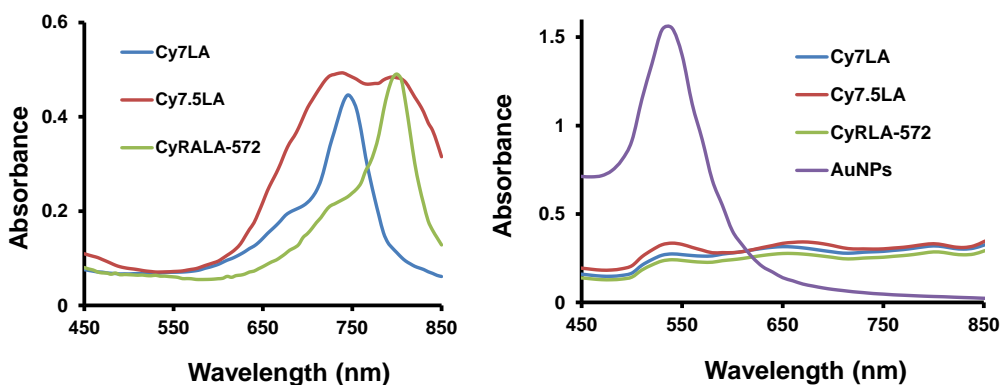
Figure 4.4 Surface plasmon absorption spectra of Au-colloids containing CyRLA , Cy7LA and Cy7.5LA reporters.

Three encapsulated dyes Cy7LA, Cy7.5LA and CyRLA-572 showed strong atleast one unique SERS signal when excited at NIR laser (785 nm) and therefore could provide high sensitive multiplex detection capability (**Figure 4.5**)
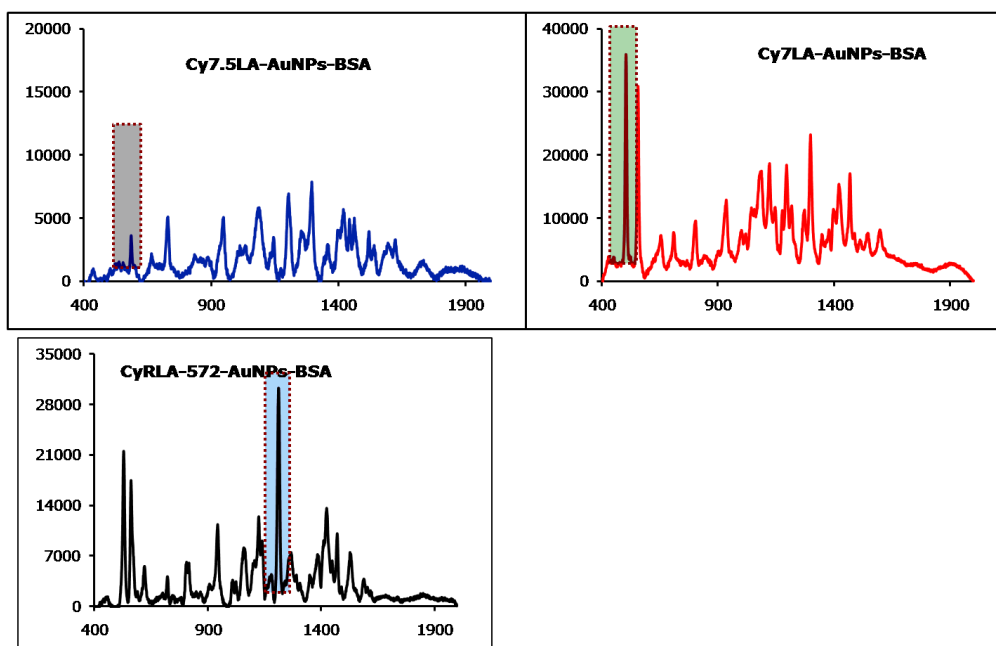
Figure 4.5 SERS spectra of BSA-encapsulated nanotags of Cy7.5LA, Cy7LA, CyRLA-572. Raman spectral range: 400 to 2000 cm.$^{-1}$, resolution: 1 cm^{-1}, acquisition time: 10 s.

90

4.3.5 SERS with multiplex peaks

Previously Maiti *et al* synthesized a highly Raman active NIR Raman reporter-set (Cy7LA, Cy7.5LA and CyNAMLA-381) as a Raman multiplex partner.[15] Similarly, in this chapter, SERS spectra of chemisorbed CyRLA, Cy7LA and Cy7.5LA on AuNPs were analyzed under the 785 nm laser and consequently their multiplexing capability was evaluated. Notably, a number of peaks are useful for uniquely identifying the three different nanotags: 503, 523, 586 cm^{-1} for Cy7.5LA, CyRLA and Cy7LA respectively (**Figure 4.6**). The combination of these cyanine Raman reporters can be useful for the construction of multiplex SERS nanotags, and we aimed to explore their application for the detection of germ layers in differentiated mESc.
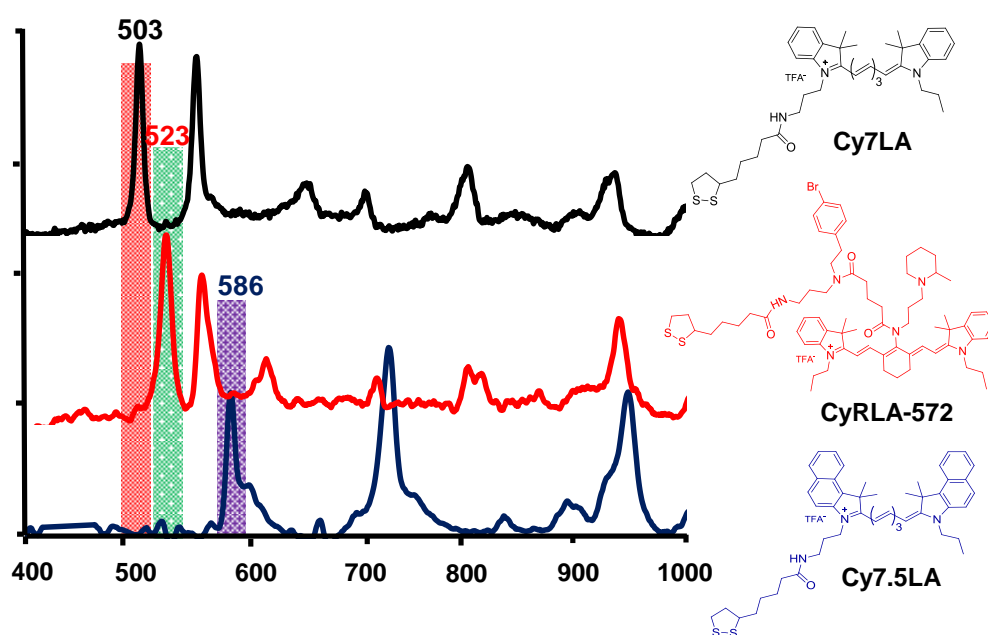
Figure 4.6 Normalized SERS spectra of Cy7.5LA, CyRLA-572 and Cy7LA after chemisorption on AuNPs. Spectra were measured using a Raman microscope (785 nm laser excitation, 30 mW laser power, acquisition

time: 10s) and plotted as average intensities (n=3). The most distinctive peaks from each reporter are highlighted in three different colours.

4.3.6 Signal stability

After encapsulating NPs-RM complexes using bovine serum albumin (BSA) and glutaraldehyde as a cross-linking agent, the excess glutaraldehyde was removed by treatment with glycine treatment and then the long-term stability of SERS-signals of CyRLA-E10-AuNPs was studied for 20 days (**Figure 4.7**). Stability of these nanotags was monitored at Raman peak of 523 cm^{-1}.
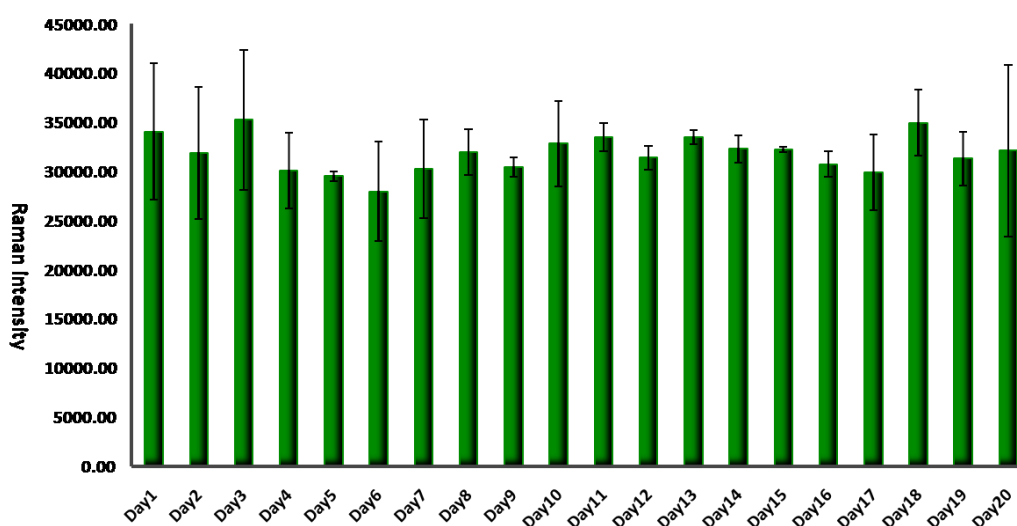
Figure 4.7 Time course SERS measurement of CyRLA-E10 nanotag. SERS intensities of the highest Raman peaks (i.e. 523 cm^{-1} for CyRLA-572) are plotted as means ± standard deviation of 5 independent measurements taken from the same sample at different time points.

Notably, there is no significant aggregation among all these nanotags and they exhibited stable SERS intensities over time, shown in **figure 4.7.** **Figure 4.8**, transmission electron microscopy (TEM) image indicates that the

size of these nanotags was around 65 nm. Here, 5 nm increments in size featured to the encapsulation BSA layer.
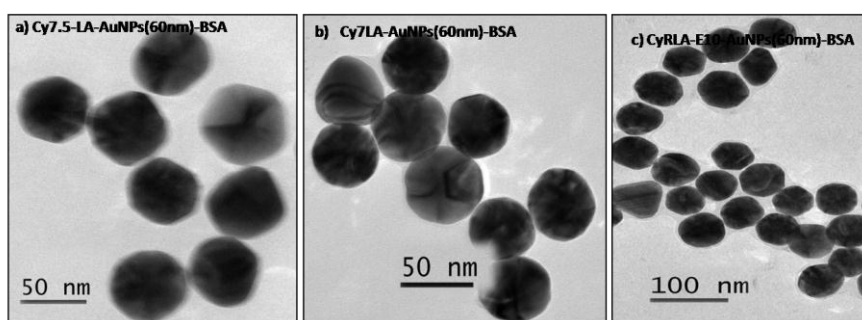
Figure 4.8 Transmission electron microscopy (TEM) images of: a) BSA-encapsulated Cy7.5LA b) Cy7LA c) CyRLA-572 nanotag; Scale bar: 50 nm for Cy7 and Cy7.5 . 100 nm for CyRLA-572

4.3.7 SERS study in differentiated mouse Embryonic stem Cells (mESc)

In order to examine the multiplex differential recognition of CyRLA-572 anti-CD34, Cy7LA anti-CD184 and Cy7.5LA anti-Notch1 nanotags in three different germ layers of differentiated mESC, an equal amount of all these three nanotags were incubated with teratoma (consisted of Endoderm, mesoderm, ectoderm). After washings with PBS buffer, the SERS measurement in differentiated mouse embryonic was carried out (**Figure 4.9**). SERS spectra for anti-CD34 (mesoderm) treated teratoma resembled to the spectra of CyRLA-572, SERS signal of anti-CD184 (endoderm) treated teratoma resembled to the spectra of Cy7LA and SERS spectra from anti-Notch1 (ectoderm) treated teratoma resembled to Cy7.5LA spectra. No significant SERS signal was recorded where nanotogs without antibody was treated to the differentiated mouse embryonic stem cells (spectra is not given here).
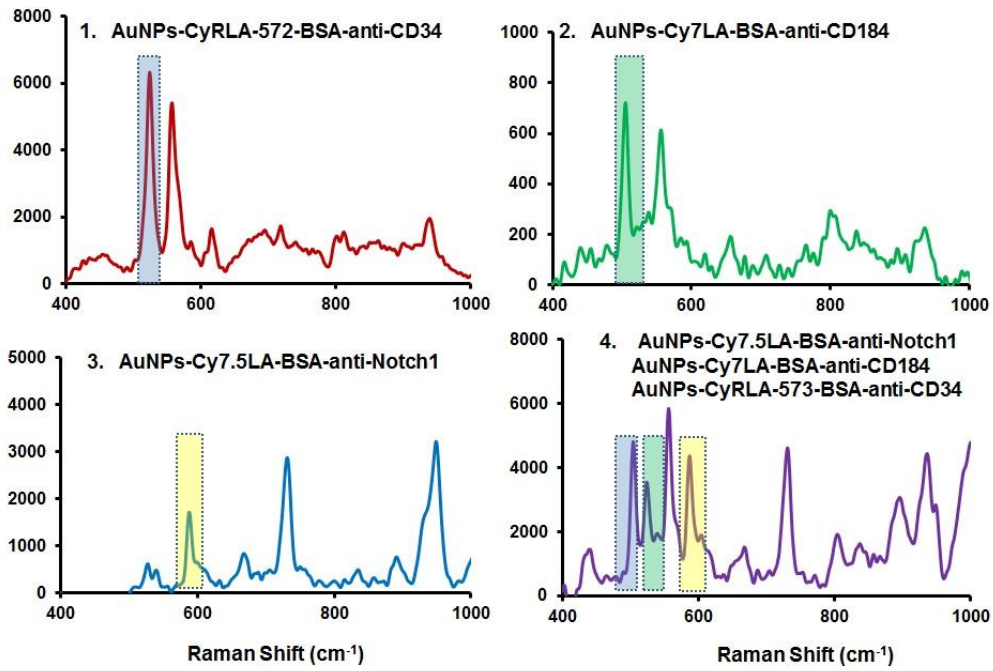
Figure 4.9 Obtained SERS signal from the differentiated mESc; (**1**) signal from mesoderm; CyRLA-572-anti-CD34 (**2**) signal from endoderm; Cy7LA-anti-CD184 (**3**) signal from ectoderm; Cy7-5LA-anti-Notch1(**4**) signal from all the three differentiated layers; CyRLA-572-anti-CD34, Cy7LA-anti-CD184 and Cy7-5LA-anti-Notch1

4.4 Conclusions

In summary, we report three lipoic acid-containing NIR active tricarbocyanine Raman reporters (CyRLA-572, Cy7LA and Cy7.5LA) as multiplex partner where Cy7LA and Cy7.5LA were previously reported as well as used for *in vivo* multiplex targeted imaging. Here, I have synthesized CyRLA library and screened them to identify Raman reporter having high Raman intensity and high signal stability and consequently used it for multiplex Raman partner with Cy7LA and Cy7.5LA to detect the three different germ layers of differentiated mESc *in vitro*.

4.5 Experimental Method

Material and method

Surface plasmon absorption spectra were measured on a SpectraMax M2 spectrophotometer (Molecular Devices), and the data analysis was performed using Microsoft excel 2007. SERS measurements were carried out in a Renishaw InVia Raman (UK) microscope with a laser beam directed to the sample through $50\times$ and $20\times$ objective lens and a Peltier cooled CCD detector in Singapore Bioimaging Consortium, Agency for Science, Technology and Research (A*STAR), Singapore. Samples were excited with a 785 nm excitation wavelength laser and Stokes shifted Raman spectra were collected in the range of 400 to 2000 cm^{-1} with 1 cm^{-1} resolution. Prior to every measurement, a calibration with a silicon standard (Raman peak centered at 523 cm^{-1}) was performed. WiRE 3.0 software package was used for data acquisition.

4.5.1 Characterization data of representative CyRLA compounds

CyRLA-442 (7 mg, 20%)
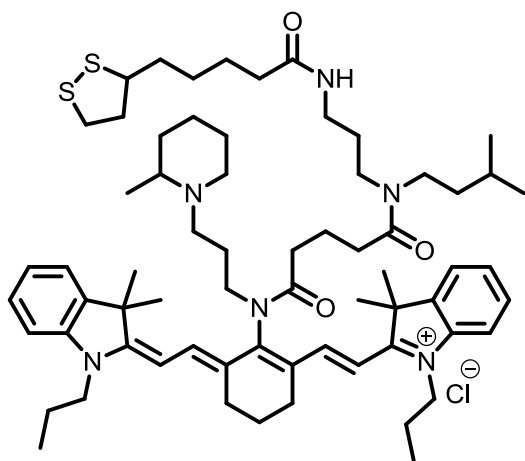
^{1}H-NMR (500 MHz, CDCl$_3$): δ 0.87-1.60 (m, 18 H), 1.65 (s, 6H), 1.66 (s, 6H), 1.7-1.92 (m, 14H), 2.14-2.72 (m, 12H), 3.03-3.28 (m, 11H), 3.48-3.72 (m, 13H), 4.0-4.1 (m, 6H), 6.12 (d, 1H, *J*=13.5 Hz), 6.24 (d, 1H, *J*=13.5 Hz), 7.04-7.44 (m, 8H), 7.52 (d, 1H, *J*=13 Hz), 7.55 (d, 1H, *J*=13Hz).

ESI-MS *m/z* (M $^+$), calc'd: 1087.7, found 1087.4

CyRLA-572 (9 mg, 17%)
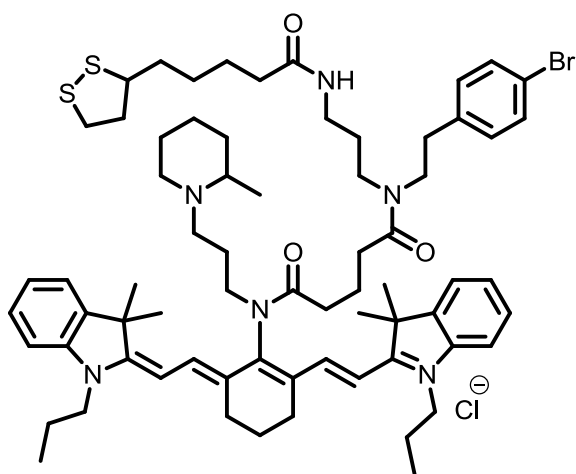
^{1}H-NMR (500 MHz, CDCl$_3$): δ 1.06-1.62 (m, 18 H), 1.66 (s, 6H), 1.68 (s, 6H), 1.69-2.06 (m, 9H), 2.18-2.78 (m, 10H), 3.04 -3.31 (m, 11H), 3.44-3.73 (m, 13H), 3.93-4.06 (m, 6H), 6.14 (d, 1H, J=14.5 Hz), 6.17 (d, 1H, J=14.5 Hz), 6.99-7.43 (m, 12H), 7.53 (d, 1H, J=14.5 Hz), 7.56 (d, 1H, J=14.5Hz). ESI-MS m/z (M$^+$), calc'd: 1199.6, found 1201.1(due to bromine isotope).

CyRLA-364 (7.5 mg, 15%)
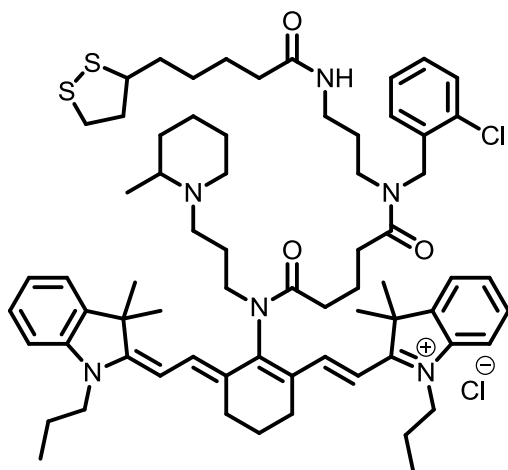
^{1}H-NMR (500 MHz, CDCl$_3$): δ 1.06-1.62(m, 18H), 1.67 (s, 6H), 1.68 (s, 6H), 1.70-1.92 (m, 9H), 1.99-2.46 (m, 10H), 2.52-2.62 (m, 6H), 2.72 (m, 2H), 3.0-3.72 (m, 15H), 4.0-4.12 (m, 6H), 4.53(s, 2H), 6.10 (d, 1H, J=14.5 Hz), 6.16 (d, 1H, J=14.5 Hz), 7.07-7.49 (m, 12H), 7.52 (d, 1H, J=15 Hz), 7.55 (d, 1H, J=15 Hz). ESI-MS m/z (M$^+$), calc'd: 1141.7, found 1141.4

CyRLA-335 (8.2 mg, 18%)
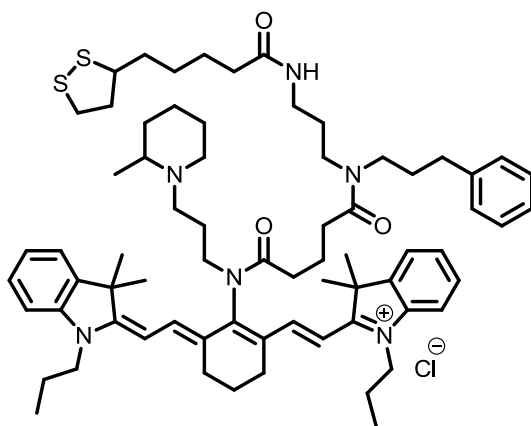
^{1}H-NMR (500 MHz, CDCl$_3$): δ 1.09-1.57 (m, 18 H), 1.61 (s, 6H), 1.63 (s, 6H), 1.71-2.03 (m, 11H), 2.16-2.80 (m, 10H), 3.05 -3.33 (m, 11H), 3.54-3.76 (m, 13H), 3.96-4.17 (m, 6H), 6.14 (d, 1H, *J*=13.5 Hz), 6.17 (d, 1H, *J*=13.5 Hz), 7.09-7.45 (m, 13H), 7.56 (d, 1H, *J*=13.5 Hz), 7.59 (d, 1H, *J*=13.5Hz). ESI-MS *m/z* (M $^+$), calc'd: 1135.7, found 1135.6

CyRLA-240 (6 mg, 12%)
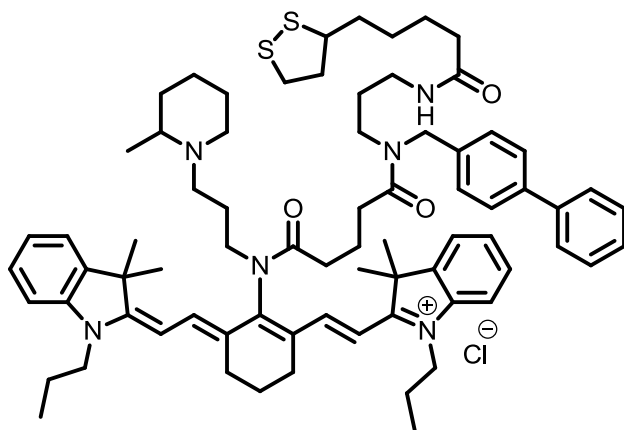
1H-NMR (500 MHz, CDCl$_3$): δ 1.04-1.51 (m, 16H), 1.62 (s, 6H), 1.64 (s, 6H), 1.69-1.90 (m, 8H), 1.99-2.43 (m, 10H), 2.50-2.61 (m, 6H), 2.76 (m, 2H), 3.05-3.74 (m, 15H), 3.97-4.13 (m, 6H), 4.64 (s, 2H), 6.10 (d, 1H, *J*=14 Hz), 6.16 (d, 1H, *J*=14 Hz), 7.05-7.53 (m, 17H), 7.54 (d, 1H, *J*=13.5 Hz), 7.57 (d, 1H, *J*=13.5 Hz). ESI-MS *m/z* (M $^+$), calc'd: 1183.7, found 1183.6

4.5.2 Synthesis CyRLA library

Synthesis of lipoic acid nitrophenol resin:

Aminomethyl nitrophenol polystyrene resin was prepared according to reported procedures. The nitrophenol resin (2 g, 2.9 mmol, 1 eq.) was swollen in 10 mL of DMF, and lipoic acid (2 g, 10 mmol, 3.3 eq.), N,N'-diisopropylcarbodiimide (1.2 mL, 12 mmol, 4 eq.) and a catalytic amount of DMAP (20 mg) were added to the resin, which was continuously shaken

for 24 h at r.t. Subsequently, the resin was washed with DCM (10×25 mL) and dried under vacuum until use.

General procedure for the synthesis of the CyRLA library

To synthesized CyRLA library, each of 1 μmol CyR library compound (80 compounds) was taken according to their plate code in the 2 mL of 96-deep well plate. About 30 mg (~ 20 μmol, 20 eq.) of active-ester resin was added to the each well of the CyR library containing plate. Then, DCM: ACN (7:1) solvent mixture of around 500 μL and catalytic amount of saturated solution of $NaHCO_3$ were poured in to each well. The plate was kept in the shaker with moderate shaking for 6 hours. Then, the solution was filtered from the resin and dried to obtain pure products.

4.5.3 Cell preparation and SERS screening

mESC was maintained on gelatinized tissue culture dishes in high-glucose DMEM supplemented with 20% ES FBS, 1% Pen Strep Glutamine, 1% Non Essential Amino acid, 0.1% β-mercaptoethanol and 100 U/ml leukemia inhibitory factor (LIF, Chemicon). For trypsinization, after removing the old media and washing by PBS (pH 7.3) the cells were incubated in their culture plates using 0.25% trypsin with 1 mM EDTA solution (Invitrogen) for 3 min at 37 °C to obtain a single cell suspension. After neutralizing the trypsin by media spin down (1500 rpm for 3min) in a falcon tube to collect the pellet which is subcultured in non gelatineted cell culture dishes in the mESC media without leukemia inhibitory factor (LIF) and incubate for a 4-6 days to make an embryonic body. After neutralizing the trypsin by media spin down (1500 rpm for 3min) in a falcon tube to collect the pellet of embryonic body which is

subcultured in gelatin coated chamber slide with mESC culture media without LIF.

4.5.4 SERS signal from mESc

When the three germ layers has formed on the slide chamber, 50 μL of each antibody conjugated three nanotags nanotags (Cy7LA-CD184, CyRLA-10-CD-34 and Cy7.5LA-Notch1 anti) were applied in three individual slide chambers of glass slide. Furthermore, one of chamber was treated with the mixture of three nanotags having three different antibodies (intensity of three nanotags were equalized at their multiplexing peaks, 503 cm^{-1} for Cy7LA, 523 cm^{-1} for CyRLA and 584 cm^{-1} for Cy7.5LA). The nanotags treated slide chamber was incubate for 2 h and washed carefully by media. Briefly, the washing steps were performed by applying 500 μL of media and removed it after 5 min incubation. This process was repeated for three times to complete removal of excess non interacting nanotags. This glass slide chamber was covered with glass slide and SERS spectra were measured. Raman experiments were performed in a Renishaw InVia Raman microscope with a laser beam directed to the sample through 50X objective lens and a Peltier cooled CCD detector. Samples were excited with a 785 nm excitation wavelength laser, and Raman spectra were collected in the range of 400 to 2000 cm^{-1} with 1 cm^{-1} resolution. Acquisition time for all spectra was 10 s.

4.5.5 Antibody conjugation of SERS nanotags

The carboxylic acids groups of BSA were activated with *N*-(3-(dimethylamino)-propyl)-*N'*-ethylcarbodiimide (EDC) (125 nmol) and *N*-hydroxysuccinimide (NHS) (125 nmol. The activated particles were then reacted with mouse monoclonal anti-CD-184, anti-CD-34 and anti-Notch1 at

25 °C for 2 h and then overnight incubation at 4 °C. Non-specific binding chemicals and antibodies were removed by centrifugation (10000 rpm, 10 min) and the final nanotags were re-suspended in PBS and stored at 4 °C.

4.6 References

1) S. Keren, C. Zavaleta, Z. Cheng, A. de la Zerda, O. Gheysens and S. S. Gambhir, *P. Natl. Acad. Sci. U.S.A.*, 2008, **105**, 5844.

2) M. Gellner, K. Kompe and S. Schlucker, *Anal. Bioanal. Chem.*, 2009, **394**, 1839.

3) K. C. Bantz, A. F. Meyer, N. J. Wittenberg, H. Im, O. Kurtulus, S. H. Lee, N. C. Lindquist, S. H. Oh and C. L. Haynes, *Phys. Chem. Chem. Phys.*, 2011, **13**, 11551.

4) K. K. Maiti, A. Samanta, M. Vendrell, K. S. Soh, M. Olivo and Y. T. Chang, *Chem.Commun* , 2011, **47**, 3514.

5) A. Matschulat, D. Drescher, J. Kneipp, ACS Nano 2010, 4, 3259.

6) K. K. Maiti, U. S. Dinish, A. Samanta, M. Vendrell, K. S. Soh, S. J. Park, M. Olivo and Y. T. Chang, *Nano Today*, 2012, **7**, 85.

7) J. J. Cunningham, T. M. Ulbright, M. F. Pera and L. H. J. Looijenga, *Nat Biotechnol*, 2012, **30**, 849.

8) H. Hentze, P. L. Soong, S. T. Wang, B. W. Phillips, T. C. Putti and N. R. Dunn, *Stem Cell Res*, 2009, **2**, 198.

9) H. Jang, Y. K. Kim, S. R. Ryoo, M. H. Kim and D. H. Min, *Chem. Commun.*, 2010, **46**, 583.

10) C. C. Lin, Y. M. Yang, Y. F. Chen, T. S. Yang and H. C. Chang, *Biosens. Bioelectron.*, 2008, **24**, 178.

11) S. Lee, H. Chon, M. Lee, J. Choo, S. Y. Shin, Y. H. Lee, I. J. Rhyu, S. W. Son and C. H. Oh, *Biosens. Bioelectron.*, 2009, **24**, 2260.

12) D. Graham, D. G. Thompson, W. E. Smith and K. Faulds, *Nat. Nanotechnol.*, 2008, **3**, 548.

13) L. Sun, K. B. Sung, C. Dentinger, B. Lutz, L. Nguyen, J. W. Zhang, H. Y. Qin, M. Yamakawa, M. Q. Cao, Y. Lu, A. J. Chmura, J. Zhu, X. Su, A. A. Berlin, S. Chan and B. Knudsen, *Nano. Lett.*, 2007, **7**, 351.

14) X. M. Qian, X. H. Peng, D. O. Ansari, Q. Yin-Goen, G. Z. Chen, D. M. Shin, L. Yang, A. N. Young, M. D. Wang and S. M. Nie, *Nat. Biotechnol.*, 2008, **26**, 83-90.

Chapter 5

Possibility of live B-Lymphocytes imaging by novel BODIPY probe: CDg6
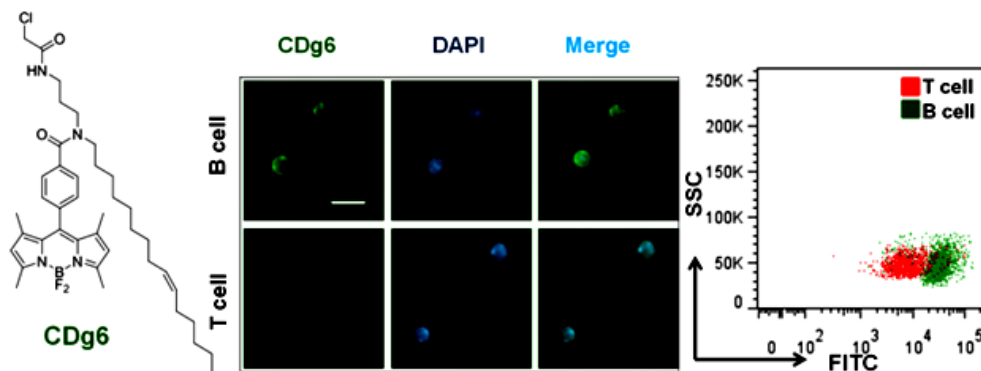
5.1 Introduction

B-and T-cells are lymphocytes, type of white blood cells which are morphologically similar. B-cells, in particular, play a large role in mediating humoral immune responses as well as in autoimmune diseases like systemic lupus erythematosus (SLE)[1] and rheumatoid arthritis[2]. Despite its well studied roles within the immune system, B-cell detection remains very challenging due to the morphological similarities between B-and T-cells. Current methods of discriminating these cells require the use of cell-specific antibodies involved in either immunophenotyping using flow cytometry or immunocytochemistry. These identification techniques while highly specific either activate the cells via antibody binding or kill the cells via fixation for immunofluorescence rendering them less desirable. These shortcomings warrant the needs to develop a novel fluorescent probe for B-cell that displays high target specificity in live cells and at the same time low potency to activate them. Fluorescent probes are powerful tools which enable us to visualize the polymeric biomolecules or cellular organelles efficiently.[3] Fluorescent small molecules are the major toolbox, have been extensively used for probe development. Several DOFL scaffolds including coumarin,[4a,b] dapoxyl,[4c] styryl,[4d] hemicyanine,[4e] rosamine,[5a] and BODIPY[5b] have been developed and their potential application to imaging probe development demonstrated. Our group have utilized combinatorial chemistry to develop several diversity-oriented fluorescence libraries (DOFL) and successfully applied them to the discovery of imaging probes for a number of biological targets.[6] Among them, BODIPY scaffold is ubiquitously chosen as a versatile fluorophore because of its high quantum yield, tunable fluorescence characteristics, high

photostability, and narrow emission bandwidth.[7] So far, numerous labeling agents and probes derived from the BODIPY scaffold have been reported and even commercialized.[8a,b] We recently reported the solution as well as solid-phase syntheses of BODIPY libraries (i.e., BD[9a,b] and BDM[10], BDD[11]). Motivated by this synthesis, I have synthesized BODIPY based library, BDR, BDRCA and BDRAC in solid phase and applied them in development of B cell imaging probe.

5.2 Objectives

B-cells are lymphocytes that play a large role in the humoral immune response of our body as well as in autoimmune diseases. Via image based high throughput screening of BODIPY based library BDR, BDRCA and BDRAC, we discovered a small molecule probe and named it Compound of Designation green 6 (CDg6) that stains mouse B-cells selectively. Here, diversity oriented solid phase synthesis was adopted to successfully modify the BODIPY core scaffold for generating these libraries. The photophysical characterization was also carried out for these libraries.

5.3 Results and Discussion

5.3.1 Synthesis of BDR Library

In our present work, we have synthesized, BODIPY-based library, BDR and its derivatives BDRCA and BDRAC using solid-phase chemistry to provide a set of structurally diverse fluorescent compounds. For the BDR library synthesis (**Scheme 5.1**), carboxylic acid containing BODIPY scaffold **2** was used as the key intermediate. The general synthetic strategy of BODIPY acid **2** involves two steps (40% overall yield) reaction process. First, BODIPY ester **1** was synthesized in situ by treating BF$_3$-OEt$_2$ after condensation

reaction between the methyl 4-(chlorocarbonyl)benzoate and 2,4-dimethyl pyrrole then followed by mild basic hydrolysis of that ester provided the key intermediate of BODIPY acid **2**. Then the structurally diverse BDR library was synthesized using previously reported robust solid phase synthesis technique.[12] The wide structural diversity was achieved as the solid phase secondary amines **5** by simple reaction between the bromopropylamine loaded resins **4** with the series of primary amines (**Chart 5.1**). Then the key intermediate **2** was coupled to this solid phase amine building block by using a standard acid– amine coupling protocol. The final step of acidic cleavage from the solid supported compounds **3** yielded 80 very pure members of the BDR library (average purity is 90% without further purification at 350 nm, **Table 5.1**).

Scheme 5.1 Synthesis of **BDR** library

80 **BDR** Compounds
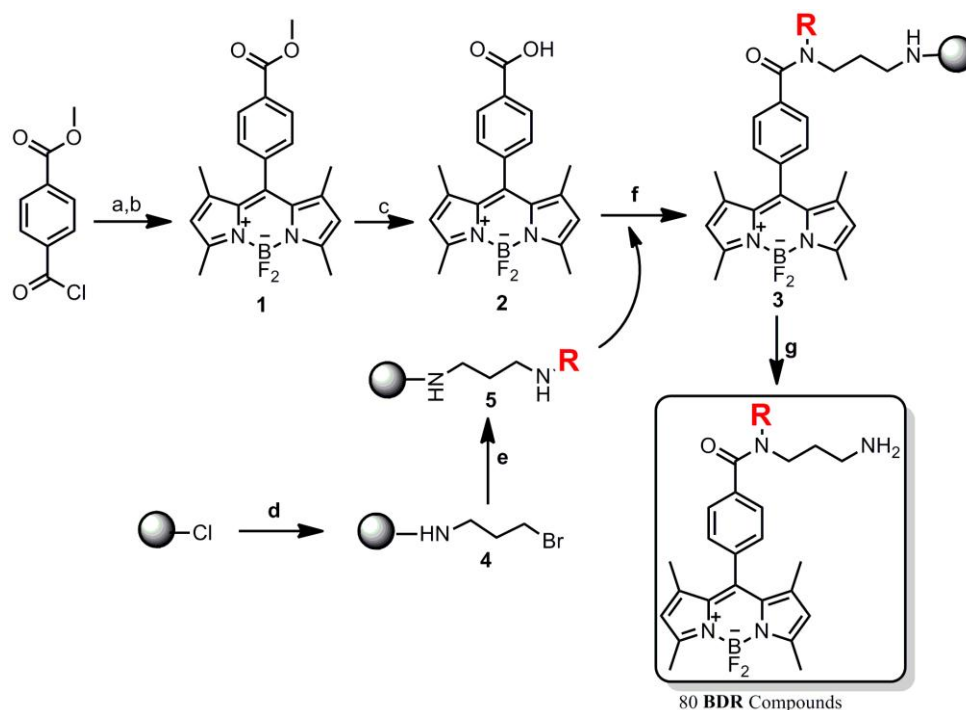
Reagents and conditions: (a) DCM, 2,4-dimethlypyrrole, r.t , 4 h.; (b) DCM, BF$_3$-OEt$_2$, TEA, rt, 12 h.; (c) MeOH:DCM (3:1), 0.2(N) KOH, r.t, 24 h.; (d) DIEA, THF, 3-bromopropylamine, r.t., 12 h.; (e) DIEA, RNH$_2$, NMP, 70 $^{\circ}$C, 12 h.; (f) DMF, HATU, DIEA, r.t. 24 h.; (g) 0.5% TFA in DCM , r.t., 40 min

This synthetic protocol provides an amino-linker in the BODIPY scaffold in addition to the structural diversity. Using that primary amine, I synthesized the acetyl and choloroacetyl version of BDR (BDRAC and BDRCA) compounds using solid phase activated ester chemistry. Firstly, active ester resins were prepared by treating the nitrophenol resin with chloroacetyl chloride. The reaction of the resulting resin with the highly reactive propylamine moiety of BDR compounds in the presence of catalytic amount of mild base NaHCO$_3$ afforded the corresponding BDRCA and BDRAC compounds (**Scheme 5.2**). The reaction was completed within 2 hours and the products were obtained after a simple filtration with an average purity of above 90% without further purification. All the library compounds showed a green range of fluorescence as expected (average excitation at 450 nm and emission at 520 nm). The quantum yield of each molecule varied from 0.3 to 0.6 reflecting diverse structural and electronic characteristics (**Figure 5.1**, **Table 5.2 and 5.3**)

Scheme 5.2 Synthesis of BDRCA and BDRAC derivatives
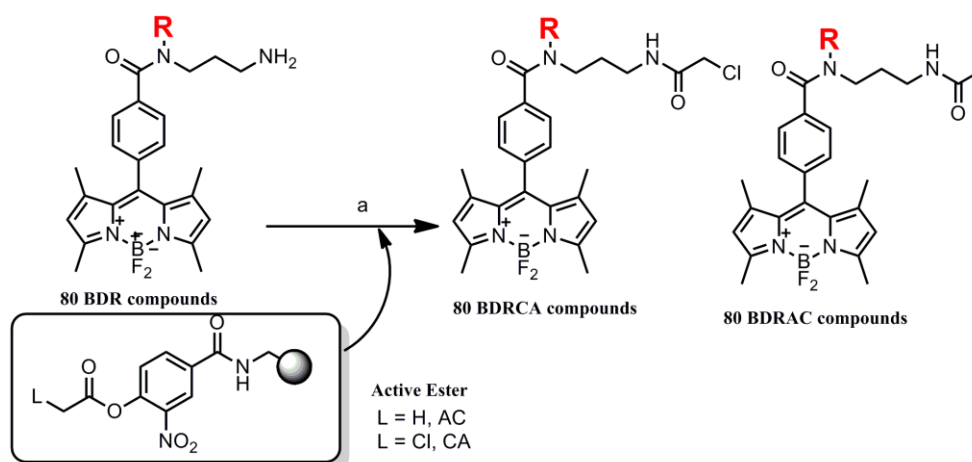
Reagents and conditions: (a) DCM/ACN (7:1), NaHCO$_3$, r.t., 2 h

Chart 5.1 Amine building blocks for BDR library

108
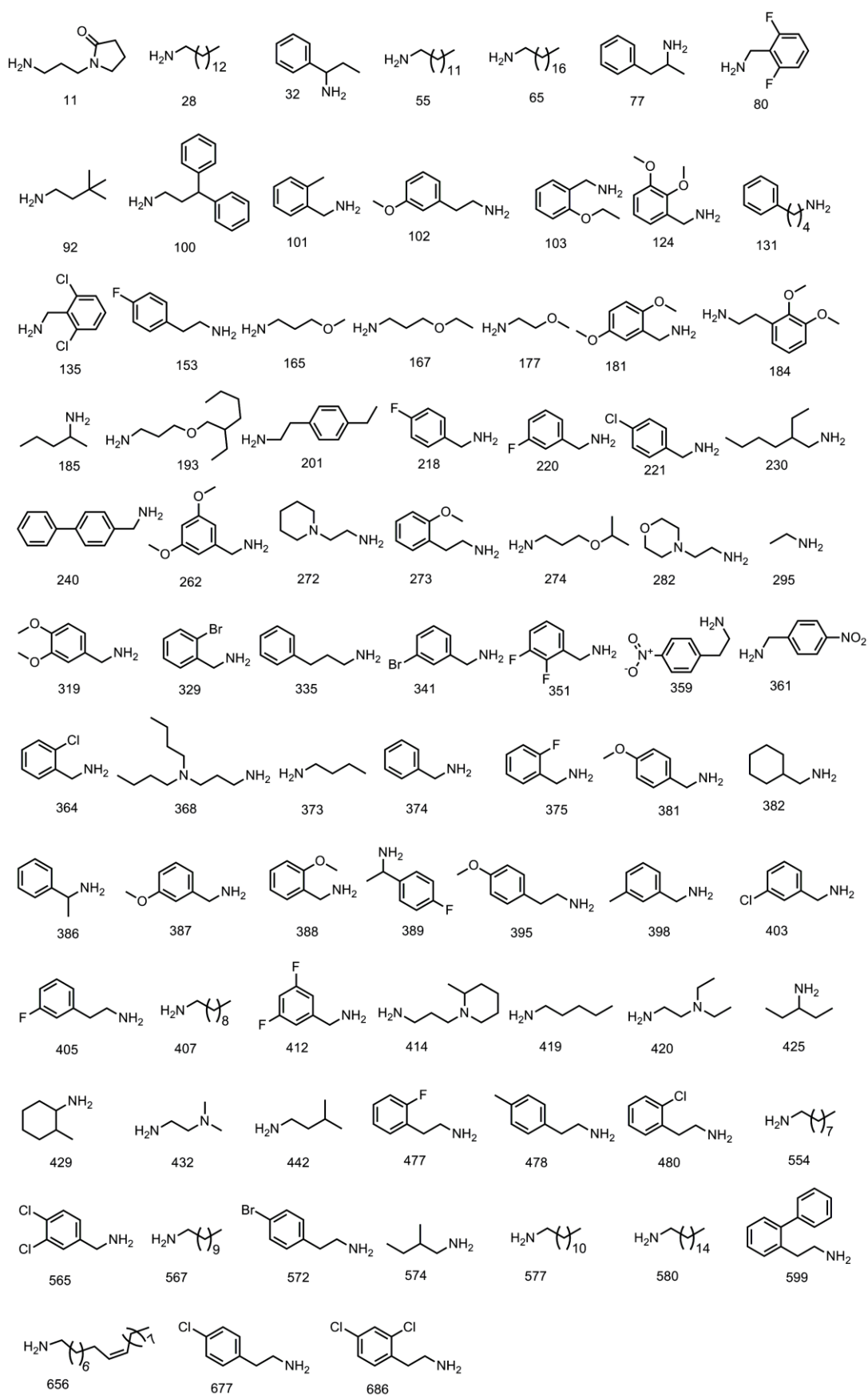
Table 5.1 Characterization by HPLC-MS and photophysical property of BDR library

Compound	M$^+$(calc.)	(M +H)	λ_{abs}(nm)	λ_{em}(nm)	ϕ^{*1}	Purity^{*2}
BDR 389	546.3	547.3	501	518	0.41	92
BDR 677	562.2	563.3	502	519	0.40	90
BDR 273	558.3	559.3	502	518	0.35	91
BDR 388	544.3	545.3	501	517	0.39	94
BDR 398	528.3	529.5	501	517	0.40	93
BDR 565	582.2	583.2	502	517	0.75	85
BDR 220	532.3	533.3	503	518	0.31	90
BDR 240	590.3	591.3	502	517	0.32	90
BDR 103	558.3	559.3	501	519	0.28	90
BDR 28	620.4	621.4	502	518	0.44	91
BDR 407	564.4	565.4	501	517	0.31	89
BDR 262	574.3	575.3	502	518	0.34	94
BDR 335	542.3	543.3	503	519	0.38	93
BDR 11	549.3	550.3	502	518	0.38	93
BDR 274	524.3	525.3	501	519	0.46	95
BDR 124	574.3	575.3	502	517	0.36	95
BDR 387	544.3	545.3	502	517	0.46	92
BDR 429	520.3	521.3	501	517	0.48	92
BDR 382	520.3	521.3	501	518	0.35	92
BDR 230	536.3	537.4	502	519	0.36	93
BDR 181	574.3	575.3	503	518	0.37	90
BDR 580	648.5	649.5	502	517	0.41	90
BDR 405	546.3	547.3	501	517	0.41	89
BDR 193	595.4	596.4	502	517	0.4	93
BDR 218	532.3	533.3	501	518	0.55	93
BDR 478	542.5	543.3	502	517	0.36	92
BDR 419	494.3	495.3	503	519	0.34	92
BDR 386	528.3	529.3	502	518	0.51	92
BDR 442	494.3	495.3	501	517	0.43	93
BDR 599	604.3	605.3	501	518	0.39	91

BDR 381	544.3	545.3	501	519	0.33	92
BDR 55	606.4	607.5	502	518	0.32	89
BDR 477	546.3	547.3	503	519	0.40	93
BDR 92	508.4	509.3	502	517	0.37	93
BDR 480	562.2	563.3	501	518	0.44	91
BDR 77	542.3	543.3	502	519	0.44	90
BDR 368	593.4	594.4	501	518	0.37	94
BDR 403	548.9	549.2	502	519	0.17	91
BDR 131	556.3	557.3	503	517	0.34	91
BDR 374	514.3	515.3	502	518	0.69	91
BDR 185	494.3	495.3	503	519	0.35	93
BDR 135	582.2	583.2	502	518	0.51	89
BDR 80	550.4	551.3	501	519	0.34	90
BDR 184	588.3	589.4	501	517	0.44	91
BDR 153	546.2	547.3	501	518	0.69	91
BDR 375	532.3	533.4	502	519	0.33	91
BDR 201	556.3	557.4	503	518	0.35	92
BDR 100	618.3	619.4	502	517	0.28	92
BDR 177	482.3	516.0	501	517	> 0.99	91
BDR 412	550.4	551.4	501	517	0.37	91
BDR 319	574.3	575.3	502	518	0.22	91
BDR 686	596.2	597.3	501	517	0.35	92
BDR 567	578.4	579.4	502	519	0.36	91
BDR 395	558.3	559.3	502	518	0.58	92
BDR 554	550.4	551.4	501	517	0.9	90
BDR 351	550.2	551.3	501	518	0.34	94
BDR 101	528.4	529.4	502	519	0.40	90
BDR 364	548.2	549.2	503	518	0.40	90
BDR 414	563.3	564.4	502	519	0.31	91
BDR 329	592.3	593.4	501	517	0.32	90
BDR 221	548.2	549.2	502	517	0.4	94
BDR 572	606.2	607.2	502	517	0.51	90
BDR 656	674.5	675.5	502	518	>0.99	90

Compound	M^+(calc.)	(M+H)(exp.)	λ_{abs}(nm)	λ_{em}(nm)	ϕ^{*1}	Purity^{*2}
BDR 432	495.3	496.3	501	519	0.41	90
BDR 373	480.2	481.3	501	518	0.77	89
BDR 425	494.3	495.4	502	517	0.54	89
BDR 102	558.3	559.3	501	518	>0.99	90
BDR 574	494.3	495.3	502	519	0.48	90
BDR 272	535.3	536.3	502	517	0.48	89
BDR 577	592.4	593.4	501	518	0.86	90
BDR 420	523.3	524.3	501	519	0.29	90
BDR 282	537.3	538.3	502	518	0.59	90
BDR 295	494.2	495.3	503	517	0.96	93
BDR 165	546.3	547.3	502	517	0.82	91
BDR 167	510.3	511.3	501	517	0.75	88
BDR 65	676.5	677.5	502	518	0.50	92
BDR 32	542.3	543.3	501	517	0.27	91
BDR 359	573.3	574.4	502	519	0.31	92
BDR 361	559.3	560.3	502	518	0.40	91
BDR 341	594.1	595.2	501	517	0.61	90

Table 5.2 Characterization by HPLC-MS and photophysical property of BDRCA library

Compound	M^+(calc.)	(M+H)(exp.)	λ_{abs}(nm)	λ_{em}(nm)	ϕ^{*1}	Purity^{*2}
BDRCA 389	622.2	623.3	501	518	0.46	90
BDRCA 677	638.2	639.2	502	519	0.29	88
BDRCA 273	634.3	635.3	502	519	0.37	89
BDRCA 388	620.2	621.2	502	518	0.45	92
BDRCA 398	604.3	605.3	501	518	0.42	91
BDRCA 565	658.2	659.3	502	519	0.43	87
BDRCA 220	608.2	533.3	503	519	0.53	92
BDRCA 240	666.3	667.4	502	519	0.39	92
BDRCA 103	634.3	635.3	502	519	0.65	91
BDRCA 28	696.4	697.4	502	517	0.39	91
BDRCA 407	640.3	641.3	502	517	0.31	95

BDRCA 262	650.3	651.4	502	519	0.31	92
BDRCA 335	618.3	619.3	503	518	0.41	91
BDRCA 11	625.3	626.3	502	519	0.42	91
BDRCA 274	600.3	601.3	502	519	0.39	90
BDRCA 124	650.3	651.3	502	519	0.41	89
BDRCA 387	620.2	621.3	502	518	0.35	92
BDRCA 429	596.3	597.3	502	518	0.34	90
BDRCA 382	596.3	597.3	502	517	0.72	93
BDRCA 230	612.3	613.3	502	518	0.37	94
BDRCA 181	650.3	651.3	503	518	0.41	90
BDRCA 580	724.4	725.4	502	518	0.31	91
BDRCA 405	622.2	623.2	502	519	0.45	91
BDRCA 193	670.4	671.4	502	518	0.50	95
BDRCA218	608.2	609.2	502	518	0.44	92
BDRCA 478	618.3	619.3	502	517	0.36	91
BDRCA 419	570.3	571.3	503	519	0.44	91
BDRCA 386	604.3	605.3	502	518	0.35	90
BDRCA 442	570.3	571.4	501	519	0.62	89
BDRCA 599	680.3	681.3	502	519	0.46	92
BDRCA 381	620.2	621.3	502	518	0.38	90
BDRCA 55	682.4	683.4	502	519	0.37	93
BDRCA 477	622.2	623.2	503	518	0.45	94
BDRCA 92	584.3	585.2	502	519	0.36	90
BDRCA 480	638.2	638.2	502	518	0.48	90
BDRCA 77	618.3	619.4	502	519	0.53	92
BDRCA 368	669.4	670.3	502	519	0.50	93
BDRCA 403	624.2	625.2	502	519	0.32	92
BDRCA 131	632.3	633.4	503	517	0.85	93
BDRCA 374	590.2	591.3	502	519	0.37	87
BDRCA 185	570.3	571.3	503	518	0.38	92
BDRCA 135	658.2	659.3	502	517	0.38	91
BDRCA 80	626.2	627.2	501	519	0.40	91
BDRCA 184	664.3	665.3	502	519	0.50	93

BDRCA 153	658.2	659.2	502	517	0.50	95
BDRCA 375	608.2	609.2	502	519	0.46	92
BDRCA 201	632.3	633.4	503	519	0.45	90
BDRCA 100	694.3	695.3	502	518	0.41	90
BDRCA 177	558.2	559.4	502	519	0.79	92
BDRCA 412	626.2	627.2	502	518	0.43	93
BDRCA 319	650.3	651.3	502	519	0.26	92
BDRCA 686	672.1	673.2	502	519	0.35	93
BDRCA 567	654.4	655.5	502	519	0.39	87
BDRCA 395	634.3	635.3	502	518	0.50	92
BDRCA 554	626.3	627.3	501	519	0.50	91
BDRCA 351	626.2	627.3	502	519	0.45	91
BDRCA 101	604.3	605.3	502	517	0.54	93
BDRCA 364	624.2	625.2	503	518	0.46	95
BDRCA 414	639.3	640.4	502	519	0.97	92
BDRCA 329	704.1	705.1	502	519	0.44	90
BDRCA 221	624.2	625.3	502	519	0.40	94
BDRCA 572	682.2	683.3	502	518	0.42	95
BDRCA 656	750.5	751.5	502	518	0.47	92
BDRCA 432	571.3	572.4	501	519	0.34	91
BDRCA 373	556.3	557.3	502	519	0.54	91
BDRCA 425	570.3	571.3	502	519	0.53	95
BDRCA 102	634.3	635.3	501	519	0.44	92
BDRCA 574	570.3	571.3	502	518	0.41	91
BDRCA 272	611.3	612.3	502	518	0.83	91
BDRCA 577	668.4	669.4	501	519	0.52	90
BDRCA 420	599.3	600.3	502	519	0.45	89
BDRCA 282	613.3	614.3	502	519	0.31	92
BDRCA 295	572.2	573.2	503	519	0.39	93
BDRCA 165	586.3	587.3	502	519	0.55	87
BDRCA 167	752.5	753.5	501	519	0.56	92
BDRCA 65	618.3	619.3	502	519	0.43	91
BDRCA 32	685.2	686.2	501	519	0.65	91

Compound	M+(calc.)	(M+H)(exp.)	λ_{abs}(nm)	λ_{em}(nm)	ϕ	Purity
BDRCA 359	671.2	672.2	502	519	0.42	93
BDRCA 361	704.1	705.1	502	519	0.61	95
BDRCA 341	564.2	565.2	501	517	0.52	92

Table 5.3 Characterization by HPLC-MS and photophysical property of BDRAC library

Compound	M+(calc.)	(M+H)(exp.)	λ_{abs}(nm)	λ_{em}(nm)	ϕ[*1]	Purity[*2]
BDRAC 389	588.2	589.4	501	518	0.46	90
BDRAC 677	604.2	585.3	502	519	0.29	88
BDRAC 273	600.3	601.3	502	519	0.37	89
BDRAC 388	586.3	587.3	502	518	0.45	92
BDRAC 398	570.3	570.6	501	518	0.42	91
BDRAC 565	624.2	624.0	502	519	0.43	87
BDRAC 220	574.2	555.2	503	519	0.53	92
BDRAC 240	632.3	613.4	502	519	0.39	92
BDRAC 103	600.3	601.4	502	519	0.65	91
BDRAC 28	662.4	643.4	502	517	0.39	91
BDRAC 407	606.4	607.3	502	517	0.31	95
BDRAC 262	616.3	597.0	502	519	0.31	92
BDRAC 335	584.3	585.1	503	518	0.41	91
BDRAC 11	591.3	572.0	502	519	0.42	91
BDRAC 274	566.3	567.5	502	519	0.39	90
BDRAC 124	616.3	617.3	502	519	0.41	89
BDRAC 387	586.3	587.1	502	518	0.35	92
BDRAC 429	562.3	562.7	502	518	0.34	90
BDRAC 382	562.3	562.6	502	517	0.72	93
BDRAC 230	578.3	579.5	502	518	0.37	94
BDRAC 181	616.3	617.2	503	518	0.41	90
BDRAC 580	690.4	691.3	502	518	0.31	91
BDRAC 405	588.2	587.3[&]	502	519	0.45	91
BDRAC 193	636.4	617.4	502	518	0.50	95
BDRAC218	574.2	555.2	502	518	0.44	92

BDRAC 478	584.3	565.0	502	517	0.36	91
BDRAC 419	536.3	517.2	503	519	0.44	91
BDRAC 386	570.3	571.2	502	518	0.35	90
BDRAC 442	536.3	537.4	501	519	0.62	89
BDRAC 599	646.3	645.1$^{\&}$	502	519	0.46	92
BDRAC 381	586.3	587.3	502	518	0.38	90
BDRAC 55	648.4	629.2	502	519	0.37	93
BDRAC 477	588.2	569.4	503	518	0.45	94
BDRAC 92	550.3	551.0	502	519	0.36	90
BDRAC 480	604.2	585.3	502	518	0.48	90
BDRAC 77	584.3	565.2	502	519	0.53	92
BDRAC 368	635.4	636.3	502	519	0.50	93
BDRAC 403	590.2	591.2	502	519	0.32	92
BDRAC 131	598.3	599.2	503	517	0.85	93
BDRAC 374	556.2	537.1	502	519	0.37	87
BDRAC 185	536.3	536.7	503	518	0.38	92
BDRAC 135	624.2	625.1	502	517	0.38	91
BDRAC 80	592.2	592.2	501	519	0.40	91
BDRAC 184	630.3	631.4	502	519	0.50	93
BDRAC 153	588.3	568.7	502	517	0.50	95
BDRAC 375	574.2	574.5	502	519	0.46	92
BDRAC 201	598.3	598.6	503	519	0.45	90
BDRAC 100	660.3	659.2$^{\&}$	502	518	0.41	90
BDRAC 177	524.2	524.6	502	519	0.79	92
BDRAC 412	592.2	572.6	502	518	0.43	93
BDRAC 319	616.3	616.7	502	519	0.26	92
BDRAC 686	638.2	639.3	502	519	0.35	93
BDRAC 567	620.4	620.5	502	519	0.39	87
BDRAC 395	600.3	581.0	502	518	0.50	92
BDRAC 554	592.3	593.3	501	519	0.50	91
BDRAC 351	592.2	591.4$^{\&}$	502	519	0.45	91
BDRAC 101	570.3	551.1	502	517	0.54	93
BDRAC 364	590.2	591.2	503	518	0.46	95

BDRAC 414	605.3	606.4	502	519	0.97	92
BDRAC 329	634.2	615.0	502	519	0.44	90
BDRAC 221	590.2	571.0	502	519	0.40	94
BDRAC 572	648.2	649.0	502	518	0.42	95
BDRAC 656	716.5	717.4	502	518	0.47	92
BDRAC 432	537.3	538.0	501	519	0.34	91
BDRAC 373	522.3	522.6	502	519	0.54	91
BDRAC 425	536.3	537.3	502	519	0.53	95
BDRAC 102	600.3	581.0	501	519	0.44	92
BDRAC 574	536.3	537.1	502	518	0.41	91
BDRAC 272	577.3	578.4	502	518	0.83	91
BDRAC 577	634.4	635.3	501	519	0.52	90
BDRAC 420	565.3	546.3	502	519	0.45	89
BDRAC 282	579.3	580.5	502	519	0.31	92
BDRAC 165	538.3	539.0	502	519	0.55	87
BDRAC 167	552.3	551.4[&]	501	519	0.56	92
BDRAC 65	718.5	699.4	502	519	0.43	91
BDRAC 32	584.3	585.2	501	519	0.65	91
BDRAC 359	615.3	596.1	502	519	0.42	93
BDRAC 361	601.3	582.2	502	519	0.61	95
BDRAC 341	634.2	615.3	501	517	0.52	92
BDRAC 295	494.3	495.2	503	519	0.39	93

*1 Quantum yields were measured in DMSO, using tetramethyl BODIPY as a standard (ϕ : 0.64, in DMSO). *2 Purities were determined according to UV absorption at 350 nm.ESI-MS positive spectra, HPLC conditions: A: H_2O-HCOOH: 99.9:0.1. B: CH_3CN-HCOOH: 99.9:0.1; gradient 100% A to 95% B (6 min), isocratic 95% B (6-8.2min), gradient 95% B to 100% A (8.2-9 min), isocratic 100% A (9-10 min). Reversephase Phenomenex C18 Luna column (4.6 x 50 mm^2) 3.5 μm, flow rate: 1.0 mL/min. [&] negative mode.
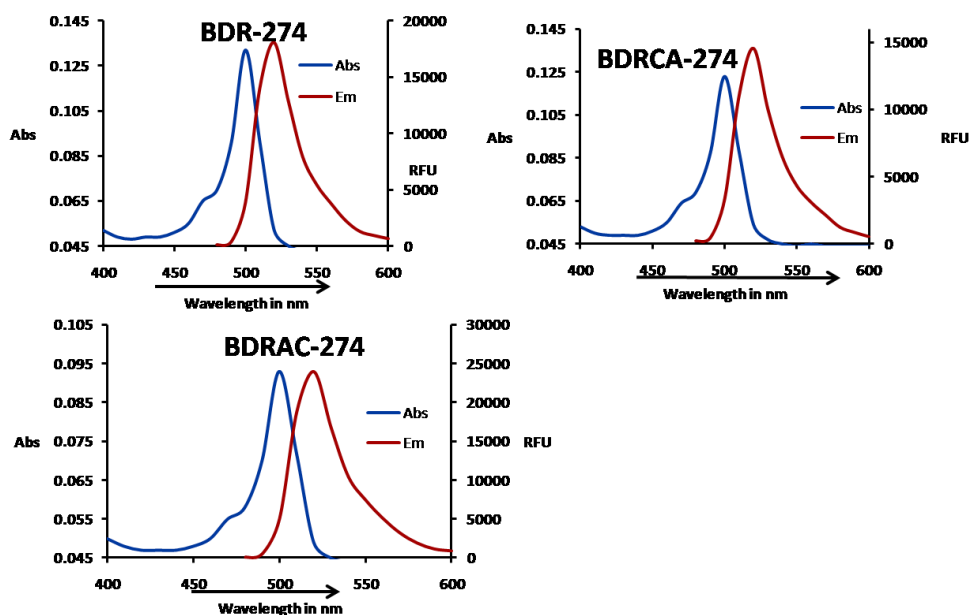
Figure 5.1 Absorption and emission of representative BDR, BDRCA and BDRAC compound.

5.3.2 Discovery of B cell probe

After the synthesis, a high throughput screening was carried out using all these compounds to discover a BODIPY based novel B cell probe. To do that, first each of B-cells and T-cells were obtained from mouse splenocytes after indirect immunomagnetic negative selection due to concern of cell activation by magnetic beads. Then, the separated B-cells and T-cells were a breast seeded in 384 well plate and subsequently 240 compounds from BDR, BDRCA and BDRAC libraries were treated at a concentration of 1 μM. After incubation for 1 h and 4 h, images were acquired using the ImageXpressMICRO system (Molecular Device), a fully-integrated hardware and software system for automated acquisition and analysis of high contents fluorescence cell images. From 1 h incubation staining, we realized that none of our compounds show either B or T-cell selective staining. At the 4 h incubation, Compound of Designation green 6(**CDg6**, λex/λem = 502/518 nm)

117

that presents selective staining only for B-cell not T-cell was chosen as hits (**Figure 5.2-b**) and validated using flow cytometric analysis with the same separated B and T-cell as image screening. (**Figure 5.2-c**).
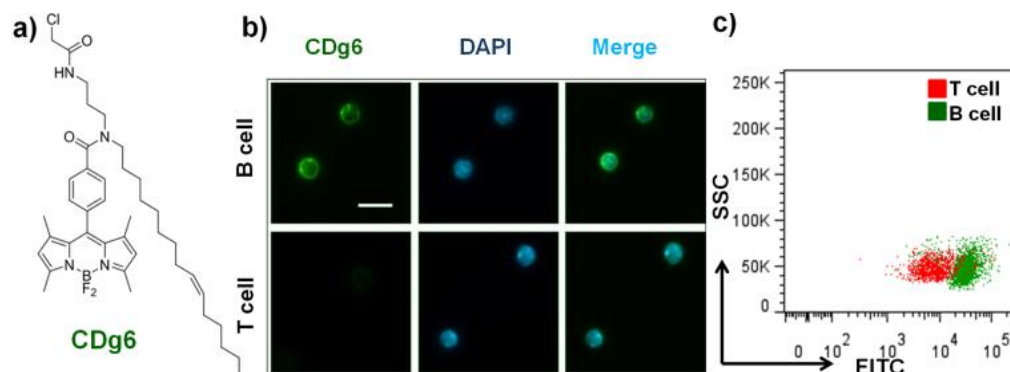
Figure 5.2 Discovery of B-cell selective probe: **CDg6** a) Chemical structure of **CDg6** b) B-cell and T-call were prepared from mouse splenocytes after negative selection using magnetic beads and incubated with 1 μM of **CDg6** for 4 h and 1 μg/mL of Hoechst 33342 for nucleus staining. Scale bar: 10 μm c) Flow Cytometric analysis of separated mouse B-and T-cells with 1 μM of CDg6 at 37°C.

5.3.3 Optimization of B cell staining kinetics

For the optimization of B cell staining kinetics, splenocytes were loaded on flow cytometry every 20 min after staining of **CDg6** at 1 μM at 37 °C (**Figure 5.3-a**). Splenocytes at 90 min after incubation started to show 70% of separation until 240 min, while none of incubation time at 4 °C show difference at all (**Figure 5.3-b**).

118
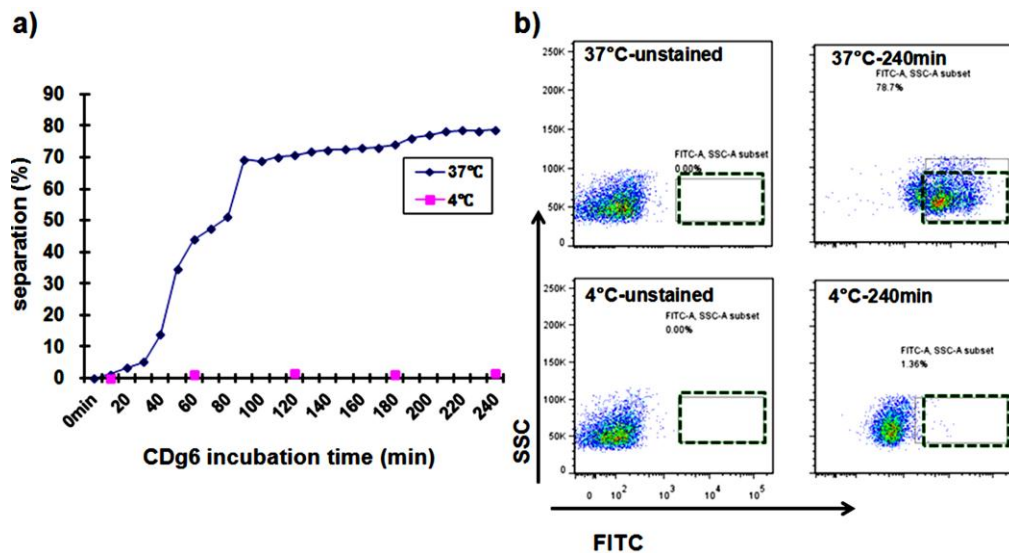
Figure 5.3 B cell staining kinetics using CDg6 a) Seperation kinetics using CDg6 b) Flow Cytometric analysis with time of stained and unstained cells.

5.3.4 Localization of CDg6 in B-cells

From the 60x fluorescence image, CDg6 seems to localize at the plasma membrane of B-cells from splenocytes. To confirm the membrane localization, we use confocal microscopy to obtain high magnification and resolution images of B-cells in conjunction with commercially available CellMask^{TM} plasma membrane stain. From **figure 5.4** below, similar staining pattern was observed between CDg6 and the commercial dye confirming its plasma membrane localization.
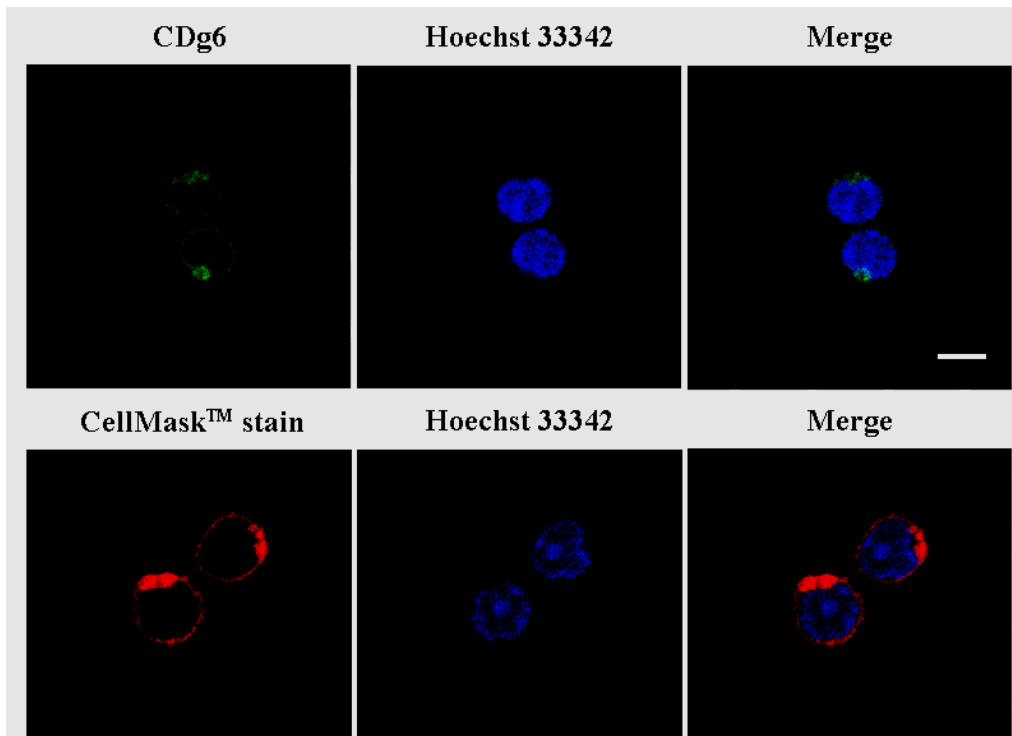
Figure 5.4 Comparison of staining localization of CDg6 with Invitrogen CellMask^{TM} plasma membrane stain. Top panel: cells stained with CDg6. Bottom panel: cells stained with CellMask^{TM} plasma membrane stain. Cells were mounted on a glass slide, CDg6 (FITC filter), Hoechst 33342 (DAPI filter) and CellMask^{TM} plasma membrane stain (Cy5) images were taken using the Nikon Confocal Microscope quipped with x 100 objective lens. Scale bar: 5 μm.

5.3.5 Cytotoxicity of CDg6 in B-cells

To assess the cytotoxicity of CDg6, B-cell viability upon incubation with increasing concentrations of CDg6 with respect to non-CDg6 treated cells was compared. From **figure 5.5**, we observed that even at high concentrations of CDg6 (5 μM), cell viability across a 48 hour period stays similar to non-CDg6 treated cells. In this respect, the low cytoxicity of CDg6 enables high cell survival rates at the recommended 1 μM working concentration.
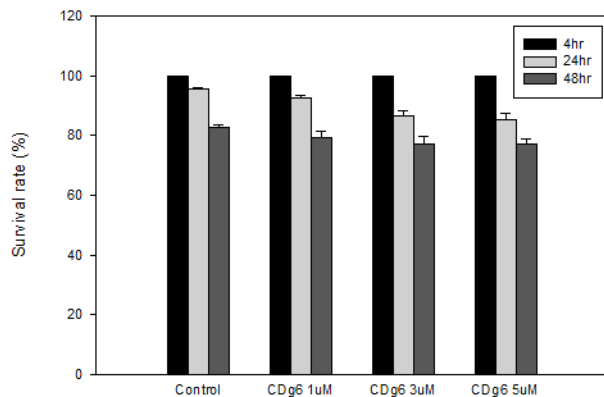
Figure 5.5 Comparison of B-cell survival rates in non-CDg6 treated cells versus CDg6 treated cells at 1 μM, 3 μM and 5 μM over 48 h. The error bars are s.d. over triplicates at each time point and experiment set.

5.3.6 Application of CDg6 for isolation of B cell from mouse splenocytes

To investigate the possibility of **CDg6** for separating B-cells from mouse splenocytes which exist in B and T-cell together, we performed Fluorescent Activated Cell Sorter (FACS) after 4 h staining of **CDg6** at 1 μM. Mouse splenocytes were separated as two populations by fluorescent intensity of **CDg6** (**Figure 5.6-a**). After that, **CDg6** [bright] cells were physically sorted out and confirmed with immunostaining of CD45R antibody that represents B-cell of mouse spleen (**Figure 5.6-b**). For further validation of **CDg6**, we first stained with **CDg6** and CD45R antibody together and loaded them on flow Cytometry to check whether both of them are double stained or not (**Figure 5.7-a**). And also cells were allowed to observe under fluorescent microscopy from FITC and Cy5 filters for **CDg6** and CD45R antibody, respectively (**Figure 5.7-b**). while, **CDg6** [bright] cells were overlapped with CD45R clearly, no double staining with CD3e antibody that represents T-cell of mouse spleen

shows in flow Cytometry (**Figure 5.7-c**) as well as fluorescent images(**Figure 5.7-d**).
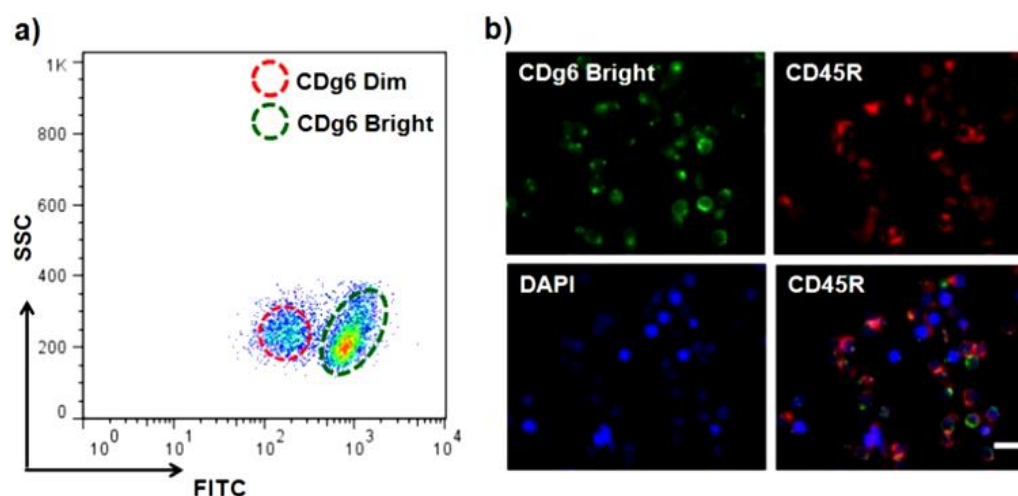
Figure 5.6 Isolation of B-cells with **CDg6** in mouse splenocytes a) FACS dot plot image of **CDg6** stained B-cell not T-cell. b) **CDg6** **bright** cells after sorting were immunostained with CD45R antibody for B-cell and 1 μg/mL of Hoechst 33342 for nucleus. All images taken by fluorescent microscopy were merged together. Scale bar: 10 μm. FITC filter used for CDg6 staining, Cy5 for CD45R antibody and DAPI for Hoechst 33342.
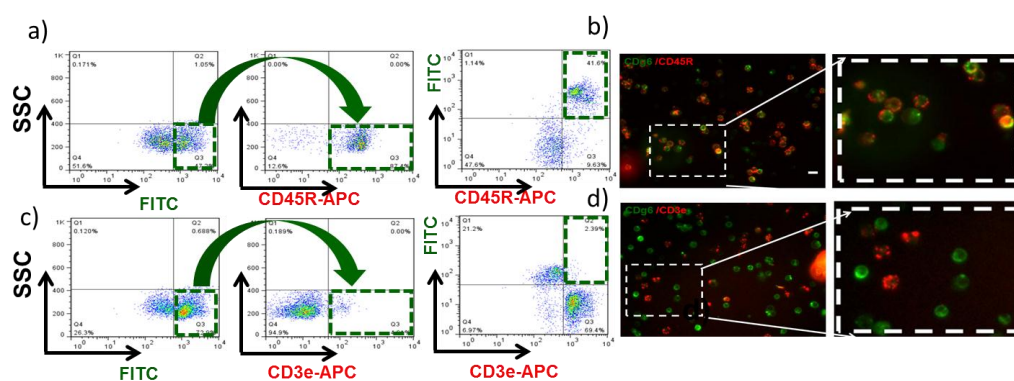
Figure 5.7 Selective staining of B-cell against T-cell by **CDg6** a) Flow Cytometry dot plot image CDg6 (x-axis) and CD45R antibody staining (y-axis) b) The fluorescent images of double staining CDg6 (green) and CD45R antibody (red) and white dot box image zoomed in left. c) Flow Cytometry dot plot image of CDg6 (x-axis) and CD43e antibody staining (y-axis) d) The fluorescent images of double staining of CDg6 (green) and CD3e antibody (red) and white dot box image zoomed in left. Scale bar: 10 μm.

5.3.7 Structural Activity Relationship studies

It is noted that the **CDg6** contains 18-carbon alkyl chain which is derived from the olylamine as the part of structural diversity. Oleyl amine has one un-saturation at the 9th position in the alkyl chain and we assumed that it may have a role in the B-cell staining. Hence, we decided to check the effectiveness of B-cell staining in the saturated form of the BDR-derivatives. The BDR derivative (BDRCA-65) of 18-carbon saturated alkyl chain from the stearylamine has also B-cell staining capability and can be considered as the B-cell hit. As 18-carbon chain has been a hit, there is a huge curiosity to check the effect of chain length variation in other BDR derivatives (**Table 5.4**).
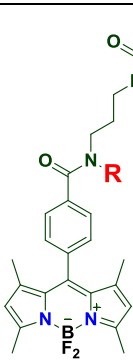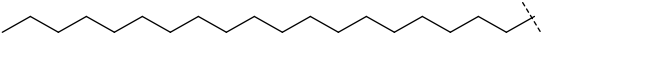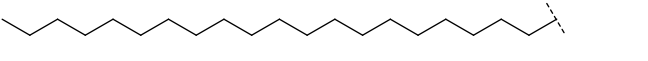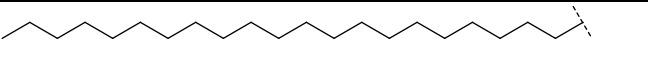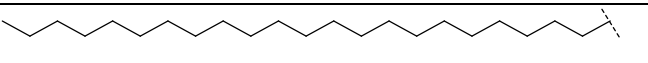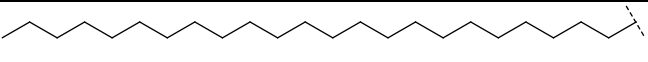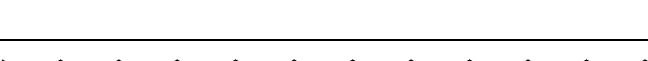
Table 5.4 Structure of derivatives with alkyl chain length between 4 –18 carbon long.

General structure	**R** group with Carbon atoms	Compound
		BDRCA-373
		BDRCA-419
		BDRCA-554
		BDRCA-407
		BDRCA-567
		BDRCA-577
		BDRCA-55
		BDRCA-28
		BDRCA-580
		BDRCA-65

After all these it became interesting to see the Structural Activity Relationships beyond the 18-carbon alkyl chain. Hence, we synthesized BDR derivatives having alkyl chain length up to 24 carbons (**Table 5.5**). Among

them, TB-G-19CA, TB-G-21CA, TB-G-23CA and TB-G-24CA (19, 21, 23 and 24 alkyl chain containing BODIPY respectively) were synthesized by using the previously described BDRCA synthesis protocol. For the TB-G-20C and TB-G-22C synthesis, modified protocol was used.

Table 5.5 Structure of derivatives with alkyl chain length between 19 –24 carbon long.

Structure	**R** group with Carbon atoms	Compound
		TB-G-19CA
		TB-G-20CA
		TB-G-21CA
		TB-G-22CA
		TB-G-23CA
		TB-G-24CA

Scheme 5.3 Synthesis of 20 and 22 carbon chain BDRCA derivatives

124
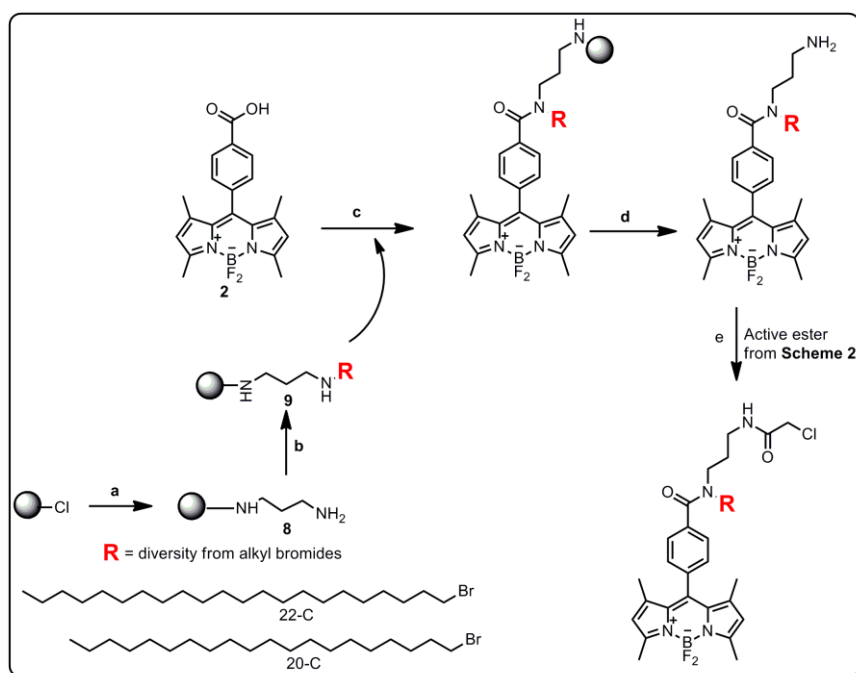
Reagents and conditions: (a) DCM, propane-1,3-diamine, r.t., 12 h.; (b) DIEA, RCH$_2$Br, NMP, 70 ^{o}C, 12 h.; (c) DMF, HATU, DIEA, r.t. 24 h.; (d) 0.5% TFA in DCM , r.t., 40 min.; (e) DCM/ACN (7:1), NaHCO$_3$, r.t., 2 h

5.3.8 Alkyl chain length effect on B cell staining

Then, the result of these compounds indicates that the newly synthesized BDR derivatives of more than 18 carbons also have B-cell staining. To check whether this theory corresponds with selectivity of B-cell staining as well as separation of two populations, we carried out flow Cytometry with splenocytes after staining of all the BDR compounds which have different alkyl chain length at 1 μM for 4 h at 37°C (**Figure 5.8-a**). From 14 to18 carbon compounds showed two separated populations and we confirmed bright separation of 18 carbon compound by immunostaining. 18-carbon [bri] population was overlapped with CD45R for B-cell antibody (**Figure 5.8-b**), not CD3e for T-cell antibody (**Figure 5.8-c**). It suggests that the alkyl chain length nearer to the 18-carbon is more effective for B-cell selectivity.

125
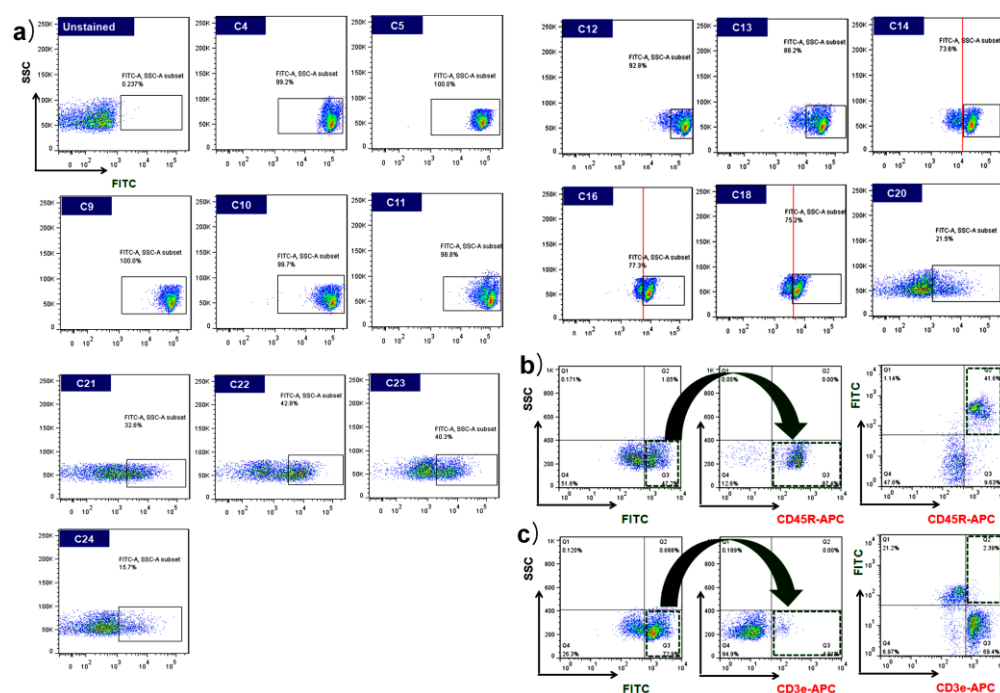
Figure 5.8 Alkyl chainlegth effect in B cell staining: a) Flow Cytometric analysis of separated mouse B-and T-cells with 1 µM of various long chain derivatives b) and c) B- cell and T cell antibody confirmation.

5.4 Conclusions

In summary, we have developed a novel bioimaging probe CDg6 for B-cell detection which exhibits comparable selectivity for B-cells as antibodies without activating them and having low toxicity. The experimental results presented herein demonstrate the utility of CDg6 for the facile identification and isolation of B-cells from splenocytes and peripheral blood lymphocytes without the aid of antibodies with high degree of efficiency. To the best of our knowledge, no B-cell selective fluorescent probe has been reported yet. This new probe will be a useful tool to aid the study of B-cell detection, proliferation and migration in the immune system which is key information in the study of role of B-cell in autoimmune diseases and humoral immunity.

5.5 Experimental methods

Material and methods

Amine and few bromide building block and all other chemicals and solvents for the synthesis were purchased from the Alfa Aesar, Fluka, Acros, MERCK, and Sigma Aldrich and were used without any purification. Merck Silica Gel 60 (particle size: 0.04-0.063 mm, 230-400 mesh) was used for the normal phase column chromatographic purification. From BeadTech Inc., Korea, 2-chlorotrityl alcohol resin (1.37 mmol/g) was purchased. For analytical characterization of BDR compounds HPLC-MS (Agilent-1200 series) with a DAD detector and a single quadrupole mass spectrometer (6130

series) with an ESI and sometimes with an APCI probe were used. Analytical process, except specified: eluents: A: H_2O (0.1% HCOOH), B: ACN (0.1% HCOOH), C_{18} (2) Luna column (4.6 x 50mm^2, 5μm particle size) was used. ^{1}H-NMR and ^{13}C-NMR spectra were recorded on both Bruker Avance 300 MHz and 500 MHz NMR spectrometer, and chemical shifts are expressed in parts per million (ppm) and approximate coupling constants were calculated in Hz. Quantum yields and all other photophysical properties of BDR derivatives were performed in Biotek reader spectrophotometer (Molecular Devices) instrument and the obtained data were analyzed using the Microsoft Office Excel 2007.

5.5.1 Characterization data for CDg6 (BDRCA-656) and other BDR derivatives

CDg6 (9 mg, 25%)
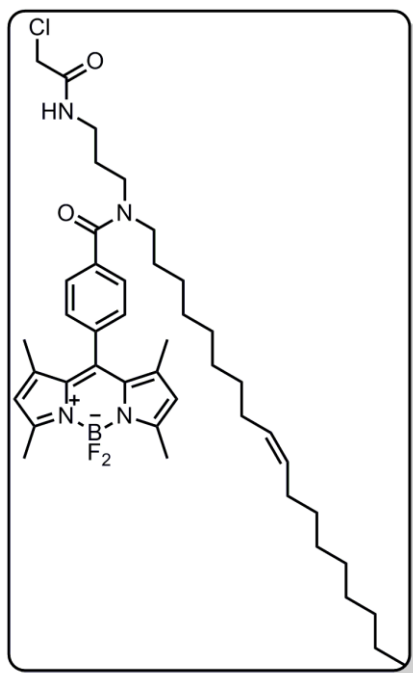
LCMS (APCI): calc for $C_{43}H_{62}BClF_2N_4O_2$ (M+H) 751.46; found: 751.5

HRMS (APCI): calc for $C_{43}H_{62}BClF_2N_4O_2$ (M+H) 751.4622; found: 751.4702

^{1}H-NMR (500 MHz, CDCl$_3$): δ 7.50 (d, 2H, J= 8.0 Hz), 7.37 (d, 2H, J= 8.0 Hz), 5.94 (s, 2H), 5.29-5.33 (m, 2H), 4.07 (s, 2H), 3.62 (t, 2H, J=5.5 Hz), 3.39 (t, 2H, J=5.5 Hz), 3.16 (t, 2H, J=7 Hz), 2.55 (s, 6H), 1.39 (s, 6H), 1.03-1.25 (m, 30H), 0.85 (t, 3H, J=7 Hz).

^{13}C-NMR (125 MHz, CDCl$_3$): δ 164.16, 164.12, 155.96, 145.23, 142.71, 128.40, 127.22, 121.46, 53.31, 50.87, 49.57, 42.72, 41.68, 39.43, 36.29, 31.89, 31.86, 29.73, 29.69, 29.65, 29.51, 29.43, 29.34, 29.30, 29.16, 29.09, 28.97, 27.46, 27.39, 27.22, 27.17, 27.12, 26.75, 26.59, 14.64, 14.60, 14.01, 14.07

BDRCA-28 (8 mg, 15%)
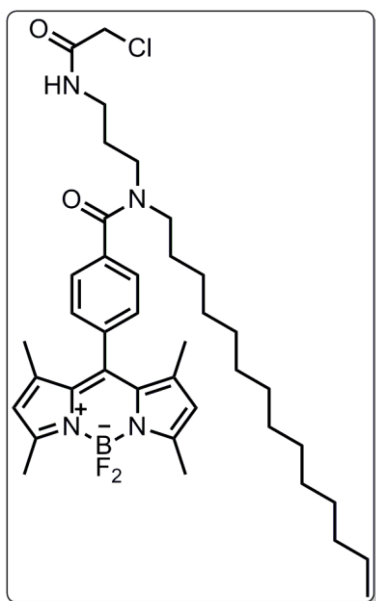
LCMS (APCI): calc for $C_{39}H_{56}BClF_2N_4O_2$ (M+H) 697.42; found: 697.4

HRMS (APCI): calc for $C_{39}H_{56}BClF_2N_4O_2$ (M+H) 697.4153; found: 697.4232

^{1}H-NMR (500 MHz, CDCl$_3$): δ 7.49 (d, 2H, J=8 Hz), 7.36 (d, 2H, J=8 Hz), 5.98 (s, 2H), 4.06 (s, 2H), 2.54 (s, 6H), 1.85 (t, 2H, J=6 Hz)), 1.46-1.52 (m, 4H), 1.38 (s, 6H), 1.03-1.23 (m, 26 H), 0.86 (t, 3H, J=7 Hz)

BDRCA-55 (5 mg, 10%)
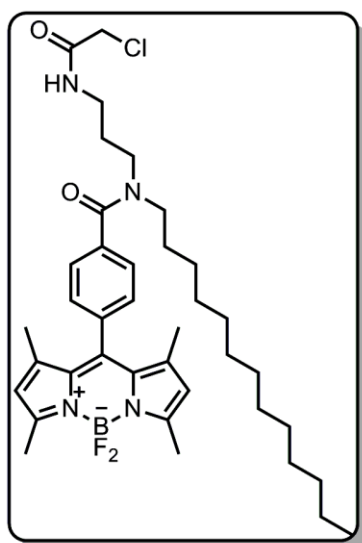
LCMS (APCI): calc for $C_{38}H_{54}BClF_2N_4O_2$ (M+H) 683.40; found: 683.40

HRMS (APCI): calc for $C_{38}H_{54}BClF_2N_4O_2$ (M+H) 683.3996; found: 683.4076

^{1}H-NMR (500 MHz, CDCl$_3$): δ 7.50 (d, 2H, *J*=8 Hz), 7.37 (d, 2H, *J*=7.5 Hz), 5.99 (s, 2H), 4.07 (s, 2H), 2.55 (s, 6H), 2.09 (m, 2H), 1.63 (m, 12H), 1.40 (s, 6H), 1.25 (m, 4H), 0.71-0.86 (m, 15H)**.**

BDRCA-65 (10 mg, 20%)
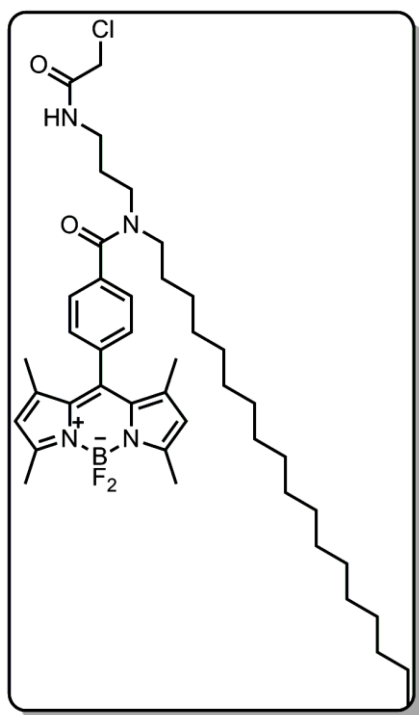
LCMS (APCI): calc for $C_{43}H_{64}BClF_2N_4O_2$ (M+H) 753.48; found: 753.5

HRMS (APCI): calc for $C_{43}H_{64}BClF_2N_4O_2$ (M+H) 753.4779; found: 753.4859

^{1}H-NMR (500 MHz, CDCl$_3$): δ 7.50 (d, 2H, J=8.5 Hz), 7.37 (d, 2H, J=8 Hz), 5.99 (s, 2H), 4.07 (s, 2H), 2.55 (s, 6H), 1.85 (m, 2H), 1.504-1.518 (m, 4H), 1.40 (s, 6H), 1.03-1.27 (m, 34 H), 0.87 (t, 3H, J=6.5 Hz).

BDRCA-407 (10 mg, 25%)
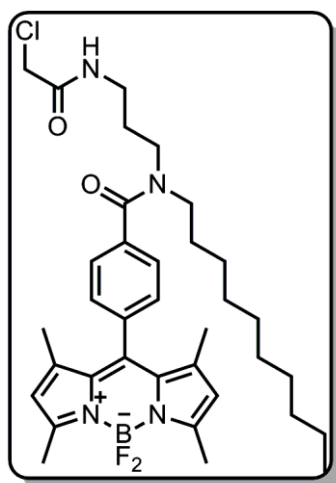
LCMS (APCI): calc for $C_{35}H_{48}BClF_2N_4O_2$ (M+H) 641.35; found: 641.4

HRMS (APCI): calc for $C_{35}H_{48}BClF_2N_4O_2$ (M+H) 641.3527; found: 641.3606

^{1}H-NMR (500 MHz, CDCl$_3$): δ 7.50 (d, 2H, J=8.5 Hz), 7.36 (d, 2H, J=8 Hz), 5.98 (s, 2H), 4.06 (s, 2H), 2.55 (s, 6H), 1.84-1.86 (m, 2H), 1.46-1.51 (m, 4H), 1.39 (s, 6H), 1.03-1.27 (m, 18 H), 0.86 (t, 3H, J=7 Hz)

BDRCA-554 (12 mg, 20%)
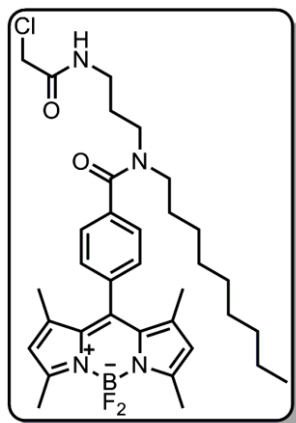
LCMS (APCI): calc for $C_{34}H_{46}BClF_2N_4O_2$ (M+H) 627.34; found: 627.30

HRMS (APCI): calc for $C_{34}H_{46}BClF_2N_4O_2$ (M+H) 627.3370; found: 627.3449

^{1}H-NMR (500 MHz, CDCl$_3$): δ 7.50 (d, 2H, J=8 Hz), 7.37 (d, 2H, J=8 Hz), 5.99 (s, 2H), 4.07 (s, 2H), 2.55 (s, 6H), 1.84-1.86 (m, 2H), 1.47-1.57 (m, 4H), 1.40 (s, 6H), 1.03-1.27 (m, 16 H), 0.86 (t, 3H, J=7 Hz)

BDRCA-567 (6 mg, 18%)
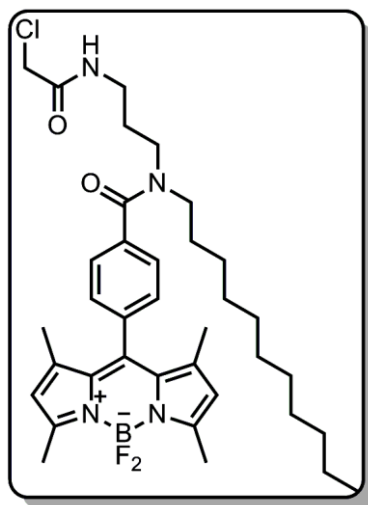
LCMS (APCI): calc for $C_{36}H_{50}BClF_2N_4O_2$ (M+H) 655.37; found: 655.40

HRMS (APCI): calc for $C_{36}H_{50}BClF_2N_4O_2$ (M+H) 655.3683; found: 655.3762

^{1}H-NMR (500 MHz, CDCl$_3$): δ 7.50 (d, 2H, J=8 Hz), 7.36 (d, 2H, J=8 Hz), 5.99 (s, 2H), 4.07 (s, 2H), 2.55 (s, 6H), 1.84-1.86 (m, 2H), 1.50-1.52 (m, 4H), 1.39 (s, 6H), 1.03-1.27 (m, 20 H), 0.86 (t, 3H, J=6.5 Hz)

BDRCA-577 (5 mg, 12%)
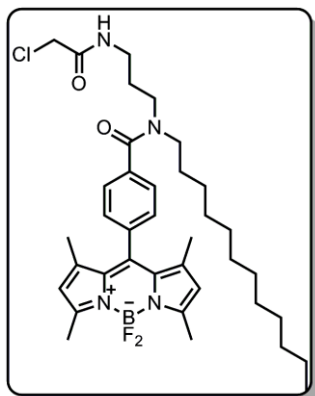
LCMS (APCI): calc for $C_{37}H_{52}BClF_2N_4O_2$ (M+H) 669.38; found: 669.4

HRMS (APCI): calc for $C_{37}H_{52}BClF_2N_4O_2$ (M+H) 669.3840; found: 669.3919

^{1}H-NMR (500 MHz, CDCl$_3$): δ 7.50 (d, 2H, *J*=8 Hz), 7.37 (d, 2H, *J*=8 Hz), 5.98 (s, 2H), 4.07 (s, 2H), 3.63-3.64 (m, 2H), 3.39-3.40 (m, 2H), 3.16 -3.19 (m, 2H), 2.55 (s, 6H),.4 (s, 6H), 1.03-1.25 (m, 22 H), 0.86 (t, 3H, *J*=7 Hz)

BDRCA-580 (8 mg, 22%)
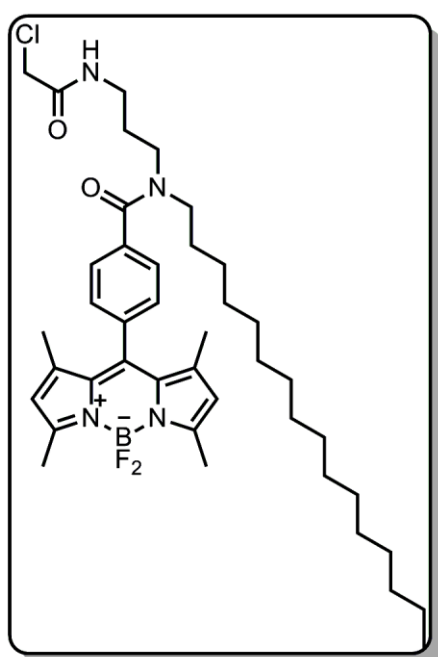
LCMS (APCI): calc for $C_{41}H_{60}BClF_2N_4O_2$ (M+H) 725.45; found: 725.5

HRMS (APCI): calc for $C_{41}H_{60}BClF_2N_4O_2$ (M+H) 725.4466; found: 725.4546

^{1}H-NMR (500 MHz, CDCl$_3$): δ 7.50 (d, 2H, *J*=8.5 Hz), 7.37 (d, 2H, *J*=8 Hz), 5.99 (s, 2H), 4.07 (s, 2H), 3.39-3.4 (m, 2H), 3.18-3.19 (m, 2H), 2.55 (s, 6H), 1.85-1.86 (m, 2H), 1.38 (s, 6H), 1.03-1.24 (m, 28 H), 0.87 (t, 3H, *J*=7 Hz)

BDR-28 (10 mg, 20%)
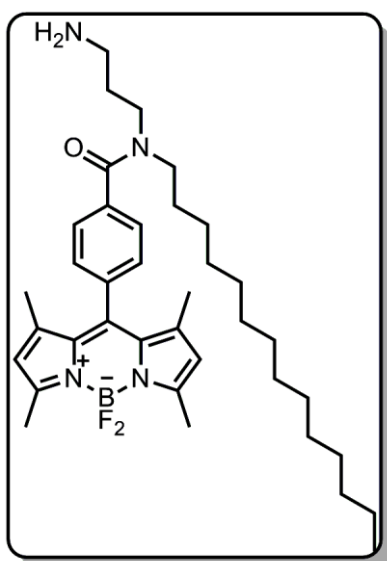
LCMS (ESI): calc for $C_{37}H_{55}BF_2N_4O$ (M+H) 621.44; found: 621.40

^{1}H-NMR (500 MHz, CDCl₃): δ 7.51 (d, 2H, J=10 Hz), 7.37 (d, 2H, J=5.5 Hz), 5.98 (s, 2H), 2.55 (s, 6H), 1.97-2.24 (m, 6H), 1.38 (s, 6H), 1.03-1.23 (m, 26 H), 0.87 (t, 3H, J=3.5 Hz)

BDR-55 (7 mg, 18%)
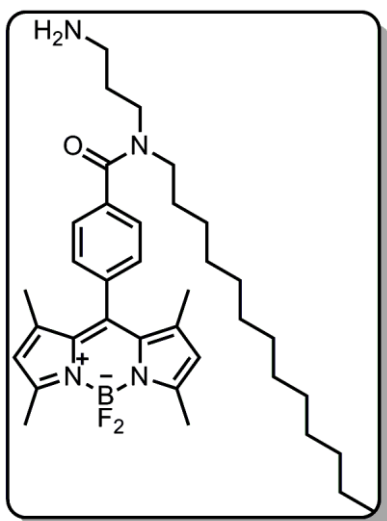
LCMS (ESI): calc for $C_{36}H_{53}BF_2N_4O$ (M+H) 607.43; found: 607.40

¹H-NMR (500 MHz, CDCl$_3$): δ 7.54 (d, 2H, *J*=7 Hz), 7.38 (d, 2H, *J*=7 Hz), 5.98 (s, 2H), 2.55 (s, 6H), 2.16-2.22 (m, 2H), 2.04-2.10 (m, 4H), 1.38 (s, 6H), 1.07-1.18 (m, 10H), 0.72-0.84 (m, 17H)**.**

BDR-65 (12 mg, 25%)
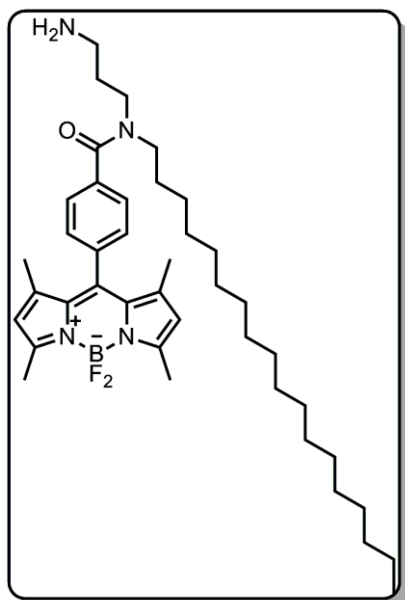
LCMS (ESI): calc for C$_{41}$H$_{63}$BF$_2$N$_4$O (M+H) 677.51; found: 677.40

¹H-NMR (500 MHz, CDCl$_3$): δ 7.51 (d, 2H, *J*=9 Hz), 7.37 (d, 2H, *J*=7 Hz), 5.98 (s, 2H), 2.55 (s, 6H), 2.06-2.21 (m, 6H), 1.38 (s, 6H), 1.03-1.23 (m, 34 H), 0.87 (t, 3H, *J*=7 Hz)

BDR-407 (15 mg, 30%)
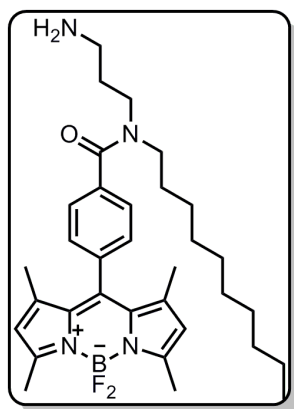
LCMS (ESI): calc for C$_{33}$H$_{47}$BF$_2$N$_4$O (M+H) 565.38; found: 565.40

¹H-NMR (500 MHz, CDCl₃): δ 7.53 (d, 2H, *J*=10 Hz), 7.37 (d, 2H, *J*= 5.5 Hz), 5.98 (s, 2H), 2.55 (s, 6H), 2.16-2.20 (m, 6H), 1.39 (s, 6H), 1.03-1.23 (m, 18 H), 0.86 (t, 3H, *J*=7 Hz).

BDR-554 (15 mg, 30%)
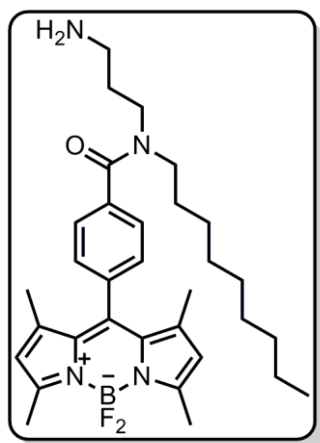
LCMS (ESI): calc for C₃₂H₄₅BF₂N₄O (M+H) 551.37; found: 551.4

¹H-NMR (500 MHz, CDCl₃): δ 7.52 (d, 2H, *J*=7 Hz), 7.37 (d, 2H, *J*=5.5 Hz), 5.98 (s, 2H), 2.55 (s, 6H), 2.02-2.24 (m, 6H), 1.38 (s, 6H), 1.04-1.27 (m, 16 H), 0.85 (t, 3H, *J*=7 Hz).

BDR-567 (9 mg, 23%)
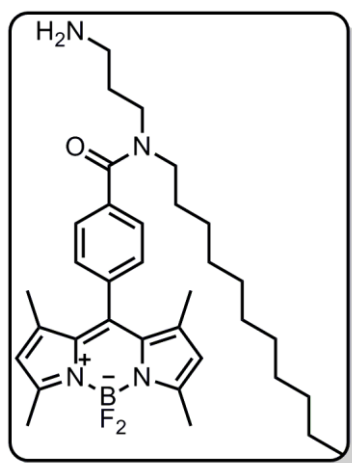
LCMS (ESI): calc for C₃₄H₄₉BF₂N₄O (M+H) 579.40; found: 579.50

¹H-NMR (500 MHz, CDCl₃): δ 7.52 (d, 2H, *J*=6.5 Hz), 7.37 (d, 2H, *J*=7.5 Hz), 5.98 (s, 2H), 2.55 (s, 6H), 2.16-2.20 (m, 6H), 1.38 (s, 6H), 1.04-1.25 (m, 20 H), 0.86 (t, 3H, *J*=6.5 Hz)

BDR-577 (6 mg, 15%)
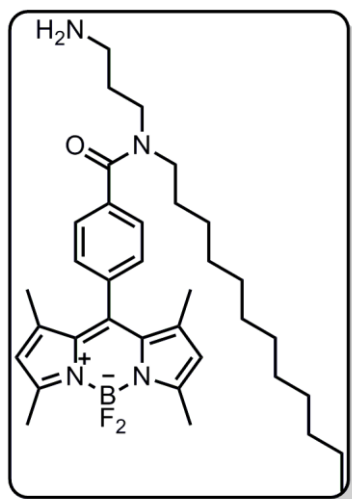
LCMS (ESI): calc for C₃₅H₅₁BF₂N₄O (M+H) 593.41; found: 593.40

¹H-NMR (500 MHz, CDCl₃): δ 7.50 (d, 2H, *J*=8 Hz), 7.38 (d, 2H, *J*=6 Hz), 5.98 (s, 2H), 2.55 (s, 6H), 2.04-2.16 (m, 6H), 1.38 (s, 6H), 1.23-1.25 (m, 22 H), 0.86 (t, 3H, *J*=6.5 Hz).

BDR-580 (13 mg, 25%)
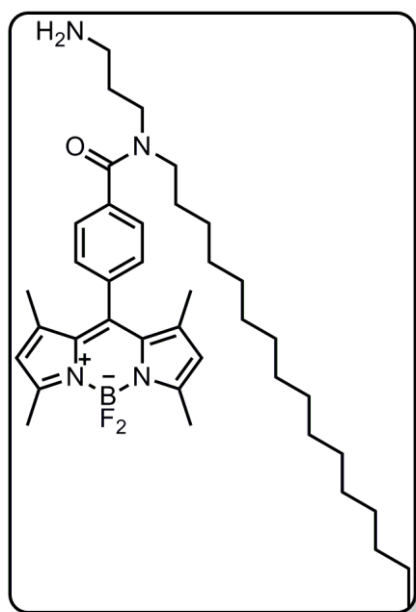
LCMS (ESI): calc for $C_{39}H_{59}BF_2N_4O$ (M+H) 649.47; found: 649.60

^{1}H-NMR (500 MHz, CDCl$_3$): δ 7.52 (d, 2H, J=7 Hz), 7.38 (d, 2H, J=7.5 Hz), 5.98 (s, 2H), 2.55 (s, 6H), 2.16-2.22 (m, 6H), 1.38 (s, 6H), 1.19-1.24 (m, 28 H), 0.87 (t, 3H, J=6.5 Hz)

BDR-656 (15 mg, 30%)
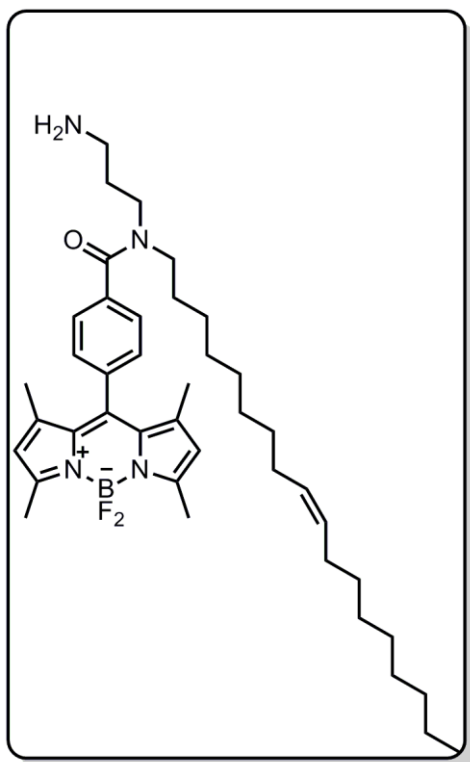
LCMS (ESI): calc for $C_{41}H_{61}BF_2N_4O$ (M+H) 675.49; found: 675.40

^{1}H-NMR (500 MHz, CDCl$_3$): δ 7.52 (d, 2H, J=7.0 Hz), 7.37 (d, 2H, J=7.0 Hz), 5.98 (s, 2H), 5.29-5.34 (m, 2H), 3.19 (t, 2H, J=6.5 Hz), 2.55 (s, 6H), 1.97 (t, 4H, J=6.5 Hz) 1.38 (s, 6H), 1.03-1.24 (m, 30H), 0.86 (t, 3H, J=7 Hz).

^{13}C-NMR (125 MHz, CDCl3): δ 156.07, 142.59, 136.76, 136.32, 131.10, 130.09, 130.01, 129.69, 129.69, 129.54, 128.53, 127.63, 121.52, 53.40, 49.98, 41.79, 37.16, 32.58, 31.88, 29.72, 29.67, 29.50, 29.46, 29.34, 29.30, 29.10, 28.96, 27.21, 27.13, 26.73, 25.59, 25.48, 22.66, 14.60, 14.09

Characterization by HPLC-MS (APCI) of BODIPY derivatives: greater than 18-carbon alkyl chain

HPLC conditions: A: H_2O-HCOOH: 99.9:0.1. B: CH_3CN-HCOOH: 99.9:0.1; gradient 5% B to 100% B (7 min), isocratic 100% B (7-18 min), gradient 100% B to 95% B(18-18.1 min), isocratic 5% B (18.1-20 min). Reversephase Phenomenex C_{18} Luna column (4.6 x 50 mm^2) 3.5 μm, flow rate: 1.0 mL/min.

TB-G-19CA (orange solid, 3.5 mg, 20%)
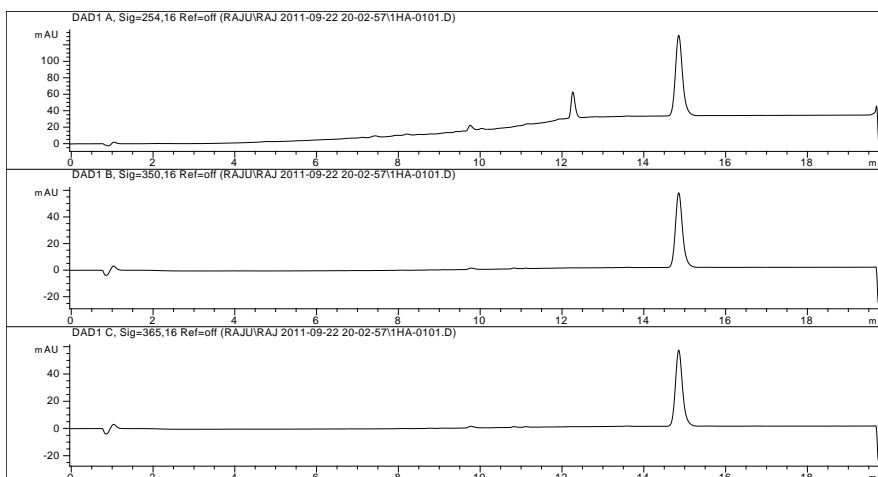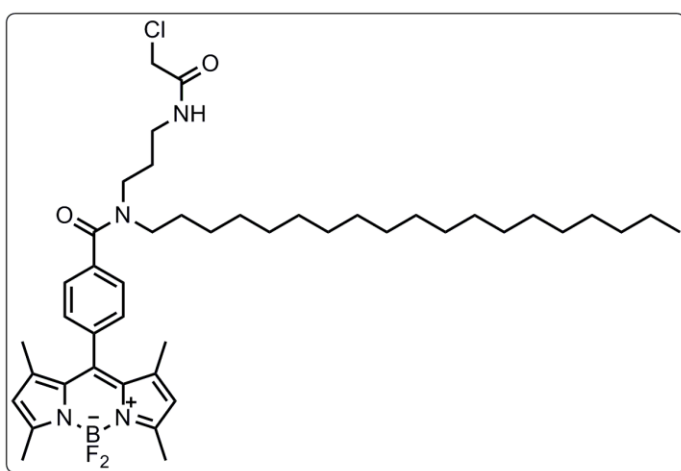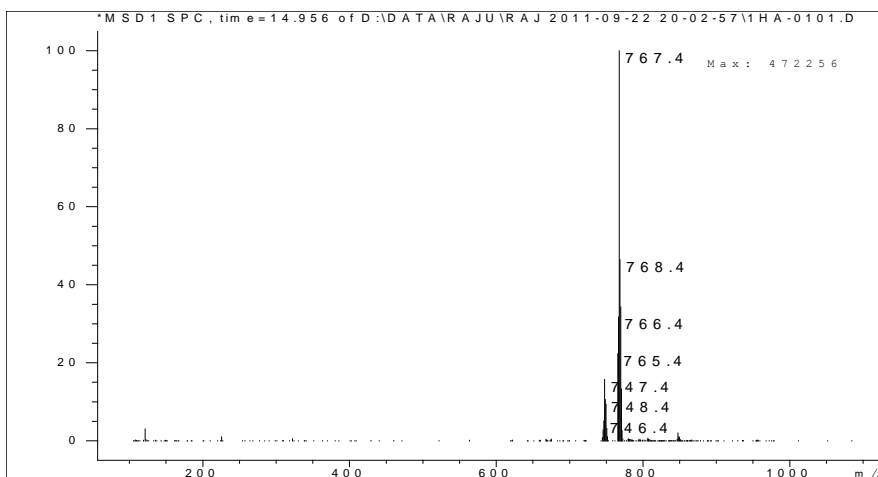
TB-G-20CA (orange solid, 3 mg, 15%)

139
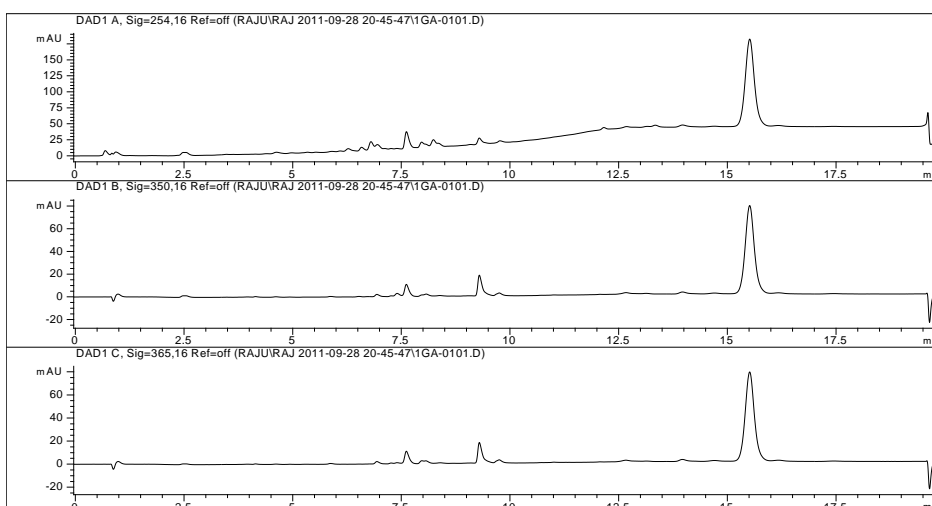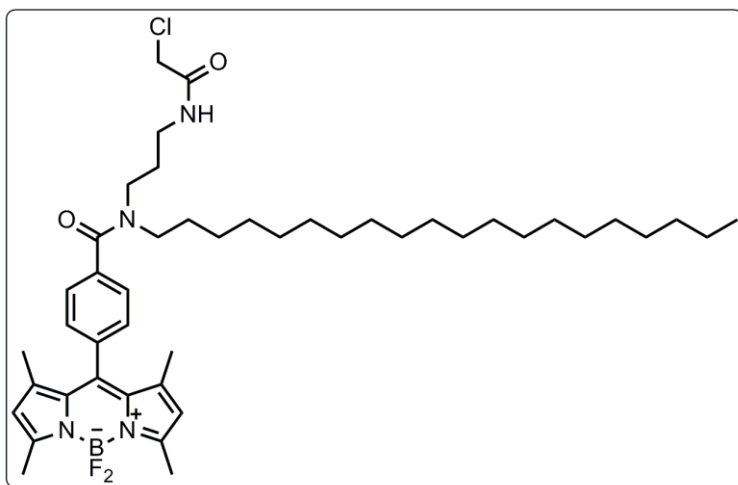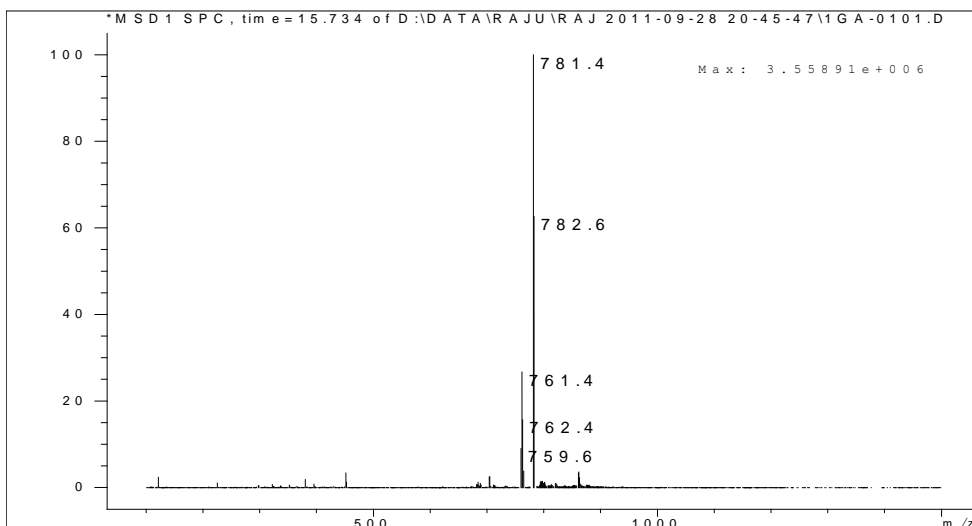
TB-G-21CA (orange solid, 1.5 mg, 8%)

140

Max: 1.32301e+006

795.4

797.4

798.4

777.4
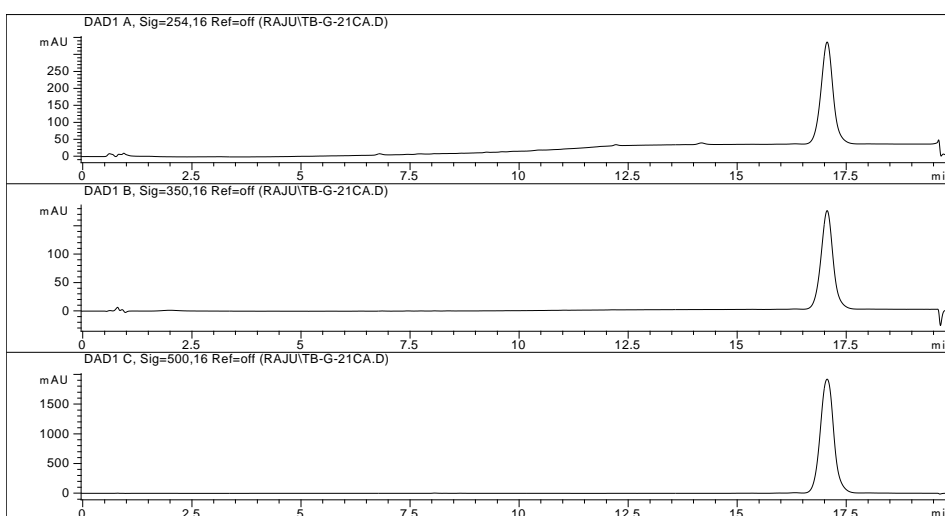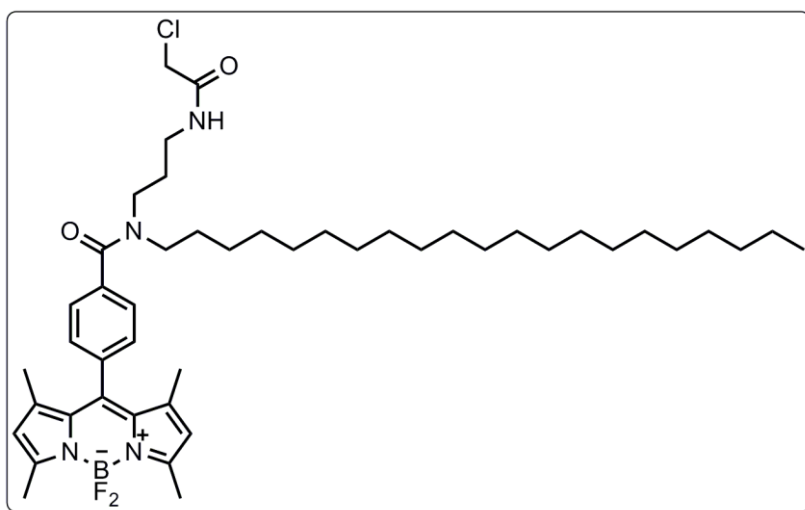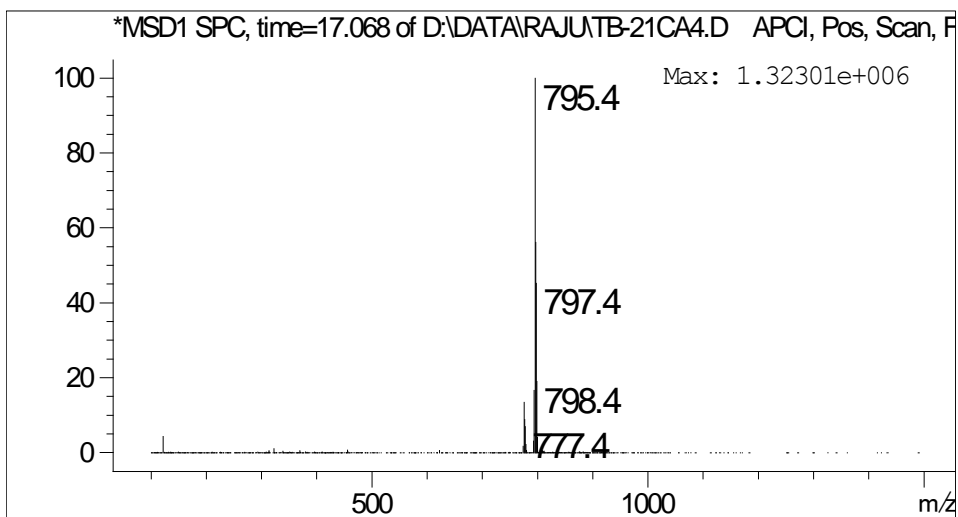
TB-G-22CA (orange solid, 2 mg, 12%)

DAD1 A, Sig=254,16 Ref=off (RAJU\TB-22CA1.D)

DAD1 B, Sig=350,16 Ref=off (RAJU\TB-22CA1.D)

DAD1 C, Sig=500,16 Ref=off (RAJU\TB-22CA1.D)
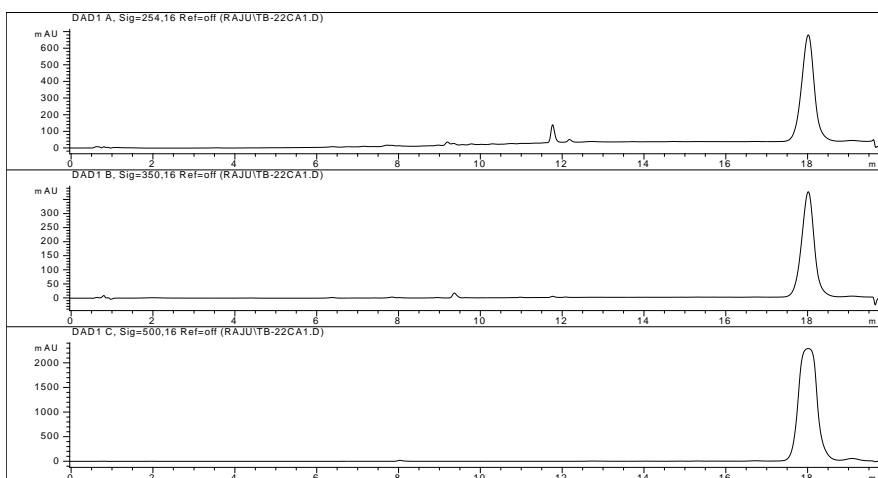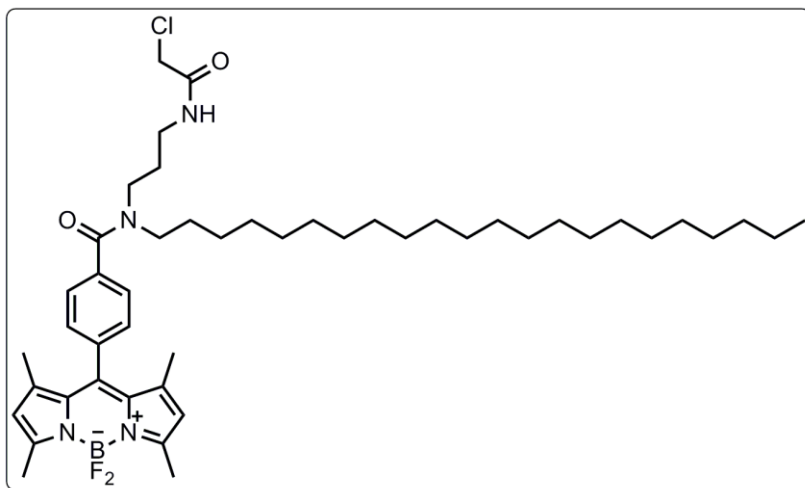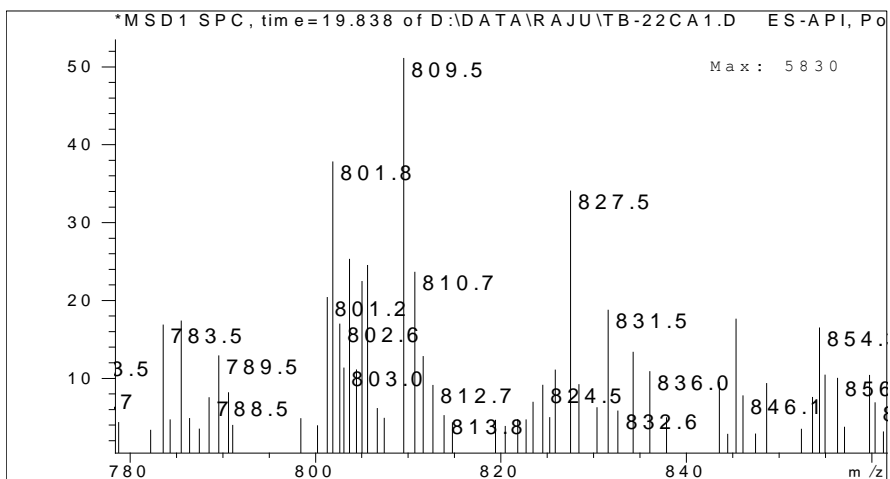
TB-G-23CA (orange solid, 1.3 mg, 6%)
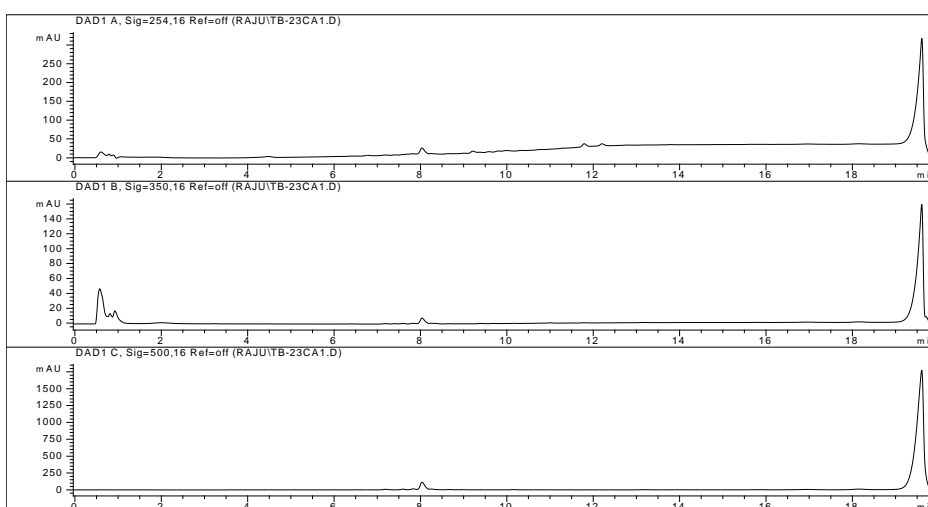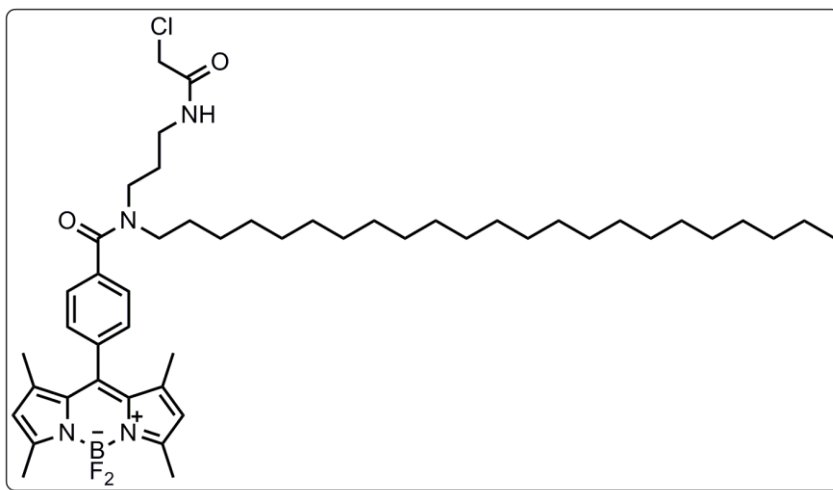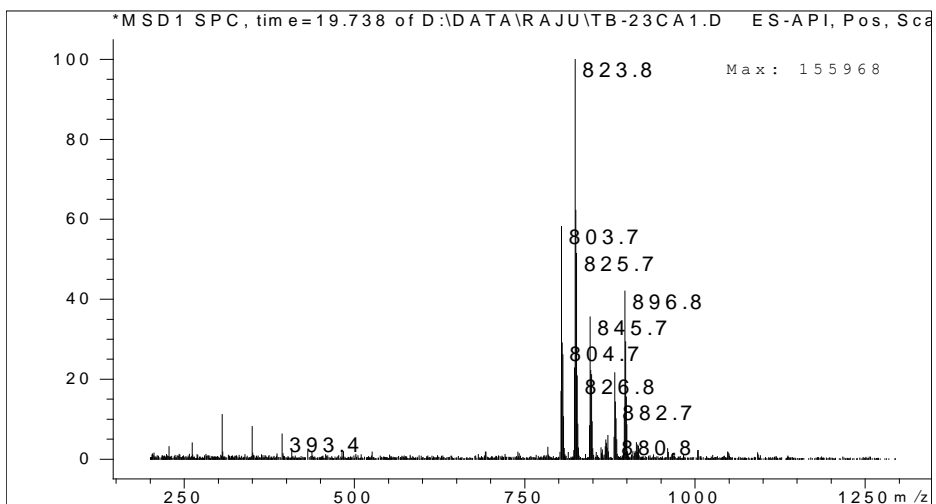
TB-G-24CA (orange solid, 0.8 mg, 6%)

*MSD1 SPC, time=18.690 of D:\DATA\RAJU\24-CA1.D   APCI, Pos, Scan, Frag: 200, "E

Max: 1.61126e+006
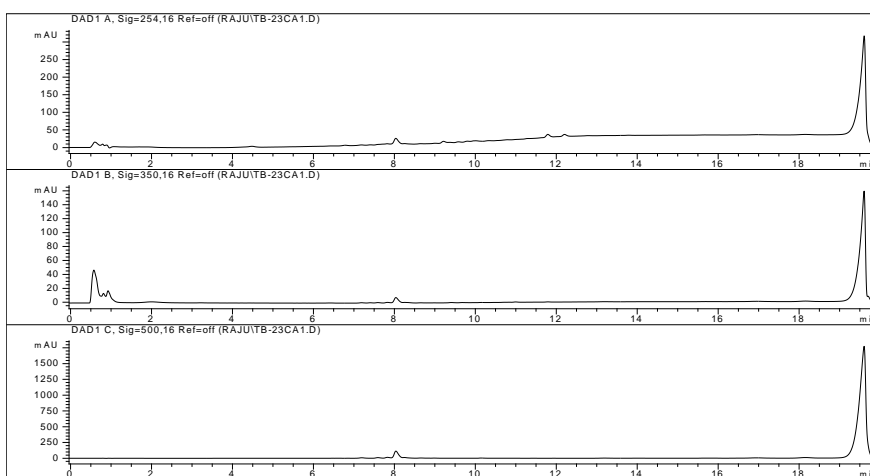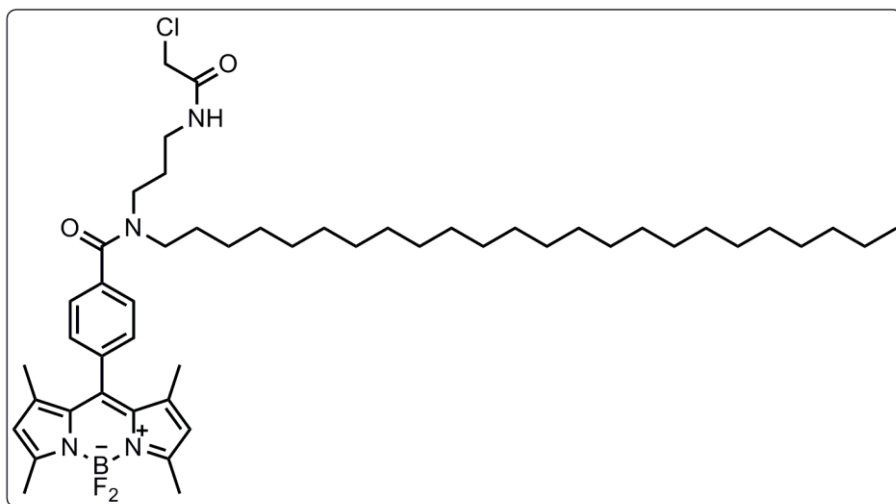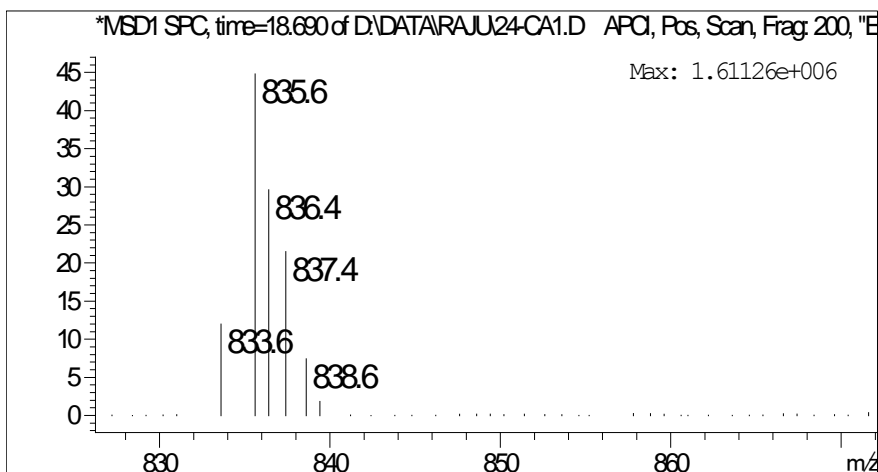
5.5.2 Synthesis procedure and characterization

Compound **1**
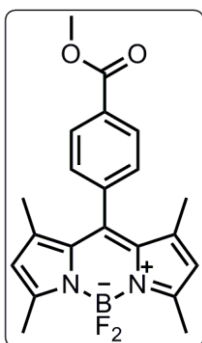
Methyl 4-(chlorocarbonyl)benzoate (1 g, 5.03 mmol, 1 eq.) and 2,4-dimethyl pyrrole (1.05 mL, 11.07 mmol, 2.2 eq.) were dissolved in DCM (100 mL) and the reaction mixture was stirred under nitrogen at room temperature for 4 hours until reaction was completed. Then the BF$_3$-OEt$_2$ (4.8 mL, 35.21 mmol, 7 eq.) and Triethylamine (3.4 mL, 25.15 mmol, 5 eq.) were added *in situ* to the reaction mixture and stirred at room temperature for 12 hours. After complete of reaction, the reaction mixture was washed with water and then organic layer was collected (3 x 100 mL) and purified by a normal-phase silica column using Hexane-EtOAc (ranging from 100:0 to 90:10) as the eluting solvent and got) pure orange colored solid compound **1**. Yield: 700 mg, 36%.

LCMS (ESI): calc for C$_{21}$H$_{21}$BF$_2$N$_2$O$_2$ (M-H) 382.17; found: 381.10

¹H-NMR (500 MHz, CDCl₃): δ 8.05 (d, 2H, *J*=8.0 Hz), 7.27 (d, 2H, *J*=8.0 Hz), 5.85 (s, 2H), 3.83 (s, 3H), 2.42 (s, 6H), 1.22 (s, 6H).

^{13}C-NMR (125 MHz, CDCl₃): δ 166.42, 155.96, 142.83, 140.18, 139.81, 130.89, 130.78, 130.33, 129.47, 128.35, 121.44, 52.35, 14.57, 14.46.

Compound **2**
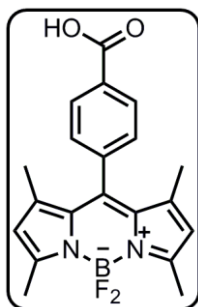
The compound 1(700 mg, 1.83 mmol, 1eq.) was dissolved in solvent mixture of DCM:MeOH (3:1)(v/v) (500 mL). Then, 90 mL of 0.2 N KOH in H₂O (1.06 g, 18.3 mmol, 10 eq) was added to the solution. The resulting mixture was stirred at room temperature for 24 hours. After complete hydrolysis, the reaction mixture was quenched with 100 mL of AcOH-H2O (1:1) and then MeOH was removed from the reaction mixture under reduced pressure. Then the DCM was added to solution and the organic layer was collected (3 x 100 mL), washed with water and purified by a normal-phase silica column using Hexane-EtOAc (ranging from 100:0 to 40:60) as the eluting solvent to obtain pure orange colored solid compound 2. Yield: 670 mg, 99%.

LCMS (ESI): calc for C₂₁H₂₁BF₂N₂O₂ (M-H) 367.15; found: 367.20

¹H-NMR (500 MHz, DMSO-d₆): δ 8.04 (d, 2H, *J*=8.0 Hz), 7.31 (d, 2H, *J*=8.0 Hz), 6.17 (s, 2H), 2.44 (s, 6H), 1.33 (s, 6H). ^{13}C-NMR (125 MHz, DMSO-d₆): δ 154.32, 142.21, 141.61, 130.03, 129.41, 126.54, 120.86, 20.79, 13.70, 13.47

General procedure for the preparation of solid supported secondary amines

Most of the general procedures for the preparation of resins which were either used in diversified library synthesis or the derivatization of library compounds have been covered in the chapter 2 and chapter 3. Here the few more procedures are given that have been used for the SAR studies.

General procedure for synthesis of solid supported secondary amines with alkyl bromide

For each reaction, resin (solid supported 3-diaminoproane) (25 mg, 0.025 mmol, 1 eq, 1 mmol/g) was suspended in 500 μL of N-Methylpyrrolidone (NMP) in a 2 mL of glass vial. 7 eq. of each alkyl-bromide (0.7 mmol) and 14 eq. of DIEA (1.4 mmol) were then added to the reaction mixture .The reaction mixture was then shaken for overnight at 70 $^{\circ}$C temperature in the heat block and then the resin was filtered through 5 mL syringe fitted with cartridge and washed with DMF (5X 3 mL), methanol (5X 3mL), and dichloromethane (5X 3mL). The solid supported secondary amine resins obtained, were dried and used for next step reactions.

General procedure for synthesis of BDR library

To synthesize BDR library, each of (solid supported secondary amine) resin (50 mg, 0.035 mmol, 1eq, 0.7 mmol/g) was suspended in 3 mL of DMF in a 10 mL syringe then 25 mg, 0.07 mmol, 2 eq **1**, 30 mg, 0.77 mmol, 2.2 eq 2-(7-Aza-1H-benzotriazole-1-yl)-1,1,3,3-tetramethyluronium hexafluorophosphate (HATU) and 30 μL, 0.168 mmol, 4.8 eq DIEA were added. At a time 40 individual reaction mixtures were placed on orbital shaker for 24 h at room temperature and after completion of the reaction the resin was

filtered through 10 mL cartridge and then washed with DMF (5X 5mL), methanol (5X 5mL), and dichloromethane (5X 5mL) consecutively. The resin was dried under high vacuum to afford solid supported compounds resin **2** and then the subsequently the dried resin of 50 mg was treated with 0.5% TFA in dichloromethane (5 mL) for 10X 4 mins. The solution was drained in to the 20 mL vial followed by quenched with 100 μL of 7 (N) NH_3 in methanol and then organic layer was washed with the saturated $NaHCO_3$ solution, and then the organic layer was separated and then purified by using short column and dried using Speed Vacuum to afford the BDR library products (orange solid with average 25% yield). Each of BDR compound was primarily characterized by HPLC-MS. The representative products are characterized by HPLC-MS, HR-MS, ^{1}H-NMR, ^{13}CNMR.

General procedure for synthesis of BDRCA and BDRAC libraries

To synthesized BDRCA and BDRAC libraries, each of 1 μmol BDR library compound (80 compounds) was taken according to their plate code in the 2 mL of 96-deep well plate. About 30 mg (~ 20 μmol, 20 eq.) of respective active-ester resin was added to the each well of the BDR library containing plate. Then, DCM:ACN (7:1) solvent mixture of around 500 μL and catalytic amount of saturated solution of $NaHCO_3$ were poured in to each well. The plate was kept in the shaker with moderate shaking for 2 hours. Then, the solution was filtered from the resin and dried to obtain pure products.

5.5.3 Cytotoxicity assay of CDg6 on purified B-cells

Stock solution of 10^6 cells/mL of purified mouse B-cells isolated from spleen was prepared as described above. 1 μM, 3 μM and 5 μM of CDg6 were used in this assay. To three wells of a 96-well plate, 100 μL of cell culture

medium was added to serve as negative control. 100 μL of each stimulant was added in triplicate sets to the remaining wells. To each well, 100 μL of B-cells were added (10^5cells/well) and the cells homogenously mixed with the stimulants via repeated inversion of the micropipette tip. The plates were then incubated at 37 ^{o}C, 5% CO_2 for 4 hour, 24 hour and 48 hour respectively. 1 μM of Hoechst 33342 (Invitrogen) was added to each well for cell counting using ImageXpressMICRO system (Molecular Device).

5.5.4 Isolation of B cell and T cell

Isolation of T cells

Spleen and blood (500 μL from heart) were obtained from six or seven week old C57BL/6J mouse. T cells were isolated from spleen and blood cells using indirect immunomagnetic separation. Red blood cells (RBCs) lysis was achieved using a 0.165M solution of NH_4Cl (Sigma-Aldrich). Biotinylated monoclonal antibodies to mouse CD45R/B220, CD11b (Integrin αM chain) Ly-6G and Ly-6C (Gr-1) and TER-119/Erythroid Cells (Ly-76) were added and incubated for at 4°C. BD IMag™ Streptavidin Particles Plus – DM (BD Bioscience Co.) were then added and bind to cells bearing biotinylated antibodies. The tube containing the labeled cell suspension was then placed within the magnetic field of the BD IMagnet™ (BD Bioscience Co.) with IMag buffer (BD Bioscience Co.). T cell isolation was achieved via depletion of cells committed to the B-lymphocytic, myeloid (monocytic and granulocytic), and erythroid lineages. The purity of the isolated T cells was 92% as assessed by flow cytometric analysis.

Isolation of B cells

Spleen, bone marrow and blood (500 µL from heart) were obtained from six or seven week old C57BL/6J mouse. B cells were isolated from spleen, bone marrow and blood cells using indirect immunomagnetic separation. RBCs lysis was achieved using a 0.165M solution of NH_4Cl (Sigma-Aldrich). Biotinylated monoclonal antibodies to mouse CD3e (CD3 ε chain), CD4, CD8, CD11b (Integrin αM chain), Ly-6G and Ly-6C (Gr-1) and TER-119/Erythroid Cells (Ly-76) were then added and incubated for at 4 ^{o}C. BD IMag™ Streptavidin Particles Plus – DM (BD Bioscience Co.) were then added and bind to cells bearing biotinylated antibodies. The tube containing the labeled cell suspension was then placed within the magnetic field of the BD IMagnet™ (BD Bioscience Co.) with IMag buffer (BD Bioscience Co.). B cell isolation was achieved via depletion of cells committed to the T-lymphocytic, myeloid (monocytic and granulocytic), and erythroid lineages. The purity of the isolated B cells was 91% as assessed by flow cytometric analysis.

5.5.5 B- Cell screening

Dulbecco's Modified Eagle Medium (DMEM) (4.5g/L glucose) (Gibco) + 10% Fetal Bovine Serum (FBS) + 0.1% Beta-mercaptoethanol + 1% Penicilin Streptomycin (P/S) was used as the medium for cell culture. T- and B- cells from mouse spleen were used for image based screening of DOFL. 5000 T-cell and B-cells isolated using immunomagnetic separation were placed in each well on a 384-well plate. Cells were counted in hematocytometer and cell viability was assessed by Trypan blue staining. DOFLs screens and analysis to detect compounds showing high fluorescent cell image was performed with all the BDR derivatives using the following

procedures. 1 μM of BDR derivatives dissolved in dimethyl sulfoxide (DMSO) was added to each well in the 384-well plate and incubated at 37 ^{o}C. 1 μM of Hoechst 33342 (Invitrogen) dye was added 15 minutes prior to screening. After incubation for 1 hour and 4 hour, images were acquired using the ImageXpress^{MICRO} system (Molecular Device) which is a fully-integrated hardware and software system for automated acquisition and analysis of high contents fluorescence cell images. The image information was converted into digital information for high-throughput and high-content analysis. In parallel, we double checked the images manually. The compounds which stain only B-cell selectively were chosen as hits and subjected to subsequent secondary screening and flow cytometric analysis.

5.5.6 Flow cytometry

300,000 each of splenocytes, peripheral blood lymphocytes, bone marrow cells, isolated T- and B- cells were incubated with 1 µM of compounds for 4 h at 37°C with cell culture medium. After incubation the cells were washed with Phosphate Buffered Saline (PBS) without Ca^{2+} and Mg^{2+} at pH 7.3 and resuspended in 100 µL of PBS. The cells are then mixed with a combination of 0.5 µL each of PE-Cy5 conjugated monoclonal antibodies to mouse CD3e and biotin-conjugated monoclonal antibodies to mouse CD45R/B220 and incubated for 25 minutes at 4 °C. In testing out the maturity state of B-cells, the cells are mixed with a combination of 0.5 µL each of APC conjugated monoclonal antibodies to mouse CD45R/B220 and biotin-conjugated monoclonal antibodies to mouse IgD incubated for 25 minutes at 4°C. After incubation, the cells were again washed with PBS and suspended in 100 µL of PBS before 0.5 µL Streptavidin-APC-cy7 was added for three-color flow cytometry.

5.5.7 Localization study

8 µL of CellMask™ Deep Red plasma membrane stain (Invitrogen) was added to 1 mL of B-cells (10^5 cells/mL) in a 5 mL polystyrene tube (8 µg/mL working concentration) and incubated for 5 minutes at 37 °C. The cells were washed, mounted on a glass slide and imaged immediately using confocal microscopy.

5.6 References

1) P. E. Lipsky, *Nat. Immunol.* 2001, **2**, 764.

2) T. Dörner and G. R. Burmester, *Curr. Opin. Rheumatol.* 2003, **3**, 246.

3) E. J. Sutton, T. D. Henning, B. J. Pichler, C. Bremer and H. E. Daldrup-Link, *Eur. Radiol.* 2008, **18**, 2021. (a) M. S. Schiedel, C. A. Briehn and P. Bauerle, *Angew. Chem., Int. Ed.* 2001, **40**, 4677.; (b) K. Sivakumar, F. Xie, B. M. Cash, S. Long, H. N. Barnhill and Q. Wang, *Org. Lett.* 2004, **6**, 4603; (c) J. Min, J. W. Lee, Y. H. Ahn and Y. T. Chang, *J. Comb. Chem.* 2007, **9**, 1079.; (d) Q. Li, J. S. Lee, C. Ha, C. B. Park, G. Yang, W. B. Gan and Y. T. Chang, *Angew. Chem., Int. Ed.* 2004, **43**, 6331.; (e) S. Wang and Y. T. Chang, *J. Am. Chem. Soc.* 2006, **128**, 10380.

4) Y. H. Ahn, J. S. Lee and Y. T. Chang, *J. Am. Chem. Soc.* 2007, **129**, 4510.; (b) J. S. Lee, N. Y. Kang, Y. K. Kim, A. Samanta, S. Feng, H. K. Kim, M. Vendrell, J. H. Park and Y. T. Chang, *J. Am. Chem. Soc.* 2009, **131**, 10077.

5) J. S. Lee, Y. K. Kim, M. Vendrell and Y. T. Chang, *Mol. Biosyst.* 2009, **5**, 411.; A.Loudet and K. Burgess, *Chem. Rev.* 2007, **107**, 4891.

6) H. S. Hendrickson, E. K. Hendrickson, I. D. Johnson and S. A. Farber, *Anal. Biochem.* 1999, **276**, 27.; (b) A. E. Thumser and J. Storch, *Moll. Cell. Biochem*, 2007, **299**, 67.

7) J. S. Lee, H. K. Kim, S. Feng, M. Vendrell and Y. T. Chang, *Chem. Commun.* 2011, **47**, 2339.; (b) J. S. Lee, N. Y. Kang, Y. K. Kim, A. Samanta, S. Feng, H. K. Kim, M. Vendrell, J. H. Park and Y. T. Chang, *J. Am. Chem. Soc*. 2009, **131**, 10077.

8) M. Vendrell, G. G. Krishna, K. K. Ghosh, D. Zhai, J. S. Lee, Q. Zhu, Y. H. Yau, S. G. Shochat, H. Kim, J. Chung and Y. T. Chang, *Chem. Commun.* 2011, **47**, 8424.

9) D. Zhai, S. C. Lee, M. Vendrell, L. P. Leong and Y. T. Chang, *ACS Comb. Sci,* 2012, 14, 81.

10) R. K. Das, A. Samanta, H. H. Ha and Y. T. Chang, *RSC Adv*. 2011, **1**, 573.

Chapter 6

Synthesis of Rhodol library (RDR) and development of mitotic phase probe
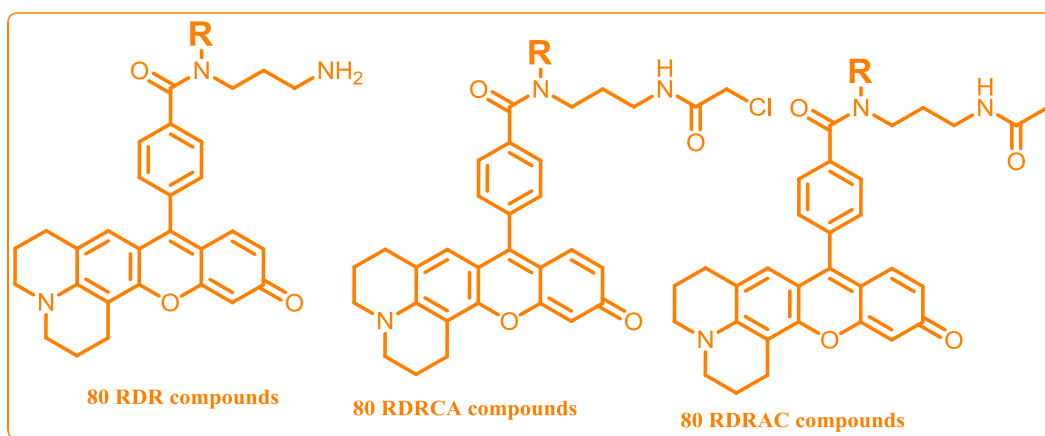
6.1 Introduction

Fluorescence techniques have extensively been used and are still enjoying rising interest from chemistry to many areas of biology due to high sensitivity, simplicity, quick response, rich of molecular information, and ability to spatial imaging.[1] However, the possibility of using fluorescence techniques for a particular purpose is often restricted by the availability of suitable fluorescent molecules. Moreover, there are very few, theoretical approaches for rational design of fluorescent probes.[2] On the other hand, combinatorial assembly of libraries of fluorescent molecules has been demonstrated to be a very powerful and promising approach[3] with a number of remarkable discoveries of novel fluorescent probes[4]. Therefore, synthesis of fluorescent library using biologically less explored scaffolds may have higher chance to discover novel fluorescent probes. As a candidate scaffold, we focused on rhodol for systematic library generation due to its limited examples about the applications in probe development process. So far, rhodol dyes have been effectively employed as scaffolds for fluorescence probes to detect hydrogen peroxide, zinc ion, peroxynitrite, and hypoxia. Rhodol[5] is the hybrid structure of fluorescein and rhodamine. It also named "Rhodafluor"[6]. This scaffold shows excellent photophysical properties such as high extinction coefficients, quantum yields, photostability, and solubility in a variety of solvents, yet low pH-dependence[5b]. Moreover, the fluorescence property such as emission wavelength and quantum yield can easily be tuned by changing the substitution patterns of the nitrogen atom in a similar manner to rhodamine.[7] Although, they inherit excellent photophysical properties there are limited availability of rhodol based fluorescent probes,[6,8] probably owing

155

to lack of enough synthetic reports . Utilizing all these opportunities and adopting our robust solid phase synthesis methodology, I synthesized diversity oriented rhodol library, RDR, RDRCA and RDRAC and utilized these compounds in the mitotic phase screening in live cells to find out live mitotic phase visualizing agent.

6.1.1 Cell division: mitosis

Cell cycle is a crucial process where a parent cell divides into two or more daughter cells. Overall, the cell cycle development consists of four different phases[9]: G1 phase, S phase, G2 phase, and mitosis. Mitosis is very important for the living organism for many reasons. It critically helps in growth, cell replacement, regeneration and vegetative reproduction of a living organism. However, uncontrolled mitotic cell division causes neoplasia. Neoplasia[10] (the formation of new strange tissues) occurs when a cell suffers mutation in its genetic material, loses the ability to control its own division and the failure is transmitted to its descendants. Cancers are malignant neoplasias. The term malignant means that neoplastic cells can disseminate to distant sites invading other organs and tissues. Neoplasias whose cells cannot disseminate to distant sites are called benign neoplasias. Moreover, according to the recent study, the monitoring of cell proliferation and its distinction during the cell cycle progression is an essential part in cell biology and regenerative medicine[11].

During the mitotic process one eukaryotic cell divides into two cells identical to the parent cell (generally identical, since alterations in genetic material can occur, more or less organelles may be distributed between the daughter cells, etc.). In the mitotic cell cycle, the cell is created and finishes when it is divided

by mitosis creating two daughter cells. Mitosis[12] propagates through the 4 different stages: prophase, metaphase, anaphase, and telophase. During the mitosis, mitotic apparatus display critical role in cell division. Mitotic apparatus consists of the set of aster fibers, radial structures around each centriole pair, plus the spindle fibers, fibers that extend across the cell between the two centriole pairs located in opposite cell poles[13]. The mitotic apparatus appears in prophase and has important role in the orientation and gripping of chromosomes and other cellular elements causing them to separate and migrate to opposite cell poles.

To monitor and quantify cell division in live cells, and reliably distinguish between acytokinesis and endoreduplication, there are few current approaches which are limited and complicated in determination of stem cell pool identities[11]. Thus, there is an urgent demand to develop novel fluorescent probe for monitoring cell proliferation.

6.2 Objectives

Here we developed the solid phase diversity-synthesis methodology of 80-member rhodol library RDR. These RDR compounds were further diversified to their corresponding actyl (RDRAC) and chloroacetyl (RDCA) derivatives using a simple but powerful solid phase activated ester chemistry. Next, we performed the full photophysical characterisation of these rhodol libraries. With the interest to develop mitotis phase selective fluorescent probe, RDR, RDRCA and RDRAC libraries were screened against RPE1:H2B:GFP cells which were seeding in 384-well plate, synchronized by Tubulyzine B and then compound RDR-567 was identified as a mitotic phase

probe that can distinguish between interphase and mitotic phase cells using micropsope.

6.3 Results and discussion

6.3.1 Design and synthesis

In this particular section, the synthesis characterisation and the applications of RDR libraries are discussed. As shown in the **Scheme 6.1**, the general synthetic strategy of rhodol acid involves five steps reactions. At first, methyl protection (**1**) of 8-hydroxyjulolidine was carried out obtain the good yield in Friedel-Crafts reaction which was performed with methyl 4-(chlorocarbonyl) benzoate in presence of $AlCl_3$ to get compound **2**. In the following step, demethylation was performed to obtain compound **3** using BBr_3 as the demethylating agent. Now, the methanesulfonic acid mediated standard ring cyclization reaction was carried out using resorcinol and demthylated product to obtain the corresponding rhodol ester, **4** which was then hydrolyzed using 2 N KOH , a standard base catalyzed ester hydrolysis method to obtain corresponding rhodol acid.

Scheme 6.1 Synthesis of RDR acid
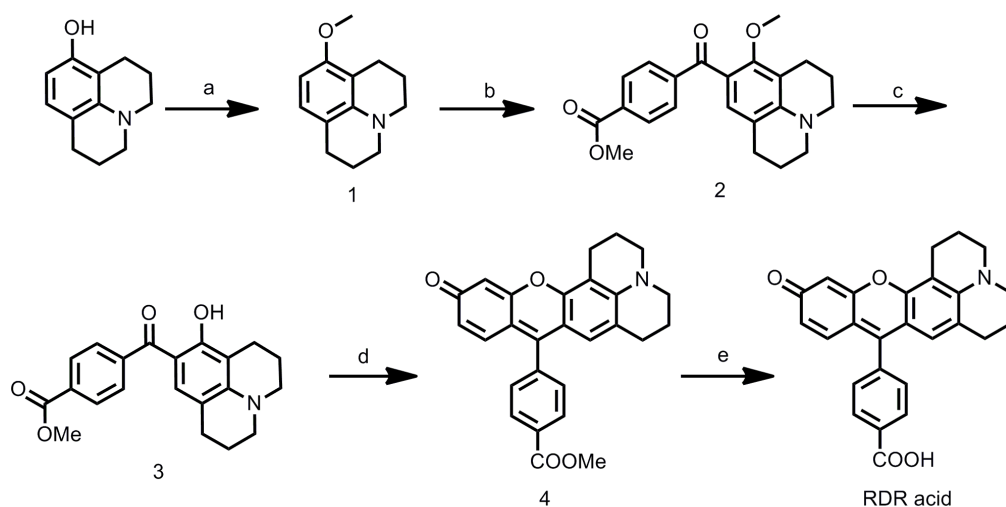
Reagent and conditions (a) $(CH3)_2SO_4$, NaH, THF, rt; (b) methyl 4-(chlorocarbonyl)benzoate, $AlCl_3$, DCM, 0 °C, 2 h; (c) BBr_3, DCM, -78 °C, 2 h; (d) Resorcinol, $MeSO_3H$, seal tube, 80 °C, 2 h; (e) 2 N KOH, MeOH, rt, 2 h.

After synthesizing rhodol acid, our robust solid phase methodology as discussed in the chapter 2 was applied to synthesize RDR library (**Scheme 6.1 and 6.2, Chart 6.1**). Then, RDRCA and RDRAC compounds were synthesized according to the previous mention protocol (chapter 3). All the compounds in the library were characterized by HPLC-MS and 80 relatively pure compounds (average purity is 90%, measured at 350 nm (**Table 6.1, 6.2 and 6.3**) were collected for further study. Excellent photophysical properties are reflected from the displaying quantum yield and spectral characteristists (**Table 6.1, 6.2 & 6.3 and Figure 6.1**).

Scheme 6.2 Synthesis of RDR library
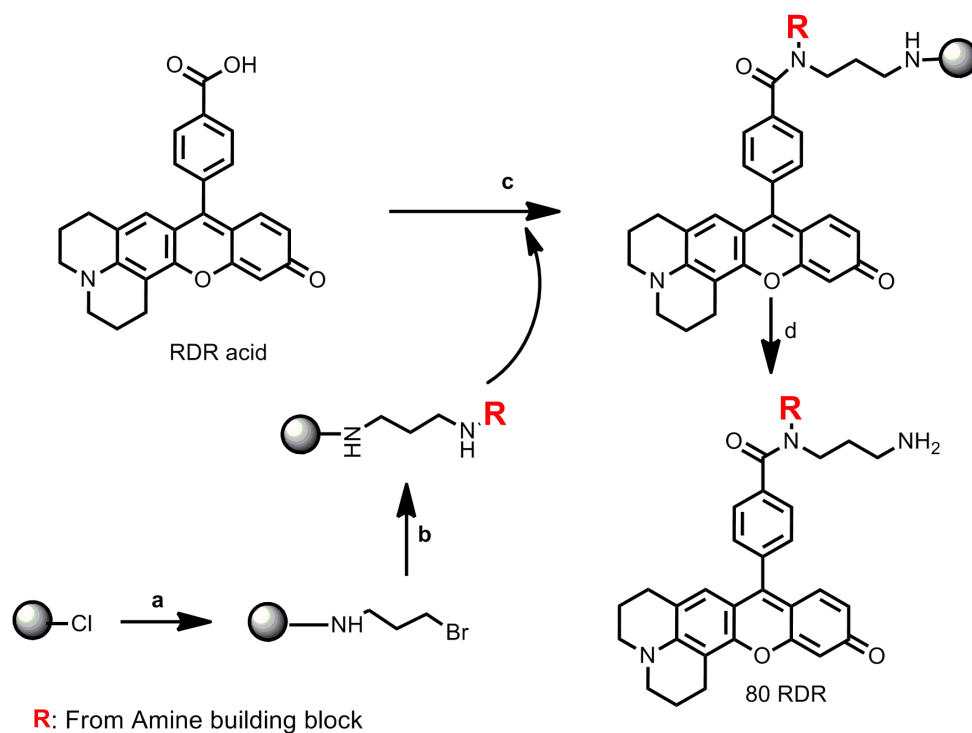
RDR acid

R: From Amine building block

80 RDR

Reagents and conditions: (a) DIEA, THF, 3-bromopropylamine, r.t., 12 h.; (b) DIEA, RNH$_2$, NMP, 70 ^{o}C, 12 h.; (c) HATU, DIEA, r.t. 24 h.; (d) 1% TFA in DCM , r.t., 10 min.

Chart 6.1 Amine building blocks for RDR library
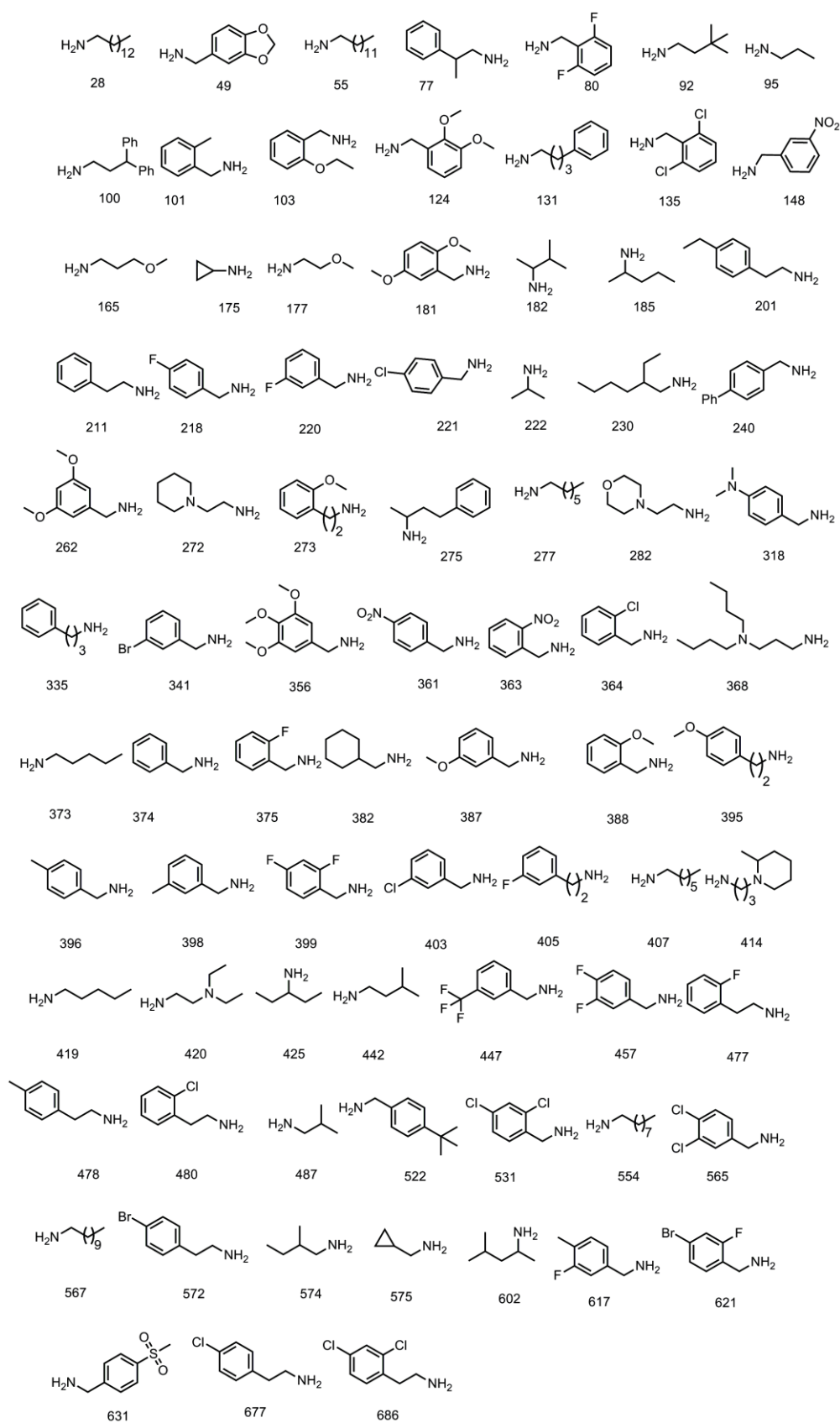
Scheme 6.3 RDRCA and RDRAC library synthesis
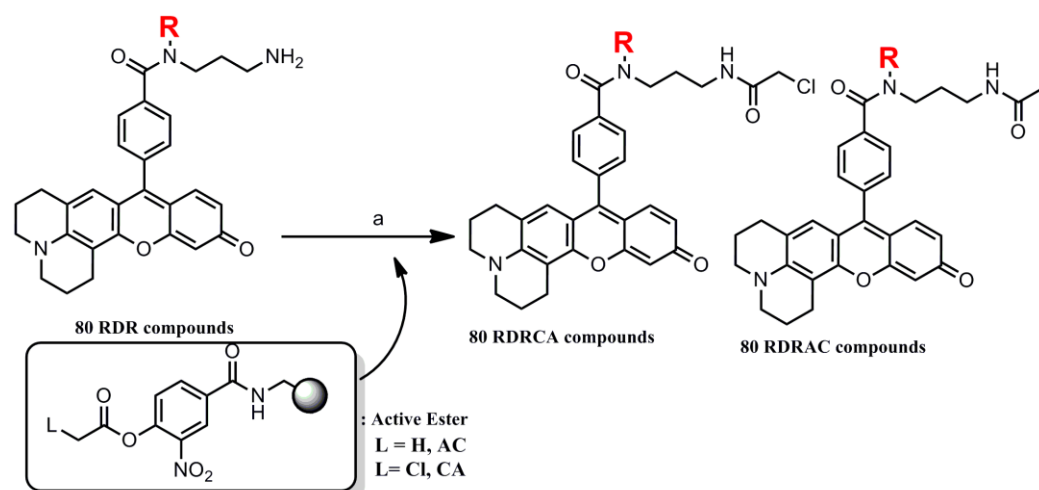
Reagent and Conditions (a) DCM/ACN (1:1), NaHCO$_3$, 2 h, r.t

Table 6.1 HPLC-MS characterization and photophysical property of RDR library

Compound	M$^+$(calc.)	M$^+$(exp.)	λ_{abs}(nm)	λ_{em}(nm)	ϕ*[1]	purity*[2]
RDR 28	663.4	664.4	545	587	0.45	93
RDR 49	601.3	602.2	546	587	0.49	93
RDR 55	649.4	650.4	544	586	0.40	96
RDR 77	585.3	586.4	545	586	0.44	93
RDR 80	593.2	594.2	545	586	0.42	92
RDR 92	551.3	552.4	545	587	0.37	97
RDR 100	661.3	662.4	545	587	0.36	95
RDR 101	571.3	572.4	546	587	0.36	95
RDR 103	601.3	602.4	545	586	0.35	92
RDR 95	509.3	510.4	545	586	0.36	95
RDR 124	617.3	618.4	546	587	0.40	91
RDR 131	599.3	600.4	545	586	0.36	91
RDR 135	625.2	626.2	546	587	0.38	93
RDR 148	602.3	603.2	546	587	0.39	92
RDR 165	539.3	540.4	546	587	0.38	92
RDR 175	507.3	508.2	545	586	0.40	92
RDR 177	525.3	526.2	546	586	0.42	91

RDR 181	617.3	618.2	546	587	0.36	93
RDR 182	537.3	538.4	544	586	0.41	90
RDR 185	537.3	538.4	545	586	0.39	91
RDR 201	599.3	600.4	546	586	0.47	92
RDR 211	571.3	572.2	545	586	0.40	92
RDR 218	575.3	576.4	546	586	0.43	93
RDR 220	575.3	576.2	544	586	0.43	95
RDR 221	591.2	592.2	546	586	0.44	91
RDR 222	509.3	510.2	545	586	0.42	88
RDR 230	579.3	580.4	544	587	0.45	91
RDR 240	633.3	634.4	545	586	0.47	91
RDR 262	617.3	618.4	546	586	0.44	96
RDR 272	578.3	579.4	545	586	0.43	91
RDR 273	601.3	602.4	545	586	0.41	92
RDR 275	599.3	600.4	546	586	0.46	90
RDR 277	565.3	566.4	546	586	0.38	91
RDR 282	580.3	581.4	545	586	0.39	90
RDR 318	600.3	601.4	546	587	0.50	91
RDR 335	585.3	586.4	546	586	0.42	96
RDR 341	635.2	636.4	544	587	0.47	94
RDR 356	647.3	648.2	545	586	0.42	94
RDR 361	602.3	603.2	546	587	0.48	94
RDR 363	602.3	603.2	545	587	0.40	94
RDR 364	591.2	592.2	546	586	0.47	94
RDR 368	636.4	637.4	544	586	0.48	95
RDR 373	523.3	524.2	545	587	0.37	93
RDR 374	557.3	558.3	545	586	0.41	95
RDR 375	575.3	576.2	545	587	0.41	96
RDR 382	563.3	564.4	545	587	0.44	94
RDR 387	587.3	588.4	546	586	0.45	89
RDR 388	571.3	572.3	546	586	0.40	96
RDR 395	601.3	602.2	545	587	0.42	91
RDR 396	571.3	572.2	546	586	0.41	92
RDR 398	571.3	572.4	544	587	0.40	90

RDR 399	593.2	594.2	545	587	0.35	98
RDR 403	591.2	592.2	545	586	0.35	91
RDR 405	589.3	590.2	546	586	0.37	93
RDR 407	607.4	608.4	544	587	0.45	91
RDR 414	606.4	607.4	546	586	0.34	92
RDR 419	537.3	538.4	544	587	0.45	96
RDR 420	566.3	567.4	545	587	0.45	94
RDR 425	537.3	538.4	545	586	0.43	93
RDR 442	537.3	538.4	546	586	0.47	95
RDR 447	625.3	626.4	544	586	0.40	94
RDR 457	593.2	594.2	546	587	0.35	93
RDR 477	589.3	590.4	545	587	0.41	94
RDR 478	585.3	586.4	545	587	0.44	94
RDR 480	605.2	606.2	546	586	0.38	93
RDR 487	523.3	524.4	546	586	0.37	93
RDR 522	613.3	614.4	544	587	0.31	91
RDR 531	625.2	626.2	545	586	0.45	93
RDR 554	593.4	594.4	546	587	0.29	92
RDR 565	625.2	626.2	545	587	0.39	91
RDR 567	621.4	622.4	545	587	0.41	92
RDR 572	649.2	650.2	545	586	0.45	92
RDR 574	537.3	538.2	545	586	0.49	96
RDR 575	521.3	522.2	545	587	0.41	92
RDR 602	551.3	552.4	545	586	0.34	93
RDR 617	589.3	590.4	545	586	0.42	89
RDR 621	653.2	654.2	545	586	0.45	93
RDR 631	635.2	636.2	545	586	0.44	91
RDR 677	605.2	606.2	545	586	0.37	92
RDR 686	639.2	640.2	545	586	0.37	93

Table 6.2 HPLC-MS characterization and photophysical property of RDRCA library

Compound	M⁺(calc.)	M⁺(exp.)	λ_{abs}(nm)	λ_{em}(nm)	ϕ*¹	purity*²
RDRCA 28	739.4	740.4	544	586	0.34	93
RDRCA 49	677.2	678.2	544	585	0.33	92
RDRCA 55	725.4	726.4	544	586	0.38	93
RDRCA 77	661.3	662.2	544	585	0.41	96
RDRCA 80	669.2	670.2	544	586	0.29	93
RDRCA 92	627.3	628.2	544	585	0.45	92
RDRCA 100	737.3	738.2	544	586	0.31	97
RDRCA 101	647.3	648.2	544	586	0.38	95
RDRCA 103	677.3	678.2	544	585	0.40	95
RDRCA 95	585.2	586.2	544	586	0.38	92
RDRCA 124	693.3	694.2	544	585	0.34	95
RDRCA 131	675.3	676.2	544	585	0.41	91
RDRCA 135	701.2	702.2	544	585	0.39	91
RDRCA 148	678.2	679.2	544	586	0.31	93
RDRCA 165	615.2	616.2	544	586	0.42	92
RDRCA 175	583.2	584.2	544	586	0.30	92
RDRCA 177	601.2	602.2	544	586	0.40	92
RDRCA 181	693.3	694.2	544	585	0.37	91
RDRCA 182	613.3	614.2	544	586	0.32	93
RDRCA 185	613.3	614.2	544	585	0.37	90
RDRCA 201	675.3	676.4	544	586	0.47	91
RDRCA 211	647.3	648.2	544	585	0.43	92
RDRCA 218	651.2	652.2	544	586	0.38	92
RDRCA 220	651.2	652.2	544	586	0.33	93
RDRCA 221	667.2	668.2	544	585	0.37	95
RDRCA 222	585.2	586.2	544	586	0.27	91
RDRCA 230	655.3	656.2	544	586	0.29	88
RDRCA 240	709.3	710.4	544	585	0.46	91
RDRCA 262	693.3	694.2	544	586	0.34	91
RDRCA 272	654.3	655.2	544	585	0.36	96

RDRCA 273	677.3	678.2	544	586	0.47	91
RDRCA 275	675.3	676.2	544	585	0.41	92
RDRCA 277	641.3	642.2	544	586	0.30	90
RDRCA 282	656.3	657.2	544	586	0.35	91
RDRCA 318	676.3	677.2	544	585	0.45	90
RDRCA 335	661.3	662.2	544	586	0.31	91
RDRCA 341	711.1	712.0	544	586	0.18	96
RDRCA 356	723.3	724.2	544	585	0.34	94
RDRCA 361	678.2	679.2	544	586	0.31	94
RDRCA 363	678.2	679.2	544	585	0.27	94
RDRCA 364	667.2	668.2	544	586	0.45	94
RDRCA 368	712.4	713.4	544	585	0.40	94
RDRCA 373	599.3	600.2	544	586	0.29	95
RDRCA 374	633.2	634.2	544	586	0.23	93
RDRCA 375	651.2	652.2	544	585	0.23	95
RDRCA 382	639.3	640.2	544	586	0.25	96
RDRCA 387	663.2	664.2	544	585	0.40	94
RDRCA 388	647.3	648.2	544	586	0.25	89
RDRCA 395	677.3	678.2	544	585	0.43	96
RDRCA 396	647.3	648.2	544	586	0.32	91
RDRCA 398	647.3	648.2	544	586	0.41	92
RDRCA 399	669.2	670.2	544	585	0.35	90
RDRCA 403	667.2	668.2	544	586	0.32	98
RDRCA 405	665.2	666.2	544	585	0.41	91
RDRCA 407	683.3	684.2	544	586	0.28	93
RDRCA 414	682.3	683.2	544	586	0.34	91
RDRCA 419	613.3	614.2	544	585	0.30	92
RDRCA 420	642.3	643.2	544	586	0.25	96
RDRCA 425	613.3	614.2	544	585	0.32	94
RDRCA 442	613.3	614.2	544	586	0.47	93
RDRCA 447	701.2	702.2	544	585	0.35	95
RDRCA 457	669.2	670.2	544	586	0.31	94
RDRCA 477	665.2	666.2	544	586	0.37	93

Compound	M⁺(calc.)	M⁺(exp.)	λ_abs(nm)	λ_em(nm)	φ	purity
RDRCA 478	661.3	662.2	544	585	0.32	94
RDRCA 480	681.2	682.2	544	586	0.40	94
RDRCA 487	599.3	600.2	544	585	0.29	93
RDRCA 522	689.3	690.2	544	586	0.31	93
RDRCA 531	701.2	702.2	544	585	0.44	91
RDRCA 554	669.3	670.2	544	586	0.38	93
RDRCA 565	701.2	702.2	544	586	0.33	92
RDRCA 567	697.4	698.2	544	585	0.34	91
RDRCA 572	725.2	726.2	544	586	0.25	92
RDRCA 574	613.3	614.2	544	586	0.29	92
RDRCA 575	597.2	598.2	544	586	0.18	96
RDRCA 602	627.3	628.2	544	585	0.32	92
RDRCA 617	665.2	666.2	544	586	0.47	93
RDRCA 621	729.1	730.0	544	585	0.31	89
RDRCA 631	711.2	712.2	544	586	0.48	93
RDRCA 677	681.2	682.2	544	586	0.37	91
RDRCA 686	715.2	716.2	544	585	0.48	92

Table 6.3 HPLC-MS characterization and photophysical property of RDRAC library

Compound	M⁺(calc.)	M⁺(exp.)	λ_abs(nm)	λ_em(nm)	φ[*1]	purity[*2]
RDRAC 28	705.5	706.4	545	587	0.51	94
RDRAC 49	643.3	644.2	546	587	0.46	93
RDRAC 55	691.4	692.4	544	586	0.40	94
RDRAC 77	627.3	628.3	545	586	0.32	97
RDRAC 80	635.3	636.2	545	587	0.30	94
RDRAC 92	593.3	594.4	545	587	0.40	93
RDRAC 100	703.3	704.2	545	586	0.34	96
RDRAC 101	613.3	614.2	546	586	0.45	94
RDRAC 103	643.3	644.2	545	587	0.41	94
RDRAC 95	551.3	552.2	546	586	0.38	93

RDRAC 124	659.3	660.2	545	587	0.34	94
RDRAC 131	641.3	642.2	546	587	0.49	92
RDRAC 135	667.2	668.2	546	587	0.53	92
RDRAC 148	644.3	645.2	544	587	0.41	94
RDRAC 165	581.3	582.2	545	586	0.47	93
RDRAC 175	549.3	550.2	546	586	0.48	93
RDRAC 177	567.3	568.2	545	587	0.44	91
RDRAC 181	659.3	660.2	546	587	0.50	90
RDRAC 182	579.3	580.4	546	586	0.40	94
RDRAC 185	579.3	580.4	546	586	0.41	91
RDRAC 201	641.3	642.2	544	587	0.39	92
RDRAC 211	613.3	614.2	545	586	0.43	93
RDRAC 218	617.3	618.2	546	587	0.41	93
RDRAC 220	617.3	618.2	544	587	0.44	94
RDRAC 221	633.2	634.2	545	587	0.36	96
RDRAC 222	551.3	552.2	545	586	0.36	92
RDRAC 230	621.4	622.4	545	586	0.39	89
RDRAC 240	675.3	676.2	545	587	0.37	92
RDRAC 262	659.3	660.2	546	587	0.35	92
RDRAC 272	620.3	621.2	545	586	0.39	95
RDRAC 273	643.3	644.2	546	586	0.34	92
RDRAC 275	641.3	642.2	545	587	0.51	93
RDRAC 277	607.3	608.2	546	586	0.38	92
RDRAC 282	622.3	623.2	546	587	0.39	93
RDRAC 318	642.3	643.2	544	587	0.44	91
RDRAC 335	627.3	628.2	545	587	0.36	91
RDRAC 341	677.2	678.2	546	587	0.50	95
RDRAC 356	689.3	690.2	545	586	0.35	95
RDRAC 361	644.3	645.2	546	586	0.28	95
RDRAC 363	644.3	645.2	546	587	0.35	96
RDRAC 364	633.2	634.2	546	587	0.49	93
RDRAC 368	678.4	679.4	544	586	0.49	93
RDRAC 373	565.3	566.2	545	586	0.39	94

RDRAC 374	599.3	600.2	545	587	0.33	92
RDRAC 375	617.3	618.2	546	586	0.40	93
RDRAC 382	605.3	606.2	545	587	0.35	95
RDRAC 387	629.3	630.2	546	587	0.33	92
RDRAC 388	613.3	614.2	546	587	0.42	90
RDRAC 395	643.3	644.2	545	587	0.45	94
RDRAC 396	613.3	614.2	546	586	0.37	92
RDRAC 398	613.3	614.2	545	586	0.50	93
RDRAC 399	635.3	636.2	546	587	0.43	91
RDRAC 403	633.2	634.2	546	587	0.56	94
RDRAC 405	631.3	632.2	544	586	0.27	92
RDRAC 407	649.4	650.2	545	586	0.42	94
RDRAC 414	648.4	649.2	546	587	0.34	92
RDRAC 419	579.3	580.4	545	586	0.35	91
RDRAC 420	608.3	609.2	546	587	0.42	95
RDRAC 425	579.3	580.2	546	587	0.45	93
RDRAC 442	579.3	580.2	546	587	0.37	94
RDRAC 447	667.3	668.2	544	587	0.37	93
RDRAC 457	635.3	636.2	545	586	0.42	93
RDRAC 477	631.3	632.2	546	586	0.46	92
RDRAC 478	627.3	628.2	544	587	0.37	93
RDRAC 480	647.3	648.2	545	587	0.37	95
RDRAC 487	565.3	566.2	545	586	0.44	94
RDRAC 522	655.3	656.4	545	586	0.21	94
RDRAC 531	667.2	668.2	546	587	0.55	92
RDRAC 554	635.4	636.4	545	586	0.38	93
RDRAC 565	667.2	668.0	546	587	0.46	93
RDRAC 567	663.4	664.4	546	587	0.31	94
RDRAC 572	691.2	694.2	544	587	0.42	93
RDRAC 574	579.3	580.4	545	586	0.47	93
RDRAC 575	563.3	564.2	546	586	0.31	95
RDRAC 602	593.3	594.4	545	587	0.36	93
RDRAC 617	631.3	632.2	546	587	0.38	94

RDRAC 621	695.2	696.2	546	586	0.43	90
RDRAC 631	677.3	678.2	546	586	0.50	94
RDRAC 677	647.3	648.2	544	586	0.35	92
RDRAC 686	681.2	682.2	545	587	0.36	90

*1 Quantum yields were measured in DMSO, using Rhodamine B as a standard (ϕ : 0.49, in DMSO).*2 Purities were determined according to UV absorption at 350 nm.

ESI-MS positive spectra, HPLC conditions: A: H_2O-HCOOH: 99.9:0.1. B: CH_3CN-HCOOH: 99.9:0.1; gradient 100% A to 95% B (6 min), isocratic 95% B (6-8.2min), gradient 95% B to 100% A (8.2-9 min), isocratic 100% A (9-10 min). Reversephase Phenomenex C18 Luna column (4.6 x 50 mm^2) 3.5 μm, flow rate: 1.0 mL/min.
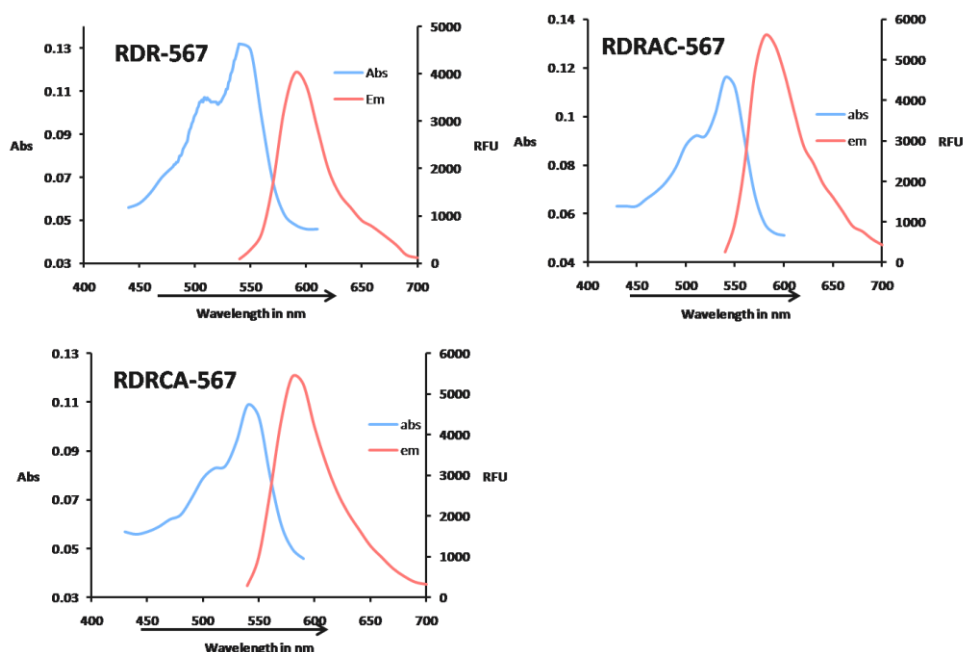
Figure 6.1 Absorption and emission of RDR, RDRCA, RDRAC

6.3.2 Discovery of Mitotic phase probe

For the mitotic cell imaging, RPE1:H2B:GFP (retinal pigmented epithelial cell line stably expressed with histone H2B fused to GFP) cells and M-phase synchronized RPE1:H2B:GFP cells were screened with the RDR

library compounds. Here tubulin binding compound, Tubulyzine B was used for (10 μM for 24 h) the synchronization. The compounds with various concentrations and with the duration of 1 h were used for the primary screening. The staining results (**Figure 6.2**) indicate that one of our RDR compounds, RDR-567 (RDR-H2) stained brightly to the synchronized cells compared to the control cells.
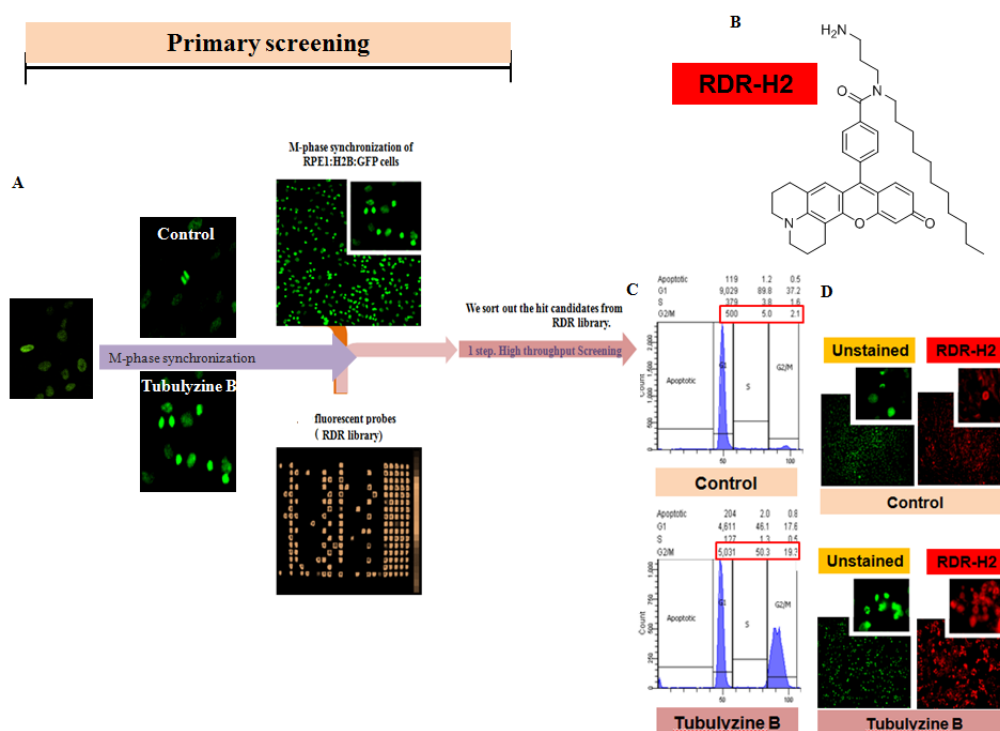
Figure 6.2 Live cell imaging of mitotic cells by RDR-567. A) The work flow of primary screening for seeking M-phase probes. (B) The structure of RDR-567. (C) Representative FACS data showed cell cycle arrested at G_1 phase (control, DMSO) after DMSO treatment for 24 h. Tubulyzine B-treated RPE1:H2B:GFP cells resulted in a clear accumulation of G_2/M phase (red box).(D) Representative Texas red (red)/GFP (green) image showed RDR-567 signal (red) and GFP signal (green) at M-phase (control, Tubulyzine B) after RDR-567 (1 μM) treatment for 1 h. Upper panel, control with RDR-567; down panel, Tubulyzine B with RDR-567; Our probes-treated cells were taken an image using ImageXpress Macro^{TM} cellular imaging system with 10X

phase contrast at 1 h. These data are representative of at least three independent experiments.

6.3.3 Dose dependent study

To check the dose dependent staining pattern of our probe, different concentrations of RDR-567/H2 were treated against the control of RPE1:H2B:GFP cells and tubulyzine B-treated RPE1:H2B:GFP cells. Consequently, **figure 6.3** demonstrated the dose-dependency of RDR-567 stained RPE1:H2B:GFP cells. Here, control and tubulyzine B-treated RPE1:H2B:GFP cells were tretaed with RDR-567 (0.1, 0.2, 0.4, 0.8 and 1.6 µM) for 1 h.
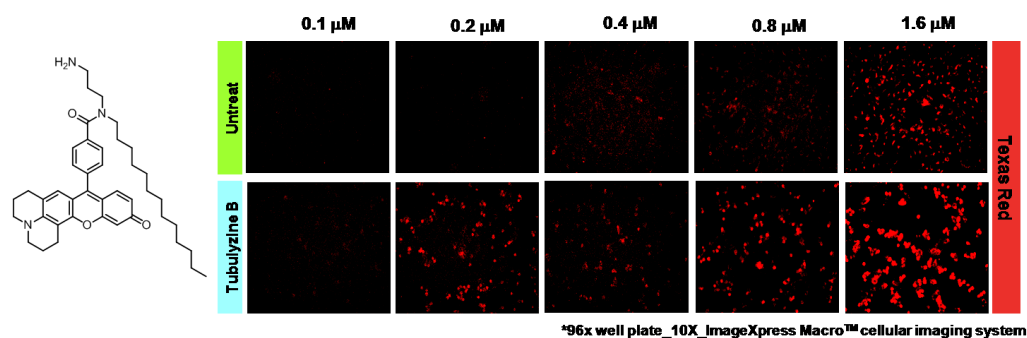
Figure 6.3 Selective staining of M-phase cells by RDR-567 (A) The structure of RDR-567. (B) dose-dependent RDR-567 stained RPE1:H2B:GFP cells. Control and Tubulyzine B-treated RPE1:H2B:GFP cells were added by RDR-567 (0, 0.1, 0.2, 0.4, 0.8, 1.6 µM) for 1 h. These data are representative of at least three independent experiments (Texas Red signal).

6.3.4 Monitoring the M-phase progression in live cells

The **figure 6.4-A** (time course images) indicates that our probe can nicely distinguish between the interphase and mitosis of the cell cycles. Mitosis cells are nicely stained with our probe. During the mitosis cell

staining, the signal intensity from the probe also increases with time (**Figure 6.4-A and B**)
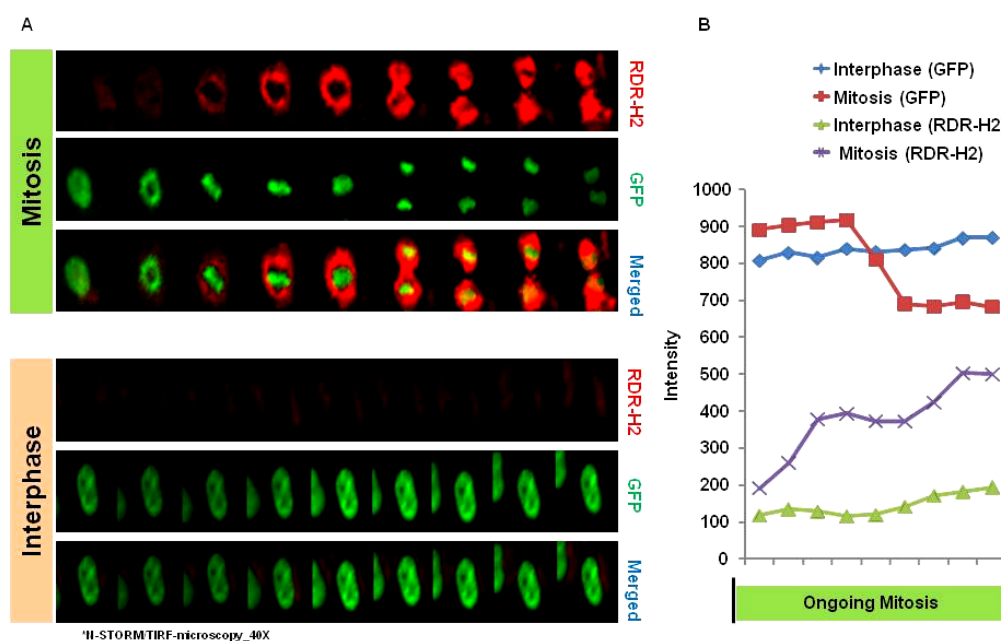
Figure 6.4 Monitoring the M-phase progression in live cells with RDR-H2 **(A)** Representative GFP (🟩 Texas Red (🟥 image showed hit candidate signal at M-phase after RDR-H2 (0.8 μM) treatment for 3 h. To obtain the live cell imaging, fluorescence microscopy was performed on a Nikon N-STORM/TIRF (40X) microscopy with a CoolSNAPHQ digital camera. (B) The intensity graph of mitosis phase-dependent changes in RPE1:H2B:GFP cells with RDR-H2. These data are representative of at least three independent experiments.

6.4 Conclusions

In conclusion, I successfully synthesized rhodol libraries (RDR, RDRCA and RDRAC) using efficient solid phase method. To the best of our knowledge, this is the first systematic report of rhodol library synthesis. Moreover, these compounds inherit excellent photophysical properties. As a result, compounds are suitable enough to utilize them in biological function detection or in probe discovery. Preliminary staining results/finding and with

further detailed study in future may render a suitable mitotic phase probe that can provide a convenient approach for developing detailed predictive models of cell cycle progression.

6.5 Experimental methods

Material and methods

Amine and few bromide building block and all other chemicals and solvents for the synthesis were purchased from the Alfa Aesar, Fluka, Acros, MERCK, and Sigma Aldrich and were used without any purification. Merck Silica Gel 60 (particle size: 0.04-0.063 mm, 230-400 mesh) was used for the normal phase column chromatographic purification. From BeadTech Inc., Korea, 2-chlorotrityl alcohol resin (1.37 mmol/g) was purchased. For analytical characterization of RDR compounds HPLC-MS (Agilent-1200 series) with a DAD detector and a single quadrupole mass spectrometer (6130 series) with an ESI and sometimes with an APCI probe were used. Analytical process, except specified: eluents: A: H_2O (0.1% HCOOH), B: ACN (0.1% HCOOH), C_{18} (2) Luna column (4.6 x $50mm^2$, 5μm particle size) was used. ^{1}H-NMR and ^{13}C-NMR spectra were recorded on both Bruker Avance 500 MHz NMR spectrometer, and chemical shifts are expressed in parts per million (ppm) and approximate coupling constants were calculated in Hz. Quantum yields and all other photophysical properties of RDR derivatives were performed in Spectramax M2 instrument and the obtained data were analyzed using the Microsoft Office Excel 2007.

6.5.1 Synthesis and characterization of intermediate for RDR acid
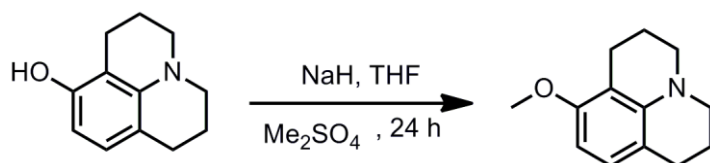
To a suspension of 8-hydroxyjulolidine (1.0 g, 5.3 mmol) and sodium hydride (0.45 g, 11 mmol) in THF (50 mL), dimethylsulfate (1.0 mL, 11 mmol) was added in ice-bath and the mixture was stirred at room temperature for 24 hrs. The reaction mixture was then evaporated and extracted with EtOAc three times. The combined organic layers were washed with water and brine, dried over $MgSO_4$ and evaporated to give the crude product. This was purified by silica gel column chromatography (eluent: Hexane : EtOAc = 5 : 2, Rf = 0.88) to obtain the pure product as viscous oil. Yield: (0.7 g, 65%); LCMS (ESI): calc for $C_{13}H_{17}NO$ (M+H) 204.1; found: 204.2
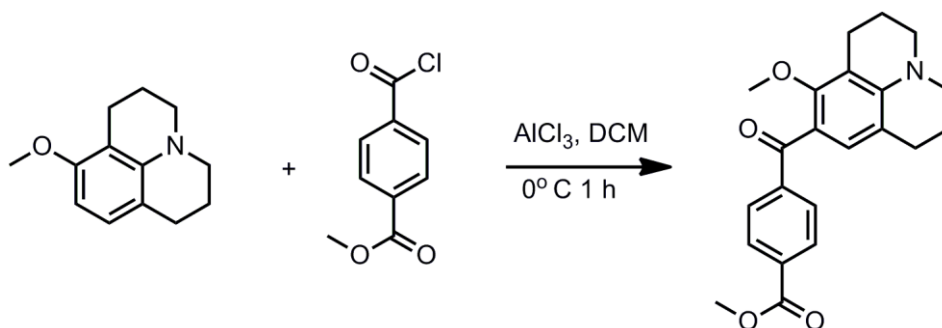
To a solution of methyl 4-(chlorocarbonyl) benzoate (1.1 g, 5.6 mmol) and $AlCl_3$ (0.80 g, 5.6 mmol) in CH_2Cl_2 (60 mL), **1** (1.1 g, 5.6 mmol) was slowly and the mixture was stirred under nitrogen at 0°C for 1hrs. The mixture was poured into aqueous HCl and extracted with CH_2Cl_2 three times. The organic layers were washed with brine, dried over $MgSO_4$ and evaporated to give the crude products. This was dissolved in 50 mL of MeOH and a catalytic amount of sulfuric acid was added. The reaction mixture was heated at reflux 3 hrs with stirring and cooled to room temperature. The solvent was removed

on the rotary evaporator and extracted with EtOAc and H_2O three times. The

organic phase was dried over $MgSO_4$ and evaporated. This was purified by

silica gel column chromatography (eluent: Hexane : EtOAc = 5 : 1, Rf = 0.37)

to obtain the pure product as yellow solids. Yield: 0.44 g (24 %).   ^{1}H- NMR

(500 MHz, $CDCl_3$); δ 1.96 (m, 4H), 2.69 (t, 2H, J=6Hz), 2.74 (t, 2H, J=6Hz),

3.25 (m, 4H), 3.46 (s, 3H), 3.93 (s, 3H), 7.06 (s, 1H), 7.79 (d, 2H, J=9Hz),

8.07 (d, 2H, J=9Hz). LCMS (ESI): calc for $C_{22}H_{23}NO_4$ (M+H) 366.2; found:

366.2
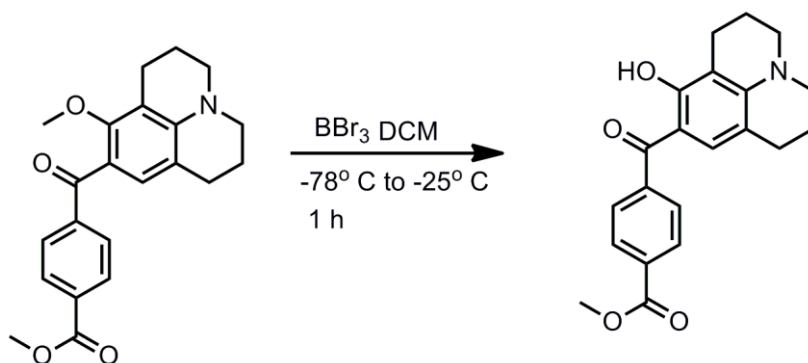
To a stirred solution of **2** (0.42 g, 1.15 mmol) in 10 mL of dry CH_2Cl_2,

a solution of 10 mL of BBr_3 (5 mmol) in $CH_2Cl_2$was added at -78℃. After 1

hr, the mixture was warmed to -25℃. After completion, the mixture was

quenched with saturated sodium bicarbonate. The mixtured was extracted with

CH_2Cl_2 three times. The combined organic layers were washed with water and

brine, dried over $MgSO_4$ and evaporated to give the crude product. It was

recrystallized from EtOH/H_2O solution to the pure product as red solids.

Yield: 24 mg (60 %); ^{1}H- NMR (500 MHz, Methanol-d_4); δ 1.95 (m, 4H), 2.54

(t, 2H, J=6Hz), 2.74 (t, 2H, J=6Hz), 3.27 (m, 4H), 3.95 (s, 3H), 6.82 (s, 1H),

7.62 (d, 2H, J=8.5Hz), 8.12 (d, 2H, J=8.5Hz). ^{13}C-NMR (125 MHz,

Methanol-d_4); δ 19.89, 20.67, 21.71, 27.38, 29.69, 49.82, 50.22, 52.31, 105.7,

108.16, 112.87, 128.40, 129.35, 130.84, 131.4, 143.4, 149.42, 161.41, 166.59, 196.37. LCMS (ESI): calc for $C_{21}H_{21}NO_4$ (M+H) 352.1; found: 352.2
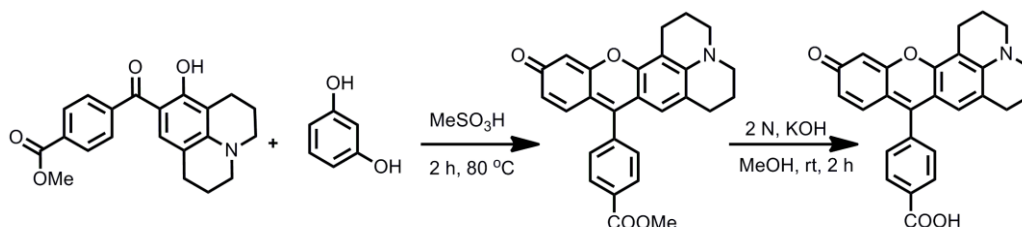
3 (200 mg, 0.56 mmol) and resorcinol (100 mg, 0.91 mmol) were combined in methanesulfonic acid acid (1.0 ml) in a sealed tube and heated at 80℃ for 2.0 hrs. The cooled brick melt was pulverized. The solid was collected on a frit, washed thoroughly with hot water and dried in vacuo. This was purified by silica gel column chromatography (Eluent: CH_2Cl_2 : MeOH = 10 : 1, Rf = 0.42) to obtain the pure product as red solids. Yield: 25 mg (10 %);   **4** (25 mg, 0.058 mmol) and 0.06 ml of 2 N KOH (0.12 mmol) solution were taken in methanol and stirred at rt for 2 hrs. Reaction was monitored by TLC. Then methanol was removed in vacuum and then compound from aqueous layer was extracted with DCM. The organic layer was dried over vacuum and crude was purified by silica gel column chromatography (Eluent: CH_2Cl_2 : MeOH = 9 : 1, Rf = 0.40). . Yield: 10 mg (40 %). ^{1}H-NMR (500 MHz, Methanol-d$_4$): δ 1.95 (m, 4H), 2.16-2.20 (m, 6H), 2.54 (t, 2H, J=6Hz), 2.74 (t, 2H, J=6Hz), 3.27 (m, 4H), 3.95 (s, 3H), 6.1 (s, 1H), 6.31 (d, 1H, J=5Hz), 6.42 (d, 1H, J=5Hz), 6.82 (s, 1H), 7.62 (d, 2H, J=8.5Hz), 8.12 (d, 2H, J=8.5Hz).

LCMS (ESI): calc for $C_{26}H_{21}NO_4$ (M+H) 412.1; found: 412.2

Characterization data for RDR-H2 (RDR-567) compound
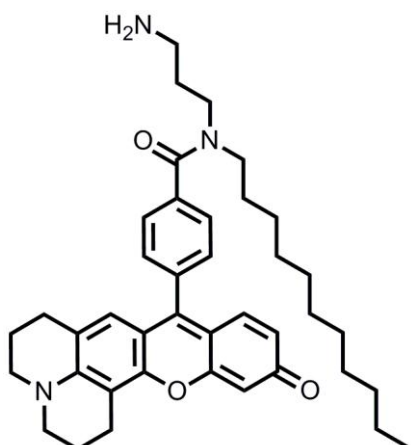
LCMS (ESI): calc for $C_{40}H_{51}N_3O_3$ (M+H) 622.4; found: 622.4

^{1}H- NMR (500 MHz, Methanol-d_4); δ 0.89 (t, 3H, J=6.5 Hz), 1.01-1.22 (m, 16 H), 1.92 (m, 4H), 2.12-2.21 (m, 6H),2.53 (t, 2H, J=6Hz), 2.75 (t, 2H, 6Hz), 3.26 (m, 4H), 3.96 (s, 3H), 6.14 (s, 1H), 6.32 (d, 1H, J=5Hz), 6.41(d, 1H, J=5Hz), 6.81 (s, 1H), 7.61 (d, 2H, J=8.5Hz), 8.11 (d, 2H, J=8.5Hz). ^{13}C-NMR (125 MHz, Methanol-d_4); δ 7.81, 12.98, 13.01, 19.00, 19.14, 20.04, 22.29, 25.59, 26.10, 27.18, 28.17, 28.62, 29.06, 29.22, 29.33, 31.61, 37.07, 41.91, 46.53, 49.41, 50.98, 51.44, 102.10, 116.04, 116.36, 126.81, 127.01, 127.68, 129.85, 130.92, 133.60, 153.41, 154.31, 156.52.

LC-MS of RDR-H2
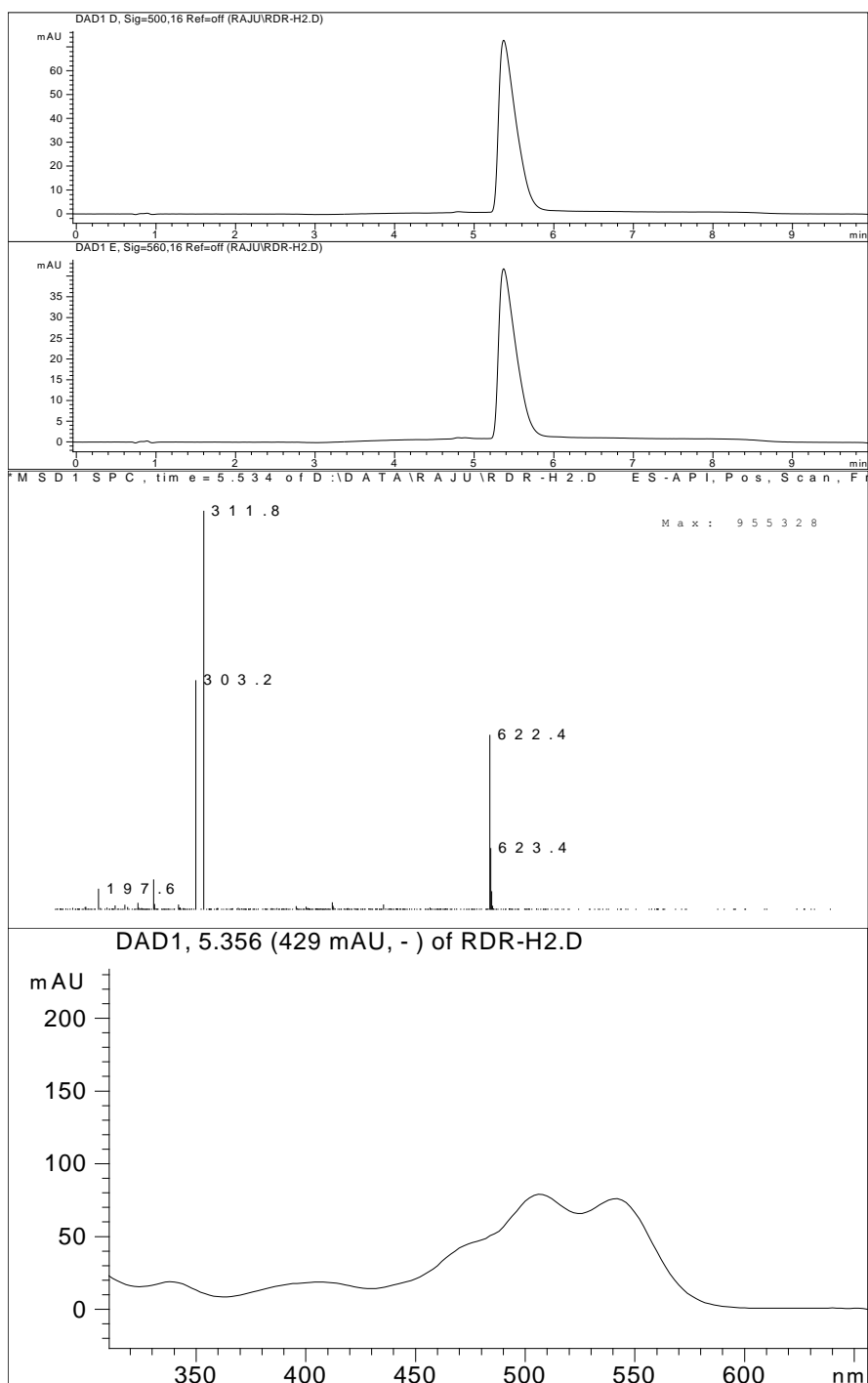
6.5.2 Live mitotic cell imaging using ImageXpress Macro^{TM} cellular imaging system

Mitotic block was induced to RPE:H2B:GFP cells by treatment with or without tubulyzine B (10 μM) for 24 h before analysis. For synchronization of

mitosis, RPE1:H2B:GFP cells were seeding in 96 (or 12) xwell plate, synchronized by Tubulyzine B (10 μM) for 24 h. RDR-H2/567 treated- cells at 0.1 to 1 μM were stained for 1 h. To visualize the nuclear, our probe-stained cells were added 1 μM of Hoechst 33342 from 30 min. The live cell images were taken by well randomly using ImageXpress Macro™ cellular imaging system with 10X phase contrast objectives at various time points throughout the experiment. All controls in subsequent experiments included 0.1% DMSO. To obtain the live cell imaging with spectrum, fluorescence microscopy was performed on a A1P+ confocal microscope (100X) or N-STORM/TIRF (40X) microscopy with a CoolSNAP HQ digital camera.

6.5.3 Cell culture

RPE1:H2B:GFP (retinal pigmented epithelial cell line stably expressed with histone H2B fused to GFP) cells were cultured on a cell culture dish in Dulbecco's Modified Eagle Medium (Sigma) with 10% FBS and 1% PS.

6.5.4 Cell synchronization

For synchronization of Mitosis, RPE1:H2B:GFP cells were seeding in 384xwell plate, synchronized by Tubulyzine B (10 μM) for 24 h. Test reagent treated- cells were stained at 1 μM of Hoechst 33342 from 30 min. The live cell images were taken for an image using ImageXpress Macro™ cellular imaging system with x10 phase contrast objectives at various time points throughout the experiment. All controls in subsequent experiments included 0.1% DMSO. To obtain the live cell imaging, fluorescence microscopy was performed on a Nikon Ti inverted microscope with a CoolSNAP HQ digital camera.

6.5.5 Cell cycle analysis

For synchronization of mitosis, RPE1:H2B:GFP cells were seeding in 384xwell plate, synchronized by Tubulyzine B (10 μM) for 24 h. RDR-567/H2 (0.8 μM) treated- cells were stained for 1 h. For FACS analysis with PI staining and live condition, cell samples were harvested with trypsinization. To stain the DNA content, cells were fixed with cold 100% Methanol and stained with PI at a final concentration f 10 μg/ml. To stain the DNA content in live cells, our probe-stained cells were added 1 μM of Hoechst 33342 from 30 min. Cell cycle phase distributions were analyzed by flow cytometry (BD Bioscience).

6.6 References

1) J. R. Lakowicz, Principles of Fluorescence Spectroscopy, 3rd ed.; Springer US: New York, 2006.

2) (a) A. P. de Silva, H. Q. Gunaratne, T. Gunnlaugsson, A. J. Huxley, C. P. McCoy, J. T. Rademacher and T. E. Rice, *Chem. Rev.*, 1997, **97**, 1515.; (b) J. F. Callan, A. P.de Silva and D. C. Magri, *Tetrahedron* 2005, **61**, 8551–8588.; (c) K. Tanaka, T. Miura, N. Umezawa, Y. Urano, K. Kikuchi, T. Higuchi and T. Nagano, *J. Am. Chem. Soc.*, 2001, **123**, 2530.; (d) T. Miura, Y. Urano, K. Tanaka, T. Nagano, K. Ohkubo and S. Fukuzumi, *J. Am. Chem. Soc.*, 2003, **125**, 8666.; (e) Y. Gabe, Y. Urano, K. Kikuchi, H. Kojima and T. Nagano, *J Am Chem Soc*, 2004, **126**, 3357-3367.

3) (a) S. Kauffman and A. D. Ellington, *Curr. Opin. Chem. Biol.*, 1999, **3**, 256.; (b) N. S. Finney, *Curr. Opin. Chem. Biol.*, 2006, **10**, 238-245.

4) (a) J. V. Mello and N. S. Finney, *J. Am. Chem. Soc.*, 2005, **127**, 10124.; (b) S. Wang and Y. T. Chang, *J. Am. Chem. Soc.*, 2006, **128**,

10380-10381. (c) Y. H. Ahn, J. S. Lee and Y. T. Chang, *J Am Chem Soc*, 2007, **129**, 4510-4511.

5) (a) L. G. Lee, G. M. Berry and C. H. Chen, *Cytometry*, 1989, **10**, 151.; (b) J. E. Whitaker, R. P. Haugland, D. Ryan, P. C. Hewitt and F. G. Prendergast, *Anal Biochem*, 1992, **207**, 267.

6) S. C. Burdette and S. J. Lippard, *Inorg. Chem.*, 2002, **41**, 6816.

7) R. P. Haugland, The Handbook: A Guide to Fluorescent Probes and Labeling Technologies, 10th ed.; Molecular Probes: Eugene, OR, 2005

8) (a) M. A. Clark, K. Duffy, J. Tibrewala and S. J. Lippard, *Org. Lett.*, 2003, **5**, 2051. (b) B. C. Dickinson and C. J. Chang, *J. Am. Chem. Soc.*, 2008, **130**, 9638.

9) I. Neganova and M. Lako, *J. Anat.*, 2008, **213**, 30.

10) R. D. Barnard and A. Oppenheim, *Brit. Med. J.*, 1962, 943-&.

11) M. Hesse, A. Raulf, G. A. Pilz, C. Haberlandt, A. M. Klein, R. Jabs, H. Zaehres, C. J. Fugemann, K. Zimmermann, J. Trebicka, A. Welz, A. Pfeifer, W. Roll, M. I. Kotlikoff, C. Steinhauser, M. Gotz, H. R. Scholer and B. K. Fleischmann, *Nat. Commun.*, 2012, **3**.

12) M. Vleugel, E. Hoogendoorn, B. Snel and G. J. P. L. Kops, *Dev. Cell*, 2012, **23**, 239.

13) (a) K. L. Crossin and D. H. Carney, *Cell,* 1981, **23,** 61.; (b) A. Sakaue-Sawano, H. Kurokawa, T. Morimura, A. Hanyu, H. Hama, H. Osawa, S. Kashiwagi, K. Fukami, T. Miyata, H. Miyoshi, T. Imamura, M. Ogawa, H. Masai and A. Miyawaki, *Cell,* 2008, **132,** 487.

Chapter 7

Solid phase Synthesis Coumarin dye Library
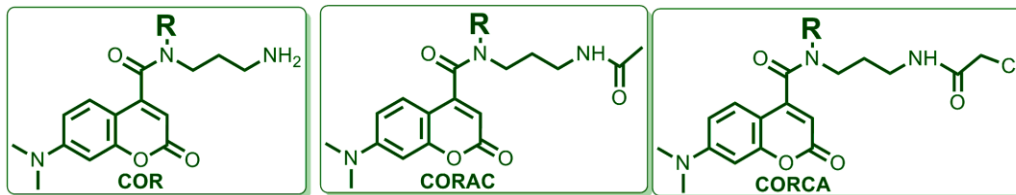
7.1 Introduction

Functional fluorescent molecules are useful in many fields of scientific research, including analytical chemistry or cell biology. For example, fluorescent molecules, whose fluorescence properties can be changed by binding to or reacting with ions, small molecules, or enzymes, enable us to estimate the concentration or activity of the targets.[1,2] Although some theoretical approaches to the design of such sensors have been reported, [2,3] most currently available sensors were developed empirically. Combinatorial synthesis of libraries of fluorescent molecules is an effective approach.[4] Chang *et al* have developed libraries of styryl dyes bearing DNA sensitive fluorescent sensors[5] and an amyloid sensors,[6] and Finney *et al.* developed a fluorescent Hg^{2+} sensor via construction of a library.[7] Coumarins are of interest because of their pharmacological activity[8] and photophysical properties, and they have been applied as laser dyes[9] and fluorophores for fluorescent sensors.[10] Bauerle *et al.*[11] and Wang *et al.*[12] reported coumarin libraries with diversity at the 3-position via Suzuki Miyaura, Heck, Sonogashira Hagihara, or Husigen cycloaddition reactions; they obtained coumarins with a wide range of absorbance, fluorescence wavelength, and fluorescence intensity. This work also confirmed the conclusion that electron-donating groups at 7-position of coumarins [13] showed strong enhancement of the fluorescence and dominated the emission color. Keeping all that in mind, we opted a coumarin scaffold which contains dimethyl amino group at 7- position for better photophysical property and acid group at 4-position for diversification. Over all, we constructed a coumarin library (COR, CORCA and CORAC) with diversity at the 4-position using our efficient solid phase synthesis to explore these

compounds in the evalution of biological function via cell based and in vitro screening.

7.2 Objectives

Herein, we report the diversity oriented solid synthesis of coumarin library. To the best of our knowledge, this the first report of coumarin library where modification has been performed in the 4-postion of the coumarin scaffold. This chapter mainly covers the synthesis and evaluations of the photophysical properties of coumarin library and their future prospect for the study of biological functions.

7.3 Results and Discussion

For the COR library synthesis (**Scheme 7.1**), carboxylic acid containing coumarin scaffold **1** was used as the key intermediate. The general synthetic strategy of coumarin acid **2** involves two steps (40% overall yield) reaction process. First, coumarin ester **1** was synthesized according to procedures (Song *et al.*)[14], with modifications, by Pechmann cyclization of 3-dimethylamino phenol with diethyloxalacetate (DEOA), then followed by basic hydrolysis of that ester provided the key intermediate of coumarin acid **2**.Then the structurally diverse COR library was synthesized using previously reported robust solid phase synthesis technique.[15] Here, the wide structural diversity was introduced by the use of solid phase secondary amines 5 utilizing a simple reaction between the bromopropylamine loaded resins **4** with the series of primary amines (**Chart 7.1**). Then the key intermediate of coumarin acid **2** was coupled to this solid phase amine building block by using a standard acid–amine coupling protocol. The final step of acidic cleavage

from the solid supported compounds 3 yielded 80 very pure members of the COR library (average purity is 90% without further purification at 350 nm, **Table 7.1, 7.2 and 7.3**).

Scheme 7.1 Synthesis of COR library.

R: From Amine building block
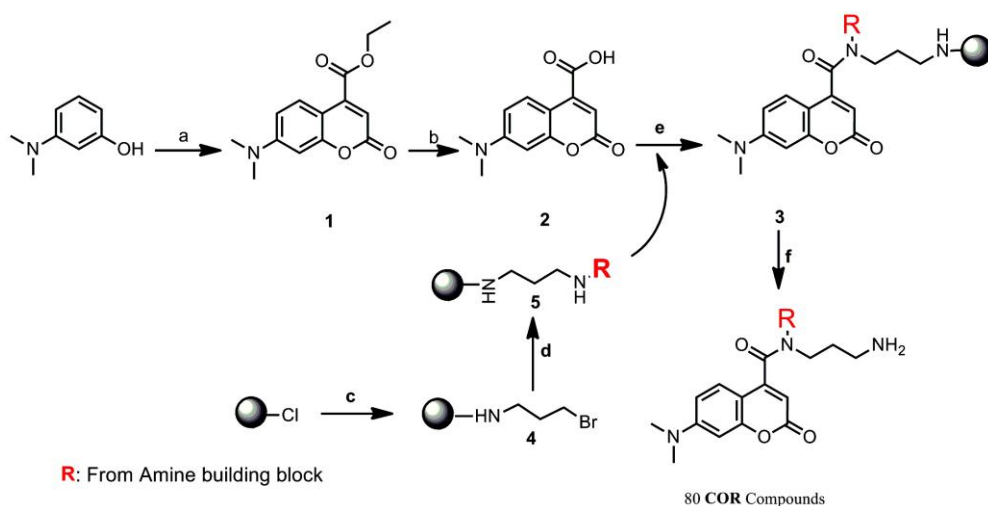
80 **COR** Compounds

Reagents and conditions (a) Sodium ditheyloxalacetate, $ZnCl_2$, EtOH, reflux, 15 h.; (b) 2M LiOH, $THF:H_2O$ (3:1), 0 ^{o}C to rt, 0.5 hr.; (c) DIEA, THF, 3-bromopropylamine, r.t., 12 h.; (d) DIEA, RNH_2, NMP, 70 ^{o}C, 12 h.; (e) DMF, HATU, DIEA, r.t. 24 h.; (f) 2% TFA in DCM , r.t., 40 min.

Then, CORCA and CORAC compounds were synthesized according to the previous mention protocol (chapter 3). All the compounds in the library were characterized by HPLC-MS and 80 relatively pure compounds (average purity is 90%, measured at 350 nm (**Table 7.1, 7.2 and 7.3**) were collected for further study. The high stokes shift of this library is reflected from the spectral characteristics (**Figure 7.1, Table 7.1, 7.2 and 7.3**)

186

Scheme 7.2 CORCA and CORAC library synthesis
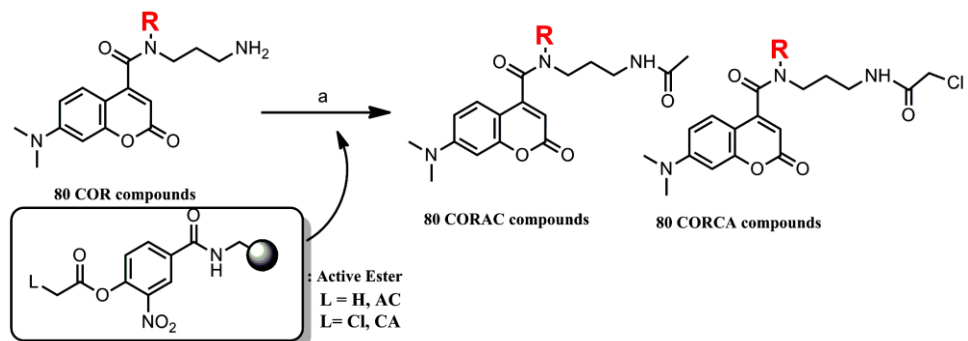
Reagents and conditions: (a) DCM/CAN (7:1), sat. NaHCO$_3$, rt, 2 hrs.

Chart 7.1 Amine building blocks for COR library
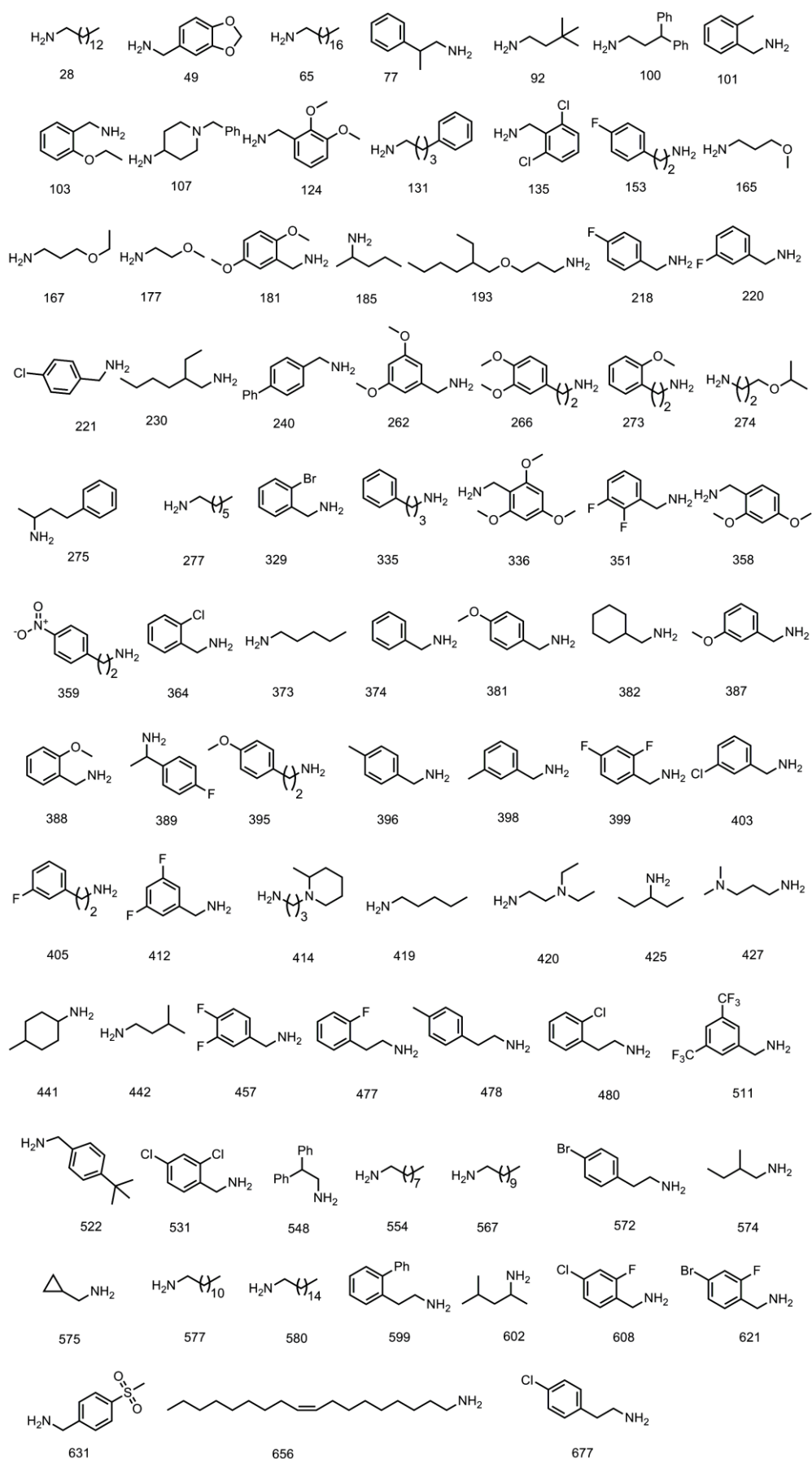
Table 7.1 HPLC-MS characterization and photophysical property of COR library

Compound	M^+(calc.)	M^+(exp.)	λ_{abs}(nm)	λ_{em}(nm)	ϕ*[1]	purity*[2]
COR 28	485.4	486.4	386	530	0.26	90
COR 49	423.2	424.2	386	530	0.22	95
COR 65	541.4	542.4	386	530	0.19	96
COR 77	407.2	408.2	386	530	0.25	93
COR 92	373.2	374.2	386	530	0.24	90
COR 100	483.3	484.4	386	530	0.29	89
COR 101	393.2	394.2	386	530	0.18	94
COR 103	423.2	424.2	386	530	0.31	92
COR 107	462.3	463.2	386	530	0.19	92
COR 124	439.2	440.2	386	530	0.21	95
COR 131	421.2	422.2	386	530	0.33	92
COR 135	447.1	448.2	386	530	0.27	94
COR 153	411.2	412.2	386	530	0.25	94
COR 165	361.2	362.2	386	530	0.25	89
COR 167	375.2	376.2	386	530	0.27	90
COR 177	347.2	348.2	386	530	0.19	91
COR 181	439.2	440.2	386	530	0.3	90
COR 185	359.2	460.2	386	530	0.26	91
COR 193	459.3	460.2	386	530	0.22	93
COR 218	397.2	398.2	386	530	0.18	90
COR 220	397.2	398.2	386	530	0.14	92
COR 221	413.2	414.2	386	530	0.17	90
COR 230	401.3	402.2	386	530	0.26	95
COR 240	455.2	456.2	386	530	0.28	92
COR 262	439.2	440.2	386	530	0.19	93
COR 266	453.2	454.2	386	530	0.14	90
COR 273	423.2	424.2	386	530	0.25	91
COR 274	389.2	390.2	386	530	0.13	92
COR 275	421.2	423.2	386	530	0.2	93
COR 277	387.3	388.2	386	530	0.19	94

COR 329	457.1	458.2	386	530	0.17	92
COR 335	407.2	408.2	386	530	0.32	92
COR 336	469.2	470.2	386	530	0.22	92
COR 351	415.2	416.2	386	530	0.21	93
COR 358	439.2	440.2	386	530	0.22	92
COR 359	438.2	439.2	386	530	0.17	90
COR 364	413.2	414.2	386	530	0.12	94
COR 373	345.2	346.2	386	530	0.21	95
COR 374	379.2	380.2	386	530	0.16	96
COR 381	409.2	410.2	386	530	0.19	92
COR 382	385.2	386.2	386	530	0.15	93
COR 387	409.2	410.2	386	530	0.13	94
COR 388	409.2	410.2	386	530	0.15	95
COR 389	411.2	413.2	386	530	0.12	93
COR 395	423.2	424.2	386	530	0.19	95
COR 396	393.2	394.2	386	530	0.19	96
COR 398	393.2	394.2	386	530	0.3	90
COR 399	415.2	416.2	386	530	0.12	89
COR 403	413.2	414.2	386	530	0.18	94
COR 405	411.2	412.2	386	530	0.19	91
COR 412	415.2	416.2	386	530	0.13	92
COR 414	430.3	431.2	386	530	0.11	92
COR 419	359.2	360.2	386	530	0.19	94
COR 420	390.3	391.2	386	530	0.18	91
COR 425	359.2	360.2	386	530	0.17	92
COR 427	376.2	377.2	386	530	0.2	91
COR 441	385.2	386.2	386	530	0.24	92
COR 442	359.2	360.2	386	530	0.19	93
COR 457	415.2	416.2	386	530	0.17	94
COR 477	411.2	412.2	386	530	0.29	92
COR 478	407.2	408.2	386	530	0.17	95
COR 480	427.2	428.2	386	530	0.18	92
COR 511	515.2	516.2	386	530	0.16	91

Compound	M⁺(calc.)	M⁺(exp.)	λ_abs(nm)	λ_em(nm)	φ	Purity
COR 522	435.3	436.2	386	530	0.19	92
COR 531	447.1	448.0	386	530	0.24	94
COR 548	469.2	470.4	386	530	0.22	90
COR 554	415.3	416.2	386	530	0.27	91
COR 567	443.3	444.2	386	530	0.2	91
COR 572	471.1	472.2	386	530	0.26	92
COR 574	359.2	360.2	386	530	0.21	92
COR 575	343.2	344.2	386	530	0.21	91
COR 577	457.3	458.2	386	530	0.24	92
COR 580	513.4	514.4	386	530	0.2	92
COR 599	469.2	470.2	386	530	0.28	95
COR 602	373.2	374.2	386	530	0.25	96
COR 608	431.1	432.2	386	530	0.19	93
COR 621	475.1	476.2	386	530	0.22	90
COR 631	457.2	458.2	386	530	0.24	88
COR 656	539.4	540.4	386	530	0.32	90
COR 677	427.2	428.2	386	530	0.32	89

Table 7.2 HPLC-MS characterization and photophysical property of CORCA library

Compound	M⁺(calc.)	M⁺(exp.)	λ_abs(nm)	λ_em(nm)	φ*¹	Purity*²
CORCA 28	561.3	562.2	388	528	0.33	91
CORCA 49	499.2	500.2	388	528	0.22	92
CORCA 65	617.4	618.4	388	528	0.31	94
CORCA 77	483.2	484.2	388	528	0.29	90
CORCA 92	449.2	450.2	388	528	0.22	90
CORCA 100	559.2	560.2	388	528	0.24	88
CORCA 101	469.2	470.2	388	528	0.16	93
CORCA 103	499.2	500.2	388	528	0.23	91
CORCA 107	538.2	539.2	388	528	0.02	94
CORCA 124	515.2	516.2	388	528	0.17	93

CORCA 131	497.2	498.2	388	528	0.29	91
CORCA 135	523.1	524.2	388	528	0.17	92
CORCA 153	487.2	488.2	388	528	0.24	93
CORCA 165	437.2	438.2	388	528	0.27	91
CORCA 167	451.2	452.2	388	528	0.25	91
CORCA 177	423.2	424.2	388	528	0.27	92
CORCA 181	515.2	516.2	388	528	0.2	90
CORCA 185	435.2	436.2	388	528	0.26	92
CORCA 193	535.3	536.2	388	528	0.29	94
CORCA 218	473.2	474.2	388	528	0.12	94
CORCA 220	473.2	474.2	388	528	0.18	96
CORCA 221	489.1	490.2	388	528	0.21	91
CORCA 230	477.2	478.2	388	528	0.32	96
CORCA 240	531.2	532.2	388	528	0.18	95
CORCA 262	515.2	516.2	388	528	0.2	93
CORCA 266	529.2	530.2	388	528	0.27	95
CORCA 273	499.2	500.2	388	528	0.29	92
CORCA 274	465.2	466.2	388	528	0.24	93
CORCA 275	497.2	498.2	388	528	0.21	91
CORCA 277	463.2	464.2	388	528	0.28	93
CORCA 329	533.1	534.2	388	528	0.21	95
CORCA 335	483.2	484.2	388	528	0.22	92
CORCA 336	545.2	546.2	388	528	0.3	92
CORCA 351	491.1	492.2	388	528	0.23	92
CORCA 358	515.2	516.2	388	528	0.29	97
CORCA 359	514.2	515.2	388	528	0.04	96
CORCA 364	489.1	490.2	388	528	0.18	93
CORCA 373	421.2	422.2	388	528	0.27	94
CORCA 374	455.2	456.2	388	528	0.19	93
CORCA 381	485.2	486.2	388	528	0.21	95
CORCA 382	461.2	462.2	388	528	0.32	93
CORCA 387	485.2	486.2	388	528	0.2	92
CORCA 388	485.2	486.2	388	528	0.26	94

CORCA 389	487.2	488.2	388	528	0.1	95
CORCA 395	499.2	500.2	388	528	0.3	95
CORCA 396	469.2	470.2	388	528	0.23	92
CORCA 398	469.2	470.2	388	528	0.2	91
CORCA 399	491.1	492.2	388	528	0.16	89
CORCA 403	489.1	490.2	388	528	0.19	93
CORCA 405	487.2	488.2	388	528	0.23	91
CORCA 412	491.1	492.2	388	528	0.2	91
CORCA 414	506.3	507.2	388	528	0.08	90
CORCA 419	435.2	436.2	388	528	0.32	93
CORCA 420	466.2	467.2	388	528	0.13	94
CORCA 425	435.2	436.2	388	528	0.29	94
CORCA 427	452.2	453.2	388	528	0.06	92
CORCA 441	461.2	462.2	388	528	0.27	94
CORCA 442	435.2	436.2	388	528	0.26	93
CORCA 457	491.1	492.2	388	528	0.16	94
CORCA 477	487.2	488.2	388	528	0.25	92
CORCA 478	483.2	484.2	388	528	0.4	94
CORCA 480	503.1	504.2	388	528	0.25	93
CORCA 511	591.1	592.2	388	528	0.18	93
CORCA 522	511.2	512.2	388	528	0.27	92
CORCA 531	523.1	524.2	388	528	0.18	93
CORCA 548	545.2	546.2	388	528	0.29	92
CORCA 554	491.3	492.4	388	528	0.32	91
CORCA 567	519.3	520.4	388	528	0.34	91
CORCA 572	547.1	548.2	388	528	0.27	93
CORCA 574	435.2	436.2	388	528	0.24	95
CORCA 575	419.2	420.2	388	528	0.29	94
CORCA 577	533.3	534.2	388	528	0.31	93
CORCA 580	589.4	590.4	388	528	0.38	92
CORCA 599	545.2	546.2	388	528	0.32	92
CORCA 602	449.2	450.2	388	528	0.3	92
CORCA 608	507.1	508.2	388	528	0.19	93

Compound	M⁺(calc.)	M⁺(exp.)	λ_abs(nm)	λ_em(nm)	φ*¹	purity*²
CORCA 621	551.1	552.0	388	528	0.17	95
CORCA 631	533.1	534.2	388	528	0.16	91
CORCA 656	615.4	616.4	388	528	0.34	92
CORCA 677	503.1	504.2	388	528	0.26	92

Table 7.3 HPLC-MS characterization and photophysical property of CORAC

library

Compound	M^+(calc.)	M^+(exp.)	λ_{abs}(nm)	λ_{em}(nm)	ϕ*¹	purity*²
CORAC 28	527.4	528.4	383	530	0.3	91
CORAC 49	465.2	466.2	383	530	0.31	92
CORAC 65	583.4	584.4	383	530	0.46	94
CORAC 77	449.2	450.2	383	530	0.22	92
CORAC 92	415.2	416.4	383	530	0.23	92
CORAC 100	525.3	526.2	383	530	0.23	88
CORAC 101	435.2	436.2	383	530	0.05	93
CORAC 103	465.2	466.2	383	530	0.2	92
CORAC 107	504.3	505.2	383	530	0.04	94
CORAC 124	481.2	482.2	383	530	0.07	93
CORAC 131	463.2	464.4	383	530	0.22	94
CORAC 135	489.1	490.2	383	530	0.16	93
CORAC 153	453.2	454.2	383	530	0.45	92
CORAC 165	403.2	404.2	383	530	0.31	90
CORAC 167	417.2	418.2	383	530	0.22	92
CORAC 177	389.2	390.2	383	530	0.41	93
CORAC 181	481.2	482.2	383	530	0.17	91
CORAC 185	401.2	402.2	383	530	0.4	92
CORAC 193	501.3	502.2	383	530	0.35	92
CORAC 218	439.2	440.2	383	530	0.26	91
CORAC 220	439.2	440.2	383	530	0.22	93
CORAC 221	455.2	456.2	383	530	0.33	92
CORAC 230	443.3	444.4	383	530	0.36	93
CORAC 240	497.2	498.4	383	530	0.14	91

CORAC 262	481.2	482.2	383	530	0.56	92
CORAC 266	495.2	941.7	383	530	0.36	92
CORAC 273	465.2	466.2	383	530	0.46	91
CORAC 274	431.2	432.2	383	530	0.52	93
CORAC 275	463.2	464.4	383	530	0.14	92
CORAC 277	429.3	430.2	383	530	0.17	92
CORAC 329	499.1	500.2	383	530	0.51	93
CORAC 335	449.2	450.4	383	530	0.21	91
CORAC 336	511.2	512.2	383	530	0.42	92
CORAC 351	457.2	458.2	383	530	0.26	92
CORAC 358	481.2	482.2	383	530	0.33	91
CORAC 359	480.2	481.2	383	530	0.42	92
CORAC 364	455.2	456.2	383	530	0.28	93
CORAC 373	387.2	388.2	383	530	0.41	92
CORAC 374	421.2	422.2	383	530	0.3	93
CORAC 381	451.2	452.2	383	530	0.28	91
CORAC 382	427.2	428.4	383	530	0.36	92
CORAC 387	451.2	452.2	383	530	0.11	94
CORAC 388	451.2	452.2	383	530	0.39	94
CORAC 389	453.2	454.2	383	530	0.22	94
CORAC 395	465.2	466.4	383	530	0.34	96
CORAC 396	435.2	436.2	383	530	0.28	94
CORAC 398	435.2	436.2	383	530	0.45	90
CORAC 399	457.2	458.2	383	530	0.04	91
CORAC 403	455.2	456.2	383	530	0.58	93
CORAC 405	453.2	454.2	383	530	0.75	92
CORAC 412	457.2	458.2	383	530	0.17	91
CORAC 414	472.3	473.2	383	530	0.03	91
CORAC 419	401.2	402.2	383	530	0.42	93
CORAC 420	432.3	433.2	383	530	0.14	92
CORAC 425	401.2	402.2	383	530	0.55	92
CORAC 427	418.3	419.2	383	530	0.15	89
CORAC 441	427.2	428.4	383	530	0.28	91

CORAC 442	401.2	402.2	383	530	0.35	89
CORAC 457	457.2	458.2	383	530	0.55	89
CORAC 477	453.2	454.2	383	530	0.42	92
CORAC 478	449.2	450.2	383	530	0.44	93
CORAC 480	469.2	470.2	383	530	0.32	91
CORAC 511	557.2	558.2	383	530	0.46	92
CORAC 522	477.3	478.4	383	530	0.21	91
CORAC 531	489.1	490.2	383	530	0.25	90
CORAC 548	511.2	512.2	383	530	0.28	90
CORAC 554	457.3	458.2	383	530	0.39	94
CORAC 567	485.3	486.4	383	530	0.47	93
CORAC 572	513.1	514.2	383	530	0.2	92
CORAC 574	401.2	402.2	383	530	0.5	92
CORAC 575	385.2	386.2	383	530	0.31	96
CORAC 577	499.3	500.4	383	530	0.33	95
CORAC 580	555.4	556.4	383	530	0.13	93
CORAC 599	511.2	512.4	383	530	0.33	92
CORAC 602	415.2	416.2	383	530	0.19	92
CORAC 608	473.2	474.2	383	530	0.21	91
CORAC 621	517.1	518.2	383	530	0.08	94
CORAC 631	499.2	500.2	383	530	0.38	89
CORAC 656	581.4	582.2	383	530	0.27	91
CORAC 677	469.2	470.2	383	530	0.26	96

*1 Quantum yields were measured in DMSO, using Dansylamide as a standard (ϕ : 0.66, in DMSO). *2 Purities were determined according to UV absorption at 350 nm.ESI-MS positive spectra, HPLC conditions: A: H_2O-HCOOH: 99.9:0.1. B: CH_3CN-HCOOH: 99.9:0.1; gradient 100% A to 95% B (6 min), isocratic 95% B (6-8.2min), gradient 95% B to 100% A (8.2-9 min), isocratic 100% A (9-10 min). Reversephase Phenomenex C18 Luna column (4.6 x 50 mm^2) 3.5 μm, flow rate: 1.0 mL/min.
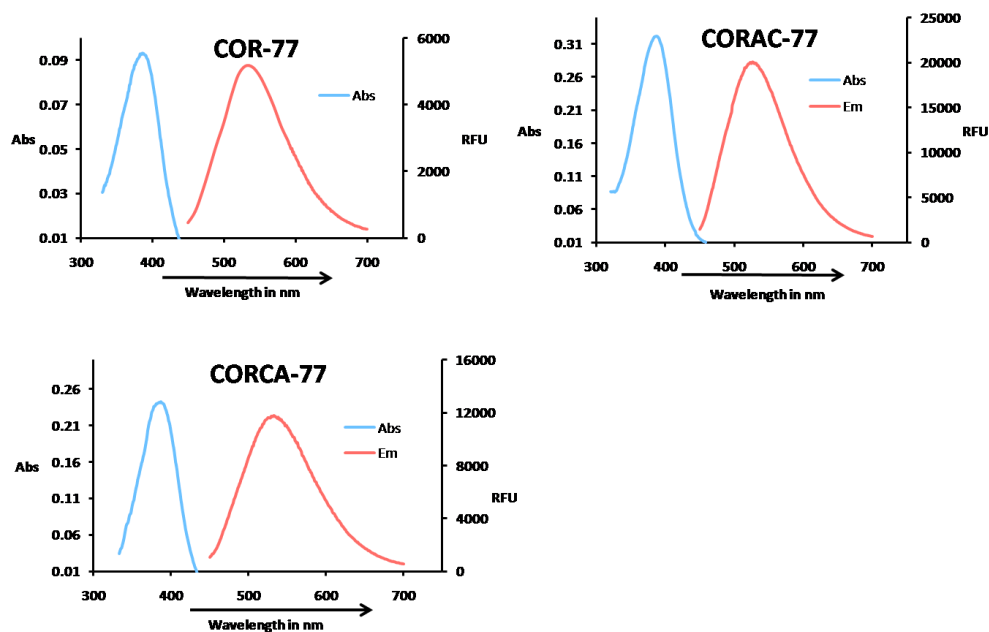
Figure 7.1 Absorption and emission spectra of representative COR, CORCA and CORAC compound.

7.4 Conclusions

I have succesufully synthesized large stoke shift (~ 150 nm) coumarin dye library, COR, in solid phase. I have also successfully modified them with chloroacteyl and acetyl version (CORCA and CORAC). These set of library could be used in bio-imaging applications as well as construction of longer wavelength FRET dyes.

7.5 Experimental methods

Material and methods

Amine and few bromide building block and all other chemicals and solvents for the synthesis were purchased from the Alfa Aesar, Fluka, Acros, MERCK, and Sigma Aldrich and were used without any purification. Merck Silica Gel 60 (particle size: 0.04-0.063 mm, 230-400 mesh) was used for the normal phase column chromatographic purification. From BeadTech Inc., Korea, 2-chlorotrityl alcohol resin (1.37mmol/g) was purchased. For analytical

197

characterization of COR compounds HPLC-MS (Agilent-1200 series) with a DAD detector and a single quadrupole mass spectrometer (6130 series) with an ESI was used. Analytical process, except specified: eluents: A: H_2O (0.1% HCOOH), B: ACN (0.1% HCOOH), C_{18} (2) Luna column (4.6 x 50mm^2, 5µm particle size) was used. ^{1}H-NMR and ^{13}C-NMR spectra were recorded on both Bruker Avance 300 MHz and 500 MHz NMR spectrometer, and chemical shifts are expressed in parts per million (ppm) and approximate coupling constants were calculated in Hz. Quantum yields and all other photophysical properties of COR derivatives were performed in Spectramax M2 instrument and the obtained data were analyzed using the Microsoft Office Excel 2007.

7.5.1 Synthesis of Coumarin acid
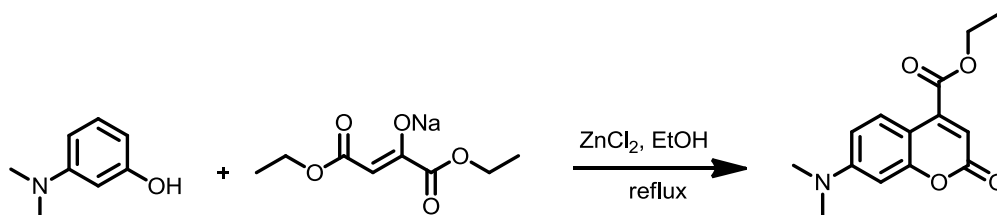
To synthesize coumarin ester **1**, m-dimethylaminophenol (12 g, 87.5 mmol), sodium diethyloxalacetate (20.2 g, 96.2 mmol, 1.1 equiv.) and ZnCl $_2$ (14.31 g, 105 mmol) were dissolved in absolute ethanol (50 mL). The reaction mixture was heated at reflux for 15 h. The reaction mixture was cooled to room temperature. Then, the reaction mixture was poured into ice-water. The precipitate formed was filtered and air-dried and purified by silicagel colum chromatography (eluent: DCM: MeOH = 15: 1, Rf = 0.30) to obtain orange solid (10 g, 43%).^{1}H- NMR (500 MHz, Methanol-d$_4$); δ 1.67 (t, 3H, *J*=7Hz), 3.31 (s, 3H), 4.68 (q, 2H, *J*=7Hz), 6.75 (d, 1H, *J*=2Hz), 6.79 (s, 1H), 6.99 (dd, 1H, *J*=9Hz), 8.28 (d, 1H, *J*=9Hz). ^{13}C-NMR (125 MHz, Methanol-d$_4$); δ

14.05, 62.07, 98.21, 105.62, 109.42, 111.92, 127.44, 142.90, 152.84, 156.62, 161.49, 14.54.

LCMS (ESI): calc for $C_{14}H_{15}NO_4$ (M+H) 261.1; found: 262.0
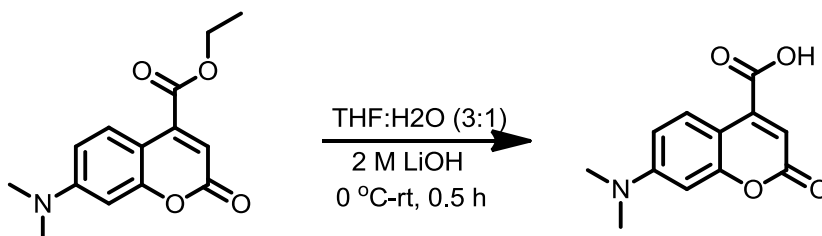
To Coumarin ester **1** (10 g, 36.32 mmol) was dissolved in THF–H$_2$O (3 :1) (60 mL) and cooled to 0 °C. 2 M LiOH solution (36.3 mL, 72.64 mmol, 2.0 equiv.) was added dropwise. The reaction mixture was stirred at room temperature for 0.5 h. Water (60 mL) was added, the aqueous layer was extracted with Et$_2$O (3 X50 mL). The aqueous layer was acidified to pH 2 by a 2 M HCl solution. Crude compound was extracted out from the aqueous layer with DCM (5X 50 ml). Organic layer was dried to get crude product which was purified by silica gel column chromatography (eluent: DCM : MeOH = 8 : 1, Rf = 0.45) to obtain the pure product as yellow solids. Yield: (4 g, 44%). ^{1}H- NMR (500 MHz, Methanol-d$_4$); δ 3.06 (s, 6H), 6.06 (s, 1H), 6.53 (d, 1H, *J*=2Hz), 6.75 (d, 1H, *J*=9Hz), 7.75 (d, 1H, *J*=9Hz). ^{13}C-NMR (125 MHz, Methanol-d$_4$); δ 40.09, 96.50, 105.71, 107.42, 110.52, 129.17, 154.64, 157.81, 165.21.

LCMS (ESI): calc for $C_{12}H_{11}NO_4$ (M-H) 232.1; found: 232.2

7.5.2 General procedure for solid phase synthesis of COR library

All the general procedures for the coumarin library synthesis is similar and given in chapter 2.

7.6 References

1) J. R. Lackowitz, Principles of Fluorescence Spectroscopy, 3rd ed.; Springer Science: New York, 2006.

2) A. P. de Silva, H. Q. Gunaratne, T. Gunnlaugsson, A. J. Huxley, C. P. McCoy, J. T. Rademacher and T. E. Rice, *Chem. Rev.*, 1997, **97**, 1515-1566.

3) (a) T. Miura, Y. Urano, K. Tanaka, T. Nagano, K. Ohkubo and S. Fukuzumi, *J. Am. Chem. Soc.*, 2003, **125**, 8666-8671.; (b) Y. Urano, M. Kamiya, K. Kanda, T. Ueno, K. Hirose and T. Nagano, *J. Am. Chem. Soc.*, 2005, **127**, 4888.

4) (a) N. S. Finney, *Curr. Opi. Chem. Biol.* 2006, **10**, 238.; (b) Q. Zhu , H.S.Yoon , P. B.Parikh, and Y.T. Chang and Yao, S. Q. *Tetrahedron Lett*. 2002, **43**, 5083.; (c) H. Cao, V. Chang, R. Hernandez and M. D. Heagy, *J. Org. Chem.*, 2005, **70**, 4929.

5) J. W. Lee, M. Jung, G. R. Rosania and Y. T. Chang, *Chem. Commun.* 2003, 1852.

6) Q. A. Li, J. S. Lee, C. Ha, C. B. Park, G. Yang, W. B. Gan and Y. T. Chang, *Angew. Chem. Int. Edit.*, 2004, **43**, 6331.

7) J. V. Mello and N. S. Finney, *J. Am. Chem. Soc.*, 2005, **127**, 10124.

8) (a) K. R. Romines, J. K. Morris, W. J.Howe, P. K Tomich,. M. M. Horng, K.T. Chong, R. R. Hinshaw, D. J. Anderson, J. W. Strohbach, S. R. Turner, S. A. Mizak, *J. Med. Chem*, 1996, **39**, 4125.; (b) I. Raad, R. Terreux, P. Richomme, E. L. Matera, C. Dumontet, J. Raynaud and D. Guilet, *Bioorg. Med. Chem.*, 2006, **14**, 6979.

9) R. S. Koefod and K. R. Mann, *Inorg. Chem.* 1989, **28**, 2285.

10) (a) H. Komatsu, T. Miki, D. Citterio, T. Kubota, Y. Chindo, Y. Kitamura, K. Oka and K.Suzuki, *J. Am. Chem. Soc.* 2005, **127**, 10798.; (b)K. Setsukinai, Y.Urano, K. Kikuchi, T. Higuchi and T. Nagano, *J. Chem. Soc., Perkin Trans.* **2** 2000, 2453.

11) M.S. Schiedel, C. A. Briehen and P. Bauerle, *Angew. Chem. Int. Ed.* 2001, **40**, 4677.

12) K. Silvakumar, F.Xie, B. M. Cash, S. Long, H. N. Barnhill and Q. Wang, *Org. Lett.* 2004, **6**, 4603.

13) K. Sivakumar, F. Xie, B. M. Cash, S. Long, H. N. Barnhill and Q. Wang, *Org. Lett.*, 2004, **6**, 4603.

14) H. Y. Song, M. H. Ngai, Z. Y. Song, P. A. MacAry, J. Hobley and M. J. Lear, *Org. Biomol. Chem.*, 2009, **7**, 3400.

15) R. K. Das, A. Samanta, H. H. Ha and Y. T. Chang, *RSC Adv.*, 2011, **1**, 573.

Chapter 8

8.1 Conclusions

It is quite obvious from the available wide range of literature reports that the progress of diversity orientedfluorescent library approach along with the high throughput screening lead to novel bio-imaging probes/sensors discovery in a relatively faster manner. However, for the case presented here, efficient solid phase chemistry needs to be devised to provide a robust synthetic route for generating a large number of fluorescent libraries in a short span of time. In this view, I developed an elegant solid phase route to systemically apply in the synthesis of fluorescent libraries that cover wide emission color spectra from Vis to NIR. We designed the novel diversity oriented fluorescent libraries where each library contains single emission wavelength to develop both cell imaging and *in vivo* imaging probe. Single wavelength with different structural diversity provided a useful toolbox as it allowed easier structural activity relationships studies (B cell probe development).

Based on the previous work by our group, I have synthesized ultraphotostable , NIR cyanine dye libraries (CyR and its CA, AC and lipoic acid derivatives) utilizing CyNA-414 , the most photostable dye from CyNA library. From macrophage screening of CyR derivatives, we developed a novel *in vivo* imaging macrophage probe (CyRCA-E4). From the SERS screening of the CyRLA compounds, we discovered the highly SERS-active compound CyRLA-E10 which has been utilized as the multiplexing partner with the Cy7LA and Cy7.5LA compounds to detect teratoma *in vitro*. Modifying the stable tetramethyl BODIPY scaffold, I have synthesized BDR library and its

CA and AC derivatives to generate green emission compounds. From the cell based screening, we discovered a B-cell selective probe CDg6. For the SARs study, I synthesized BODIPY derivatives containing long alkyl chains (upto 24 carbons). I also synthesized BODIPY derivative with different colors emissions keeping the chain length (18-C) same using condensation and coupling reactions.

Rhodol scaffold, a mixed hybrid from rhodamine and fluorescein was employed to produce longer wavelength, dye library (RDR and its CA, AC derivatives) in the range of orange emission color. Rhodol library inherited excellent photophysical properties such as good quantum yield, high extinction coefficient. Using cell based screening, we primary results for discovering mitotic phase specific probe, RDR-H2 which specifically stains to the mitosis compared to the inter phase cells.

I synthesized COR library and its respective chloroacetyl (CA) and acetyl derivatives (AC) to cover the large stokes shift (150 nm), green emission dyes. Here, based on the previous work and the studies, I opted a coumarin scaffold which contains dimethyl amino group at 7- position for better photophysical property and acid group at 4-position for diversification. Over all, I constructed a coumarin library (COR, CORCA and CORAC) with diversity at the 4-position using our efficient solid phase synthesis to explore these compounds in the evaluation of biological function via cell based and in vitro screening.

8.2 Future prospectives

Bio-imaging research needs arsenals of fluorescent probes to be developed. To accelerate the discovery of new bioimaging probes, we have

developed a new chemical toolbox that contains a set of fluorescent dyes with diverse structural, chemical and spectral properties. Due to the unbiased construction of these fluorescent dyes, varieties of *in vitro* or cell imaging probes can be developed using the high-throughput screening. Our simple but robust solid phase synthesis methodology would be applicable in designing and synthesizing new fluorescent libraries. Additionally, although, I have recently finished the coumarin library synthesis, due to the lack of enough time, we did not perform the cell based or *in vitro* screening using these compounds. The screening may offer coumarin based sensors or probes for further biological research.

The bio-imaging techniques recently have been attracted much attention for the development of new fluorescence probes based on single fluorophores. However, single emission intensity as a sensing signal can readily be perturbed[1] by environmental factors, such as pH, temperature, and solvent polarity. Hence, the development of precise fluorometrical analysis under complex biological assay may pave way the cellular bioimaging studies. Generally, single fluorophores are suffered from their unknown concentration and inhomogeneous location inside the cells[2]. Therefore, probes consisting two different wavelengths may represent an intriguing avenue for extracting biological information from living subjects since they can be monitored with safe, noninvasive optical imaging techniques. Our research group have been successfully demonstrated (as described in chapter 1) the potentiality of diversity oriented fluorescence library approach (DOFLA) to develop chemosensors/probes[3] for a number of biomolecules in one dimensional single fluorophore approach. Utilizing our DOFL approach and my fluorescent

libraries resources, two dimensional fluorescent libraries can be constructed to visualize the biological events to increase the chance of lead compound generation from high throughput screening (HTS).

8.3 References

1) Y. Kurishita, T. Kohira, A. Ojida and I. Hamachi, *J. Am. Chem. Soc.*, 2010, **132**, 13290.

2) Y. Sako, *Mol. Syst. Biol.*, 2006, **2**, 56.

3) (a) G. R. Rosania, J. W. Lee, L. Ding, H. S. Yoon and Y. T. Chang, *J. Am. Chem. Soc.*, 2003, **125**, 1130. (b) S. L. Wang and Y. T. Chang, *Chem. Commun.*, 2008, 1173. (c) S. L. Wang and Y. T. Chang, *J. Am. Chem. Soc.*, 2006, **128**, 10380. (d) Y. H. Ahn, J. S. Lee and Y. T. Chang, *J. Am. Chem. Soc.*, 2007, **129**, 4510.